



University of HUDDERSFIELD

University of Huddersfield Repository

Zhen, Dong

A Study of Non-stationary Signal Processing for Machinery Condition Monitoring

Original Citation

Zhen, Dong (2012) A Study of Non-stationary Signal Processing for Machinery Condition Monitoring. Doctoral thesis, University of Huddersfield.

This version is available at <http://eprints.hud.ac.uk/id/eprint/17812/>

The University Repository is a digital collection of the research output of the University, available on Open Access. Copyright and Moral Rights for the items on this site are retained by the individual author and/or other copyright owners. Users may access full items free of charge; copies of full text items generally can be reproduced, displayed or performed and given to third parties in any format or medium for personal research or study, educational or not-for-profit purposes without prior permission or charge, provided:

- The authors, title and full bibliographic details is credited in any copy;
- A hyperlink and/or URL is included for the original metadata page; and
- The content is not changed in any way.

For more information, including our policy and submission procedure, please contact the Repository Team at: E.mailbox@hud.ac.uk.

<http://eprints.hud.ac.uk/>

**A STUDY OF NON-STATIONARY
SIGNAL PROCESSING FOR
MACHINERY CONDITION
MONITORING**

*A thesis submitted to the University of Huddersfield for the degree of Doctor of
Philosophy in the School of Computing and Engineering*

2012

Dong Zhen

School of Computing and Engineering

LIST OF CONTENTS

List of Contents	2
List of Figures	6
List of Tables	9
List of Abbreviations and Notations	10
Abstract.....	15
Declaration.....	17
Copyright	18
Acknowledgements.....	19
Publications.....	20
Chapter 1 Introduction.....	22
1.1 Motivation and background	23
1.2 Introduction to condition monitoring	24
1.3 Acoustic-based condition monitoring	26
1.4 Aims and objectives of the research.....	28
1.5 Organisation of thesis.....	29
Chapter 2 Non-stationary Signal Processing.....	32
2.1 Introduction to signal processes	33
2.2 Non-stationary processes	34
2.2.1 Definition of non-stationary signal	34
2.2.2 Non-stationary processes in machinery condition monitoring	36
2.3 Time domain analysis	38
2.4 Spectral analysis.....	40
2.5 Time-frequency domain analysis	42
2.5.1 Spectrograms	42

2.5.2	Wigner-Ville distribution.....	43
2.5.3	Wavelet transform.....	44
2.5.4	Fractional Fourier transform.....	45
Chapter 3 Dynamic Time Warping.....		48
3.1	Introduction to dynamic time warping.....	49
3.2	Classical dynamic time warping	50
3.2.1	The definition.....	50
3.2.2	Properties	51
3.2.3	Warping path.....	52
3.3	Dynamic time warping limitations.....	54
3.3.1	Definition of singularity.....	54
3.3.2	Computational complexity.....	57
3.4	Dynamic time warping improvements	57
3.4.1	Singularity improvement	58
3.4.2	Time complexity improvement.....	65
3.5	Phase properties of singularities.....	68
Chapter 4 Dynamic Time Warping of Motor Current Signals for Fault Diagnosis of A Reciprocating Compressor		73
4.1	Introduction to motor current signal analysis	74
4.2	Reciprocating compressor test	75
4.2.1	Test rig	75
4.2.2	Current transducer.....	77
4.2.3	Experimental setup	78
4.3	Phase current signal.....	78
4.3.1	Electromagnetic relationship of the phase current signal	79
4.3.2	The characteristics of phase current signal	81
4.4	Phase compensation based dynamic time warping	83
4.4.1	Phase estimation	84
4.4.2	Algorithm implementation strategies.....	85
4.5	Faults detection and classification	88

4.5.1	Dynamic time warping alignment.....	88
4.5.2	Feature extraction and fault diagnosis	90
4.5.3	Results and discussion	93
Chapter 5 The Characteristics of Vibro-acoustic Signals from Internal Combustion Engines		98
5.1	Introduction to engine acoustics	99
5.2	Engine test facilities and setup	100
5.2.1	The test engine specification.....	100
5.2.2	Measurement instrumentation.....	102
5.2.3	Data acquisition system	107
5.2.4	Test procedures	107
5.3	The characteristics of engine noise and vibration	109
5.3.1	The time domain statistics of engine acoustics and vibration	109
5.3.2	Spectrum analysis of engine acoustics and vibration	115
5.4	Room modes	119
5.5	Fuel monitoring based on engine acoustics	121
Chapter 6 Combustion as the Source of Vibro-acoustics From an Engine Fuelled By Biodiesel Blends		126
6.1	Researches on the performance of engine fuelled by biodiesel	127
6.2	Combustion parameters.....	128
6.2.1	Cylinder pressure	130
6.2.2	Heat release rate.....	132
6.2.3	Ignition delay	135
6.2.4	Cumulative heat release	136
6.3	Vibration and noise from combustion.....	137
Chapter 7 Analysis of Engine Vibro-acoustic Signal Based on Fractional Fourier Transform		141
7.1	Researches on engine vibro-acoustics.....	142
7.2	Statistical characteristics of vibration and acoustic signals	143
7.2.1	Variations of engine vibro-acoustic signals.....	143

7.2.2	Coherent power spectrum analysis	147
7.3	The time-frequency distribution of engine acoustics	150
7.3.1	The Wigner-Ville distribution	150
7.3.2	Wigner-Ville distribution analysis of engine acoustics	151
7.4	The fractional Fourier transform	152
7.4.1	Definition of fractional Fourier transform and its properties	153
7.4.2	Band-pass filter based on fractional Fourier transform	155
7.4.3	Combustion noise extraction	156
7.5	Feature extraction and classification	158
Chapter 8 Combustion Diagnosis Based on Engine Acoustics Using Wavelet Analysis		161
8.1	Introduction to engine acoustics analysis using continuous wavelet transform	162
8.2	The continuous wavelet transform	163
8.2.1	Definition of continuous wavelet transform	164
8.2.2	Properties of continuous wavelet transform	165
8.2.3	Morlet wavelet	166
8.3	Time synchronous average.....	168
8.4	Feature extraction and RMS linear classification	171
Chapter 9 Conclusions and Future Work		176
9.1	Review of thesis objectives and achievements	177
9.2	Conclusions	179
9.2.1	Conclusions regarding the fault diagnostics of the compressor using the motor electrical current signal.....	180
9.2.2	Conclusions regarding the condition monitoring of diesel engines.....	181
9.3	Research contributions to new knowledge.....	182
9.4	Suggestions for further research.....	184
Appendix A		186
Appendix B		188
References		193

LIST OF FIGURES

Figure 1-1 Classification of maintenance strategies	23
Figure 1-2 The three main steps in a condition monitoring system.....	25
Figure 3-1 Time series aligned by DTW.....	50
Figure 3-2 Optimal warping path selected by dynamic programming	53
Figure 3-3 Examples of singularities in DTW application	55
Figure 3-4 Singularities located at the ends	56
Figure 3-5 Step patterns: a) the step patterns in classic DTW; b) the step pattern improvement	59
Figure 3-6 Comparisons of signal alignment by DTW, DDTW and FBDTW	61
Figure 3-7 The alignment of points based on the warping paths produced by DTW, DDTW and FBDTW	63
Figure 3-8 Optimal warping paths produced by DTW, DDTW and FBDTW.....	64
Figure 3-9 Global constraints for time complexity improvement.....	66
Figure 3-10 Comparison of point alignment after processing by DTW and PDTW	67
Figure 3-11 SD of DTW residual signals with different phase shifts	69
Figure 3-12 The singularity effect of DTW with phase compensation.....	71
Figure 3-13 Comparison of SD of DTW residual signals.....	72
Figure 4-1 Photos of the test facility and data acquisition system.....	76
Figure 4-2 The experimental setup	77
Figure 4-3 Current transducer	77
Figure 4-4 Waveform and spectra of stator current signals from a compressor with healthy and faulty valve leakage	82
Figure 4-5 A flow diagram of the DTW based method	84
Figure 4-6 DTW processing motor current signal	89
Figure 4-7 Waveforms of residual signals for faulty cases in one sliding window	91
Figure 4-8 DTW residual signal based detection and diagnosis	92

Figure 4-9 Spectrum sideband based detection and diagnosis.....	93
Figure 4-10 Envelope signal based detection and diagnosis.....	94
Figure 4-11 Comparison of standard deviation for three analysis techniques.....	96
Figure 5-1 The test rig photo.....	100
Figure 5-2 Microphones and preamplifier	103
Figure 5-3 Schematic diagram of the engine test system.....	103
Figure 5-4 Microphone used for measuring the acoustic signals.....	104
Figure 5-5 Vibration accelerometer	105
Figure 5-6 Pressure sensor	106
Figure 5-7 Data acquisition equipment (model YE6261B)	107
Figure 5-8 SPL comparisons under different operating conditions	110
Figure 5-9 Variations of SPL versus speed and load	111
Figure 5-10 Raw acoustic signals under various loads and speeds.....	112
Figure 5-11 Combustion pressure under various loads.....	113
Figure 5-12 Raw vibration signals under various loads and speeds	114
Figure 5-13 RMS of the raw vibration signals from the test engine.....	115
Figure 5-14 Spectrum of acoustic signals under different speeds.....	116
Figure 5-15 Spectrum of acoustic signals under various conditions	117
Figure 5-16 1/3 octave band spectra of acoustic signals.....	118
Figure 5-17 Difference spectrum of acoustic signals under different speeds	121
Figure 5-18 Acoustic signals under various fuels supplied in one cycle	122
Figure 5-19 Variations of SPL under different operating conditions	123
Figure 5-20 Variations of SPL filtered by high-pass filter	124
Figure 5-21 1/3 octave band spectra of acoustic signals.....	125
Figure 6-1 Cylinder pressure, heat release rate for diesel engine	129
Figure 6-2 Cylinder pressure at a speed of 1300rpm under different loads.....	130
Figure 6-3 Cylinder pressure at a load of 420N m under different speeds	131
Figure 6-4 HRR at speed of 1100rpm and under different loads.....	133
Figure 6-5 HRR at 210 N m load under different speeds for biodiesels.....	134
Figure 6-6 HRR at a speed of 1100rpm under different loads for biodiesel blends ...	135
Figure 6-7 Cumulative heat release at a speed of 1300rpm and different loads	137

Figure 6-8 Normalised cylinder pressure, body vibration and engine acoustic	138
Figure 6-9 Combustion noise generation diagram	139
Figure 7-1 Vibration signals at a speed of 1300rpm under different loads.....	144
Figure 7-2 Acoustic signals at a speed of 1300rpm under different loads.....	145
Figure 7-3 Spectrum of vibration signals under different conditions	146
Figure 7-4 Spectrum of acoustic signals under different conditions.....	147
Figure 7-5 Engine noise source model.....	148
Figure 7-6 Coherent power spectrum analysis of engine noise	149
Figure 7-7 WVD of engine noise at loads of 105N m and 420N m.....	152
Figure 7-8 Time-frequency plane and a set of coordinates (u, v) rotated by an angle α relative to the original coordinates (t, ω)	154
Figure 7-9 Energy distributions on the fractional plane	156
Figure 7-10 WVD of engine noise processed by FRFT filter.....	157
Figure 7-11 Variations of SPL for different fuels.....	158
Figure 8-1 The Morlet wavelet	167
Figure 8-2 TSA acoustic signals under different operating conditions and fuel types	170
Figure 8-3 RMS values of TSA acoustic signals under different fuel types.....	171
Figure 8-4 Contour plots of the results for different fuel types at the speed of 900rpm	172
Figure 8-5 Contour plots of the results for different fuel types at the speed of 1300rpm	173
Figure 8-6 Comparison of the RMS values between different loads and fuel types...	174

LIST OF TABLES

Table 4-1 Electrical specification of current transducer	78
Table 4-2 Faults and Loads in using Experimental testing	78
Table 5-1 Specifications of the test engine	101
Table 5-2 Specification of the microphone CHZ-211	104
Table 5-3 Specification of the preamplifier	104
Table 5-4 Technical specification of the accelerometer	106
Table 5-5 Test operating setup-1	108
Table 5-6 Test operating setup-2.....	108
Table 5-7 Properties of biodiesel	109
Table 5-8 Lower order room modes.....	119
Table 6-1 Crank angles at the start of combustion for fuels at different engine conditions	136

LIST OF ABBREVIATIONS AND NOTATIONS

List of abbreviations

AET	acoustic emission technology
AE	acoustic emission
AR	autoregressive model
ARMA	autoregressive moving average
AM	amplitude modulation
B25	25% biodiesel
B50	50% biodiesel
B100	100% biodiesel
CBM	condition based maintenance
CM	condition monitoring
CWT	continuous wavelet transform
DTW	dynamic time warping
DWT	discrete wavelet transform
DDTW	derivative dynamic time warping
EMD	empirical mode decomposition
FFT	fast Fourier transform
FT	Fourier transforms

FRFT	fractional Fourier transform
FBDTW	feature based dynamic time warping
HRR	heat release rate
IMFs	intrinsic mode functions
LHV	lower heating value
PCA	principal component analysis
PDTW	piecewise dynamic time warping
RMS	root mean square
RSD	relative standard deviation
STFT	short-time Fourier transforms
SNR	signal-to-noise ratio
SD	standard deviation
SPL	sound pressure level
TSA	time synchronous average
TDC	top dead centre
WVD	Wigner-Ville distribution
WT	wavelet transform

List of notation

A_{ref}	Estimated amplitude of reference signal	[A]
a	Dilation parameter	[-]
b	Translation parameter	[-]
C	Accumulative distance matrix	[-]
D	Distance matrix	[-]
d_{ij}	Point-to-point Euclidean distance	[-]
$d_w(\cdot)$	Accumulated distance	[-]
$d^*(\cdot)$	Optimal warping path	[-]
$dQ/d\theta$	Heat release rate	[KJ/deg]
F_s	Sampling frequency	[Hz]
$f(\cdot)$	Frequency components	[Hz]
$G(\cdot)$	Cross power spectrum	[-]
$H_i(t)$	Transfer function	[-]
I	The amplitude of the supply current	[A]
i_A	Instantaneous current signal in phase A	[A]
$K_\alpha(\cdot)$	The kernel function of FRFT	[-]
$L^2(R)$	Space of square integral complex functions	[-]
L_{min}	Minimum length of sliding window	[-]
$n(t)$	Background noise	[-]

(n_x, n_y, n_z)	Room mode	[-]
$O(\cdot)$	Computational complexity	[-]
P	Number of pole pairs	[-]
\mathbf{P}	In-cylinder gas pressure	[Pa]
p	Transform order of the FRFT	[-]
Q_c	Accumulative heat release	[m]
R^α	Operator of FRFT	[-]
R	Transmission ratio of compressor	[-]
RSD	Relative standard deviation	[-]
S	Speed of compressor	[rpm]
$s_{(\cdot)}$	Time series	[-]
T	Interaction torque	[N m]
ΔT	Oscillatory torque	[N m]
V	In-cylinder volume	[m ³]
W	Warping paths	[-]
$W_f(\cdot)$	Continuous Wigner-Ville distribution	[-]
$w(t)$	Time window	[-]
$W_{fw}(t, \omega)$	Wigner-Ville distribution of windowed signal	[-]
$WT(\cdot)$	Wavelet transform	[-]
X	A time series	[-]

x_{ref}	Reference signal	[A]
Y	A time series	[-]
$\alpha_{(\cdot)}$	Angular displacement	[rad]
$\Delta\alpha_{(\cdot)}$	Angular oscillation	[rad]
α	Rotation angle for FRFT	[rad]
γ	Ratio of specific heats	[-]
$\gamma_{(\cdot)}^2$	Coherent function	[-]
$\theta_{(\cdot)}$	Phase angular	[rad]
θ	Crank angular	[deg]
ε	Positive integer window width	[-]
$\Delta\omega$	Speed fluctuation	[rad]
$\Delta\psi, \Delta\hat{\psi}$	Window radius	[m]
$\psi_{a,b}(\cdot)$	Wavelet function	[-]
$\psi(t)$	Time domain Morlet	[-]
$\hat{\psi}(\omega)$	Frequency domain Morlet	[-]
\emptyset_A	Instantaneous magnetic flux	[Wb]
\emptyset	Amplitude of magnetic flux	[Wb]
$\hat{\eta}(\omega)$	Correction term to Morlet function	[-]

ABSTRACT

Machinery condition monitoring techniques are carried out based on the knowledge of the characteristics of signals obtained from a machine or plant. These signals are often non-stationary signals whose frequency changes over time due to the time-varying natures of machine operations and fault effects. Conventional signal processing techniques are developed based on stationary signals and cannot reveal the time information of the frequency changes. The work undertaken in this research presents a generic study of non-stationary signal processing for machinery condition monitoring.

Starting with examining the concept of non-stationary signals, it can be identified that most condition monitoring signals fall into two main categories: weak non-stationary signals, such as motor electrical current signal and strong non-stationary signal such as machinery vibration and acoustic signals.

For developing techniques to process these two typical non-stationary signals, two experiments were carried out to obtain these them. Firstly, an induction motor drive system was set up based on a two-stage reciprocating compressor; the motor current signals were then acquired for compressor fault detection and diagnosis. Secondly, a set of vibration and acoustic measurement instrumentation was set up based on a diesel engine test system. The engine vibration and acoustic signals were collected for further analysis for engine combustion condition monitoring. The engine was fuelled by different biofuels during data collection allowing a new and efficient method of verifying different sustainable fuels to be developed based non-intrusive vibro-acoustic measurements in conjunction with non-stationary signal analysis methods.

A time domain based method, dynamic time warping, was validated and improved for analysing the motor current signal to detect and classify the common faults of reciprocating compressors. Based on the limitations of classical dynamic time warping, a phase estimation and compensation approach is developed to reduce the singularity effect of classical dynamic time warping in order to obtain accurate diagnostic results. A sliding window was also designed to improve computing efficiency. The diagnostic results show that the accuracy and reliability of detection and classification by the proposed dynamic time warping method is higher than that from Fourier transform spectrum and envelope analysis. In addition, the fault detection and classification is based on a root mean square (RMS) linear classifier processes combined with the proposed dynamic time warping method, and is based entirely on time domain analysis which is easier to apply to a real-time condition monitoring system. It was proved that the proposed dynamic time warping is a novel and efficient method for cyclostationary/weak non-stationary analysis.

Various non-stationary signal processing techniques based on time-frequency domain analysis, including Wigner-Ville distribution, fractional Fourier transform and continuous wavelet transform, are investigated to process the engine vibration and the acoustic signals for the condition monitoring of engine combustion. A sound pressure level (SPL) indicator is designed based on the Wigner-Ville distribution (WVD) analysis and the fractional Fourier transform filtering of the engine vibro-acoustic signals. The processing results demonstrate that the combustion induced acoustics can be extracted for the diagnostics of engine combustion process and for condition monitoring.

A root mean square (RMS) linear classifier is developed based on the engine acoustic analysis by time synchronous average and continuous wavelet transform, the classification demonstrates that the root mean square (RMS) values of the continuous wavelet transform coefficients can be used to evaluate the fuel for engine combustion and indicate the engine operating conditions. The analysis results verify that the engine vibro-acoustics have the potential to be used to diagnose the engine combustion process and to monitor the engine operating conditions with the application of suitable non-stationary signal processing techniques. This can be used instead of the cylinder pressure data which is both intrusive and costly to obtain.

Finally, the conclusions and achievements are given based on the entirety of this research work, and suggestions are presented for further research.

DECLARATION

No portion of the work referred to in this thesis has been submitted in support of an application for another degree or qualification of the University of Huddersfield or any other university or other institute of learning.

COPYRIGHT

1. Copyright in text of this thesis rests with the Author. Copies (by any process) either in full, or extracts, may be made only in accordance with instructions given by the Author and lodged in the University Library of Huddersfield. Details may be obtained from the Librarian. This page must form part of any such copies made. Further copies (by any process) of copies made in accordance with such instructions may not be made without the permission (in writing) of the Author.
2. The ownership of any intellectual property rights which may be described in this thesis is vested in the University of Huddersfield, subject to any prior agreement to the contrary, and may not be made available for use by third parties without the written permission of the University, which will prescribe the terms and conditions of any such agreement. Further information on the conditions under which disclosures and exploitation may take place is available from the Head of the School of Computing and Engineering.

ACKNOWLEDGEMENTS

This work has been carried out in the school of Computing and Engineering, Centre for Efficiency and Performance Engineering (CEPE) at the University of Huddersfield, U. K. It was financially funded by the Fee-waiver Scholarship scheme from the University of Huddersfield. I would like to give my grateful acknowledgements to the University of Huddersfield and CEPE group for their support during the research.

I would like to give a sincere thank to my main supervisor, Professor Andrew Ball, at the University of Huddersfield for his guidance and constant support over the duration of this research. It is his inspiration which encourages me to cope with all the faced challenges and gain the rewarding research skills.

I am especially like to thank my co-supervisor, Dr. Fengshou Gu, Senior Research Fellow at the University of Huddersfield, for his sincere and warm-hearted help both academically and personally. His support in both research and life makes me have a pleasure and fruitful time throughout the pursuit of my doctorate.

I would like to thank all the members of the Centre for Efficiency and Performance Engineering (CEPE) research group for their discussion and advice during the research.

I also appreciate the help from all the friends I have made in Huddersfield, especially Shan Lou, Zhaozong Meng and Lan Wang, they have made my time here both enjoyable and unforgettable.

Finally, special thanks extend to my parents for their unstinting support, encouragement, and high expectations.

PUBLICATIONS

1. **D. Zhen**, T. Wang, F. Gu, and A. D. Ball, "Fault diagnosis of motor drives using stator current signal analysis based on dynamic time warping", *Mech. Syst. Signal Process.* (2012), <http://dx.doi.org/10.1016/j.ymssp.2012.07.018>.
2. **D. Zhen**, H. L. Zhao, F. Gu, and A. D. Ball, "Phase-compensation-based dynamic time warping for fault diagnosis using the motor current signal," *Measurement Science and Technology*, vol. 23, no. 5, p. 055601, May 2012.
3. **D. Zhen**, T. Wang, F. Gu, and A. D. Ball, "Acoustic measurement for combustion diagnosis of diesel engines fuelled with biodiesels," *Measurement Science and Technology*. (under review)
4. **D. Zhen**, B. Tesfa, X. Yuan, R. Wang, F. Gu, and A. D. Ball, "An investigation of the acoustic characteristics of a compression ignition engine operating with biodiesel blends," *Journal of Physics: Conference Series*, vol. 364, p. 012015, May 2012.
5. **D. Zhen**, T. Wang, F. Gu, and A. D. Ball, "Combustion Analysis of a CI Engine with Biodiesel Blends based on Vibro-Acoustic Measurement". In: *CM 2012 and MFPT 2012: The ninth International Conference on Condition Monitoring and Machinery Failure Prevention Technologies*, 2012.
6. **D. Zhen**, F. GU, X. Zhou, and A. D. BALL, "Fault Signal Enhancement using Adaptive Filtering Techniques for Gearbox Monitoring", *The 24th International Congress on Condition Monitoring and Diagnostics Engineering Management (COMADEM2011)*, pp 251-258, 2011.
7. **D. Zhen**, A. Alibarbar, X. Zhou, F. Gu, and A.D. Ball. "Electrical Motor Current Signal Analysis using a Dynamic Time Warping Method for Fault Diagnosis". *J. Phys.: Conf. Ser.* 305 012093, 2011.
8. **D. Zhen**, F. Gu, and A. D. Ball, "The Study of Acoustic Source Localization using a Small Microphone Array for Condition Monitoring". In: *Future*

- Technologies in Computing and Engineering: Proceedings of Computing and Engineering Annual Researchers' Conference 2010: CEARC'10. University of Huddersfield, Huddersfield, pp. 14-19. ISBN 9781862180932, 2010.
9. **D. Zhen**, Y. Fan, F. Gu, and A. D. Ball, "A Study of Sound Source Characteristics in Active Noise Control and Fault Diagnosis". In: Inter noise 2010-39th International congress on Noise Control Engineering, 13-16 June 2010, Lisbon, Portugal.
 10. **D. Zhen**, J. Gu, T. Wang, F. Gu, and A. D. Ball, "Diagnostic Feature Development based on Dynamic Time Warping of Dynamic Signals under Variable Machine Operating Condition". In: CM 2010 and MFPT 2010: The Seventh International Conference on Condition Monitoring and Machinery Failure Prevention Technologies, 2010.
 11. X. Tian, F. Gu, **D. Zhen**, V. T. Tran and A. D. Ball, "Investigation of Fault Diagnosis based on an Active Noise Control System". In: CM 2012 and MFPT 2012: The ninth International Conference on Condition Monitoring and Machinery Failure Prevention Technologies, 2012.
 12. F. Elbarghathi, T. Wang, **D. Zhen**, F. Gu, and A. D. BALL, "Two Stage Helical Gearbox Fault Detection and Diagnosis based on Continuous Wavelet Transformation of Time Synchronous Averaged Vibration Signals", Journal of Physics: Conference Series, vol. 364, p. 012083, May 2012.
 13. H. Zhang, Z. Q. Shi, **D. Zhen**, F. Gu, and A. D. BALL, "Stability Analysis of a Turbocharger Rotor System Supported on Floating Ring Bearings", The 25th International Congress on Condition Monitoring and Diagnostics Engineering Management (COMADEM2012), 2012.
 14. X. Zhou, Y. Shao, **D. Zhen**, F. Gu, and A. D. Ball. "Gear Fault Signal Detection based on an Adaptive Fractional Fourier Transform Filter", J. Phys.: Conf. Ser. 305 012022, 2011.

CHAPTER 1

INTRODUCTION

This chapter presents a general introduction to the machinery condition monitoring techniques. Firstly, the motivation and background of this research work are presented; secondly, maintenance strategies and condition monitoring techniques are reviewed; finally, the objectives and organisation of this research are outlined.

1.1 Motivation and background

In industrial application, the reliability of a machine is a critical aspect in the evaluation of its performance. The performance of a machine will be deteriorated over time as a result of operating under certain stresses or load. Maintenance has been introduced as an efficient way to assure a satisfactory level of reliability during the useful life of a machine [1]. Maintainability is regarded an important process for manufacturing managers especially when the cost involved in the failure and repair of equipment is taken into account [2]. Numerous maintenance actions are carried out to extend the life span of the machine or process and to avoid catastrophic accidents. Generally, maintenance is a combined action depending on an understanding of the machine and its working principles. Along with the development of maintenance techniques, there is several maintenance strategies used widely: corrective maintenance, emergency maintenance, preventive maintenance, scheduled maintenance, and condition-based maintenance [2][3]. These maintenance strategies can be classified as two main types according to their implementation characteristics, which are unplanned maintenance and planned maintenance as shown in Figure 1-1.

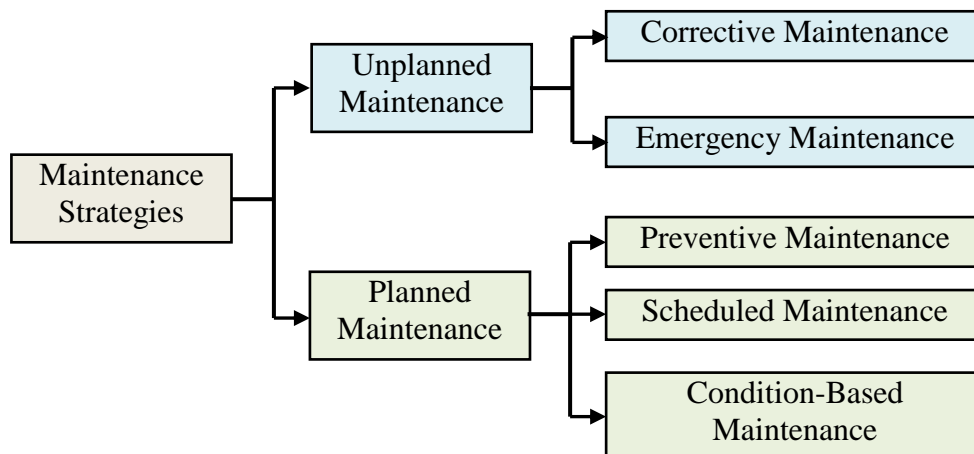


Figure 1-1 Classification of maintenance strategies

Amongst these maintenance strategies, condition-based maintenance is a popular maintenance strategy which is widely used in practice since it works to predict failure at a time sufficiently in advance of the event that action may be taken [2]. It is capable

of exploiting the maximum operating time of a system or machine and minimizing the maintenance costs involved. Condition-based maintenance is defined as preventive maintenance initiated as a result of knowledge of the condition of an item from routine or continuous monitoring [2]. Condition-based maintenance works by determining the actual operating conditions of a system or item at any point in time. Condition monitoring is a useful technique which is able to monitor the conditions of machine at all times and provides an accurate prediction of any potential failure. The main purpose of condition-based maintenance is to guide the maintenance be taken at a proper time based on the operating conditions of monitored machine. This means that the most important aspect of condition-based maintenance is the effectiveness of the method used for monitoring the status of a machine. Condition monitoring is an effective method used to monitor the operating conditions of a machine and ensures that all necessary maintenance actions can be taken at a time appropriate to the predicted failure.

1.2 Introduction to condition monitoring

Condition monitoring is defined as the continuous and periodic measurement and interpretation of data to indicate the condition of a system or plant which is then used to guide the maintenance [2]. Condition monitoring is concerned with gathering data to enable better understanding of the health or condition of an item [4]. Normally, condition monitoring is carried out when the system or plant is running, and its application is used to assess the current condition of the system or plant by analysing the measured signals using various signal processing techniques. This is in order to economically perform maintenance when a potential failure is identified at a convenient time. The assessment of the current condition of a system or item is carried out through measuring parameters which reflect the condition of a component. These measurements may also indicate the future trend of its possible deterioration.

The use of condition monitoring allows effective maintenance to be scheduled, and allows other actions to be carried out in order to avoid accidents before a failure occurs. The input of condition monitoring activity is mainly the data obtained from different

types of sensors which are used to schedule and carry out the maintenance actions. A condition monitoring system consists of three key steps [1]: data acquisition, data processing, and maintenance decision making. These are shown in Figure 1-2.



Figure 1-2 The three main steps in a condition monitoring system [1]

Various types of data can be used for condition monitoring. It depends on the kinds of sensors used in the data acquisition system. The data can be vibration, acoustic, oil analysis data, temperature, pressure, moisture, humidity, and weather or environmental data. All these data can be collected by different kind of sensors, such as accelerometers, microphones, ultrasonic sensors and acoustic emission sensors [5, 6].

Data processing is a vital step in a condition monitoring system, its purpose is to better understand and interpret the data so that efficient maintenance policies may be proposed [1]. Many kinds of algorithms and techniques have been introduced to analyze the data obtained from data acquisition system.

There are numerous methods used for making maintenance decisions in a condition monitoring system. Based on the types of data collected or the types of the sensors used for data collected, there are a variety of techniques that can and should be used for making maintenance decisions in a condition monitoring system [6].

1. Visual inspection [3][7].
2. Trend monitoring [7].
3. Vibration-based condition monitoring [7][8][9].
4. Acoustic emission monitoring [10][11][12].
5. Acoustic-based condition monitoring [7][13][14].
6. Current-based monitoring [15][16].

Among the various condition monitoring techniques, vibration monitoring is generally the most important technique in most condition monitoring systems [3]. Sometimes, all of these technologies are applied in a comprehensive condition monitoring system in order to obtain accurate conditions assessment of a machine. Especially, acoustic-based condition monitoring technique is coupled with vibration-based condition monitoring for the analysis of the conditions of a machine.

1.3 Acoustic-based condition monitoring

Sound or acoustics are related to the vibration of objects. The generation of sound is usually attributed to the vibration of solid objects and sound can be explained as vibration of the air [17]. Therefore, the vibration, acoustic or the sound noise signals are generated from the machine or processes at the same time as a machine is running and the noise produced by the machine can be used to indicate the condition of the machine. Acoustic-based condition monitoring employs the airborne sound signal with the frequency from 20Hz to 20 kHz.

Airborne sound signals can be picked up by microphones, and can be employed for condition monitoring by analysis of the airborne acoustic characteristics or the noise produced by machines or equipment. Compared with vibration sensors, microphones are easy to install and have higher frequency response ranges which can give more detailed information [7]. Acoustic signals are also easy to record, and record the total noise level of the monitored system as there are potentially a number of different sound sources in one machine. The characteristics of noise generation and the transmission of each sound source can be extracted by analyzing the airborne acoustic signal, and the sound sources can also be separated for detailed analysis through microphone array signal processing techniques [18]. Researchers have focused on the use of airborne acoustic signals for condition monitoring more frequently in recent decades. Li [13] investigated the acoustic-based condition monitoring of a diesel engine operating under different conditions, and the results showed that the extracted features from the acoustic signals generated by the test engine were able to identify the differences between the engine's normal and faulty conditions.

Even though the airborne acoustic monitoring technique is convenient to use in practice, the airborne acoustic signals are easily polluted by background noise. Gu and Ball [14] investigated *“the influences of the measurement environment on the acoustic data, the signal conditioning and the representation techniques were required to reveal the condition-indicating content of the monitored acoustic signal.”* Airborne acoustic signals need to be pre-processed to improve its signal to noise ratio (SNR) before extracting the characteristics of the sound sources from the noise signals for fault diagnosis. Albarbar, Gu and Ball [19] employed adaptive filtering techniques to enhance the diesel fuel injector needle impact excitations contained within airborne acoustic signals for better condition monitoring information. Jiang, Gu and Ball [20] introduced an effective monitoring method for diesel engine combustion based on acoustic one-port source theory and exhaust acoustics measurement, and found that *“the engine acoustic source has ability of providing an accurate representation of engine combustion events by minimizing the reflection effects in the exhaust system.”* The fact is that airborne acoustics is a sequence of waves of pressure which propagate through compressible media air [17]. During their propagation, the sound waves may be refracted and attenuated by the medium. Otherwise, if the sound sources are located in an enclosed space, the reflection caused by the boundary of the enclosed space will affect the basic characteristics of the sound source [17], and increase the difficulties of fault diagnosis.

Condition monitoring techniques are applied to assess the conditions of a machine or plant based on the measured signal collection and interpretation using various signal processing methods. The signal processing methods selected for the analysis of the measured signals are based on the characteristics of the signal itself [2]. In the machinery condition monitoring [1][2][4], most of the measured signals can be considered as non-stationary signals which contain the information related to the faults and operating conditions of the monitored machine. Non-stationary signal analysis is a critical part of machinery condition monitoring and it is necessary to study the using of appropriate signal processing methods to analyse measured non-stationary signals

based on their characteristics for accuracy feature extraction for machinery condition monitoring and fault diagnostic.

1.4 Aims and objectives of the research

The aim of this research is to study the signal processing methods for non-stationary characteristics analysis, extraction and for abnormal detection of signals in machine condition monitoring and fault diagnostics. In this research work, electrical current, engine vibration and engine acoustic signals are selected as three typical non-stationary signals. Effective signal processing algorithm and techniques are studied to be used to analyze these three typical non-stationary signals for a compressor fault diagnostic and diesel engine condition monitoring.

To test the abilities and effectiveness of the developed signal processing algorithms on feature extraction for the machine condition and fault diagnostics, experiments (see Section 4.2 and 5.2) are carried out and the proposed signal processing methods (see Section 3.2, 4.4, 4.5, 7.3-7.5, and 8.2-8.4) are used to analyse the measured signals. The results of the analysis show that the developed signal processing methods are capable of analysing the non-stationary characteristics of signals for feature extraction, weak signal enhancement, and for the detection of abnormal components. This leads to more accurate detection results for the monitoring of machinery condition and for the diagnosing of faults.

This aim is accomplished by the fulfilment of the following objectives:

- The reviewing of the signal processing methods and monitoring techniques used in machinery condition monitoring (see Chapter 2).
- The construction of a diesel engine test rig (see Section 5.2) and a reciprocating compressor test facility (see Section 4.2) for the study of machinery condition monitoring.
- Improvement of the dynamic time warping algorithm (see Chapter 4) for accurate feature extraction used for fault classification of a reciprocating compressor.

- Analysis of the characteristics of diesel engine vibro-acoustic signals (see Chapter 5).
- Analysis of the combustion process of a diesel engine (see Chapter 6) for engine combustion condition monitoring and fuel evaluation.
- The development of advanced vibro-acoustic signal processing methods (see Chapter 7 and 8) to extract the non-stationary nature for diesel engine condition monitoring.
- Analysis of the relationship between vibro-acoustic signal and the combustion process of a diesel engine under different conditions (see Section 6.3).
- The extraction of vibro-acoustic features to monitor the combustion process fuel quality of the diesel engine (see Section 7.5 and 8.4).

1.5 Organisation of thesis

A brief introduction is listed to outline the thesis as follows:

Chapter 1: This chapter presents the motivation and background of this research work and gives a brief introduction to machinery condition monitoring. The aims, objectives and organisation of thesis are also presented.

Chapter 2: To begin with, this chapter discusses the definition of non-stationary signals and the non-stationary process in machinery condition monitoring, then reviews the literature of the application of signal processing techniques in machinery condition monitoring, especially with regards to non-stationary signal processing methods.

Chapter 3: This chapter introduces the classic dynamic time warping method, its properties and its limitations. Based on the problems associated with classic dynamic time warping, the improvement of singularities and time complexity of dynamic time warping are studied. The effect of phase properties on the singularities of dynamic time warping is also discussed.

Chapter 4: This chapter concerns the use of dynamic time warping for analysing the motor electrical current signals for the fault diagnostics of a reciprocating compressor. Information about the compressor test facility is given including current transducer

specifications and the experimental setup. Taking into account the characteristics of the electrical current signal and the dynamic time warping method, phase estimation and compensation is proposed to improve the singularities of dynamic time warping for accurate fault feature extraction. Finally, the fault detection and classification results are discussed.

Chapter 5: This chapter studies the characteristics of the diesel engine vibro-acoustic signal based on the time domain statistics and the frequency domain spectrum analysis. Firstly, information regarding the diesel engine test rig is described including the test engine specifications and test rig functions. Secondly, the effects of room acoustics on the engine acoustic signals are analysed. Finally, the fuel monitoring of a diesel engine based on the engine noise analysis is also investigated and discussed.

Chapter 6: This chapter introduces the combustion process and combustion parameters variability based on the diesel engine test. The generation of the combustion produced by vibration and noise are also investigated through analysis of the characteristics of the diesel engine combustion process.

Chapter 7: This chapter employs the Wigner-Ville distribution (WVD) method to analyse the time-frequency characteristics of the engine's vibro-acoustic signals; the relationship between the combustion produced vibrations is also discussed, and noise is investigated using coherent power spectrum analysis. The combustion produced noise is extracted for the combustion process monitoring by applying a band-passed filter based on fractional Fourier transform (FRFT).

Chapter 8: This chapter describes the application of the time-frequency analysis techniques to engine noise study. The continuous wavelet transform is introduced and applied to the investigation of diesel engine noise for the combustion diagnostics. Firstly, time synchronous average (TSA) technique is employed to pre-process the engine noise for the enhancement of the signal-to-noise ratio (SNR). Next, the continuous wavelet transform with Morlet wavelet function is improved for the analysis of engine acoustic signals. Finally, the results obtained from the continuous

wavelet transform analysis are given for diesel engine combustion monitoring and fuel evaluation.

Chapter 9: This chapter summarises the results and conclusions drawn from this research. Furthermore, suggestions are also given for the future work in related research areas.

CHAPTER 2

NON-STATIONARY SIGNAL PROCESSING

This chapter reviews the definition of non-stationary signals and the signal processing techniques used in machinery condition monitoring, including time-domain analysis, frequency-domain analysis and time-frequency domain analysis. In particular, the signal processing methods used for non-stationary signal analysis, such as short-time Fourier transform, Wigner-Ville distribution, wavelet transform and fractional Fourier transform, are surveyed and discussed.

2.1 Introduction to signal processes

In machinery condition monitoring system, signal processing is the analysis and transforms action of data which has been collected from the monitored machines. There are various signal processing techniques and algorithms discussed for better understanding and interpretation of the collected data for machinery condition monitoring and fault diagnostics. The purpose of using signal processing methods in condition monitoring is to extract useful information for the assessment of the conditions of monitored machine.

The simplest way of signal processing is to examine the magnitude of the raw incoming signal as a function of time and considering it in the time domain analysis (see Section 2.1). This is, in fact, the basis of all visual inspection techniques and trend analysis. The processing in such cases consists of a comparison of the current record against the previous value with a predetermined threshold. This process is easy to implement, even when many hundreds of inputs are being monitored.

The magnitude detection in the time domain implies that machinery condition information is seeded in the changing of the signals obtained from the plant. The variation of the signals usually shows the changes of the conditions for the monitored machine. Variation of a signal in the time domain can be more salient expressed as components in the frequency domain. Therefore, frequency domain analysis is a common technique of signal processing applied in condition monitoring. Spectral analysis (see Section 2.4) is effective especially when applied to process the steady-state periodic signals, as is usually the case with monitoring machine faults that develop gradually [16].

For machinery condition monitoring, various kinds of factors, such as changes in the environment and the faults of the machine, leading to the measured signals of the operating machine contain non-stationary components [21], and generally, these non-stationary components contain information related to the faults of the machine. Non-stationary means the frequency components of the signals change over time and space. In mathematical, non-stationary signal presents as its statistical parameters vary with

time. It is therefore critical to process the non-stationary signals for fault diagnostics. Unfortunately, even though spectral analysis is the most widely used and well-established method for signal processing in machinery condition monitoring, it is unsuitable for non-stationary signal analysis and cannot reveal the inherent information found in non-stationary signals [21].

Various researchers have developed a number of signal processing techniques for non-stationary signal analysis. Time-frequency analysis (see Section 2.5) is the most popular method used for the analysis of non-stationary signals, such as short time Fourier transform (STFT) (see Section 2.5.1), Wigner-Ville distribution (WVD) (see Section 2.5.2) and wavelet transform (WT) (see Section 2.5.3). These techniques are able to provide the time-frequency representations for non-stationary signals and can be used to extract features related to the faults and conditions of the monitored machines for machinery condition monitoring.

In this chapter, the definitions of a non-stationary signal and a non-stationary process in machinery condition monitoring are discussed (see Section 2.2), and then the present available signal processing methods for machinery condition monitoring are reviewed based on the three main categories of data analysis: time-domain analysis (see Section 2.3), frequency-domain analysis (see Section 2.4) and time-frequency analysis (see Section 2.5).

2.2 Non-stationary processes

2.2.1 Definition of non-stationary signal

This section is to discuss the definitions of non-stationary signal and its properties in mathematics. Generally, a non-stationary signal is defined as a frequency component in which of the signal changes over time and space, such as in human speech where frequencies vary over time depending on the words being pronounced. In mathematics, the non-stationary signal can be defined based on the definition of the stationary signal. This means if the variation of the statistical parameters of one signal, such as mean and variance, not met the conditions of a stationary process, it can be considered a non-

stationary signal. The stationary signal can be defined as a signal whose statistical properties do not vary with time in mathematics [22]. On the contrary, processes whose statistical properties do change with time are referred to as non-stationary signals.

Strict-sense stationary:

Assuming that $\{x(t)\}$ is a random process or random signal, if its statistical properties are invariant by translation in time as:

$$p(x_1, \dots, x_n; t_1, \dots, t_n) = p(x_1, \dots, x_n; t_1 + \tau, \dots, t_n + \tau) \quad (2-1)$$

where p denotes the statistical probability of $\{x(t)\}$ and $\{x(t + \tau)\}$, x_n ($n = 1, 2, 3, \dots$) is the value of the random process at time t_n ($n = 1, 2, 3, \dots$), and τ is the time shift.

These random processes can be considered as strict-sense stationary for every moment they are invariant by temporal translation regardless of the time shift τ applied to them.

Wide-sense stationary:

A signal will be stationary if the statistical properties of the signal are objected to the following conditions [22]:

- (1) Its average value is constant:

$$\bar{x} = E[x(t)] = \text{constant} \quad (2-2)$$

- (2) Its autocorrelation function depends only on the time shift τ :

$$R_{xx}(t, t + \tau) = E(t + \tau) = R_{xx}(\tau) \quad (2-3)$$

where \bar{x} is the average value of the random process $\{x(t)\}$, $E(\cdot)$ is the expected value calculation, and R_{xx} is the autocorrelation function of $\{x(t)\}$.

The probability density of one signal should vary randomly when the signal is not stationary. Otherwise, there is a special kind of non-stationary signal which can be referred to as a cyclostationary signal, whose statistical properties are periodic. Hence, each cycle of this signal can be regarded as the realization of the same random process.

The cyclostationary signal can also be classified into strict-sense and wide-sense cyclostationary signals based on the mathematic theory.

Strict-sense cyclostationary:

If the probability density is a periodic of T as in equation (2-4), a random signal $\{x(t)\}$ can be considered as strict-sense cyclostationary signal with the periodic of T .

$$p(x_1, \dots, x_n; t_1, \dots, t_n) = p(x_1, \dots, x_n; t_1 + T, \dots, t_n + T) \quad (2-4)$$

where p denotes the statistical probability of $\{x(t)\}$, $x_n (n = 1, 2, 3, \dots)$ is the value of the signal at time $t_n (n = 1, 2, 3, \dots)$, and T is the periodic of the probability density.

Wide-sense cyclostationary:

A random process is classified as wide-sense cyclostationary if its autocorrelation function is a periodic function [23] with the periodic of T for all t and τ :

$$R_{xx}(t, \tau) = E\{x(t - \tau/2)x^*(t + \tau/2)\} = R_{xx}(t + T, \tau) \quad (2-5)$$

where $x^*(t)$ is the complex conjugate of $x(t)$. $E(\cdot)$ is the expected value calculation, and R_{xx} is the autocorrelation function of $\{x(t)\}$, τ is the time shift.

It can be seen that most of the measured signals in machinery condition monitoring can be considered as non-stationary signal since their characteristics of statistical parameters are not conform to that of stationary signal.

2.2.2 Non-stationary processes in machinery condition monitoring

According to the definition of non-stationary signal, it is very common that strong non-stationary components are presented in the measured signals in the field of machinery condition monitoring and damage assessment. This is because of the changes of the experimental environment and because of the faults in the monitored machine itself. If based on the strict definition of a stationary signal, almost all the measured signals in machinery condition monitoring can be classified into non-stationary signals. Some of

the data should be considered as weak non-stationary or cyclostationary signals based on the definition of wide-sense stationary signal and cyclostationary signal.

Generally, the non-stationary process is very common when a machine operates under different conditions. For example, the transient signals generated during machine start-up, shutdown or the changing of direction can provide information about machine conditions which cannot be revealed from stationary signals. In addition, when the experimental environment changes and if faults occur during the machine's operation, the non-stationary process is produced and results in non-stationary signals in the collected data. These non-stationary components contain critical information for machine condition monitoring and fault detection as a result of its mechanism.

Signals, such as vibration, acoustic, electrical current and so on, collected from the machine during its operation are all combined with non-stationary components which contain useful information related to the conditions and faults of the machine. This cannot be identified through analysis of the signals by stationary signal processing techniques. Individually, vibration and acoustic signals can be considered as strong non-stationary signals since strong transient signals are also included when the operating conditions and the experimental environment are changed. As well as this, when some faults occur, non-stationary or transient signals will contribute to the measured vibration and acoustic signals. Electrical current signal contains nonlinear components because of the corresponding electromagnetic force produced by the nonlinear interaction of the linkage flux of the motor [24]. The current signal presents non-stationary behaviour related to the machine operating process and the electrical phase fluctuation. Based on the definition of wide-sense cyclostationary signals and the characteristics of electrical current signals (see Section 4.3), this non-stationary behaviour can be considered as a cyclostationary process [25]. According to the non-stationary process in machinery condition monitoring, non-stationary signal processing techniques need to be studied and developed in order to obtain more accurate analysis results.

2.3 Time domain analysis

Time domain analysis is based on the time series by plotting its amplitude against time. In time-domain analysis, the characteristic features of signals, such as mean, peak, peak-to-peak interval, standard deviation, crest factor, root mean square (RMS), skewness, kurtosis, are calculated and used to describe the statistics of signals. These features are usually called time-domain features or statistical parameters. A widely used time-domain analysis approach is time synchronous average (TSA) [26] (see Section 8.3). The objective of time synchronous average is to use the ensemble average of the raw signal to remove or reduce noise and effects from other sources, so as to enhance the signal components of interest. Time synchronous average is based on the knowledge of the revolution period of rotating part of a machine, if the revolution specifications obtained, the time synchronous average can be used to highlight the signal-to-noise ratio of either stationary or non-stationary signals, for accurate analysis results obtained based on the time domain.

Another useful method of time-domain analysis is dynamic time warping (see Section 3.2) which is an algorithm for aligning two time series which are similar, but out of synchronization and generally of differing lengths [27]. The two raw signals can be compared directly in the time domain after they are pre-processed by the dynamic time warping to get accurate detection results. The underlying principle behind dynamic time warping is to stretch or compress two time series locally in order to make one resemble the other as much as possible. Dynamic time warping is a widely used method and has been applied in many areas, such as word recognition [28], speed recognition [29] and online signature matching [30]. Therefore, dynamic time warping has the ability to process the non-stationary or nonlinear data for non-stationary components analysis in the time domain, especially for amplitude modulation signal analysis.

Empirical mode decomposition (EMD) is also an effective method used for signal processing in the time domain, especially for the non-stationary or nonlinear data analysis [31]. Empirical mode decomposition will break down a signal into its intrinsic

mode functions (IMFs). The intrinsic mode functions are defined as a class of functions which can be used to indicate the local properties of the analytical non-stationary signals [31]. As the frequency of non-stationary or nonlinear data changes over time, the signal may involve more than one oscillatory mode. The empirical mode decomposition can decompose the signal into IMF components. An IMF satisfies two basic conditions [31]:

- (1) The number of extreme and the number of zero crossings must equal or differ at most by one in the whole data set.
- (2) The mean value of the envelope defined by the local maxima and the local minima is zero at any point.

Based on the properties of the intrinsic mode functions, the intrinsic mode functions of a signal can be decomposed by a sifting process. For further details of the algorithmic implementation one should refer to [31] in the references. Empirical mode decomposition can be used to decompose a signal into a finite sum of intrinsic mode functions based on the energy associated with various intrinsic time scales. It means empirical mode decomposition can decompose a signal into components adaptively, and each component has meaningful instantaneous frequency, different components correspond to different frequency scales. The intrinsic mode functions obtained from empirical mode decomposition provide physical insights which are crucial in engineering applications [32]. Therefore, empirical mode decomposition is particularly suitable for processing nonlinear and non-stationary signals.

There are many other time-domain analysis techniques used to analyse waveform data for machinery fault diagnostics. Jardine and Lin [1] review the time domain analysis methods used for data analysis in condition monitoring, such as pseudo-phase portrait, singular spectrum analysis, principal component analysis (PCA), and time series models including the autoregressive model (AR) and the autoregressive moving average (ARMA) model. These are used for time series modelling, feature extraction, and fault diagnostics in condition monitoring areas. Jardine and Lin pointed out that *“the application of autoregressive model or autoregressive moving average models is*

difficult due to the complexity in the modelling, especially in the need to determine order in the model.”

The advantage of time-domain analysis is that the indication of the conditions and faulty information of the monitored objects is based on the variation of the statistical parameters. The features of the measured signals are presented by the statistical parameters, such as root mean square (RMS), Kurtosis, standard deviation etc. Time-domain analysis is therefore easy to implement in an online condition monitoring system as all the statistical parameters are based on single value representation. Time-domain analysis can also avoid the shortcoming of frequency-domain analysis including aliasing, spectral leakage, sampling determination and picket-fence effect, as caused by Fourier transform (FT). If the sampling frequency of recording a signal is higher than two times of the highest frequency component of the recorded signal, Fourier transform can identify all the frequency components of the signal, but the picket-fence effect is still exist.

2.4 Spectral analysis

Frequency domain analysis gives spectral information of signals and is often used for data analysis. It is realized by transforming the signals from the time domain into the frequency domain. The advantage of frequency-domain analysis over time-domain analysis is its ability to easily identify and isolate certain frequency components of interest. The most widely used conventional analysis is spectrum analysis by means of fast Fourier transform (FFT) [1]. The main principle of spectral analysis is either to look at the spectrum in its entirety, or to simply look closely at certain frequency components of interest and then extract features from the signal. The most commonly used tool in spectrum analysis is the power spectrum. Some useful tools for spectrum analysis are graphical presentation of the spectrum, frequency filters, envelope analysis [33] and side band structure analysis [34].

Various useful spectra for processing signal have been introduced with their own advantages. Cepstrum can be used to detect harmonics and side band patterns in the power spectrum [1]. Power cepstrum is most popular. It is defined as the inverse

Fourier transform of the logarithmic power spectrum [1]. High-order spectra, such as bi-spectrum and tri-spectrum, can provide more diagnostic information than the power spectrum for non-Gaussian signals [1]. The bi-spectrum can be considered as a decomposition of the third moment of a signal over frequency and proves useful for analysing systems with asymmetric non-linear, while the tri-spectrum represents a decomposition of kurtosis over frequency [35]. Bi-spectrum analysis has been widely used in machinery diagnostics for various mechanical systems such as gears, bearings[35], rotating machines [36] and induction machines [24]. Jardine and Lin [1] reviewed the wide use of the frequency-domain analysis in machinery condition monitoring and fault diagnostics for various mechanical systems, including the application of the bi-spectrum diagonal slice to gear fault diagnostics, the use of both the bi-spectrum diagonal slice and the normalized bi-spectrum diagonal slice for bearing fault diagnostics, and the application of both the bi-spectrum and tri-spectrum to bearing fault diagnostics.

Although the application of frequency-domain analysis is popular in various areas, its limitations, caused by Fourier transform [75-78], such as aliasing, spectral leakage and picket-fence, affect its application in practice. Aliasing happens when the frequency sampling is less than twice of the highest frequency component in the signal. Aliasing causes frequency components that are higher than half of the sampling frequency to overlap with the lower frequency components. Spectral leakage is the result of the assumption in Fourier transform. The assumption of Fourier transform is that the time record for Fourier transform is exactly repeated of the signal intervals. This assumption is not established in practice. Picket-fence affects the frequency components identified by Fourier transform since it can only produce spectral analysis results in discrete frequencies. The latter two limitations, spectral leakage and picket-fence, often lead to significant errors in spectrum estimation as the weak signature related to faults in signals cannot be resolved properly for accurate fault detection and diagnostics.

2.5 Time-frequency domain analysis

The emphasis of this research focuses on the analysis of non-stationary signals for machinery condition monitoring. Hence a number of the main signal processing techniques relating to the non-stationary signal analysis are discussed. Time-frequency distribution is commonly used in conventional time-frequency analysis, which represents the energy or power of signals in two-dimensional functions of both time and frequency in order to better reveal fault patterns for more accurate diagnostics. The classical time-frequency distribution, such as short-time Fourier transforms (STFT) or spectrograms, and Wigner-Ville distribution (WVD) [28–31] are widely used for non-stationary signal analysis.

2.5.1 Spectrograms

The idea of short-time Fourier transforms is to divide an entire signal into segments with a short-time window and then to apply Fourier transform to each segment. The time-frequency distribution can be obtained by successively sliding the window along the time axis of the signal. It assumes the data to be piecewise stationary because it is applied based on the traditional Fourier spectral analysis. This assumption is not always justified in non-stationary data. It is difficult to ensure that the window size adopted always coincides with the stationary time scales. Spectrograms have some limitation in time-frequency resolution due to signal segmentation [21]. The window width must be narrow in order to localize an event in time. On the other hand, the frequency resolution requires a longer time series. This means that short-time Fourier transforms has a constant resolution for all frequencies since the same length of window is used for the analysis of the entire signal. Therefore, a good frequency resolution using a wide window for the analysis of low-frequency components, and a good time resolution using narrow window for the analysis of high-frequency components, cannot be obtained based on the short-time Fourier transforms analysis. In addition, it cannot constitute orthogonal bases during the translation of the window function in short-time Fourier transforms, so it is difficult to find a fast and effective algorithm to calculate short-time Fourier transforms because there are no orthogonal bases for short-time Fourier transforms [21]. These requirements limit the application

of spectrograms as they can only be applied to non-stationary signals with a slow change in their dynamics.

2.5.2 Wigner-Ville distribution

Wigner-Ville distribution does not have the time-frequency resolution limitations of spectrograms since it is not based on signal segmentation [21]. Wu and Chiang [37] employed Wigner-Ville distribution to analyse the non-stationary sound emission signals combined with the probability neural network for an internal combustion engine fault diagnosis. Their results showed *“the network can achieve a high recognition rate with feature extraction using the Wigner-Ville distribution method”*. Staszewski, Worden and Tomlinson [39] studied the application of the Wigner-Ville distribution in gearbox condition monitoring by analysing the gearbox vibration signals. Based on the data analysis, they concluded that *“the Wigner-Ville distribution is capable of detecting local tooth faults in spur gears, and the progression of a fault can be monitored by observing changes in features of the distribution”*. Albarbar, Gu, and Ball [41] studied the non-stationary acoustic signals of a diesel engine using Wigner-Ville distribution for fuel injection process characteristics analysis. Based on the simulation and experiment analysis, they concluded that *“through the use of joint time-frequency domain representation, Wigner-Ville distribution allows the dominating combustion frequency band in the engine acoustic signal to be defined”*. In this research work, the Wigner-Ville distribution is employed to analyse the time-frequency distribution of the engine acoustics for feature extraction to diagnose the engine combustion process and to monitor the engine conditions (see Section 7.3).

The disadvantage of Wigner-Ville distribution is the interference terms formed by the transformation itself [21]. These results from the distribution indicate that cross-terms of the input components exist in the output, this makes interpretation of the estimated distribution difficult [42]. Peng and Chu [21] pointed out the shortcomings of the Wigner-Ville distribution: *“even though the Wigner-Ville distribution can support a good concentration in the time-frequency plane, the interference terms of Wigner-Ville distribution will give the wrong impression about the signal analysis”*. Gu and Ball [43]

investigated a smoothed version of the Wigner-Ville distribution for overcoming the interference terms of the Wigner-Ville distribution in the analysis of typical vibration symptoms. They concluded that *“the smoothing is shown to reduce the presence of interference components, and also enhances the representation of noise-contaminated data”*.

2.5.3 Wavelet transform

Another transform widely used for time-frequency analysis is the wavelet transform (WT). Different from a time-frequency distribution, wavelet transform is a time-scale representation of a signal. Wavelet transform is described as a good solution in the time-frequency domain so that it can extract more information in the time domain at different frequency bands. Wavelet transform has become well known as a useful tool for various signal processing applications in the past decade [44]. Wavelet analysis of a raw signal expresses the signal in a series of oscillatory functions with different frequencies at different time by dilations via the scale parameter and translations via the time parameter. The main advantage of wavelet transform is its ability to produce a high frequency resolution at low frequencies and a high time resolution at high frequencies for signals with long duration low frequencies and short duration high frequencies. Therefore, wavelet transform is very useful in analysing data with gradual frequency changes.

Wavelet transform (see Section 8.2) has been successfully applied to data analysis in machinery fault diagnostics such as gears [45][21], bearings [46] and other mechanical systems [37]. Baydar and Ball [47] applied wavelet transform to analyse the acoustic and vibration signals to examine the ability of the acoustic signal in the detection local faults in gearboxes, the analysis results using wavelet transform suggested that *“acoustic signals are effective for the early detection of faults and may provide powerful tool to indicate the various types of progressing faults in gearboxes”*. Rubini and Meneghetti [46] developed a signal processing method based on the evaluation of wavelet transform for fatigue fault detection in rolling bearings. They compared the results with those obtained by spectral and envelope analysis to investigate the effects

of fault evolution. Many other applications of wavelet transform have been carried out on the condition monitoring and fault diagnostics in rotor systems, structures and crack detection, etc. Peng and Chu [21] reviewed machine condition monitoring and fault diagnostics using wavelets. They presented a summary of the application of wavelet transform in machine fault diagnostics in the aspects of the time-frequency analysis, the feature extraction, and the de-noising and extraction of the weak signals.

The basic wavelet transform does have some drawbacks [31]. Firstly, the leakage generated by the limited length of the wavelet function leads to difficulties in the quantitative definition of the energy-frequency-time distribution. This also makes the interpretation of the wavelet counterintuitive. For instance, wavelet transform should look for the result in the high frequency range to define a change occurring locally, but for the higher the frequency, the basic wavelet will be more localized. If a local event occurs only in the low frequency range, it will still be forced to check its effects in the high frequency range. Secondly, the non-adaptive nature of wavelet analysis will affect its analysis results, meaning that once the wavelet function is selected, it must be used to analyse all the data. The performance of the wavelet analysis mainly relies on the selection of wavelet functions [31]. Different wavelet functions result in different analysis results and the choice of an appropriate wavelet function depends on the signal itself and the purpose of the analysis. In most cases, the characteristics of the analysed signal changes over time, if a determined wavelet function is used to analyse the entire signal, some features of the analysed signal cannot be extracted accurately.

In spite of these problems, wavelet transform is still currently the best available non-stationary signal analysis method. In our research work, the wavelet analysis is also employed to analyse the characteristics of the engine acoustic and vibration signals for condition monitoring of the diesel engine (see Section 8.2 and 8.4).

2.5.4 Fractional Fourier transform

The fractional Fourier transform was first introduced as a way to solve certain classes of ordinary and partial differential equations arising in quantum mechanics by Namias in 1980 [48]. They defined “*the fractional Fourier transform based on an operational*

calculus and this can be considered as the optical version of the fractional Fourier transform". The fractional Fourier transform was then used to process the optical signal in 1993 [49] as it was easily realized with some optical instruments. Since then the fractional Fourier transform has many applications in optics. Recently, a number of researchers studied the application of the fractional Fourier transform on signal processing, especially for the processing of non-stationary signals [50].

The fractional Fourier transform (see Section 7.4) is a generalization of the classical Fourier transform and can be considered as the chirp-basis expansion from its definition [50]. The fractional Fourier transform will be defined mathematically in section 7.4. Otherwise, it can be interpreted as a rotation in the time-frequency plane. The fractional Fourier transform can reveal the characteristics of the signal changing from the time domain to the frequency domain with the order increasing from 0 to 1. The rotation property of the fractional Fourier transform shows the direct relationship between the fractional Fourier transform and the time-frequency distribution, and indicates that the fractional Fourier transform domain can be interpreted as a uniform time-frequency domain. This offers the advantage of the fractional Fourier transform, which can be applied in processing a non-stationary signal. Compared with Fourier transform, the fractional Fourier transform is more flexible and suitable for processing non-stationary signals since it processes the signals in the unified time-frequency domain.

Along with the development of the fast algorithm of the discrete fractional Fourier transform, there are many applications of the fractional Fourier transform in signal processing. Tao, Deng and Wang [50] reviewed the applications of the fractional Fourier transform in signal processing. In signal detection and parameter estimation, the fractional Fourier transform was used to detect and estimate the parameters of multi-component linear frequency modulation signals [51]. In phase retrieval and signal reconstruction, a complex signal can be completely reconstructed through phase retrieval from the magnitudes of its fractional Fourier transform. The fractional Fourier transform was also used for filters designed in the fractional Fourier transform domain, neural networks and sound analysis.

Other than those previously mentioned, there are also many other methods which can be used to process non-stationary signals, such as the evolutionary spectrum, the empirical orthogonal function expansion (EOF), Gabor transform, cyclic statistics, AM/FM signal analysis and so on [31], will not be discussed any further in this research.

In this research, one of the time-domain analysis methods to which dynamic time warping (see Chapter 3) is employed in order to process the electrical motor current signal based on entirely time domain for a two-stage coprocessor fault diagnostic (see Chapter 4). In the following chapters, three of the time-frequency domain analysis methods: Wigner-Ville distribution (see Section 7.3), wavelet transform (see Section 8.2) and the fractional Fourier transform (see Section 7.4) are investigated to process the engine vibration and acoustic signals for engine condition monitoring and combustion diagnostics.

CHAPTER 3

DYNAMIC TIME WARPING

This chapter gives a brief description of classical dynamic time warping and its limitations in application, such as singularity and computational complexity. The improvement of the singularities and the computational complexity is studied based on the definition of classical dynamic time warping. In addition, the effect of the phase properties of two time series on the singularities of the classical dynamic time warping is analysed for the improvement of the singularities with classical dynamic time warping. Novel phase compensation is then proposed and is demonstrated to have the ability of reducing the effect of singularities on maintaining the minimal value of the dissimilarity between the two time series with different phase shifts through simulation studies. The analysis results show that the proposed phase estimation and compensation method can improve the singularities of dynamic time warping effectively.

3.1 Introduction to dynamic time warping

In practice, such as speech recognition [30], signature matching [29] and condition monitoring [52], a common task with time series data is comparing one sequence with another in order to detect the differences between them for further analysis. It is often the case that two signals in the time domain have similar overall component shapes [53], but are out of synchronization and generally not of exactly the same length as shown in Figure 3-1(a). In order to find the exact dissimilarity between such two signals and as a pre-processing step before comparing them, it is necessary to match the two signals in to achieve an appropriate alignment.

Dynamic time warping (DTW) is an algorithm which can be used for efficiently aligning two time series which are out of synchronization and which do not have the same length. The underlying principle behind dynamic time warping is to stretch or compress two time series locally in order to make one resemble the other as much as possible. The distance between them is computed, after stretching, by summing the distances of the individual aligned elements as seen in Figure 3-2. Figure 3-1(b) shows the alignment of the two time series processed by dynamic time warping. It can be seen that the two signals are matched with each other after the dynamic time warping processing meaning that the comparison can then be carried out.

Dynamic time warping is a popular algorithm which is applied in many areas. Bellman and Kalaba [54] first introduced it for adaptive control processes. Dynamic time warping was popularised in the 1970s, when it was mainly applied to isolated word recognition and speech recognition [29][28] to account for differences in speaking rates between speakers and utterances. Since then, dynamic time warping has been employed for clustering and classification in countless domains including: electrocardiogram analysis [55–57], the clustering of gene expression profiles[58][59], biometrics [60][61] and process monitoring [62]. Dynamic time warping has also been used in handwriting and online signature matching [30], sign language recognition and gesture recognition, data mining and time series clustering, computer vision and animation, surveillance, protein sequence alignment and chemical engineering, music

and signal processing [63]. Recently, Zhen D. *et al* [52][64] explored the use of dynamic time warping in processing the electrical current signal from motors for condition monitoring and the research revealed promising results in that signals aligned by dynamic time warping do not lose information and therefore can be used for fault diagnosis. Dynamic time warping can be developed to suppress the supply frequency component and highlight the sideband components.

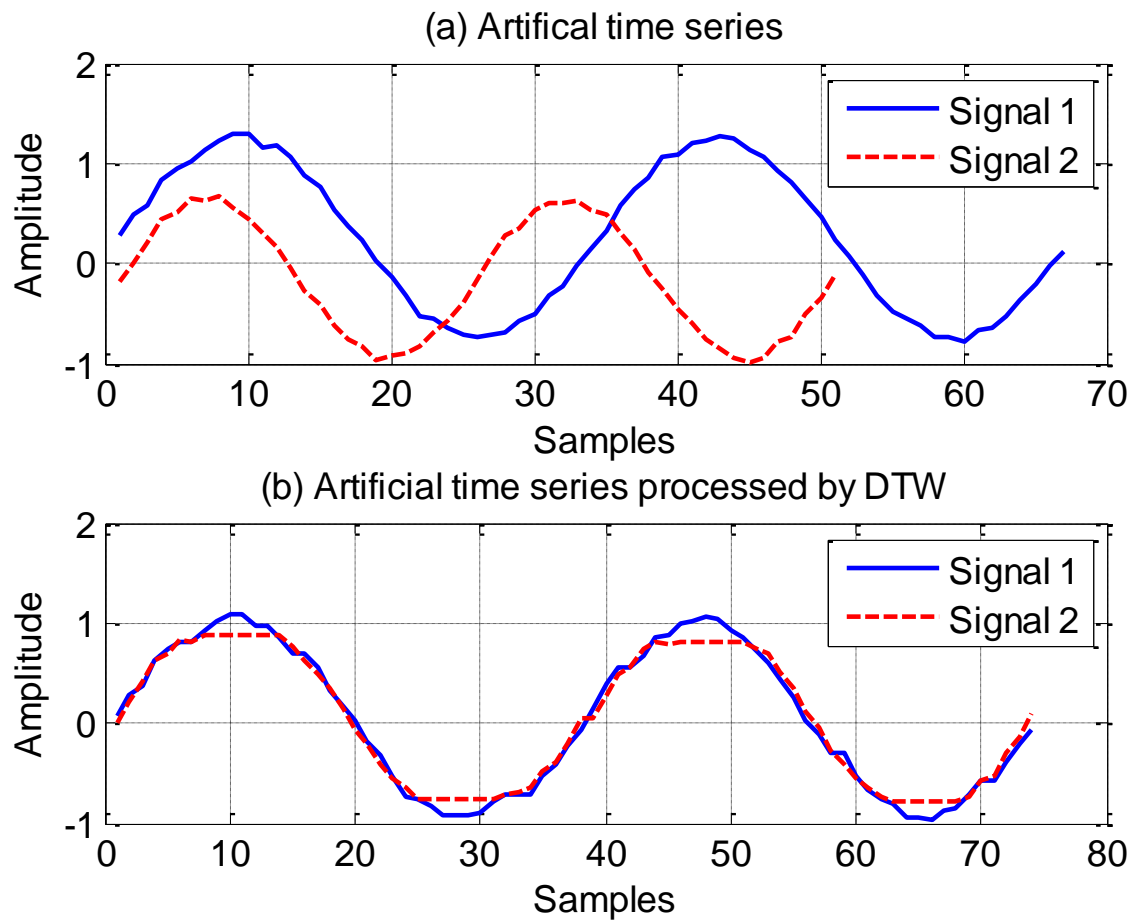


Figure 3-1 Time series aligned by DTW

3.2 Classical dynamic time warping

3.2.1 The definition

Given two time series of lengths N and M respectively

$$X = (x_1, x_2, \dots, x_N) \quad (3-1)$$

$$Y = (y_1, y_2, \dots, y_M) \quad (3-2)$$

where x_i ($i = 1, 2, \dots, N$) and y_j ($j = 1, 2, \dots, M$) are represented by the sequences of values at the points i and j in the time series X and Y , respectively.

To align the two time series for comparison, firstly a $N \times M$ distance matrix D is built. The element of the matrix $d(i, j)$ is the distance between the two points x_i and y_j which is represented by d_{ij} . Typically, the Euclidean distance is used to calculate the point-to-point distance by,

$$d_{ij} = \sqrt{x_i^2 - y_j^2} \quad (3-3)$$

Once the distance matrix has been built, the dynamic time warping algorithm is used to find the alignment path which runs through the matrix elements defining a mapping between the time series X and Y . The alignment path found by dynamic time warping is a warping path function which can be defined as W [63]. The warping path function found by dynamic time warping must conform to the certain conditions in section 3.2.2.

$$W = (w_1, w_2, \dots, w_K) \text{ With } w_k = (n_k, m_k) \quad (3-4)$$

where:

$$n_k = 1, 2, \dots, N; m_k = 1, 2, \dots, M; \text{ and } k = 1, 2, \dots, K;$$

3.2.2 Properties

The dynamic time warping algorithm needs to be applied under certain conditions [53][63]:

1. Boundary condition: $w_1 = (1, 1)$, and $w_K = (N, M)$. The starting and ending points of the warping path must be the first and the last points of the aligned time series.

2. Monotonicity condition: Given $w_k = (n_k, m_k)$ then $w_{k-1} = (n_{k-1}, m_{k-1})$, where $n_k - n_{k-1} \geq 0$ and $m_k - m_{k-1} \geq 0$. This ensures the points in W to be monotonically spaced in time.
3. Step size condition: Given $w_k = (n_k, m_k)$ then $w_{k-1} = (n_{k-1}, m_{k-1})$, where $n_k - n_{k-1} \leq 1$ and $m_k - m_{k-1} \leq 1$. The basic step size condition formulated as $w_k - w_{k-1} \in \{(1,1), (1,0), (0,1)\}$. This criterion limits the warping path from long jumps whilst aligning sequences, and restricts the allowable steps in the warping path to adjacent cells.

Noting that there are a large number of possible monotonically aligned paths increasing from (1,1) to (N, M) according to the three certain conditions. A dynamic programming algorithm is introduced to test the length of all possible distortion paths and to determine the shortest one. The dynamic programming algorithm will calculate all cumulated distances between the two time series based on the possible aligned paths found by dynamic time warping, and then extract the shortest warping path which produces the minimum cumulated distance.

The dynamic programming employs the cumulated distance $d_w(X, Y)$ between X and Y for a given warping path w , $d_w(X, Y)$ is the sum of the point-to-point distances d_{ij} along the warping path w .

$$d_w(X, Y) = \sum_{(i,j) \in w} d_{i,j} \quad (3-5)$$

Noting that $w \in W = (w_1, w_2, \dots, w_K)$ is the set of all possible warping paths. The goal of dynamic programming is to determine an optimal warping path $d^*(X, Y)$ for which the cumulated distance between X and Y is minimal.

$$d^*(X, Y) = \min_{w \in W} d_w(X, Y) \quad (3-6)$$

3.2.3 Warping path

The optimal warping path is selected based on a cumulated matrix. Figure 3-2 is an example of an optimal warping path which is selected based on a cumulated matrix for

the two signals alignment. Assuming that the cumulative distance matrix is $C = (c_{ij})$, the c_{ij} are the elements of the cumulative distance matrix C , defined as follows [63]:

1. First row: $c_{1j} = \sum_{k=1}^j d_{1k}, j \in [1: M]$.
2. First column: $c_{i1} = \sum_{k=1}^i d_{k1}, i \in [1: N]$.
3. All other elements:

$$c_{ij} = d_{ij} + \min\{c_{i-1,j-1}, c_{i-1,j}, c_{i,j-1}\}, i \in [1: N], j \in [1: M] \quad (3-7)$$

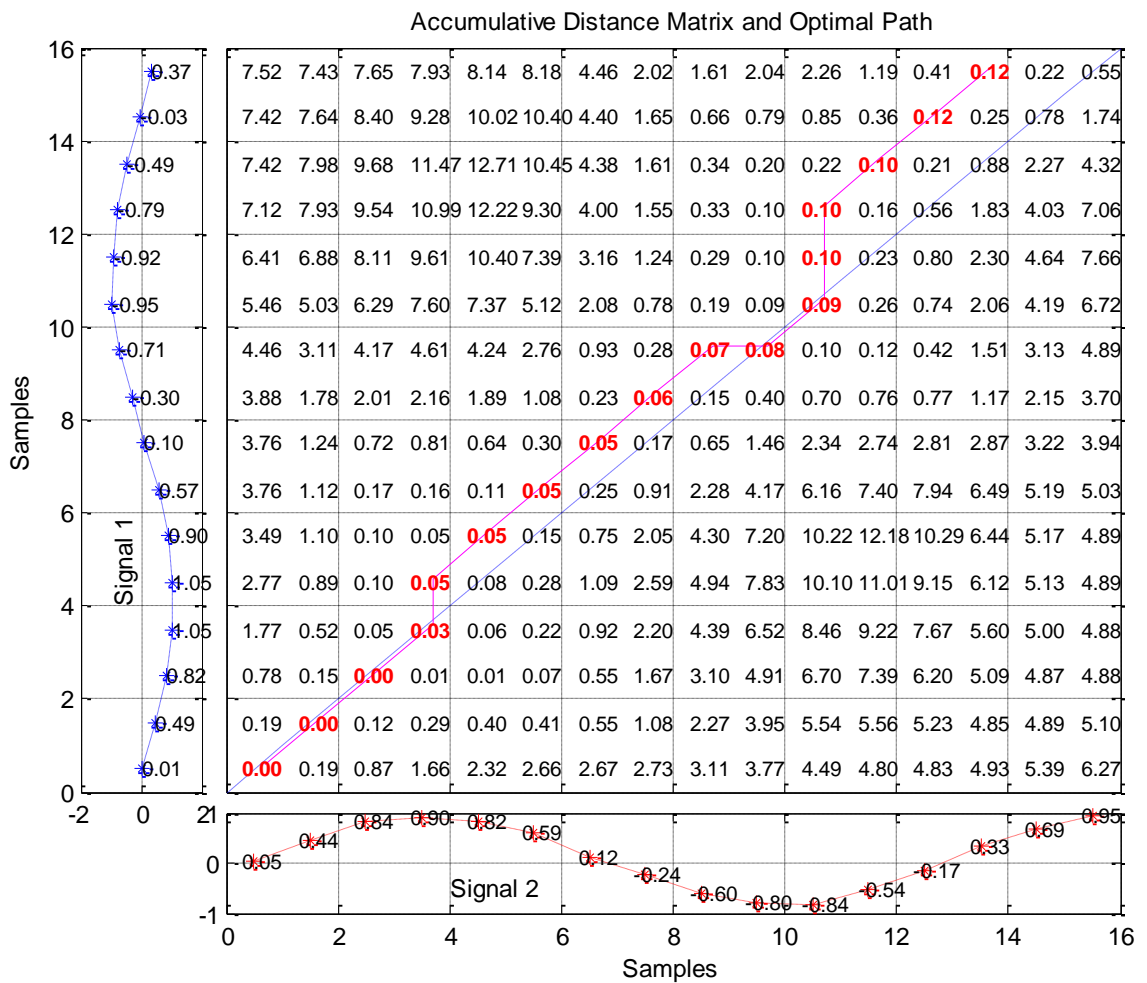


Figure 3-2 Optimal warping path selected by dynamic programming

Once the cumulative distance matrix is built, the alignment warping path can be found from the point (1,1) to (N,M) according to the Equation (3-7). According to the two aligned time series, the cumulated distance matrix has $N \times M$ entries. Therefore, the

computational complexity of the classic dynamic time warping algorithm should be $O(NM)$ [65].

3.3 Dynamic time warping limitations

Although dynamic time warping has been widely used successfully in many areas, the singularity effect and calculation time are the main limitations in its application. The singularity will affect the accuracy of the dissimilarity detection, and computational complex will limit the on-line application of algorithm since the processing capability of electronic device in some case.

3.3.1 Definition of singularity

Dynamic time warping is an effective algorithm for measuring dissimilarity between time series and has been widely used in various applications. Dynamic time warping warps the X-axis based on the variation of values in the Y-axis and the difference between the two points from the two time series is minimal in terms of values. This value comparison means that the dynamic time warping ignores the trend of the points for local accelerations and decelerations in the whole time series. This means that, dynamic time warping only considers the Y-axis value of a data point, but does not consider its local and global features. Therefore, when a single point on the one time series maps onto a large subsection of another time series, an undesirable alignment will take place during the processing of dynamic time warping, it will lead to worse dissimilarity detection. *“This undesirable alignment is called ‘singularity’”* as proposed by Eamonn and Michael [53], and can lead to inaccurate alignments. Figure 3-3 illustrates typical singularities located at samples of 8, 20, 32 and 45 in signal 2 where one point on signal 2 maps onto numerous points on signal 1.

Dynamic time warping may fail to align a pair of sequences on their common trends or patterns due to singularity effects, especially when singularities appear at the ends of the aligned time series, as seen in the sample of 68 shown in Figure 3-3 in which signal 1 is aligned to a number of different points at the end of signal 2.

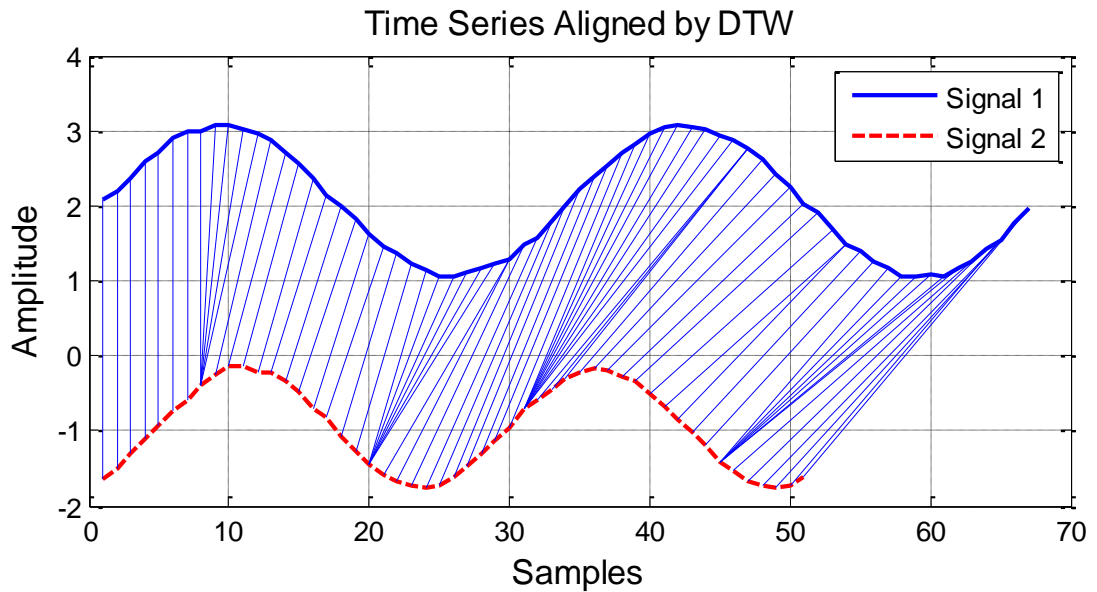


Figure 3-3 Examples of singularities in DTW application

Figure 3-4 gives a typical example of singularities located at the ends of the aligned time series during the dynamic time warping procedure. In Figure 3-4(a), signal 1 is an amplitude modulated signal whilst signal 2 is a pure sinusoidal signal. The frequency of the carrier signal of signal 1 is the same as that of signal 2, but the signals have different initial phase and amplitude. The simple sinusoid signals with different initial phase and amplitude are used in this simulation study. Its aim is to investigate the effect of initial phase and amplitude on the singularity of dynamic time warping. The two signals are aligned by dynamic time warping and the point alignments are shown in Figure 3-4(b), indicating the singularities during the dynamic time warping processing, especially at the ends of the signals. From Figure 3-4(c), it can be seen that the alignment is poor at the start and end of the aligned time series, which can lead to inaccurate dissimilarity estimation. The residual signal which results from comparing the two time series is shown in Figure 3-4(d). It is clear that the residual signal is unreliable due to the data jump at the ends caused by singularities during the dynamic time warping procedure. The singularities located at the ends may be due to the phase shift based on analysing the dynamic time warping processing as is shown in Figure 3-4 since the main difference of the two signals at their endings are their initial phases.

The singularities located at the peak points are because of the different amplitude of the two signals.

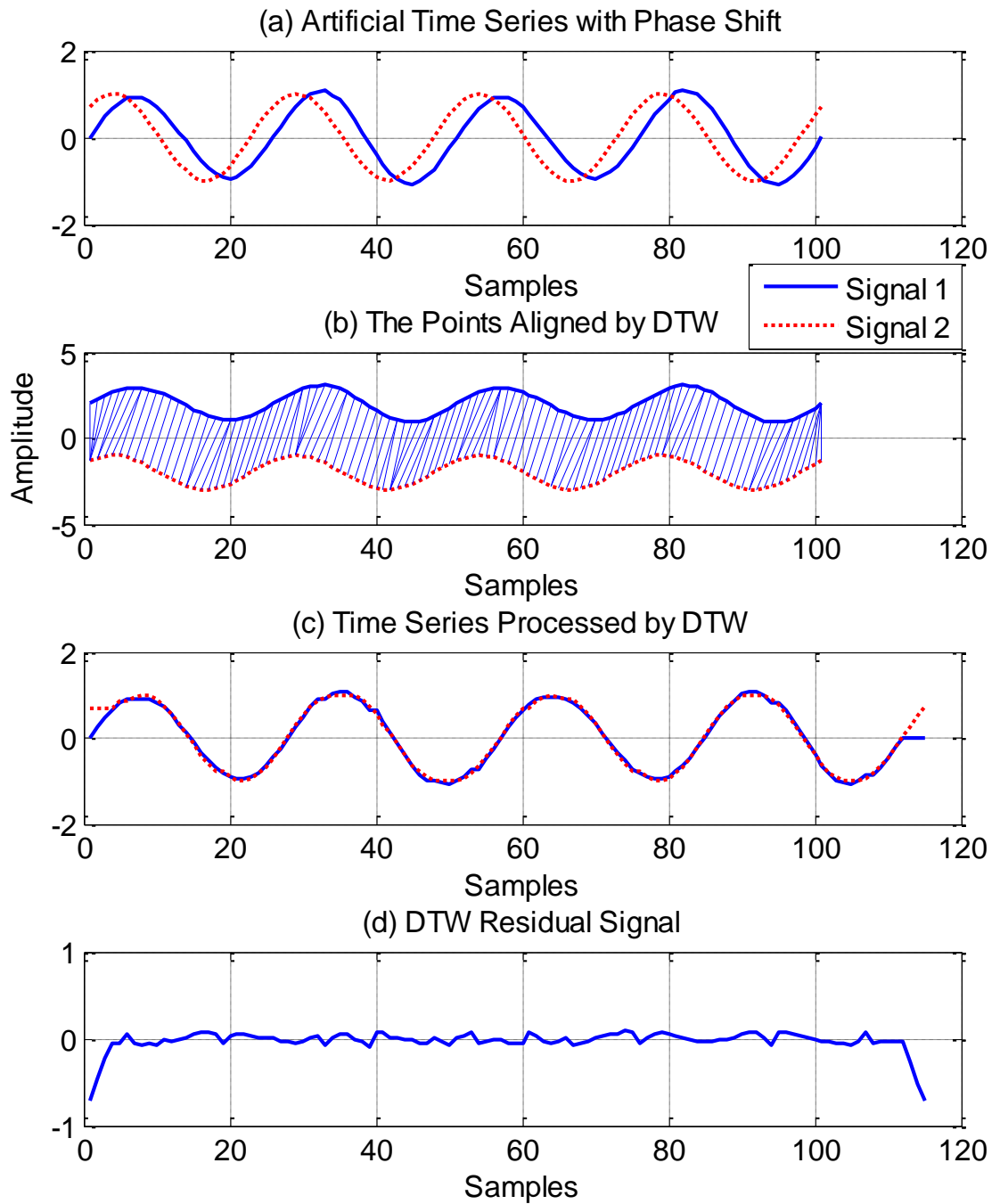


Figure 3-4 Singularities located at the ends

3.3.2 Computational complexity

In dynamic time warping application, assuming the lengths of the two time series are N and M respectively, the cumulated distance matrix will have $N \times M$ entries, therefore, the computational complexity of the dynamic time warping will be $O(NM)$ [65][66]. It means the amount of time taken by the algorithm to run is $N \times M$, indicating the algorithm needs to run $N \times M$ times. This is especially problematic for embedded systems which have limited resources.

3.4 Dynamic time warping improvements

Based on the limitations of classical dynamic time warping, various improvements have been proposed to improve classical dynamic time warping in order to enhance the accuracy of dynamic time warping alignment. Derivative dynamic time warping (DDTW) [53] is an effective method for this improvement as it has the ability of not only considering the Y-axis of the data points, but also considering the higher level features of local features. Derivative dynamic time warping estimates the first derivative of the aligned time series and replaces the value of each data point with its estimated first derivative. This can be considered as a local feature of the data point which expresses the relationship with the two adjacent neighbours. The estimation of the first derivative of a data point is the average of the data point as well as its left and right neighbour points. The first and last data points of a series cannot have its left or right neighbour points, so the derivation dynamic time warping is started from the second point of a series, and ended at the second last point. The derivative of a data point in a time series not only considering the Y-axis value of the point, but also taking into account of its local vary trend, which is better than only considering the Y-axis value of the point by calculating is Euclidean distance. It is more robust to estimate the dissimilarities than considering only two data points for the comparison. Derivative dynamic time warping considers the square of the difference of the estimated derivatives as the point-to-point distance instead of using the Euclidean distance which is used in the classical dynamic time warping.

Global features, which are the overall shapes or significant features that take place in the whole time series, may be unable to follow derivative dynamic time warping. With the purpose of capturing trends or local and global features of a time series during the alignment process, feature based dynamic time warping (FBDTW) [67] is developed to align two time series based on the local and global features of each data point and the singularities can be improved. A number of other methods have also been proposed to improve the singularities, such as windowing [29], slope weighting [29][30], and step patterns [30][68]. These methods may all moderate the effects of singularities not located at the beginning or start of the series, but the improvement is limited when the singularities occur at the start or the end of the aligned time series, leading to which larger distortion and causing inaccurate alignment.

3.4.1 Singularity improvement

The singularities allow a single point on one time series to align to a large subsection of another time series. This occurs when the algorithm tries to explain variability in the Y-axis by warping the X-axis as shown in Figure 3-3. The generation of the singularity is that the distance between two points is only consider their Y-axis values, but ignores the decreasing and increasing trends of the points in the time series. Each point of a time series not only has the property of value, but also with the properties of variation trend based on the whole series.

A variety of improvements have been proposed to process singularities. Most of these methods essentially search for a suitable warping path by constraining the possible wrappings allowed. Slope weighting is used to constrain the warping path, which allows warping paths to be constrained by restricting the slope, thereby avoiding excessively large movements in a single direction [65]. The slope is controlled by the coefficient of weighting C in equation (3-8),

$$c_{ij} = C \cdot d_{ij} + \min\{c_{i-1,j-1}, C \cdot c_{i-1,j}, c_{i,j-1}\}, i \in [1:N], j \in [1:M] \quad (3-8)$$

where C is a positive real number, the warping can be constrained by changing C 's value. The warping path is increasingly biased toward the diagonal in accordance with

the increase of C . It is not obvious how to select an appropriate parameter C in equation (3-8).

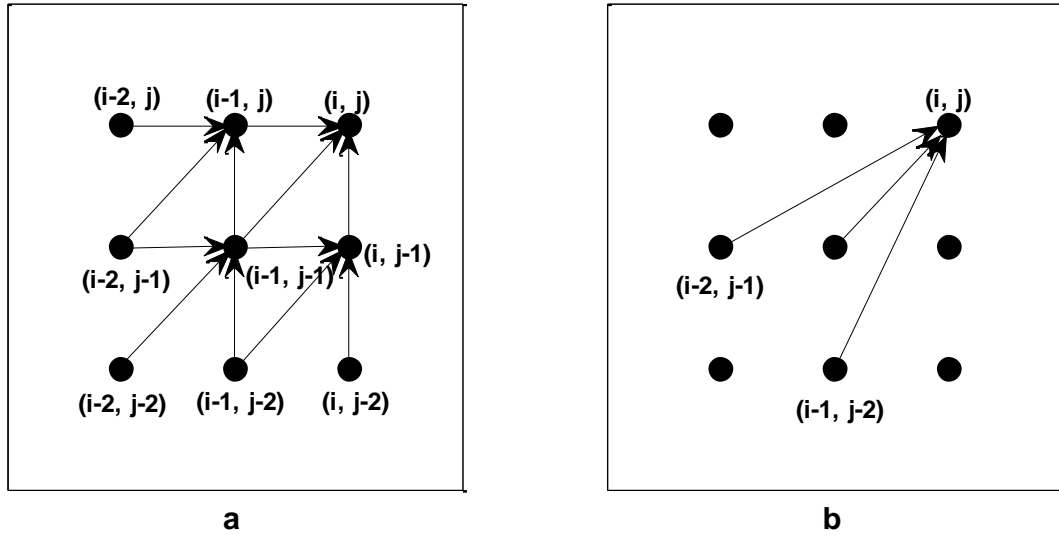


Figure 3-5 Step patterns: a) the step patterns in classic DTW; b) the step pattern improvement

Step patterns are also explored to constrain the warping path. Itakura [68] and Myers and Rabiner [30] modify the equation (3-7) to equation (3-9):

$$c_{ij} = d_{ij} + \min\{c_{i-1,j-1}, c_{i-1,j-2}, c_{i-2,j-1}\}, i \in [1:N], j \in [1:M] \quad (3-9)$$

The warping path is forced to move one diagonal step for each parallel as shown in Figure 3-5(b) to an axis by employing this equation.

Berndt and Clifford [69] employed a warping window to restrict the possible warping paths. Allowable points can be constrained to fall within a given warping window $|x_i - y_j| < \varepsilon$, where ε is a positive integer corresponding to window width. These constraints mean that the corners of the matrix are out of consideration, and also beneficially improve the computing complexity. The problem associated with this method, is that it is difficult to find a suitable window width ε because width varies according to its applications.

Classic dynamic time warping only considers the Y-axis value of a data point and does not take into account the local features of the data point. In other words, a data point of one time series not only has the feature of the Y-axis value, but also has the characteristic of a trend for local accelerations and decelerations in the time axis. In order to prevent this problem, derivative dynamic time warping is used instead as it has the ability of not only considering the Y-axis of the data points, but also considering the higher level features of local feature. The information about the shape is obtained by considering the first derivative of the time series.

In derivative dynamic time warping, the point-to-point distance d_{ij} is the square of the difference of the estimated derivatives instead of the Euclidean distance of x_i and y_j in the time series of X and Y . The method for calculating the estimated derivative of a point in a time series is indicated in equation (3-10) [53], for example, at point i in time series X .

$$D[x_i] = \frac{(x_i - x_{i-1}) + ((x_{i+1} - x_{i-1})/2)}{2}, 1 < i < N \quad (3-10)$$

This estimate is simply the average of the slope of the line through the point as well as its left and right neighbour points. Figure 3-6(b) indicates the results of two time series aligned by derivative dynamic time warping.

The derivative dynamic time warping algorithm replaces the value of each data point with its first deviation which can be considered as a local feature of that point, and which expresses its relationship with its two adjacent neighbours. Derivative dynamic time warping may lose sight of the overall shapes or significant features which happen in the entire time series when only considering the first deviations of each point in comparison. The overall shapes can be called the global features. In order to capture trends or local and global features of a time series during the alignment process, feature based dynamic time warping is developed to align two time series based on each point's local and global features rather than each point's values or first derivative [67].

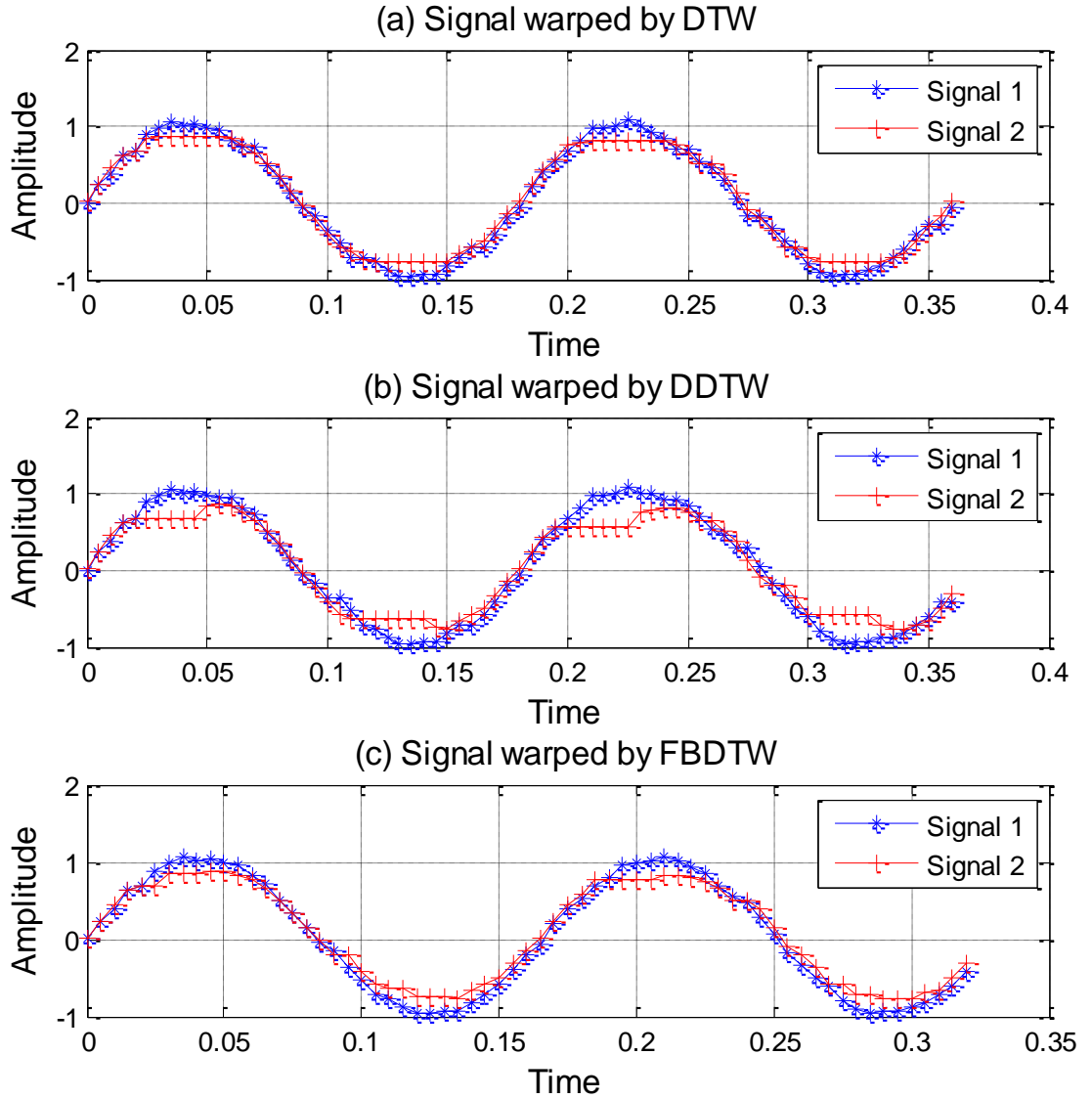


Figure 3-6 Comparisons of signal alignment by DTW, DDTW and FBDTW

In feature based dynamic time warping [67], the point-to-point distance $d_{i,j}$ consists of the local distance and the global distance evaluated which are in turn based upon both the local and global features of time series X and Y [67].

$$d_{i,j} = d_{global}(x_i, y_j) + d_{local}(x_i, y_j) \quad (3-11)$$

where $d_{local}(x_i, y_j)$ is the distance between x_i and y_j based on their local features, and $d_{global}(x_i, y_j)$ is the distance between x_i and y_j based on their global features.

The local feature of the data point x_i denoted as $f_{local}(x_i)$ is defined as a vector of two components [67]:

$$f_{local}(x_i) = (x_i - x_{i-1}, x_i - x_{i+1}) \quad (3-12)$$

The global feature of a data point x_i in a time series should reflect the position of that point in the global shape of the series, so it can be also defined as a vector of two components [67]:

$$f_{global}(x_i) = (x_i - \sum_{k=1}^{i-1} x_k / (i - 1), \quad (3-13)$$

$$x_i - \sum_{k=i+1}^M x_k / (N - i))$$

The first component of the vector is the difference between the values of x_i and the average value of the first $(i - 1)$ points in the series; the second component is the difference between the values of x_i and the average value of the last $(N - i)$ points in the series.

The distance between two time series X and Y can be evaluated according to equation (3-14) which is based upon the local and global features of each time series. When the local and global features have been calculated already, equations (3-12) and (3-13) [67] should be referred to.

$$\begin{cases} d_{local}(x_i, y_j) = |f_{local}(x_i) - f_{local}(y_j)| \\ d_{global}(x_i, y_j) = |f_{global}(x_i) - f_{global}(y_j)| \end{cases} \quad (3-14)$$

An optimal warping path can then be found by employing dynamic programming to calculate the minimal distance based upon the cumulative distance matrix C as expressed in equation (3-7). The result of the signal, warped by feature based dynamic time warping, is shown in figure 3-6(c).

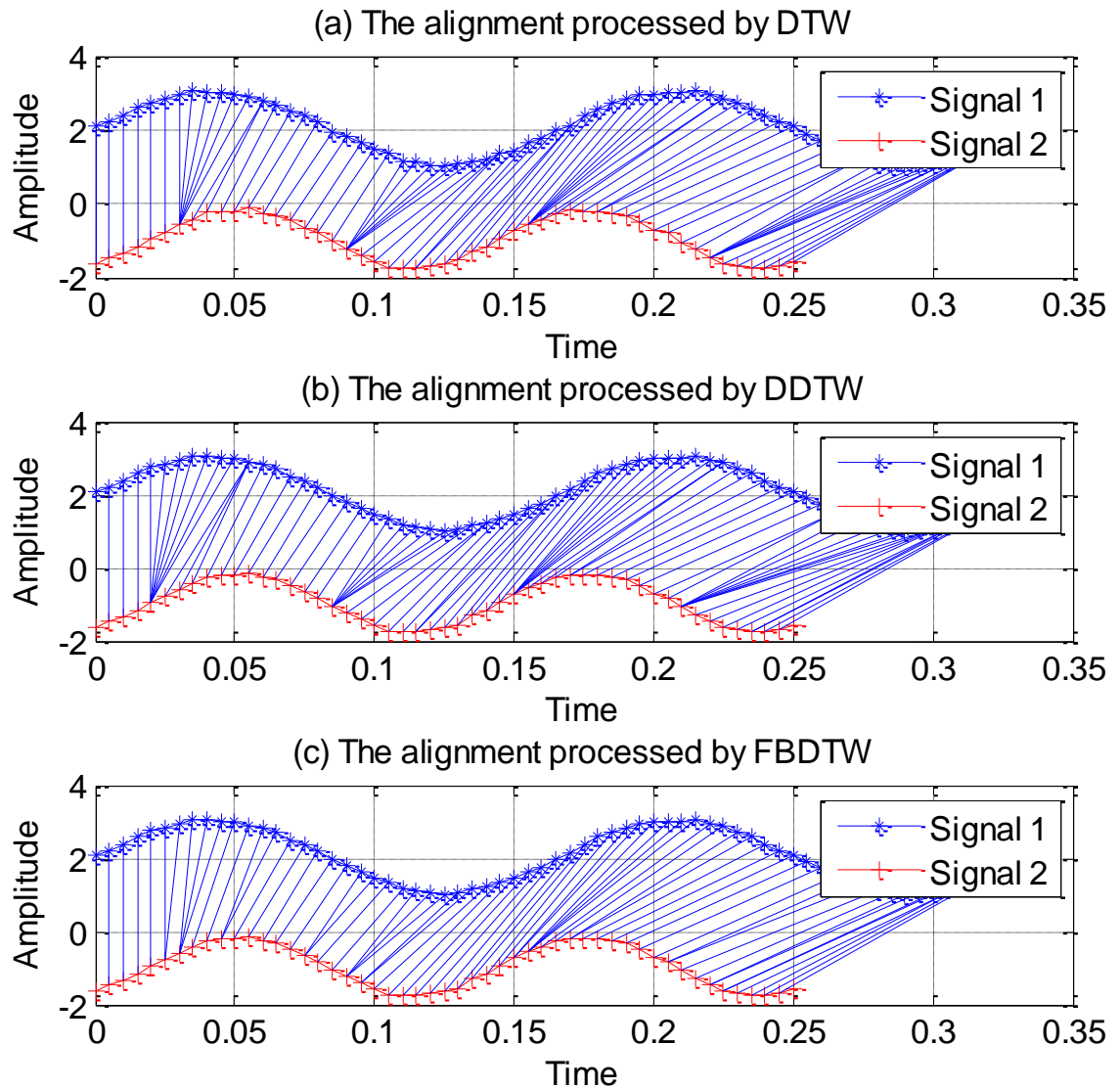


Figure 3-7 The alignment of points based on the warping paths produced by DTW, DDTW and FBDTW

The detailed alignments of the points, based on the warping paths produced by dynamic time warping (DTW), derivative dynamic time warping (DDTW) and feature based dynamic time warping (FBDTW) are shown in figure 3-7. It can be seen that the alignment of the data points processed by feature based dynamic time warping is more reasonable than that processed by dynamic time warping and derivative dynamic time warping. The improvement of singularities is obvious. The improvement of singularities is not clear according to the comparison of the data points aligned by

derivative dynamic time warping and dynamic time warping in figure 3-7. By comparing the derivative dynamic time warping and dynamic time warping signal alignments in figure 3-6(b) and figure 3-6(a), we see a slight improvement of the singularities in the derivative dynamic time warping algorithm, especially with regards to the alignment of the two central peaks.

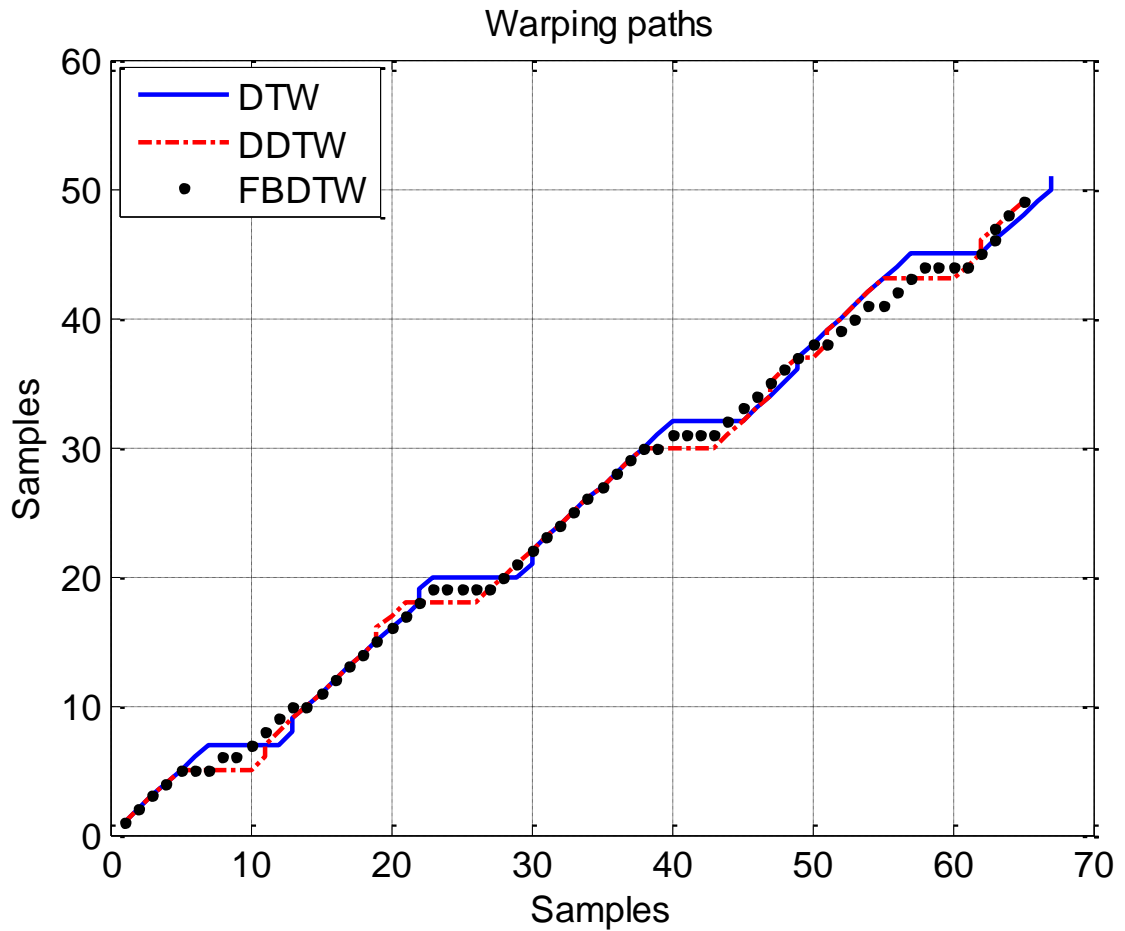


Figure 3-8 Optimal warping paths produced by DTW, DDTW and FBDTW

The optimal warping paths produced by dynamic time warping, derivative dynamic time warping and feature based dynamic time warping are shown in figure 3-8. It can be seen that the warping path of feature based dynamic time warping is closer to the diagonal of the accumulated matrix. The warping paths of dynamic time warping and derivative dynamic time warping are further away from the diagonal of the cumulated matrix compared with the warping path of feature based dynamic time warping. It has

large jumps at some points, such as at those that can be seen at points 10, 25 and 40 in the x-axis in figure 3-8, indicating the singularities effects.

Noting that both the derivation in derivative dynamic time warping (DDTW) and local or global features in feature based dynamic time warping have no definition for the first and last point in a time series, so both derivative dynamic time warping and feature based dynamic time warping calculate the optimal warping path starting with the second points of the two time series and ending with the penultimate points. Furthermore, the computational cost of derivative dynamic time warping and feature based dynamic time warping is the same as classic dynamic time warping which is $O(NM)$.

3.4.2 Time complexity improvement

In the dynamic time warping, the cumulated distance matrix calculation is the main time cost process. If the cumulated distance matrix has $N \times M$ entries, the time complexity of the dynamic time warping should be $O(NM)$ [65][66]. The time and space complexity of dynamic time warping is a critical limitation in its application. In order to improve the computational cost of the dynamic time warping algorithm, the global constraints should be considered. It can be concluded that the optimal warping paths run near the diagonal from classic dynamic time warping based on the warping path analysis. It is therefore sufficient to consider only paths lying completely inside a band around the diagonal from point (1,1) to (N, M) [27].

The ‘‘Sakoe-Chiba band’’ and ‘‘Itakura parallelogram’’ [68] are two classic global constraints used for time complexity reduction. The Sakoe-Chiba band contains all index pairs (i, j) with $|i - j| \leq r$ and a band width of $2r$, as can be seen in figure 3-9(a). The slope of this band is 45° and it holds $O(n)$ index pairs when $i = j = n$. The basic idea of Itakura parallelogram is to allow only small distortions at the beginning and the end of the time series, while larger ones are accepted in the middle [68], as can be seen in figure 3-9.

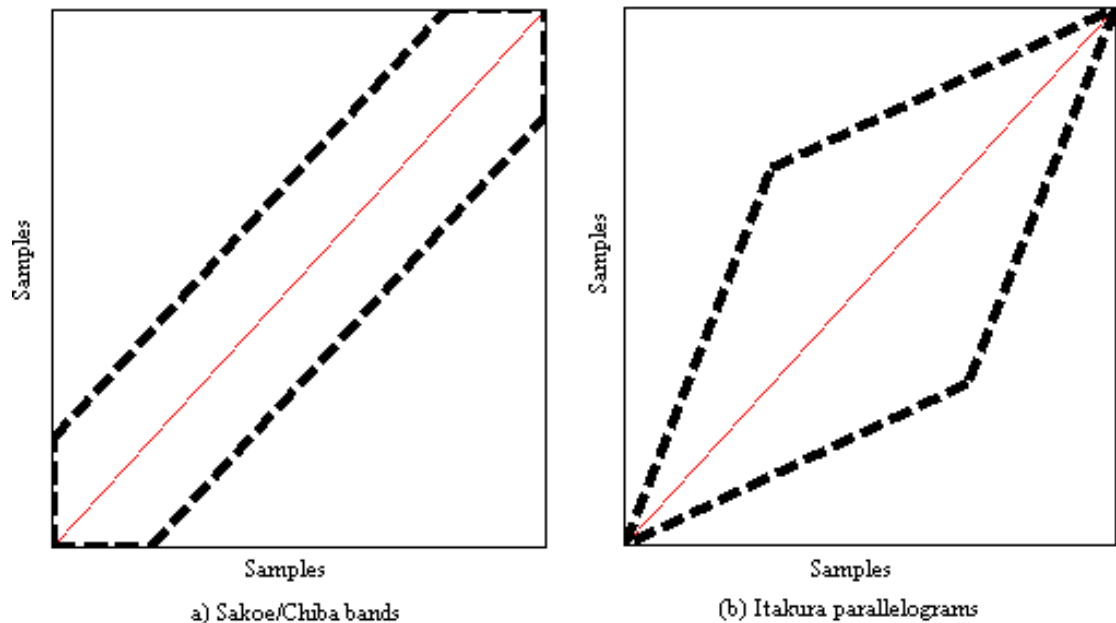


Figure 3-9 Global constraints for time complexity improvement
a) Sakoe/Chiba band; b) Itakura parallelogram

The time complexity of dynamic time warping can be reduced by employing either of the global constraints of the “Sakoe-Chiba band” or the “Itakura parallelogram”. The global constraints are easier to implement if the cumulated distance matrix is quadratic when $N = M$, normalization must be carried out when the two time series do not have the same length [27]. Another popular method to speed up dynamic time warping is that of the time-series [69]. Piecewise Dynamic Time Warping (PDTW) [70] can be developed to improve the time complexity of the dynamic time warping. The piecewise dynamic time warping operates on the reduced dimensionality representation through piecewise aggregate approximation which approximates a time series by dividing it into equal-length segments and recording the mean value of the data points which fall within each segment. The segmental signals retain the basic characteristics of the original signals even after the dimensionality reduction. Figure 3-10 shows the comparison between the dynamic time warping and piecewise dynamic time warping, two similar time series, and the point alignment between them

discovered by dynamic time warping in figure 3-10(a). Figure 3-10(b) indicates the same time series in their piecewise approximation representation by piecewise dynamic time warping. It can be seen that the segmental signals still retain the main features of the original signal after processing by piecewise dynamic time warping.

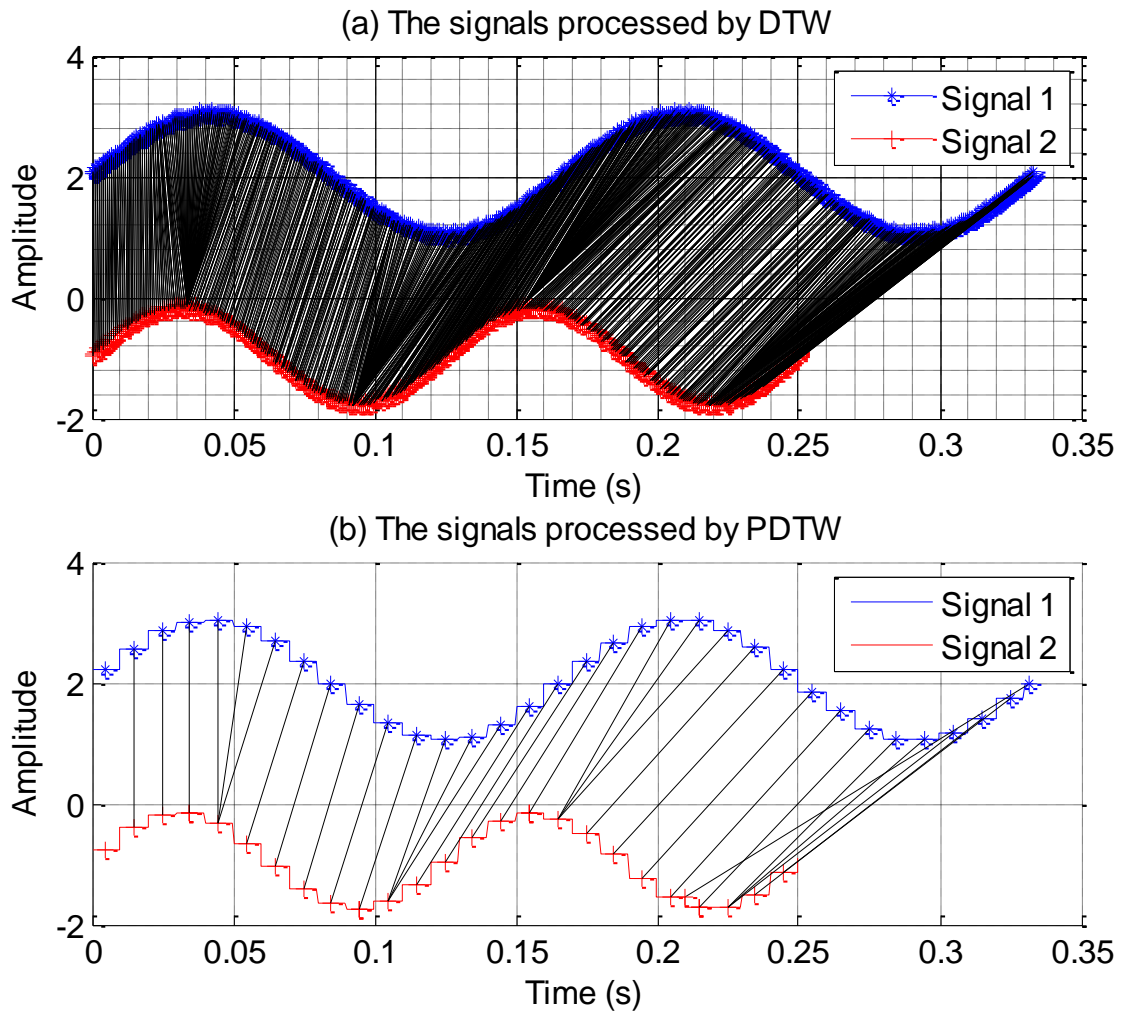


Figure 3-10 Comparison of point alignment after processing by DTW and PDTW

One important limitation of piecewise dynamic time warping is that the user must carefully choose the approximation levels used in the alignment. This means the compression rate of the dimensionality reduction should be selected appropriately. If the compression rate is higher, the resulting optimal warping path may become inaccurate or even completely useless by decreasing the sampling rate of the time

series [63]. Conversely, a lower compression rate signifies a finer approximation, but the gains in speed up of dynamic time warping are not obvious [69].

3.5 Phase properties of singularities

According to the definition of dynamic time warping, the optimal warping path is selected through finding the minimal distance in the cumulated distance matrix which is built based on the distance matrix. The elements of the distance matrix are the point-to-point Euclidean distance between the two time series. If there is a phase shift between the two time series, the Euclidean distance between the first points of the two time series is not minimal in the first column or row of the distance matrix. The distribution of the cumulated distance matrix changes accordingly and results in the optimal warping path selected [30] could not close to the diagonal of the accumulated distance matrix as much as anticipated according to step patterns. The cumulated error of the cumulated distance matrix will be increased due to the increased values in the distance matrix which is caused by the phase shift between the two time series. The cumulated error leads to inaccurate minimal distance findings in the dynamic programming of dynamic time warping and hence results in more warping jumps occurring, especially at the start and end of the aligned time series. This causes singularities as a result of the first or last point of one time series mapping onto numerous points on the other time series, as is shown in Figure 3-4(b).

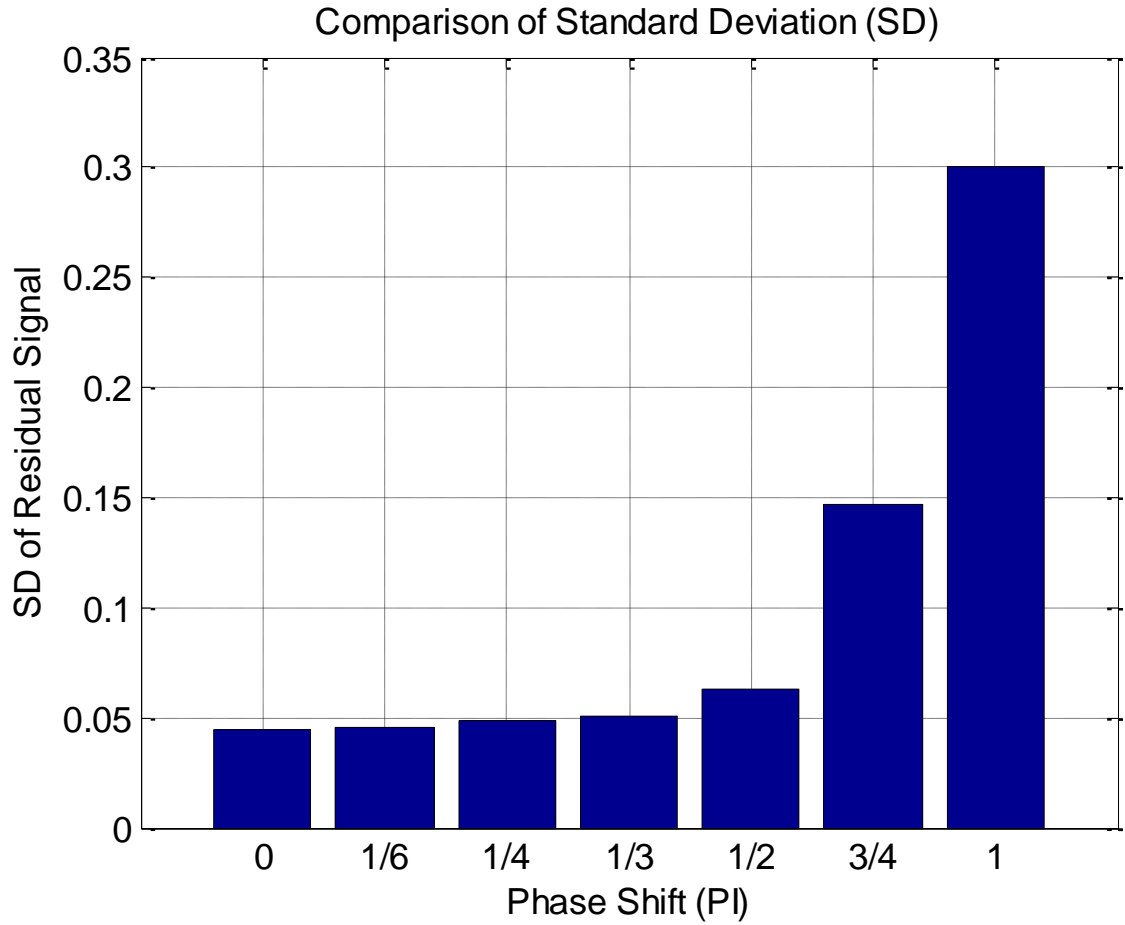


Figure 3-11 SD of DTW residual signals with different phase shifts

For the purpose of studying the impact of phase shift on singularities, different phase shifts θ_i from 0 to π between the two time series are explored. Figure 3-11 shows the standard deviation (SD) of the dynamic time warping residual signals from different pairs of time series which are of different phase shifts. The standard deviation of the residual signal can be calculated by equation (3-15)

$$SD = \sqrt{\frac{1}{N} \sum_{i=1}^N (x_i - \bar{x})^2} \quad (3-15)$$

where N is the number of the points in the residual signal, x_i is the value of the i^{th} point of the residual signal, and \bar{x} is the average value of the residual signal.

The phase shift 0 denotes that the two aligned signals have the same initial phase, whereas π means an opposite phase between two signals. It is revealed that with the increase of the phase shift, the standard deviation value of the dynamic time warping residual signal clearly increases, demonstrating that larger phase shift leads to larger cumulated errors in the cumulated distance matrix and greater data jumps in the residual signal. This shows that dynamic time warping produces different dissimilarity results at different phase shifts even if the two signatures in comparison are the same. This will lead to uncertainty of fault diagnosis when comparing measured signals with different phases as a result of different acquisition time instants.

Phase estimation and compensation of the aligned signals should be helpful to improve the singularities of dynamic time warping. Figure 3-12(a) shows the result of phase estimation and compensation of the two time series shown in Figure 3-4(a). It can be seen that the overall waveform of the two time series is now matched better after phase compensation has taken place. From the processing results of dynamic time warping shown in Figure 3-12(b) and (c) and the dynamic time warping residual signal shown in Figure 3-12(d), it is clear that the singularities at the ends of the aligned time series as shown in Figure 3-4(b) have moved out and prove that phase compensation has the ability to improve the singularity effects of dynamic time warping and reduce the data jumps at the ends of the residual signal. Hence, more accurate results of dissimilarity recognition by dynamic time warping can be obtained after processing by phase compensation.

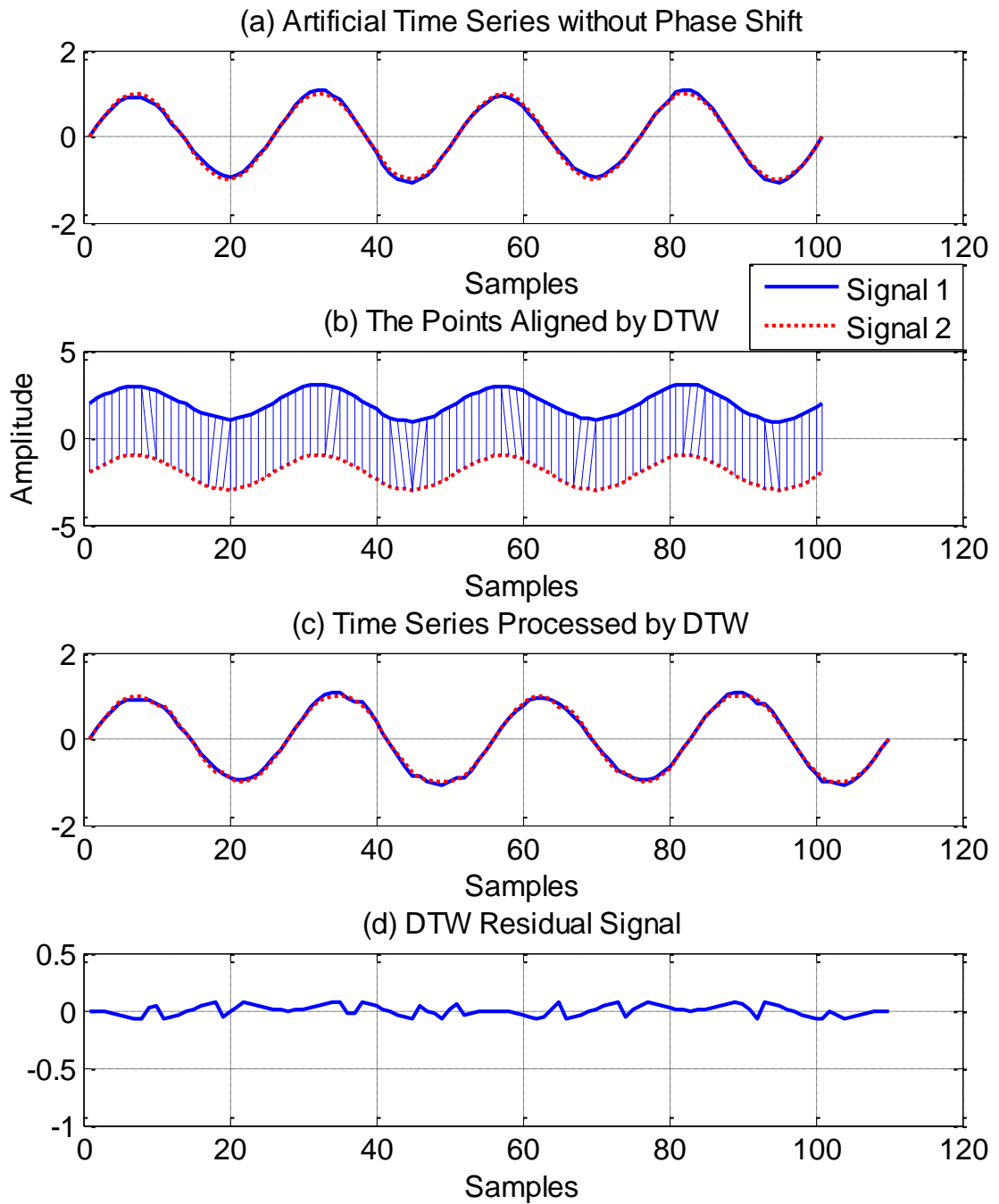


Figure 3-12 The singularity effect of DTW with phase compensation

Figure 3-13 shows the comparison of the standard deviation values between phase compensation and non-compensation. It shows that the standard deviation values increase with the phase shifts between the two time series without phase compensation. The standard deviation values of the dynamic time warping residual signals obtained

from the two time series after phase compensation are all similar. This means that the phase compensation can reduce the effect of singularities on maintaining the minimal value of dissimilarity between the two signals with different phase shifts, especially coupled with the results from Figure 3-12, showing that the phase compensation can be used to improve the singularities occurred at the beginning and ending of the aligned signals, in turn allowing accurate feature extraction for obtaining reliable fault detection and diagnosis.

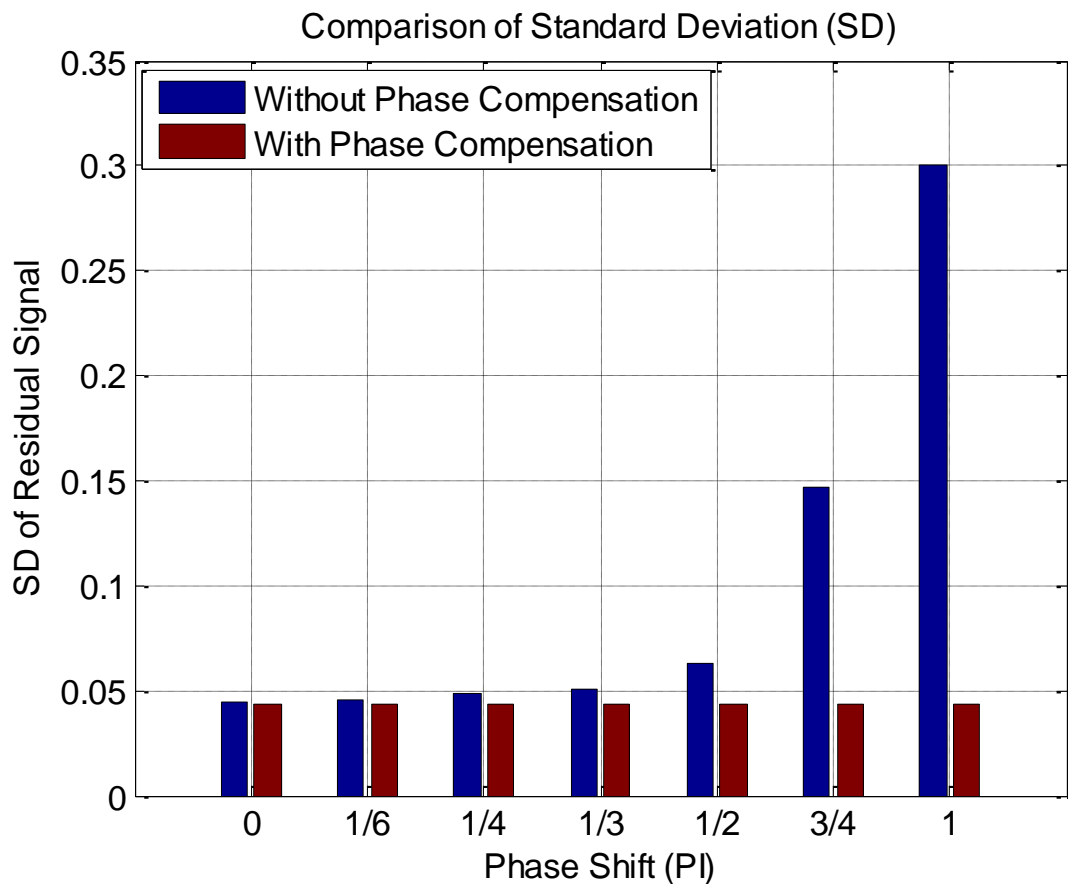


Figure 3-13 Comparison of SD of DTW residual signals

The analysis results show that the proposed phase estimation and compensation method can improve the singularities of dynamic time warping effectively. In the following chapter 4, the dynamic time warping based on phase estimation and compensation is used to analyse the electrical motor current signal for fault diagnostics of a two-stage reciprocating compressor.

CHAPTER 4

DYNAMIC TIME WARPING OF MOTOR CURRENT SIGNALS FOR FAULT DIAGNOSIS OF A RECIPROCATING COMPRESSOR

This chapter introduces the use of dynamic time warping to analyse the electrical motor current signal for fault diagnostics of a two-stage reciprocating compressor. The electrical motor current signal is a typical non-stationary signal which contains nonlinear effects due to the faults of the induction machine and its downstream mechanical equipment. Based on the limitations of the classical dynamic time warping, a phase estimation and compensation approach has been developed to reduce the singularity effect of classical dynamic time warping for the obtaining of accurate diagnostic results. A sliding window has also been designed to improve computing efficiency. The results of fault detection of a compressor demonstrate that the accuracy and reliability of detection and classification from the proposed dynamic time warping analysis is higher than those of Fourier transform spectrum and envelope analysis and the proposed method is based entirely on time domain analysis which is easier apply in real-time monitoring processes.

4.1 Introduction to motor current signal analysis

Electrical motor current signals have been widely investigated to analyse the health of the induction machine and its downstream mechanical equipment. [71][72]. As it is cost-effective in obtaining signals and allows for remote monitoring, the induction machine stator current signal is also used to detect the influence of mechanical problems resulting in rotor disturbances [71]. As well as this, the presence of load imbalance can also be detected through analysis of the induction machine stator current signals [73]. Recent studies [24] have shown that supply currents contain components related to abnormalities in downstream equipment such as compressors, pumps, rolling mills, mixers, crushers, fans, blowers and material conveyors. This technique has been used to detect specific axial flow compressor problems.

Common approaches used for fault detection are based on the comparison of correlating numerical models with measured model properties from undamaged and damaged components. Measurements are normally made in the time domain while a machine runs under different loads and speeds. The signals acquired in the test are then analysed in both the time and the frequency domains using various signal processing techniques in order to extract the diagnostic features, allowing accurate comparison between signals.

The signal processing techniques used in fault detection based on current signals are developed predominately in the frequency domain through Fourier transform (FT). Although it produces satisfactory results, the Fourier transform based method is subject to a number of generic limitations: aliasing [74], spectral leakage [75][76] and picket-fence effect [74][77] (see section 2.4). The latter two limitations can lead to significant errors in spectrum estimation, meaning that the weak signature due to faults in the signals cannot be resolved properly for accurate fault detection and diagnosis. Although many methods have been developed to improve the limitations of conventional Fourier transform, they have never eliminated them completely.

Thus it seems that techniques applied directly to the time domain signals can avoid the shortcomings of the frequency analysis as all the procedure are carried out in the time

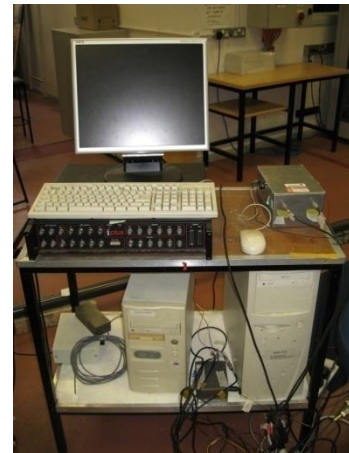
domain. In fact, time domain based methods, especially time synchronous average (TSA) [26] (see Section 8.3), have been the subject of intensive investigation in recent years for monitoring rotating machinery and have been applied successfully numerous times. However, a shaft mark signal from an additional channel is required in order to implement time synchronous average based monitoring, leading to increased cost to applications. The statistical parameters or characteristic features can be calculated from signals in the time domain, such as mean, peak, standard deviation, root mean square (RMS), and kurtosis, etc. These statistical parameters are widely used for representing the characteristics of a signal in the time domain (see Section 2.4).

This chapter presents the use of dynamic time warping (see Section 3.2) to process the motor current signals for detecting and quantifying common faults of a two-stage reciprocating compressor. Dynamic time warping is used to suppress the supply frequency component and to highlight the sideband components based on the introduction of a reference signal which has the same frequency components as the supply power. This is because the sideband components contain more useful information for the indications of faults and conditions of the monitored machine. A sliding window is designed to process the raw signal using dynamic time warping frame by frame for effective calculation (see Section 4.4.2). In addition, a phase compensation approach (see Section 4.4.1) is developed to reduce the singularity effect on the accurate detection obtained in diagnosing compressor faults.

4.2 Reciprocating compressor test

4.2.1 Test rig

The experiment is carried out based on a two-stage reciprocating compressor test rig as shown in Figure 4-1. Motor current signals of the two-stage reciprocating compressor are acquired to identify and quantify common faults of the compressor. It was demonstrated that the mechanical faults could result in rotor disturbances which can be detected through the changes in the induction machine phase current signals [78]. Motor current signals can also be used to detect the presence of load imbalance which is the imbalance in the current distribution to the load [71][24].



(a) Two-stage reciprocating compressor

(b) Data acquisition system

Figure 4-1 Photos of the test facility and data acquisition system

The reciprocating compressor has a common two-stage construction which allows air to be compressed as high as 10bar. It is driven by a 2.5kW, three-phase and four-pole induction motor through a V-belt with a transmission ratio of 3.2. During the tests, the compressor is induced with three common faults: discharge valve leakage, transmission belt looseness and inter-cooler leakage. These faults can cause reduced operating efficiency and cause potential damage to the compressors. The leakage is usually caused by mechanical vibrations while the belt looseness is a typical feature should the texture of the belt show damage.

The three types of faults are induced individually to the compressor for evaluating the effectiveness of the proposed method in detecting these faults. The valve leakage is produced by drilling a 1mm hole in the discharge valve plate. The distance between two belt pulleys is reduced by 2mm for belt looseness. The case of inter-cooler leakage is induced by adjusting the tightness of the connecting bolt for the different degrees of leakage, often a consequence of the resonance of the connection line. The experimental setup schematic is shown in Figure 4-2. It is a fact that faults induced were minor and could not easily be detected from performance measures. More details about the compressor test and setup are given in Appendix B.

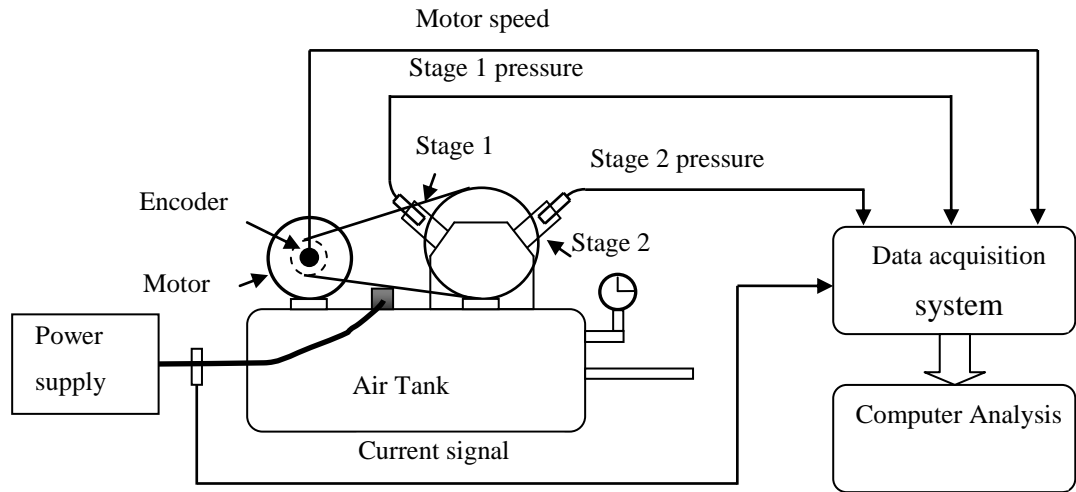


Figure 4-2 The experimental setup

4.2.2 Current transducer

A Hall Effect based current transducer with wide frequency response range is used to measure the electrical current signal in the test. The transducer converts AC/DC input current into a load independent output DC $-5V \sim +5V$. It has advantages of total galvanic isolation between input/output, high accuracy, low temperature drifting, and a wide temperature range. The electrical specification for the current transducer is shown in Table 4-1.



Figure 4-3 Current transducer

Table 4-1 Electrical specification of current transducer

Input	AC/DC 0~400A
Output	DC -5V~+5V
Frequency response	DC~1.5 kHz
Power supply	±12VDC/±15VDC/+24VDC
Accuracy	1.0%
Isolation	input/output
Insulation Voltage	AC 6000V, 1 min
Response time	20μs

4.2.3 Experimental setup

During the tests, one phase in the three-phase motor current is measured by a Hall Effect based current transducer with frequency response from DC to 1.5 kHz. The current signal is collected by a high speed ADC system at a resolution of 16-bit. For each fault the data is collected at 6 different discharge pressures: 4.8bar, 5.5bar, 6.2bar, 6.9bar, 7.6bar and 8.3bar, which covers the operating pressure range specified by the manufacturer. The fault, load and speed settings in the experimental process are listed in Table 4-2. More details about the compressor test are shown in Appendix B.

Table 4-2 Faults and Loads in using Experimental testing

Conditions	Load1 (bar)	Load2 (bar)	Load3 (bar)	Load4 (bar)	Load5 (bar)	Load6 (bar)	Nominal Speed (rpm)
Health	4.8	5.5	6.2	6.9	7.6	8.3	1400
Valve leakage	4.8	5.5	6.2	6.9	7.6	8.3	1400
Inter-cooler leakage	4.8	5.5	6.2	6.9	7.6	8.3	1400
Belt looseness	4.8	5.5	6.2	6.9	7.6	8.3	1400

Each collection is 50,000 points which is more than 2 seconds in duration for a sampling rate of 24.3 kHz for keeping more information from the original signals during analog-to-digital conversion. This data length covers about 12 compressor

cycles which is sufficient for random noise suppression in an average process. The high sampling rate allows high accuracy to be obtained in waveform parameter calculation.

4.3 Phase current signal

4.3.1 Electromagnetic relationship of the phase current signal

To study the characteristics of the motor stator current signal, the electromagnetic relationships should be analyzed in one of the three symmetric phases of a power supply system, which can be defined as phase *A* in here. Assuming the fundamental frequency of electrical supply is f_s , the instantaneous current signal [24][79] under healthy conditions can be expressed as sinusoidal signals [80],

$$i_A = I \cos(2\pi f_s t - \alpha_I) \quad (4-1)$$

where I denotes the amplitude of the supply current, and α_I is its angular. i_A is the instantaneous amplitude of the supply current in phase *A*. This current interacts with the magnetic flux in motor stator as [79],

$$\Phi_A = \Phi \cos(2\pi f_s t - \alpha_\Phi) \quad (4-2)$$

where the amplitude of the magnetic flux is Φ , and α_Φ denotes its angular displacement. Φ_A is the instantaneous amplitude of the magnetic flux in motor stator. Therefore, the torque T produced by the interaction between the current and magnetic flux can be expressed as [81]

$$T = 3P\Phi I \sin\alpha_{\Phi I} \quad (4-3)$$

where P is the number of pole pairs, and $\alpha_{\Phi I} = \alpha_\Phi - \alpha_I$ is the angular displacement between the supply current and the magnetic flux. If a fault occurs in the rotor system, and assuming the fault generates a sinusoidal wave with a frequency f_F , the current amplitude and angular displacement are I_F and α_F , respectively. This means that the additional oscillatory torque ΔT can be obtained using Equation (4-3) [24],

$$\Delta T = 3P\phi I_F \sin(2\pi f_F t - \alpha_{\phi I} - \alpha_F) \quad (4-4)$$

This oscillatory torque causes speed fluctuation $\Delta\omega$ which can be derived as,

$$\Delta\omega = \frac{P}{J} \int \Delta T dt = -\frac{3P^2\phi I_F}{4\pi^2 f_F^2 J} \cos(2\pi f_F t - \alpha_{\phi I} - \alpha_F) \quad (4-5)$$

thus, the angular oscillation is:

$$\Delta\alpha_F = \int \Delta\omega dt = \frac{3P^2\phi I_F}{4\pi^2 f_F^2 J} \sin(2\pi f_F t - \alpha_{\phi I} - \alpha_F) \quad (4-6)$$

where $\Delta\alpha_F$ is the angular oscillation with fault components in motor stator, and J is the inertia of the rotor system. The angular variation in Equation (4-6) produces phase modulation to the leakage flux. The magnetic flux in the motor stator can be expressed as [24]

$$\phi_A^F = \phi \cos(2\pi f_s t - \alpha_{\phi} - \Delta\alpha_F) \quad (4-7)$$

where ϕ_A^F is the magnetic flux with fault component in the motor stator.

This shows that the flux wave contains nonlinear effects because of the fault in the rotor system. This nonlinear interaction of linkage flux will produce a corresponding electromagnetic force and hence induce a nonlinear current signal in the stator [24]. The simplified stator current can be expressed as [24],

$$i_F = I \cos(2\pi f_s t - \alpha_I) + I_l \cos[2\pi(f_s - f_F)t - \alpha_l - \alpha_F - \varphi] - I_r \cos[2\pi(f_s + f_F)t - 2\alpha_{\phi} + \alpha_l - \alpha_F - \varphi] \quad (4-8)$$

where i_F is the stator current with fault components in the motor, and φ is the angular displacement of the motor equivalent circuit impedance at the supply frequency [24], the amplitudes of the lower and upper sideband components are denoted by I_l and I_r , respectively. Equation (4-8) is widely employed for motor condition monitoring. Fault information can be extracted by analyzing the sideband components of the current signal, such as rotor disturbances and load imbalance.

4.3.2 The characteristics of phase current signal

A reciprocating compressor system consists of a typical induction motor are used for the motor current signal collection. It has two basic working processes including compression and expansion. The working process gives rise to a periodically varying load to the driving motor due to the compressor requiring more power in compression than in expansion [81], and it is more accurately for the motor current signal measured. This varying load leads to high oscillation in the measured current signal. According to Equation (4-8), the measured current signal can be expressed as [24],

$$i_A = I \cos 2\pi f_s t + I_l \cos[2\pi(f_s - f_F)t - \alpha_l] + I_r \cos[2\pi(f_s + f_F)t - \alpha_r] \quad (4-9)$$

where α_l and α_r denote the angular displacement of the lower and upper sideband components respectively. $f_s - f_F$ and $f_s + f_F$ are distributed around the supply frequency f_s , it has similar properties with an amplitude modulation signal. The amplitude of the two sideband components will change with the degree of the fluctuation of load and speed, which means when the fluctuation of load increases with discharge pressures, the amplitude and phase of the sideband components will change accordingly. Figure 4-4 shows the stator current signals measured from the two-stage compressor under the conditions of healthy and faulty valve leakage.

It can be seen from Figure 4-4(a) that the amplitude of the current waveform from the valve leakage is slightly higher than that of the healthy condition. The current signals are modulated by a dynamic load fluctuating according to the waveform. It is also very clear that the two stator currents have similar waveforms but with clear phase shift.

In the spectra, as shown in Figure 4-4(b), the amplitude of the supply power and sidebands frequency component for the valve leakage is slightly higher than that of the healthy condition, which is consistent with the waveform in Figure 4-4(a). This indicates that the stator current signals contain useful information for compressor fault detection. The carrier frequency component at the supply frequency of 50Hz has high amplitude and the sideband components at about 50 ± 7.3 Hz are also very clear.

According to the working speed and transmission ratio of the test compressor, the load fluctuating frequency is seen at 7.3Hz.

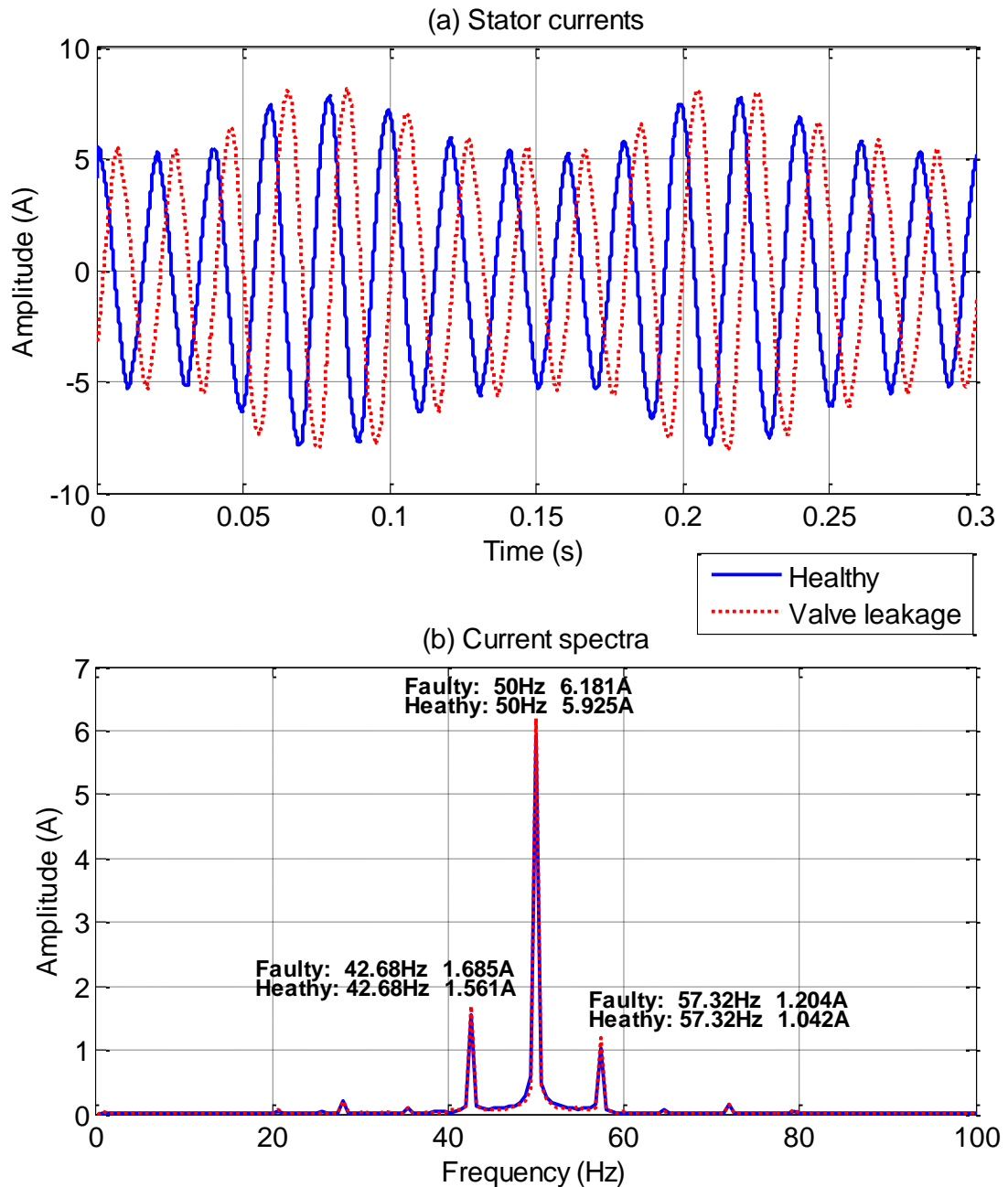


Figure 4-4 Waveform and spectra of stator current signals from a compressor with healthy and faulty valve leakage

The components at 50Hz would show spectral leakage if the frequency resolution was low due to the limitation of Fourier transform based analysis. This leakage would lead

to an error in estimating the amplitude at 50Hz, causing more difficulties in identifying and quantifying the small sidebands which are the main feature used for fault diagnosis. If the frequency resolution cannot separate the frequency components between the 50Hz and sidebands components, the sidebands components cannot be extracted properly. If the frequency resolution is high enough to identify and separate the main frequency component and its sidebands component, even the difference between the faults and healthy is small, if it is sensitivity and reliability proved by experiments carried out under different conditions, the small difference can be used to indicate a fault.

4.4 Phase compensation based dynamic time warping

According to the theoretical analysis of motor current signal, the electrical current signal can be considered as an amplitude modulation signal. The carrier signal is the supply frequency component at about 50Hz and the load fluctuating component is about 7.3Hz which corresponds to the working speed of the compressor and its transmission ratio (see equation (4-19)).

To separate the fluctuating component from the supply components as accurately as possible, the dynamic time warping based approach to data processing and fault detection is required with the data manipulation steps shown in Figure 4-5. This consists mainly of data pre-processing, dynamic time warping implementation and detection feature setup.

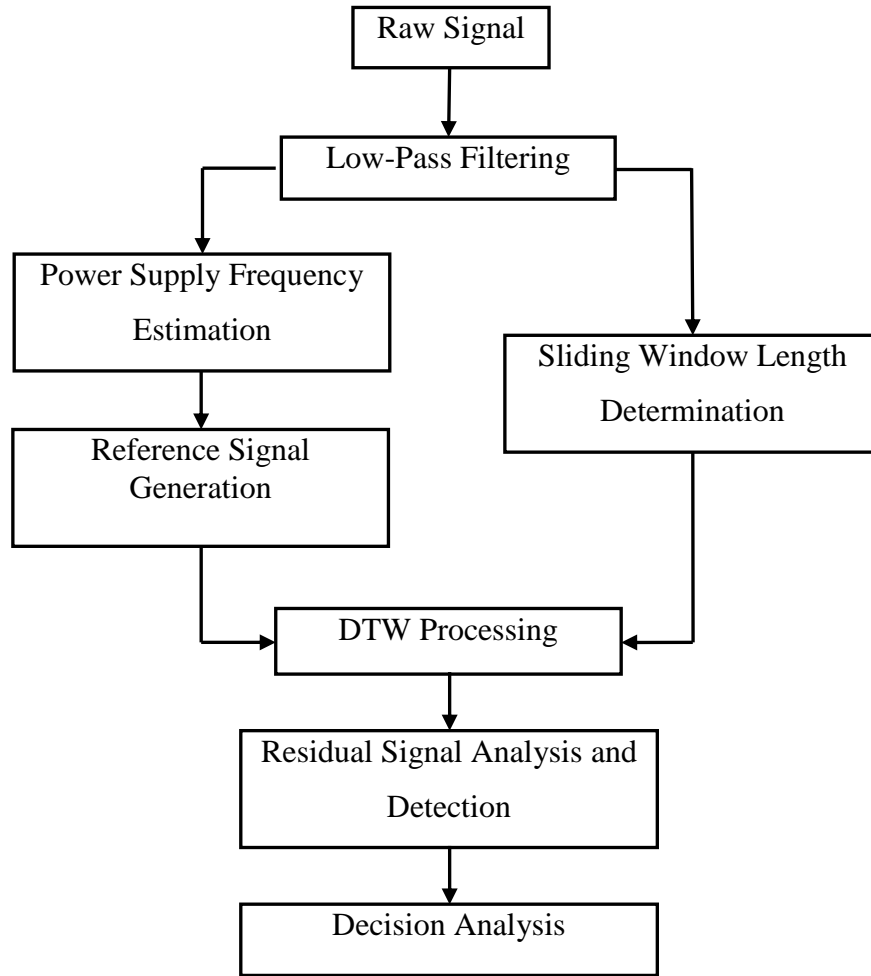


Figure 4-5 A flow diagram of the DTW based method

4.4.1 Phase estimation

To improve the singularity effects of the classic dynamic time warping, phase estimation and compensation are carried out on the two time series before dynamic time warping is implemented. An initial phase needs to be estimated for a preliminary alignment between the two aligned time series. In the proposed method, the initial phase estimation is developed by a phase matching approach. The assumption that two time series have the same length but have different initial phases is expressed in Equation (4-10)

$$s_1 = \{s_{11}, s_{12}, \dots, s_{1i}, \dots, s_{1n}\} \text{ and } s_2 = \{s_{21}, s_{22}, \dots, s_{2i}, \dots, s_{2n}\} \quad (4-10)$$

where s_1 is the first time series and s_2 is the second time series. s_{1i} ($i = 1, 2, \dots, n$) and s_{2i} ($i = 1, 2, \dots, n$) indicate the values of the first and second time series at the i^{th} point respectively.

In the initial phase estimation, the Euclidean distance given by Equation (4-11) is used to measure the differences between the two time series at different phase θ . As the phase θ varies from 0 to 2π in a step of $\pi/180$, the Euclidean distances of the two time series can be obtained.

$$D_j = \sqrt{\sum_{i=0}^n [s_{1i} - s_{2i}(\theta_j)]^2} \text{ where } j = 1, 2, \dots, N \quad (4-11)$$

where, s_{1i} indicates one time series without phase shift, and $s_{2i}(\theta_j)$ denotes another time series with a phase shift of θ_j . n is the number of points in the time series. D should have N elements according to the increase of the phase θ , where N is the number of the changes of θ . Therefore, each phase angle θ_j should correspond to one Euclidean distance D_j in the matrix D . The initial phase shift can be obtained by finding the phase angle θ_e which corresponds to the minimal Euclidean distance in the matrix D .

$$D = \{D_1, D_2, \dots, D_j, \dots, D_N\} \text{ Subject to } \theta = \{\theta_1, \theta_2, \dots, \theta_j, \dots, \theta_N\} \quad (4-12)$$

$$[D_{min}, \theta_e] = \text{Min}(D) \quad (4-13)$$

Thus the phase of the time series s_2 can be compensated using the estimated phase angle θ_e to obtain the minimal initial phase shaft compared with the time series s_1 .

4.4.2 Algorithm implementation strategies

According to the flow diagram of the proposed method for analysing the electrical current signal based on dynamic time warping, the approach can be carried out based on the following steps in details.

Step 1: Data Pre-processing

The purpose of data pre-processing is to suppress the inevitable random noise and keep the supply frequency and its sideband components which are used for compressor fault detection. It is carried out by a low-pass filter with a cut-off frequency of 120Hz to remove both the high order harmonics of supply frequency and any random noise originated from measurement and the power supply system. This will ensure that the dynamic time warping and frequency estimations can be implemented reliably.

Step 2: Reference Signal Generation

The reference signal is defined as a sinusoidal signal with the frequency and amplitude calculated from the filtered measured signal. Supposing that the filtered measured signal is $\{x_1, x_2, \dots, x_n\}$, the amplitude of the reference signal is estimated by equation (4-14) to calculate the peak value of the reference signal, as the amplitude of a signal is the peak value of the signal.

$$A_{ref} = \sqrt{2} \sqrt{\frac{1}{n} \sum_n x_n^2} \quad (4-14)$$

The frequency is estimated by the zero-cross detection method [82]. It finds the zero crossing points in a predetermined time interval and counts the number of cycles m that occur in the time interval to obtain the frequency estimation as Equation (4-15).

$$f_{ref} = F_s/m \quad (4-15)$$

where F_s is the sampling frequency. Thus the reference signal can be generated by

$$x_{ref} = A_{ref} \cos(2\pi f_{ref} t) \quad (4-16)$$

In this study, the length of the measured raw signal is 50,000 points and the sampling frequency is 24.3 kHz, which means the frequency resolution is 0.486 Hz and it is sufficient for the frequency estimation. In addition, a low-pass filter is used to restrict the bandwidth of the frequencies close to the supply frequency for accurate estimation. If the frequency estimation is inaccurate, it will affect the suppression of the supply frequency and hence lead to inaccurate dissimilarities extraction in the dynamic time warping process for fault detection and diagnostics.

Step 3: Phase Estimation and Compensation

The initial phase shifts between the measured current signal and the reference signal is estimated based on the method proposed in Section 4.4.1. The estimated phase shift θ_e can be obtained by using Equation (4-13), and hence the reference signal can be modified as Equation (4-17) to have minimal initial phase shift when compared with the filtered measured signal.

$$x_{ref} = A_{ref} \cos(2\pi f_{ref} t + \theta_e) \quad (4-17)$$

Step 4: Window Length Determination

A sliding window is designed to improve the computing efficiency of dynamic time warping implementation. The estimation of the minimum length of the sliding window for dynamic time warping processing can be found by calculating the load fluctuating components which correspond to the working speed of the compressor.

$$L_{min} = Fs/f_c \quad (4-18)$$

where Fs is the sampling frequency. The load fluctuating components can be calculated,

$$f_c = S/(60R) \quad (4-19)$$

where S and R are the speed and transmission ratio of the compressor, respectively. The actual length of the sliding window may be several times the minimal length L_{min} depending on data processing tasks. For benchmarking proposed methods with Fourier transform based methods, the length of the sliding window is set to 3 times L_{min} so that the Fourier transform based results can have a sufficient resolution for sideband feature extraction in the frequency domain [77].

In order to align the reference signal and the filtered measured signal, the length of the reference signal should be the same as that of the sliding window for high efficiency in dynamic time warping implementation and memory allocation.

Step 5: Dynamic time warping Implementation

After designing the reference signal and determining the length of the sliding window, the dynamic time warping algorithm can be applied to process the reference signal and the measured signal selected frame by frame. The two signals are aligned in the time domain after being processed by dynamic time warping, and hence a residual signal can be obtained by subtracting the reference signal from the measured signal. The dissimilarity between the two signals can be shown by the residual signal. As the window is sliding along the measured signal, the dynamic time warping can be implemented efficiently in each sliding window to reveal the differences.

Step 6: Feature Detection

The objective of applying dynamic time warping to process signals is to recognize the differences between the two signals with higher accuracy, and using the residual signal to demonstrate the differences between them. Therefore, the detection can be made through analysis of the residual signal. In the proposed dynamic time warping based method, the RMS values of the residual signal are employed to measure the amplitude of the residual signals. Compared with peak values, the RMS values produce a more reliable feature when the form of amplitude modulation varies under different operating conditions and with fault cases. Obviously, a higher RMS value indicates a greater difference between the reference signal and the measured signal and hence indicates the deviation degree of the signal from the sinusoidal due to the modulation effects under the compressor conditions.

4.5 Faults detection and classification

4.5.1 Dynamic time warping alignment

To separate the fluctuating component from the supply component as accurately as possible in motor current signals, the dynamic time warping approach based on the introduction of a reference signal which has the same frequency contents as the supply power is suggested to be applied to the current signals for the distinguishing of dissimilarities. The introduction of a reference signal is helpful to suppress the supply frequency effectively since it has the same frequency contents as the supply power.

Figure 4-6 shows the interim results of dynamic time warping processing at each key step in a typical sliding window. The measured signal is presented with an initial phase when the data is collected in Figure 4-6(a) and the reference signal is presented with 0 initial phase.

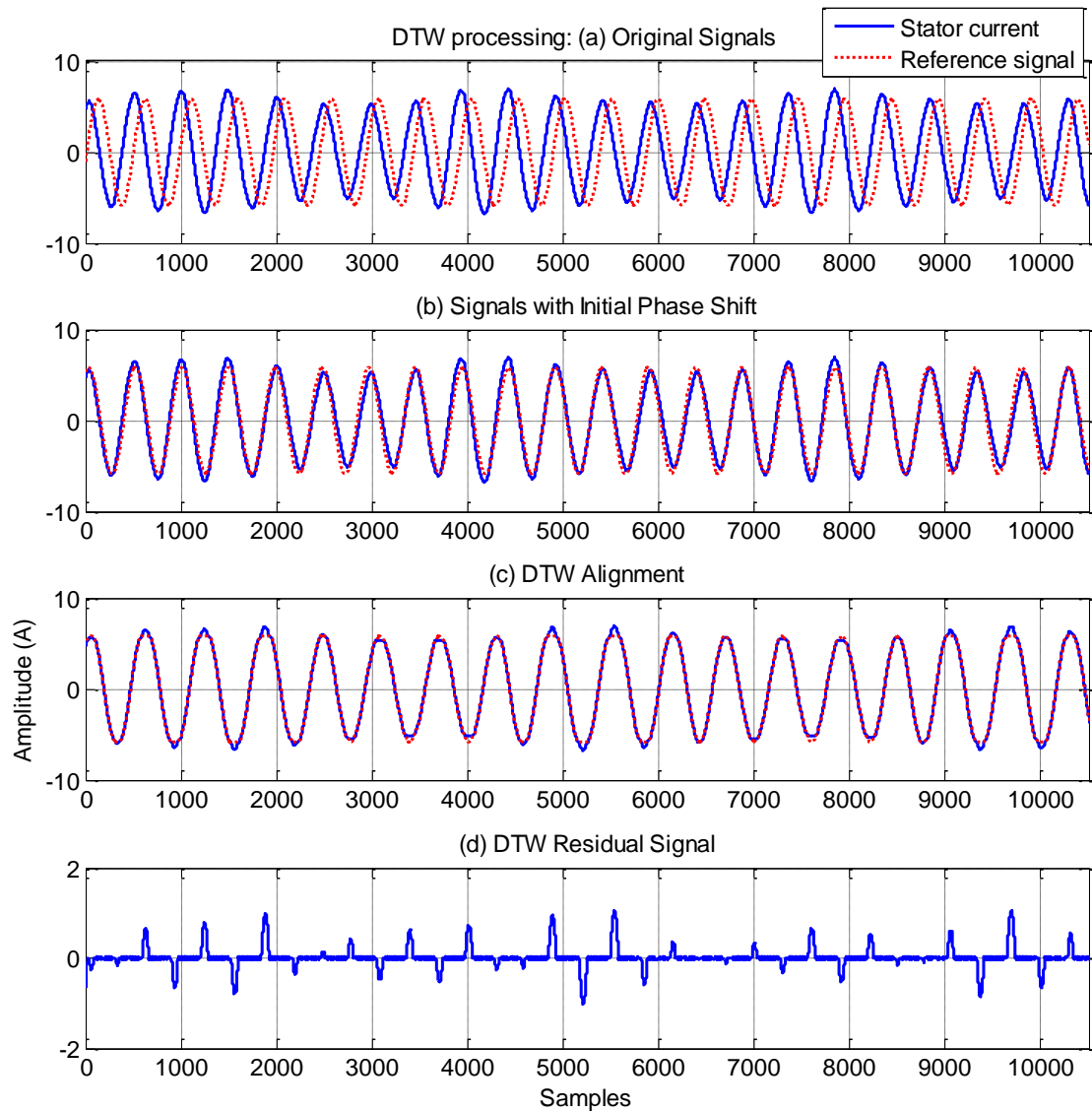


Figure 4-6 DTW processing motor current signal

Obviously, these two signals are greatly shifted from one another and cannot be directly compared. Figure 4-6(b) shows the result after phase compensation on the reference signal through the initial phase matching. It can be seen that the overall

waveforms are better matched, but many detailed portions of the waveform are still not matched sufficiently well enough for comparison. After dynamic time warping processing, the measured signal and reference signal are matched to their optimal values, as shown in Figure 4-6(c) and hence the dissimilarity can be directly revealed by subtraction. The phase estimation and compensation is a low consumption process, and its time-consumption is only 0.5% of the dynamic time warping implementation when the sampling frequency is at 24.3 kHz. Figure 4-6(d) shows the residual signal obtained by the subtraction. The residual signal highlights the major differences between the waveforms shown in Figure 4-6(a) which is around the peak portion of the amplitude modulation when the motor has been applied by higher load during the comprising process, and has the higher effects of mechanical process. As a result of this signal enhancement, a more accurate feature can be extracted from this residual signal.

4.5.2 Feature extraction and fault diagnosis

Using the proposed approach based on dynamic time warping as is presented in Section 4.4. The raw current signals are processed and subtracted by the reference signal to obtain residual signals respective to each case. During processing the sliding window is set to 10,500 points in length so that it includes 3 compressor cycles, allowing for a sufficiently good frequency resolution in Fourier transform based analysis in comparison study. Figure 4-7 presents a typical residual signal obtained by dynamic time warping for the four faulty compressor cases. Comparing the waveforms of residual current signals under different conditions, it can be found that the amplitude of the residual signals' waveform varies with different kinds of faults. The characteristics of the residual signals can be used to indicate the difference between different fault cases.

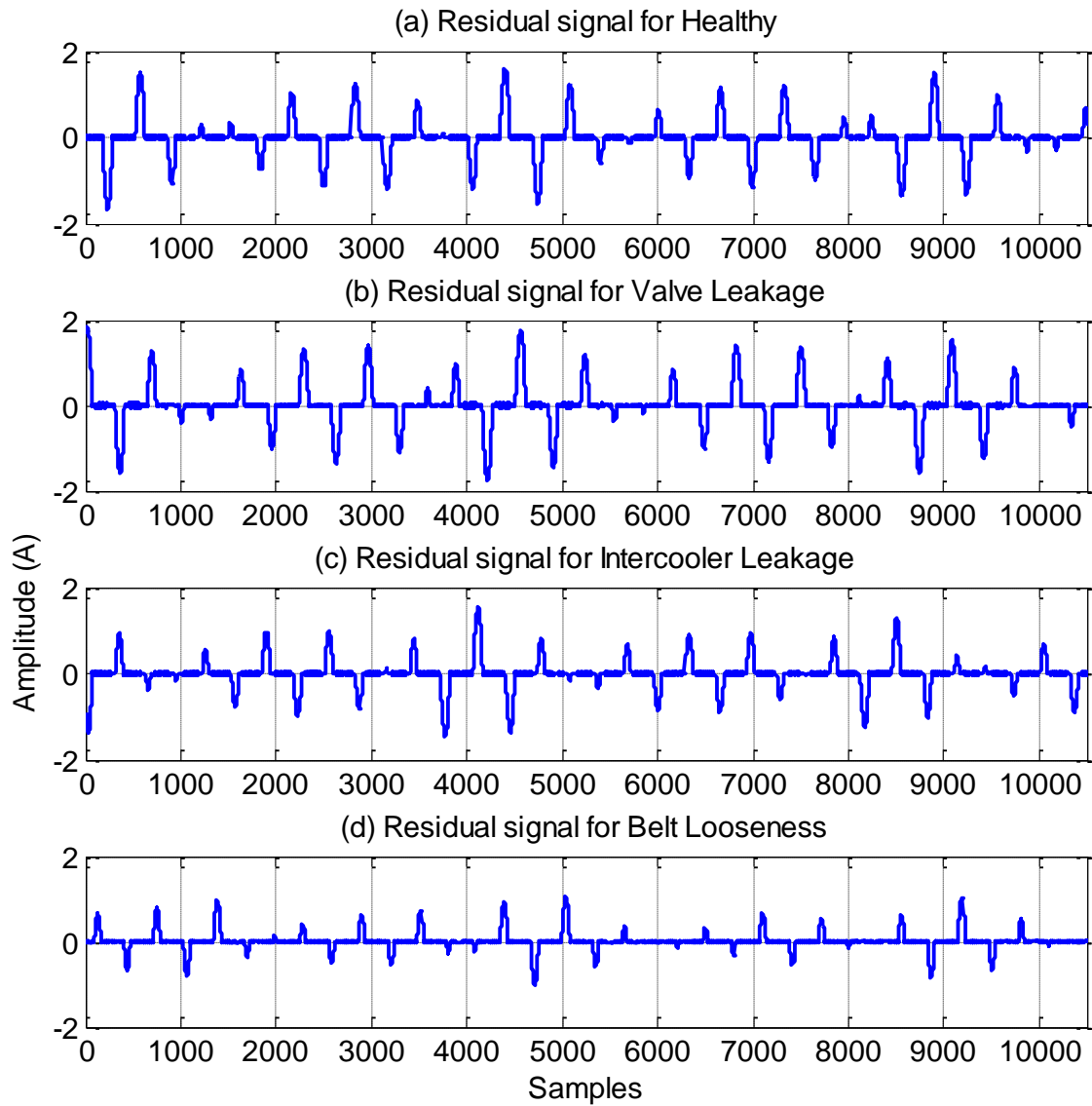


Figure 4-7 Waveforms of residual signals for faulty cases in one sliding window

To quantify these differences for separating these faulty cases, RMS values of residual signal under each fault case are calculated by equation (4-20) for the faults discrimination.

$$RMS = \sqrt{\frac{1}{n}(x_1^2 + x_2^2 + \dots + x_i^2 + \dots + x_n^2)} \quad (4-20)$$

where n is the number of points of the residual signal, x_i is the value of the i^{th} point of the residual signal.

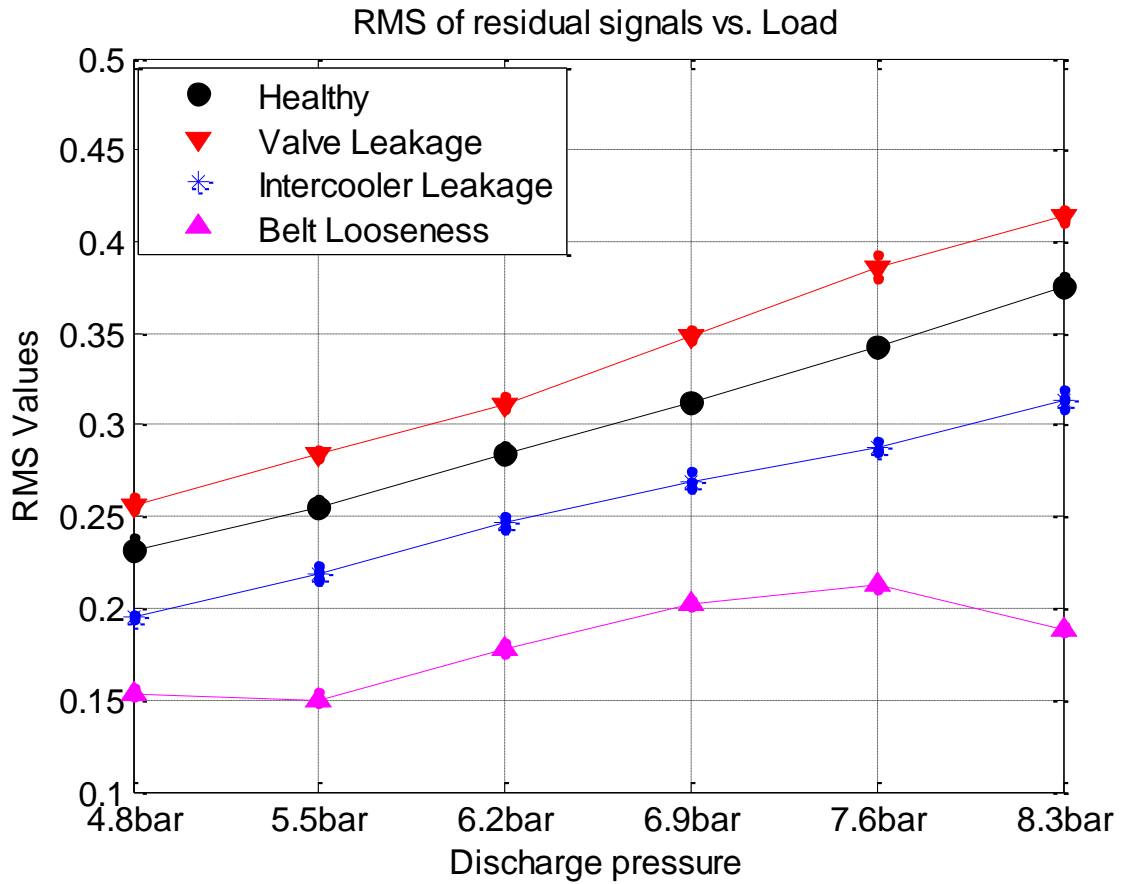


Figure 4-8 DTW residual signal based detection and diagnosis

Figure 4-8 shows the RMS of residual signals at different discharge pressures. It is clear that the RMS values of the residual current signals change with the degree of load oscillation. When the compressor operates at a constant discharge pressure, such as 6.2bar, the RMS values of the residual signals also change with the different kinds of fault cases. It can be seen that the RMS values of the residual signal under the fault of valve leakage is higher than that of healthy condition and the RMS value of the residual signal under the fault of belt looseness is the lowest in the four conditions. The RMS of residual signal falls at higher discharge pressure for the fault of belt looseness. This is because the compressor works on its non-linear working range when the discharge pressure is too higher. When the discharge pressures increase, the RMS values of the residual signals are also increase accordingly under each kind of fault

case. This means that if there is a fault in the compressor, the load fluctuation characteristic will be altered and hence the RMS values and distinctions will be different from those which occur when the compressor is healthy. Based on this analysis, the faults can be detected and diagnosed by an RMS linear classifier in association with the discharge pressures.

4.5.3 Results and discussion

To benchmark the performance of the proposed method, the modulation characteristics of the current signals are analysed by two conventional methods: Fourier transform based spectrum technique which leads to the use of a sideband amplitude as detection feature, and Hilbert transform analysis [83] which produces an envelope level as the detection feature.

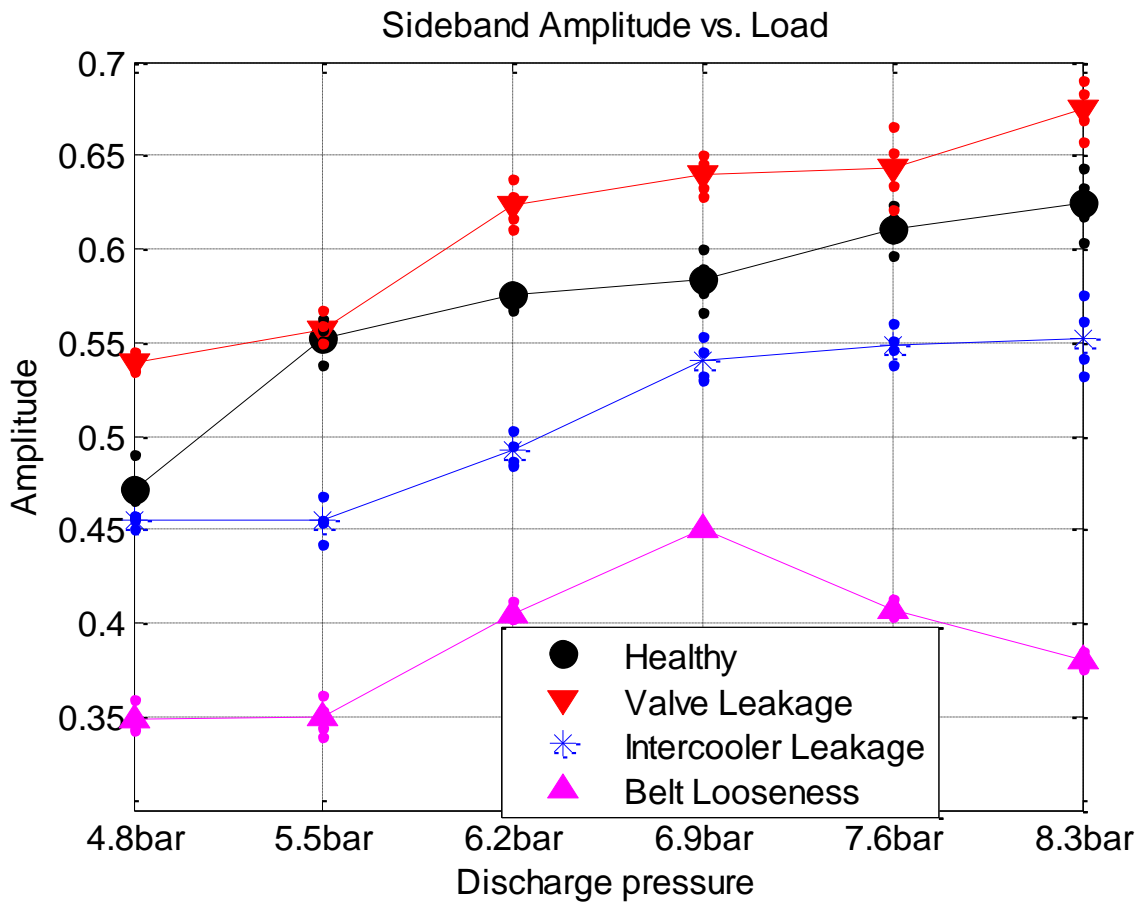


Figure 4-9 Spectrum sideband based detection and diagnosis

In performing Fourier transform calculations a Hanning window is used to reduce the spectral leakage effects. Figure 4-9 shows the results from the spectrum analysis technique. The feature extraction is carried out by extracting the spectral peak values of the sideband components which are used to reveal the differences between different operating conditions. It can be seen that the sideband amplitude is unable to produce full separation results between different fault cases under various loads. Under the discharge pressure of 5.5 bar, the valve leakage cannot be separated from healthy properly, and under the pressure of 7.6 bar, no suitable linear classifier can be used to separate the healthy and valve leakage since the detect results based on sideband analysis have large standard deviation.

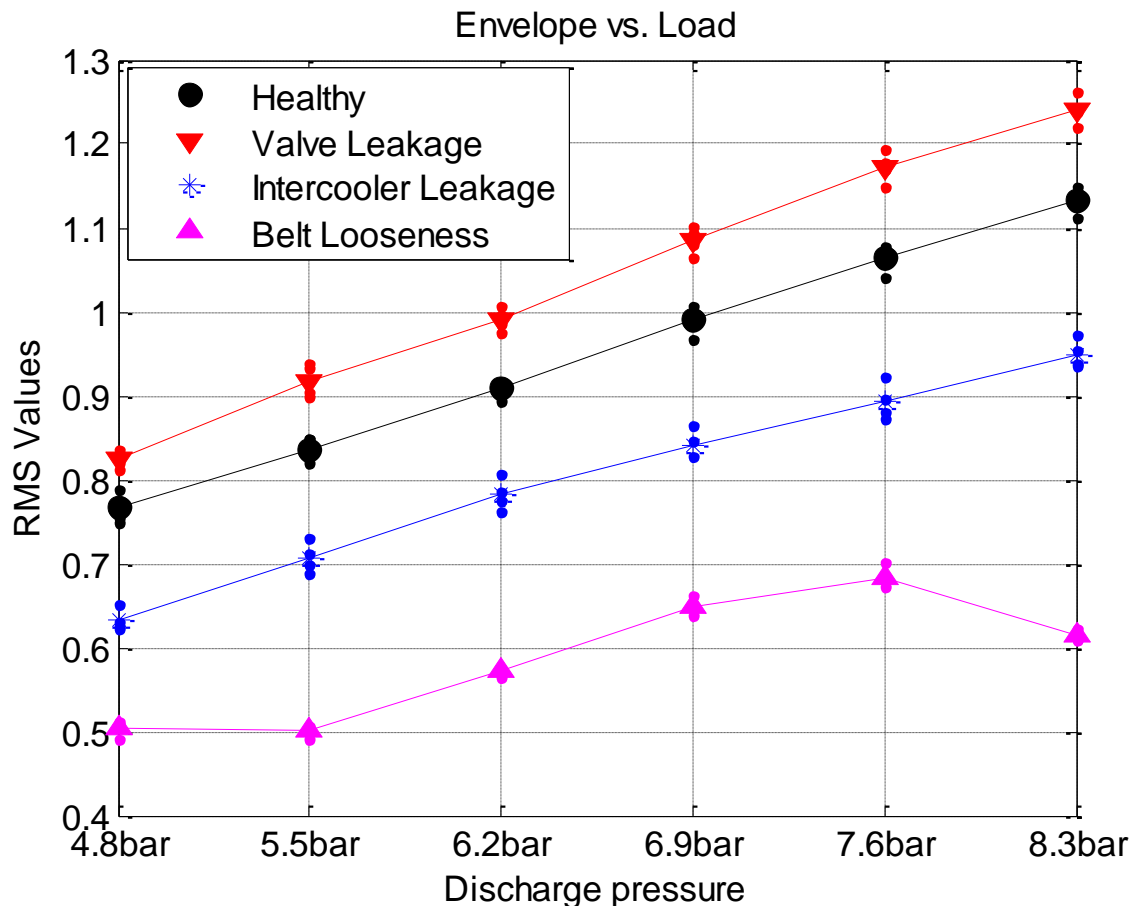


Figure 4-10 Envelope signal based detection and diagnosis

In calculating the envelope, because the main frequency band analysed feature extraction is around the supply frequency which is about 50Hz, a low-pass filter with

the cut-off frequency of 120Hz is applied to process the raw signals to suppress the inevitable noise, and then a fast Fourier transform based Hilbert transform method is used to obtain the envelope signals. Figure 4-10 shows the RMS values of envelope signals for different fault cases under different operating discharge pressures. It shows that the envelope analysis can also allow for full separation between the fault cases under the operating conditions of interest. The overall trend is very similar to that of dynamic time warping results, demonstrating that dynamic time warping is able to capture the modulation characteristics with high accuracy. As the envelope RMS values are calculated in the time domain, spectrum leakage etc may be minimised in these signals.

A careful comparison of Figure 4-10 and Figure 4-8 may also find that the deviation of envelope signals and RMS values is slightly wider than that of dynamic time warping residual RMS values. To make a detailed study, the relative standard deviation (RSD) at each pressure setting for different methods are calculated by

$$RSD = \frac{1}{\bar{x}} \sqrt{\frac{1}{N} \sum_{i=1}^N (x_i - \bar{x})^2} \quad (4-21)$$

where x_i is the RMS value for i^{th} data segment; \bar{x} is the average RMS over different data segments and N is the total segment number. The deviation of average RMS in equation (4-21) removes the influences of pressures on RMS and a comparison of deviations between different methods at each pressure can be compared more accurately.

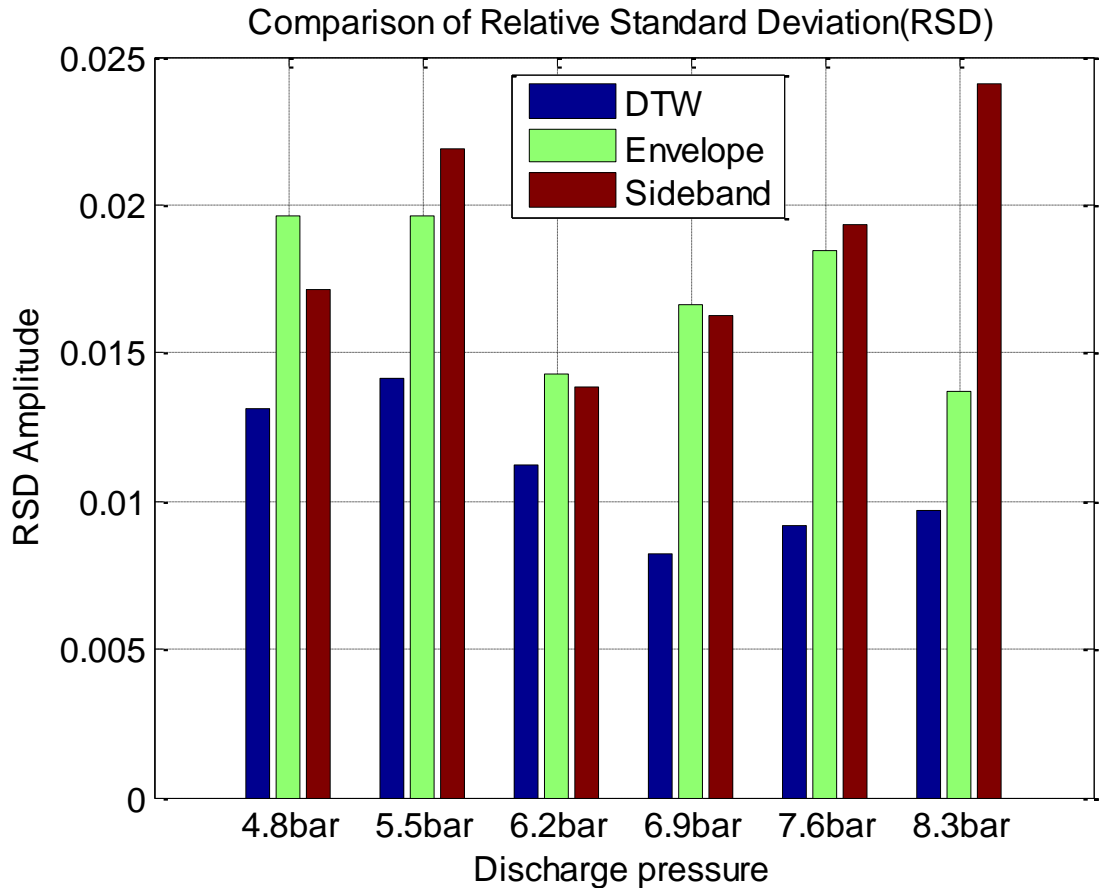


Figure 4-11 Comparison of standard deviation for three analysis techniques

Figure 4-11 shows relative standard deviation values for the three methods under different pressures. It was found that the standard deviation for dynamic time warping is the smallest, compared with the other two methods. It shows that dynamic time warping is less sensitive to noise influences and is able to produce repeatable results. It also means that the dynamic time warping method can differentiate smaller changes for earlier fault detection and diagnosis. Dynamic time warping can produce more accurate and reliable diagnostic results and be evaluated by numerous experimental studies.

This work concludes that the analysis of electrical current signals based on the dynamic time warping method has the significant potential to detect and identify the presence of incipient faults in motor driven machines. The results show that the sideband components in the current signals can be extracted through dynamic time

warping with the introduction of a reference signal of the same frequency to the supply power, this leads to a residual signal that contains mainly the sideband contents. This residual signal is then further analysed to obtain accurate and reliable features of the current signals measured under different conditions. Based on the analysis, the RMS value is developed to diagnose common compressor faults including valve leakage, intercooler leakage and belt looseness. The analysis results indicate that the dynamic time warping method can be employed to extract accurate features from the current signals and the RMS values of the residual signals can be used to differentiate the faulty from the healthy and identify the difference between other faulty cases under various loads of discharge pressures. The accuracy and reliability of detection and classification from dynamic time warping analysis is higher than that from Fourier transform spectrum and envelope analysis. The dynamic time warping processing procedure, based entirely on the time domain analysis (see Section 2.3), is easier to apply in real-time monitoring processes since it distinguishes the faults based on single value indicator, and the time cost of the algorithm can be improved by reducing the length of the sliding window.

The weak non-stationary or cyclostationary signal, as well as electrical motor current signal, was analysed using the proposed dynamic time warping based method for the condition monitoring and fault diagnosis of a two-stage reciprocating compressor. The results show the accuracy and reliability of detection and classification from the proposed dynamic time warping analysis is higher than those of Fourier transform spectrum and envelope analysis because of the results from dynamic time warping has smallest standard deviation and less sensitive to noise influences. In the following chapter 5, 6, 7, and 8, the typical strong non-stationary signals, take engine vibration and acoustics as an example, are analysed using various signal processing methods for diesel engine condition monitoring and combustion diagnosis.

CHAPTER 5

THE CHARACTERISTICS OF VIBRO- ACOUSTIC SIGNALS FROM INTERNAL COMBUSTION ENGINES

This chapter discusses the characteristics and specifications of the test engine and gives a brief description of the test rig, instrumentation and test procedures. Firstly, the engine vibration and noise characteristics from the measured vibration and acoustic signals are investigated using the time domain statistical and frequency spectral analysis methods. Secondly, the influence of room acoustics on the measurements is considered for spectral analysis. Finally, fuel monitoring is investigated based on engine noise analysis. It can be concluded that the engine's acoustic signals are easily polluted by the room modes in the lower frequency band, (below 1 kHz) and that accurate or better monitoring results can be obtained through analysing the engine acoustic signals in the higher frequency band.

5.1 Introduction to engine acoustics

The study of engine acoustics has been carried out since the early stages of engine development. The relationship between the rise of the combustion pressure and the noise produced by the engine was described by Ricardo in 1931 [84]. There are a number of engine acoustics sources, which can be divided into two categories: airborne acoustics and structure borne acoustics [85]. Airborne acoustics generated by systems and mechanisms travels through several transmission paths, whereas structure acoustics refers to noise generated by vibrations induced in the structure itself. These vibrations excite the engine surfaces and cause it to radiate noise.

The radiated noise levels from diesel engines can be affected by a variety of factors such as the engine type, the structure specifications and the operating conditions [86]. Although many previous works have provided noise level prediction criteria and design fundamentals [87][88], most of them are based on specific diesel engines. As a result, the effectiveness in predicting radiated noise levels for other engines is limited as a result of vast differences between both the specifications and working principles of different engines [7].

The objective of this chapter is to investigate the characteristics of engine noise in the time and frequency domains by employing some statistical methods such as RMS, standard deviation and finding the mean [1]. These methods are easy to interpret and implement in monitoring the conditions of the engine and give quick detection results. These features are usually called time-domain features. The frequency domain analysis of acoustic signals is another useful method in identifying and isolating the dominant components and their corresponding harmonics of interest. The aim of spectral analysis is to look at either the spectrum in its entirety or to look closely at certain frequency components of interest and thus extract features from the signal [89–91]. Here frequency domain analysis is used to reveal the dominant frequency bands which contribute to engine noise levels.

5.2 Engine test facilities and setup

The test facilities and instruments are presented in this section, particularly the test engine specification, the acoustic instruments and the data acquisition system. The test engine is one of the most commonly used heavy-duty vehicle engines, and for this research, it is equipped with specific purpose mufflers or sound insulators whose aim is to simulate the engine's working conditions as accurately as possible. Various transducers and instrumentations capable of collecting some common types of signals for general analysis purposes are mounted on the test rig. In addition, the eigenfrequencies of the test engine room are calculated based on the room acoustics theory for analyzing acoustic signals.

5.2.1 The test engine specification

The engine used for this research is a four-cylinder, four-stroke, turbocharged direct injection engine with a bore of 103 mm, a stroke of 132 mm, a displacement of 4.4 litre and a compression ratio of 18.3 [92]. Figure 5-1 shows an overview of the test rig. The major specifications of the engine are described in table 5-1.

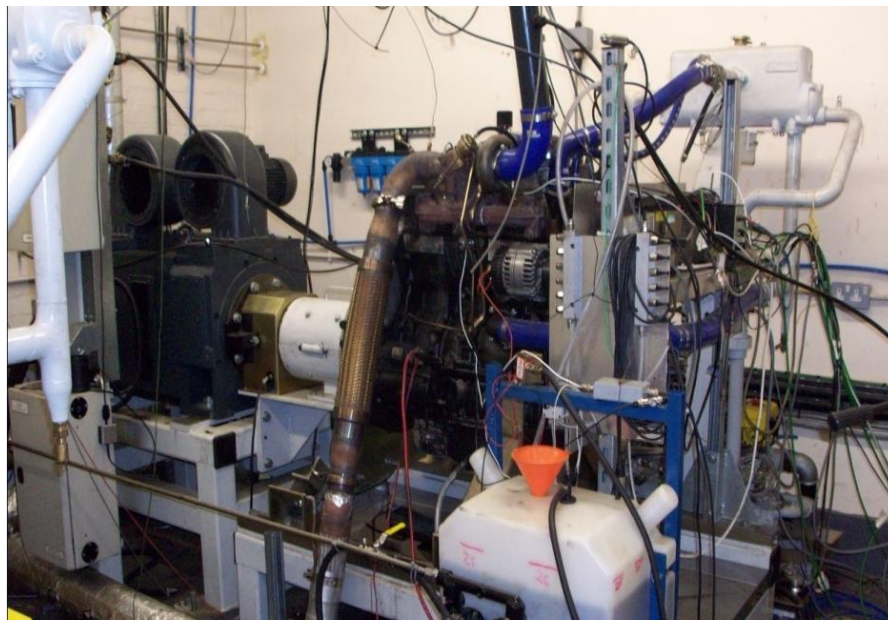


Figure 5-1 The test rig photo

Table 5-1 give only a limited number of the engine’s specifications, but more details are given in the service manual of the JCB444 T2 Diesel Engine. The test engine is placed in an engine test room with the size of 4.8m*4.2m*2.8m.

Table 5-1 Specifications of the test engine

Technical parameters	Technical data
Maker	JCB Power Systems Ltd.
Engine type	Turbocharged diesel engine
Number of cylinders	4
Firing order	1-3-4-2
Bore	103mm
Stroke	132mm
Inlet valve diameter	36.5mm
Exhaust valve diameter	33.2mm
Compressor inlet diameter	60mm
Compressor outlet diameter	60mm
Turbine inlet diameter	100mm
Turbine outlet diameter	80mm
Compression ratio	18.3:1
Number of valves	16
Injection system	Direct injection
Displacement	4.399 litre
Cooling system	Water
Speed range	850-2200 rpm
Recommended speed	850 rpm
Maximum torque	425 N m @ 1300 rpm
Maximum power	74.2 kW @ 2200 rpm

The test engine is controlled by a CP Cadet V12 Control and Data logging System. CADETV12 is an advanced, fully integrated, Windows 200-XP based engine vehicle test system. The CADETV12 has multistage environment support, full Network support using Windows 200-XP, user configurable-screen layout, a visual basic 6.0 programmer interface and control at up to 320Hz on 16 PIDS. It is integrated with high speed data acquisition (cylinder combustion analysis), engine management and control system (EMACS) and full vehicle simulation using AC or DC. The transient conditions are controlled by six of the PID loops. The outputs from the transducers are sent to the control room where the data acquisition equipment and the operating computer are located.

5.2.2 Measurement instrumentation

To obtain accurate engine test data for diesel engine condition monitoring and diagnosis techniques, the engine test system was carefully set up allowing the engine cylinder pressure variation and the changes of the engine vibration and noise under different operating conditions to be monitored.

Figure 5-3 shows the schematic diagram for the test rig and the measurement equipment used in this work. Various transducers have been installed on the test rig in order to collect the operating parameters of the engine, namely: engine noise, engine vibration, in-cylinder pressure and engine speed. These signals were collected by the following main transducers:

- Microphone
- Accelerometer
- Pressure transducer

The cylinder pressure signal is used to judge the combustion conditions of the monitored cylinder under different engine conditions. Otherwise, a magnetic pickup was used to measure the speed of the engine via the gear teeth on the flywheel. An optical encoder was also connected to the crankshaft to provide a trigger pulse once per revolution in order to synchronise data collection. A load cell was attached to the dynamometer to measure the load applied to the engine.

1. Acoustic instrumentation

The acoustic signals are measured by using BAST's microphone system composing of an electrets microphone CHZ-211 and a preamplifier YG-201. Figure 5-2 shows photos of both the microphone and the preamplifier. Tables 5-2 and 5-3 list the main specifications of the microphone and its preamplifier, respectively.

From the table it can be seen that the frequency responses of the microphone and its preamplifier are determined by the electrets microphone which has a range of up to 20 kHz. The higher frequency band can still be used for the response, drops by only a few

decibels for signals over 20 kHz with the CHZ-211 microphones in comparison with its normal response range.



(a) Microphones

(b) Preamplifier

Figure 5-2 Microphones and preamplifier

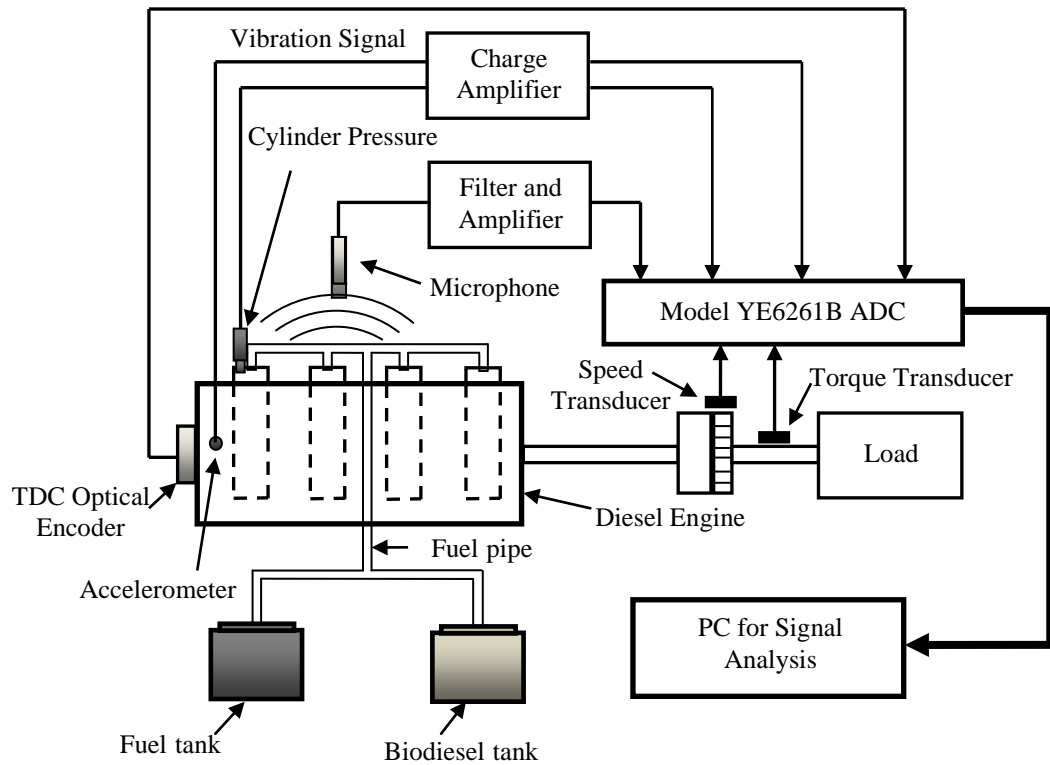


Figure 5-3 Schematic diagram of the engine test system

Table 5-2 Specification of the microphone CHZ-211

Items	Microphone CHZ-211
Sensitivity	-26±1.5dB (50mV/Pa)
Frequency response (Ref. 250Hz)	6.3Hz~20kHz (±2dB)
Sound field	Free sound field
Polarization voltage	0V
Safety limited	< 146dB
Background noise level	< 16dB
Operating temperature	-40°C~+80°C
Operating humidity	0~98 (RH, %)
Outer diameter	12.7mm
Height	17.2mm

Table 5-3 Specification of the preamplifier

Items	Preamplifier YG-201
Power supply	4mA current source
Frequency response (Ref. 250Hz)	10Hz~110kHz (±0.2dB)
Attenuation	0.3dB
Input impedance	5GΩ
Output impedance	< 100Ω
Maximum output voltages	5V
Operating temperature	-40°C~+80°C
Operating humidity	0~98 (RH, %)
Background noise level	< 7.0 uV
Length	70mm
Diameter	12.7mm

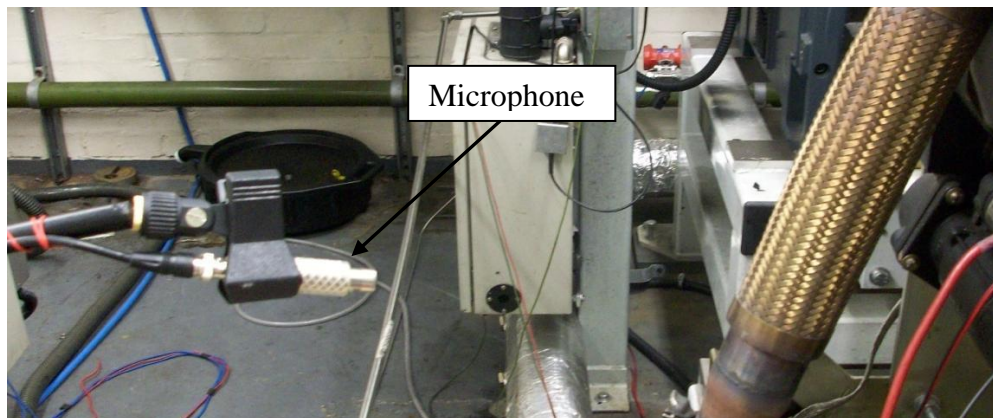


Figure 5-4 Microphone used for measuring the acoustic signals

In the test, two microphone systems are used to collect the acoustic signals generated by the engine at positions close to the engine body and the exhaust pipe respectively, at

a distance of approximately 500mm from the engine's surface and approximately 1000mm from the ground. Figure 5-4 shows one of the microphones measuring the acoustic signals produced by the engine.

2. Vibration accelerometers

Accelerometers are a widely used device for measuring the vibration of rotating machinery, and have been used extensively in machinery monitoring applications [8]. Accelerometers are rugged, compact, light-weight transducers with a wide frequency response range. The accelerometer is typically attached to the outer surface of machinery for measuring the vibration of the body or structure to which it is attached. In this research, a piezoelectric accelerometer (model CA-YD-104T) is used to measure the vibration of the test engine. Figure 5-5 shows the installation of the accelerometer in the test rig. Its technical specifications are shown in Table 5-4.

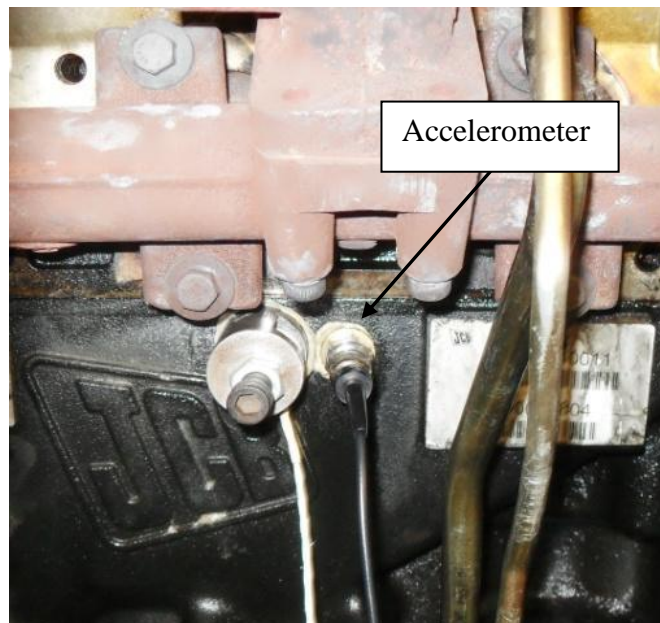


Figure 5-5 Vibration accelerometer

3. Pressure sensor

The in-cylinder combustion pressure was measured by a General Electric 4000 series pressure sensor as shown in Figure 5-6. The sensor was fixed in the combustion

chamber of cylinder number 1. The transducer has a combination of high accuracy, high overload, excellent stability and a fast dynamic response. Its operating pressure range is between 700 mbar and 700 bar gauge. It has also been specifically designed to work at high temperatures for precision measurement in internal combustion engines.

Table 5-4 Technical specification of the accelerometer

Axial sensitivity (20±5°C)	35 pC/g
Transverse sensitivity	≤ 5%
Frequency range 5%	1 to 7 kHz
Mounting resonance frequency	20kHz
Temperature effect	Refer to the temperature
Polarity	Positive direction
Isolation resistance capacitance	> 109Ω 1200 pF
Operating temperature range	-20 to + 120°C
Shock limit (± peak)	2000g
Magnetic sensitivity	2 g/T
Base strain sensitivity	0.1 g/με
Weight	33g

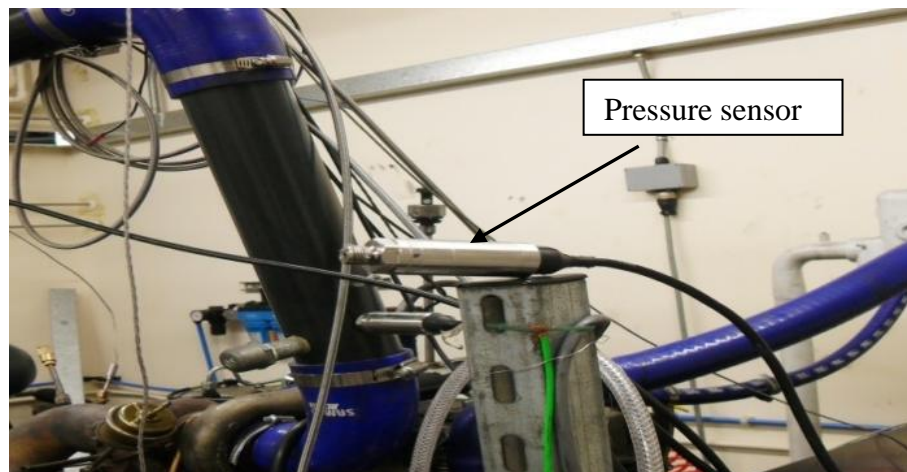


Figure 5-6 Pressure sensor

5.2.3 Data acquisition system

All the signals collected from the test rigs needed to be converted from the original analogue form to digital, and detailed analysis using a personal computer needed to take place. This can be achieved through the use of a data acquisition system.

The data acquisition system is based on a Sinocera Model YE6261B dynamic data acquisition unit. The Model YE6261B has 32 channels each with 16 bit resolution, synchronized acquisition at 100 kHz per channel, an IEEE 1394 interface, and selectable signal conditioners as can be seen in Figure 5-7. This type of data acquisition is adequate for monitoring vibration and acoustic signals as its high sampling frequency which is sufficient for keeping the key information of original analog signal during the analog-to-digital conversion.



Figure 5-7 Data acquisition equipment (model YE6261B)

5.2.4 Test procedures

Testing was carried out on the JCB444 test engine. The data was collected using related transducers for future analysis. Three accelerometers were mounted on the engine body, the exhaust pipe and the cylinder head in order to measure the vibration of the test engine in different locations to investigate the contribution of engine vibration from different engine parts to the engine acoustics. Two microphones were

installed close to the engine body and exhaust pipe in order to measure the engine noise and the pressure sensors were placed on the cylinder head. In order to compare the collected data and to perform the time domain or angular domain average of the signals, a reference point was obtained by using an optimal encoder connected to the crankshaft (at the engine's front) by a rubber rube.

For comparison purposes raw signals were collected from the sensors under normal operating conditions, meaning the engine was running without any induced faults. The engine ran under various loads and speeds supplied by diesel and biodiesel, respectively.

Table 5-5 Test operating setup-1

Fuel	Speed (rpm)	Load (N m)
Pure Diesel	1000, 1500	0, 100, 200, 300, 400
B25	1000, 1500	0, 100, 200, 300, 400
B50	1000, 1500	0, 100, 200, 300, 400
B100	1000, 1500	0, 100, 200, 300, 400

Table 5-6 Test operating setup-2

Fuel	Speed (rpm)	Load (N m)
Pure Diesel	900, 1100, 1300	105, 210, 315, 420
B50	900, 1100, 1300	105, 210, 315, 420
B100	900, 1100, 1300	105, 210, 315, 420

In the experiment, the test engine was tested with range of blends and operated at different loads and speeds in two operating setups as shown in Tables 5-5 and 5-6. In the first operating setup, for the speed and load variation, the engine was running at one of the two speeds of 1000rpm and 1500rpm, a series of loads were applied at each speed: 0, 100, 200, 300 and 400 N m. The engine was otherwise supplied by diesel and biodiesel with 25%, 50% and 100% respectively, as is shown in Table 5-5. In the second operating setup, the test engine operated at the constant speeds of 900rpm,

1100rpm and 1300rpm with loads from 105N m to 420N m with an interval of 105N m at each constant speed. The details of the operating conditions are given in Table 5-6. The test engine was fuelled with rapeseed oil (B50 and B100) as well as normal pure diesel. B50 represents the mixture of 50% rapeseed oil and 50% diesel, whereas B100 is 100% rapeseed oil. The rapeseed biodiesel is produced by a transesterification process from ‘virgin’ oil using methanol. The main physical properties such as the composition, density, lower heating value (LHV) and viscosity are presented in Table 5-7 [93].

Table 5-7 Properties of biodiesel [93]

Property	Units	Measured
Composition	% C	77
	% H	12
	% O	11
Density	Kg/m ³	879
LHV, KJ/Kg	MJ/Kg	38.5
Kinematic Viscosity	mm ² /s	4.9

5.3 The characteristics of engine noise and vibration

5.3.1 The time domain statistics of engine acoustics and vibration

The sound pressure level (SPL) is commonly used to indicate noise levels - it is derived from the RMS value of the acoustic pressure (see appendix). According to the definitions of sound energy and sound intensity, all are calculated based on the sound pressure. The sound pressure level can therefore be used to reflect the noise energy level. Although the sound pressure level is only a single value, rather than the overall noise level, it can still be used to compare the noise level changes under different conditions.

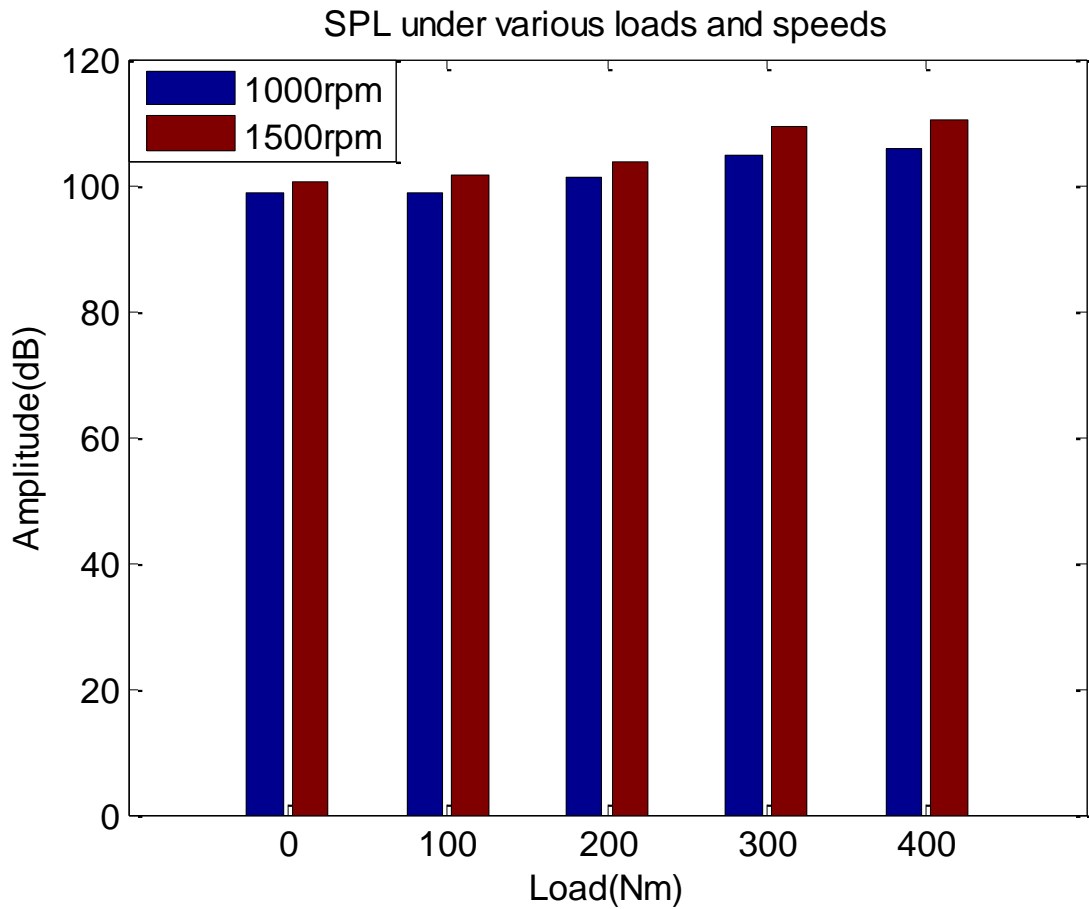


Figure 5-8 SPL comparisons under different operating conditions

Figure 5-8 shows variations of sound pressure level with respect to five different loads and two different speeds. It can be seen that as the engine loads and speeds increased, so too sound pressure level did. At 1000rpm, the difference between the minimum load and maximum load is about 7dB, and at 1500rpm, the difference is about 9.8dB. It can therefore be concluded that speeds and loads have significant influence on the measured sound levels, and the increase in sound pressure level with speed is more obvious than that of the load as can be seen in Figure 5-9.

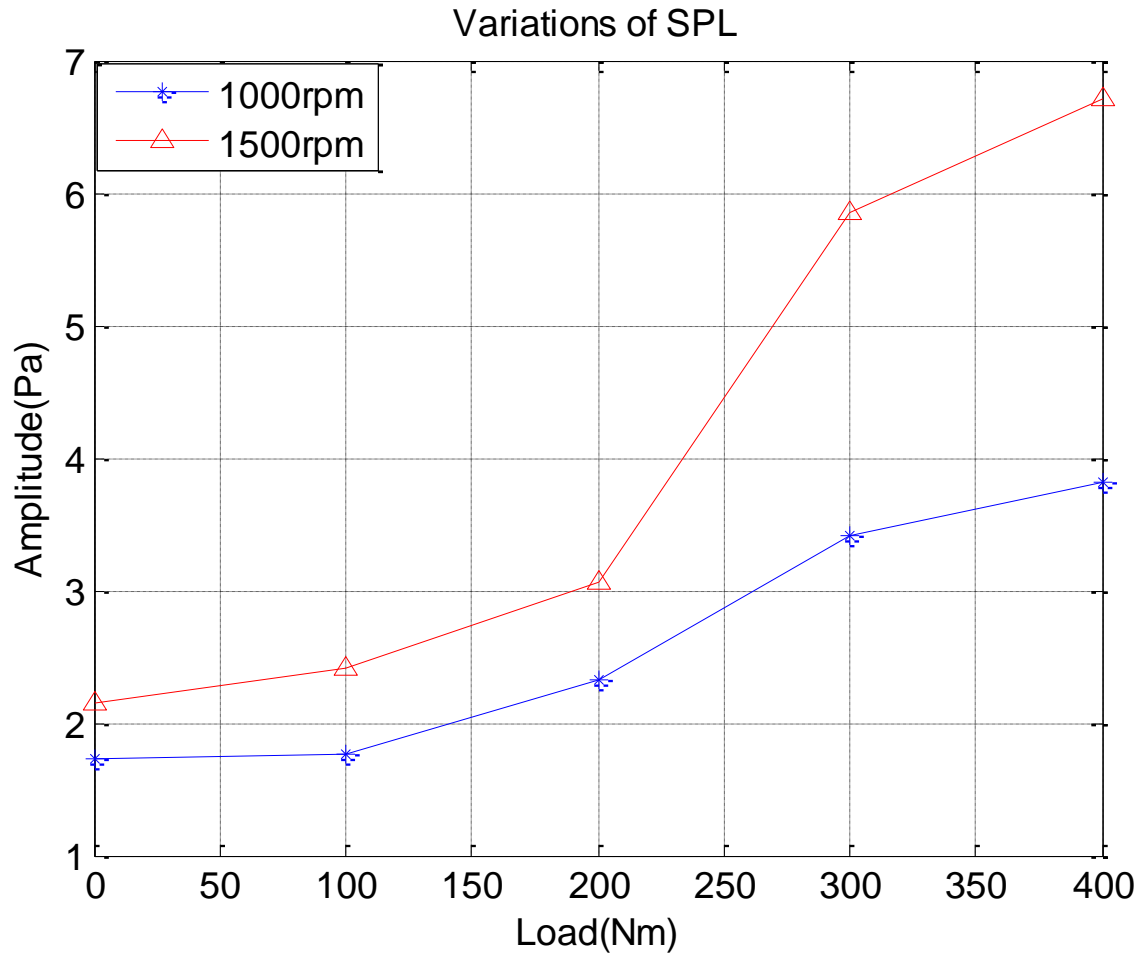


Figure 5-9 Variations of SPL versus speed and load

Figure 5-10 shows the acoustic signals of the test engine operating under the loads of 0, 100, 200, 300, and 400 N m, and a speed of 1000rpm and 1500rpm in the angular domain respectively. The results are presented based on two complete combustion cycles (1440°) [13]. Angular domain is a simple and fundamental way of presenting data, which shows the peak or RMS level of the signal which can then be used to identify changes under different engine conditions. As seen in Figure 5-10, it is clear that, with the increasing of the load at a certain speed, such as 1000rpm, the amplitudes of the acoustic signals increase correspondingly and the difference in amplitudes is obvious. The higher amplitudes represent higher sound levels as are depicted in Figure 5-8. Similarly, at a certain load, as the engine speed increases, so too does the amplitude of the acoustic signal. As the load increases the temporal pattern becomes

more obvious. There are four cyclic pattern of acoustic in every 720 degree when engine running two cyclic. At 300 N m and 400 N m the cyclic pattern of the sound is clearer than that under lower load.

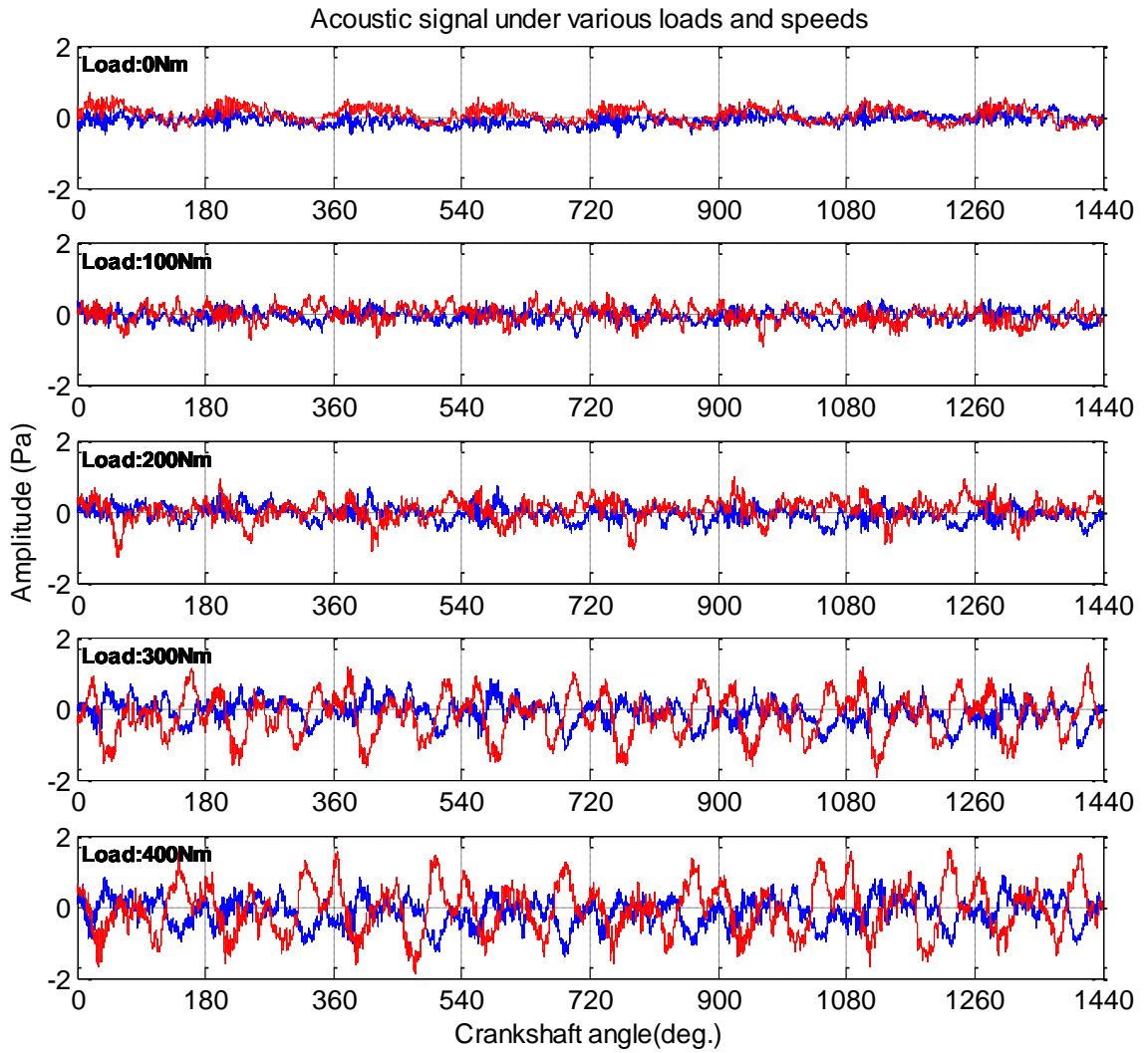


Figure 5-10 Raw acoustic signals under various loads and speeds
—: 1000rpm, - - - : 1500rpm

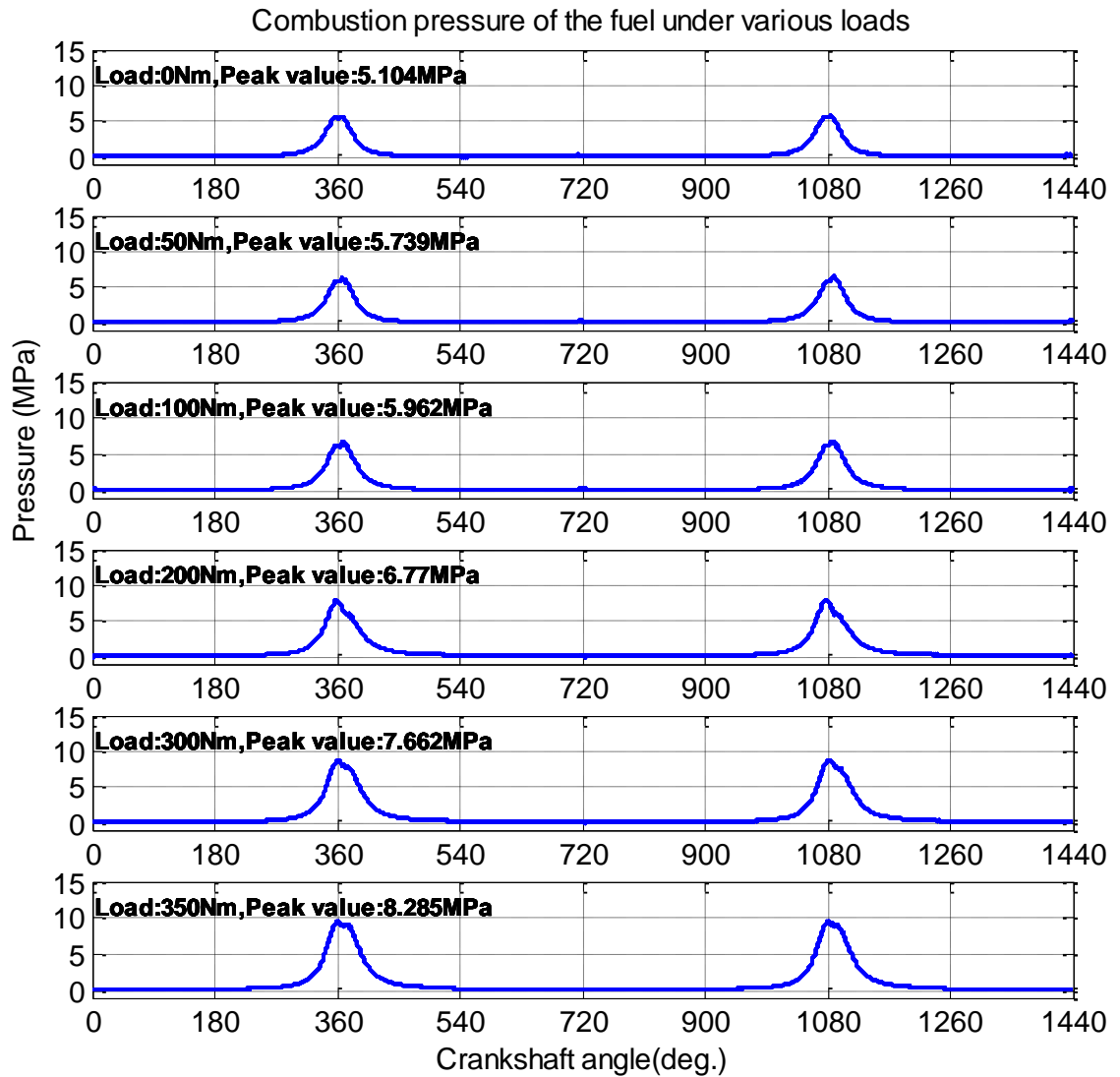


Figure 5-11 Combustion pressure under various loads

The additional excitation which increases the level of the acoustic signal is due to the higher combustion pressure of the fuel at higher loads and higher speeds. As shown in Figure 5-11, as the engine loads increase, so too does the amplitude of the in-cylinder pressure, from 5.104MPa at load of 0 N m to 8.258MPa at load of 350 N m.

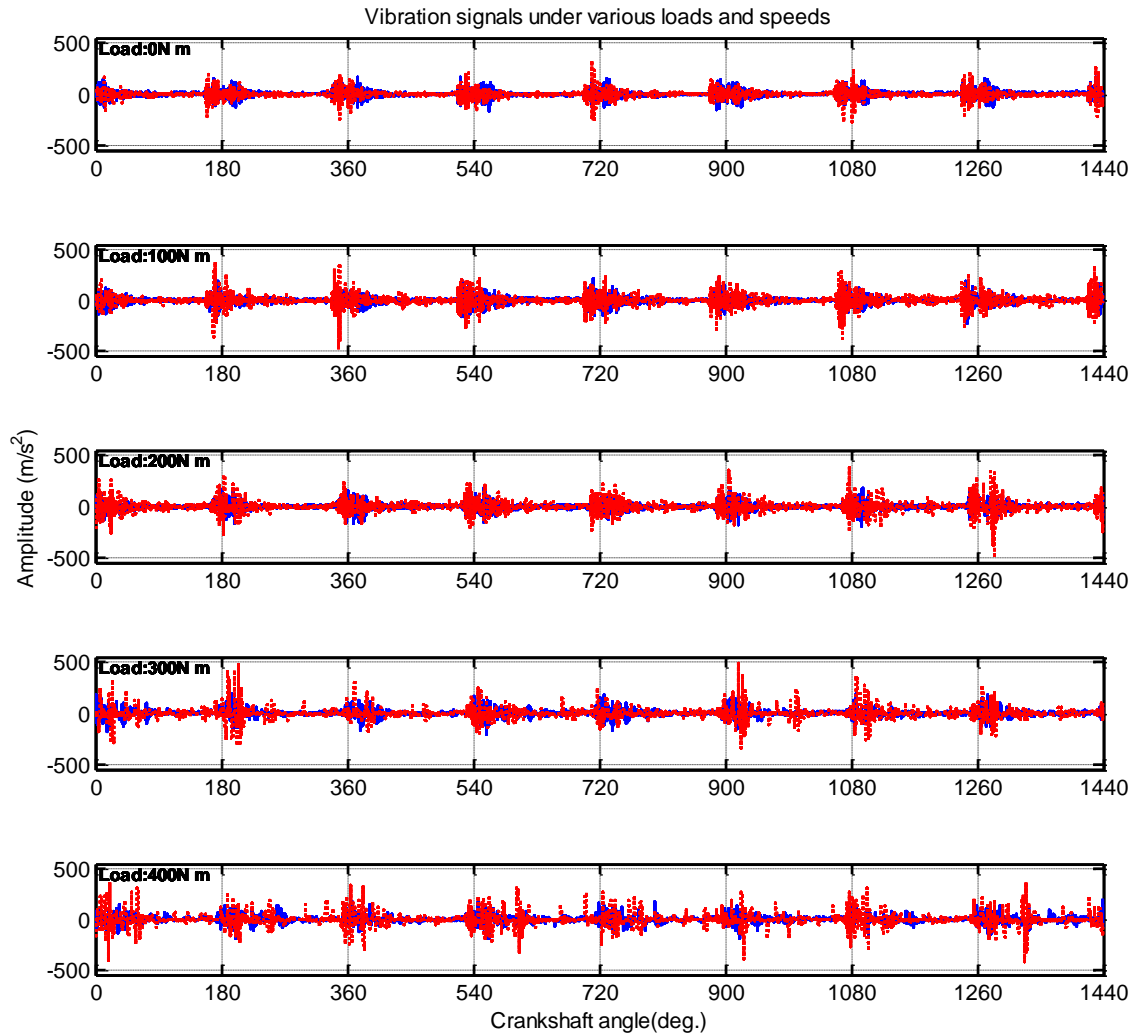


Figure 5-12 Raw vibration signals under various loads and speeds
— : 1000rpm, - - - : 1500rpm

Another additional excitation that increases the level of the acoustic signals comes as a result of the higher vibration of the engine. The higher the engine's vibration, the stronger the sound source and the more acoustic energy is radiated. Figure 5-12 shows the raw vibration signals from the engine under loads of 0, 100, 200, 300, and 400N m, and at speeds of 1000rpm and 1500rpm. It can be seen that as the speed and the engine loads increase, so too did the amplitude of the vibration from the engine. Figure 5-13 shows the RMS of the raw vibration signals from the test engine at various loads and speeds. It shows the clear trend according to the changes in the loads and speeds.

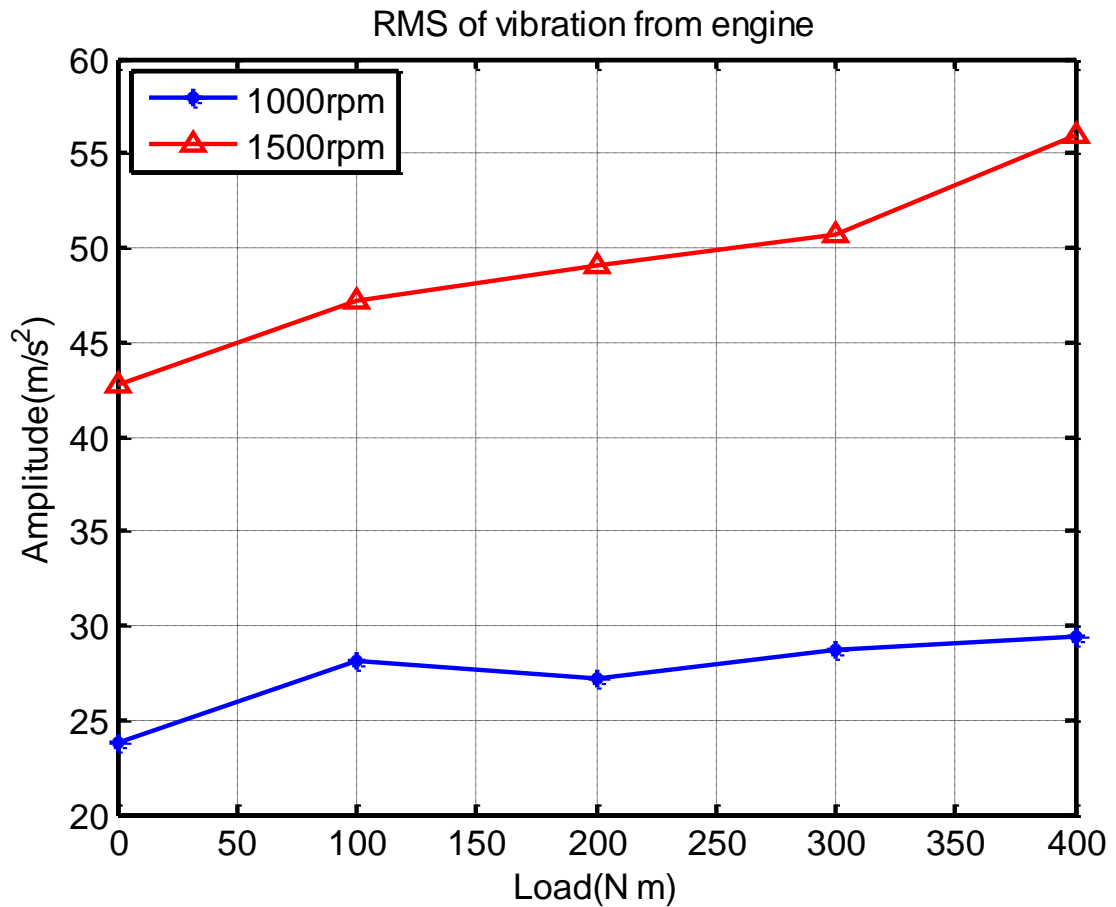


Figure 5-13 RMS of the raw vibration signals from the test engine

5.3.2 Spectrum analysis of engine acoustics and vibration

Frequency domain analysis gives spectral information of the engine acoustic signals by transforming the signal from the time domain into the frequency domain. Frequency analysis techniques have been widely used in most engine condition monitoring research, and it is an effective method for showing the differences between frequency components from the raw signals obtained under different operating conditions. Here, the obvious characteristic in the spectrum is the firing frequency and its harmonics of various loads and speeds. The acoustic energy is predominantly located in the low frequency range [20], the frequency analysis is therefore focused on the low frequency.

Figure 5-14 shows the spectrum of the engine acoustic signal with speeds of 1000rpm and 1500rpm respectively. It reveals that when the speed increases, the sound pressure

level increases accordingly. Major sound energy is located under lower frequency bands of about 3 kHz in both speeds conditions.

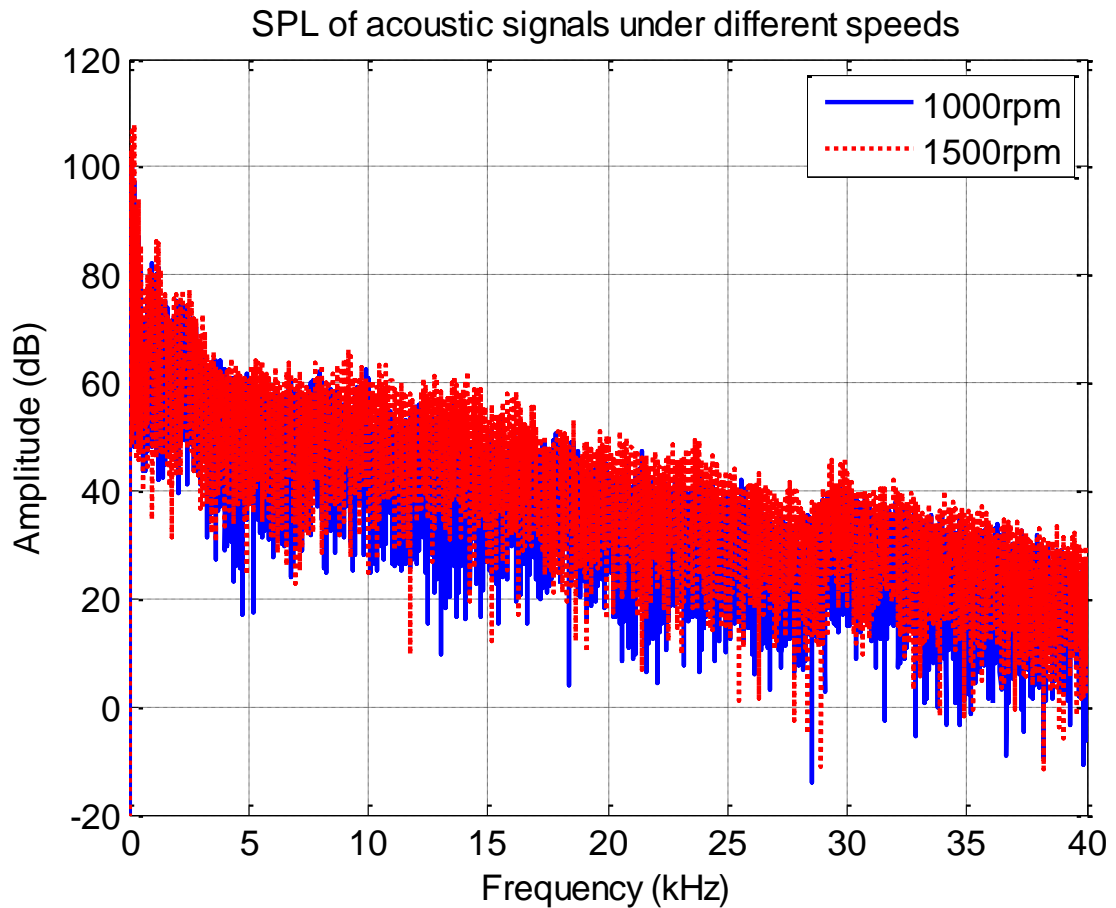


Figure 5-14 Spectrum of acoustic signals under different speeds

The firing frequencies corresponding to the rotation speeds are approximately 33Hz at a speed of 1000rpm, and about 50Hz at 1500rpm. The spectrum of the engine acoustic signals under various loads and speeds are shown in Figure 5-15. It can be seen that when the engine operates at a speed of 1000rpm, the major frequency components of the acoustic signals are the firing frequency 33Hz and its harmonics. As the loads increase from 0N m to 400N m, the amplitudes of these frequency components increase as well, and the variation are similar when the speed is 1500rpm. When the load of the engine is unchanged, for example, at the load of 300N m and 400N m as shown in Figure 5-15, the speed increases from 1000rpm to 1500rpm, the amplitudes

of the firing frequencies and their harmonics increase accordingly. This demonstrates that the speeds and loads of the engine can affect the amplitudes of the firing frequencies and their harmonics. It also shows that speed and load have a significant influence on the measured sound levels.

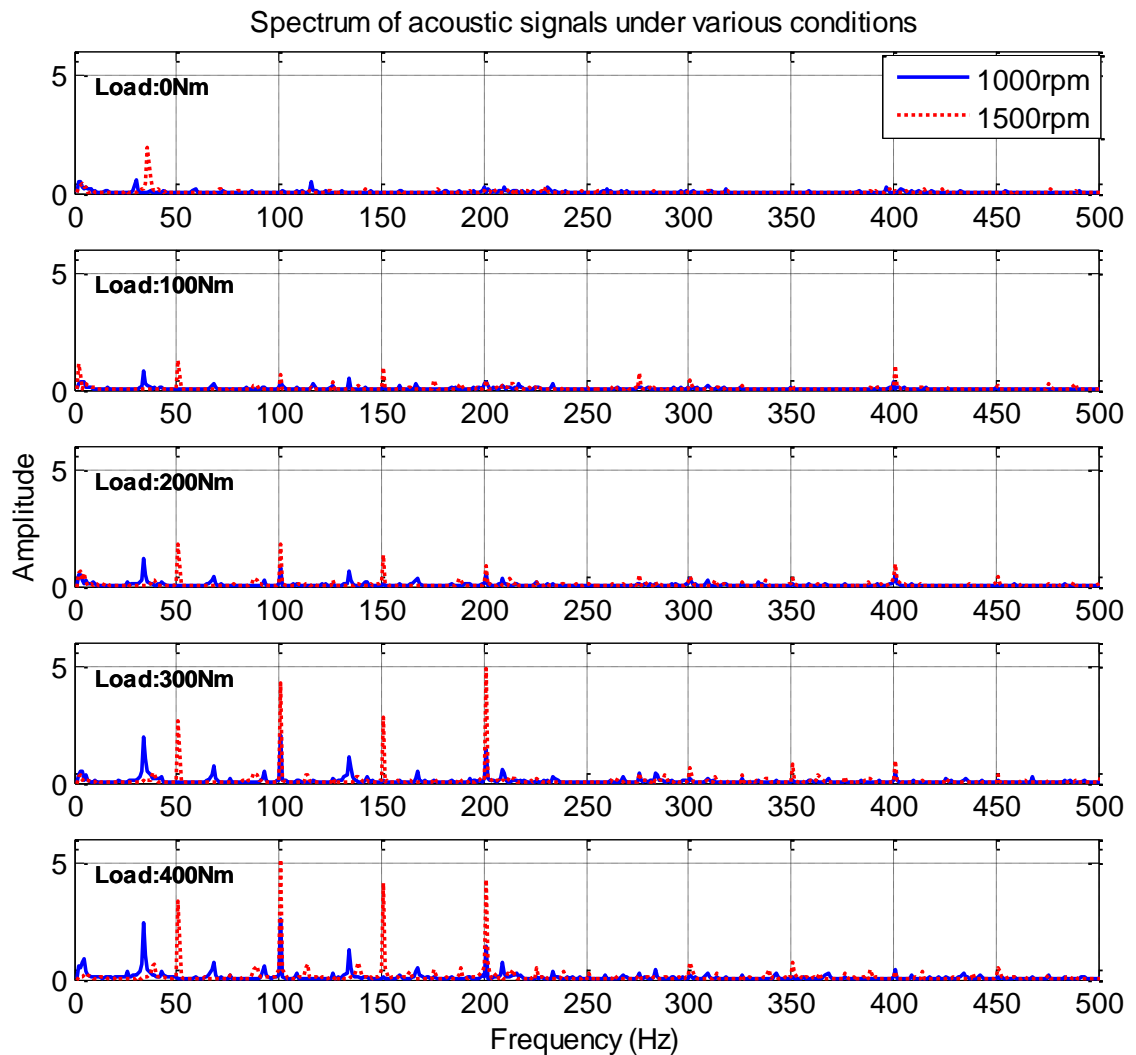


Figure 5-15 Spectrum of acoustic signals under various conditions

Octave band analysis used more frequently for analyzing the acoustic spectra in practice. This method provides more information than conventional spectral analysis or weighting networks [94] as octave analysis presents the frequency characteristics of a signal in frequency band where each frequency band covers an octave. Here the 1/3 octave band are employed to analyse the acoustic signals from the test engine

operating under various loads and speeds. Figure 5-16 shows the 1/3 octave band spectra of the acoustic signal of the test engine operating at two speeds of 1000rpm and 1500rpm with different loads of 100, 200, 300, and 400N m.

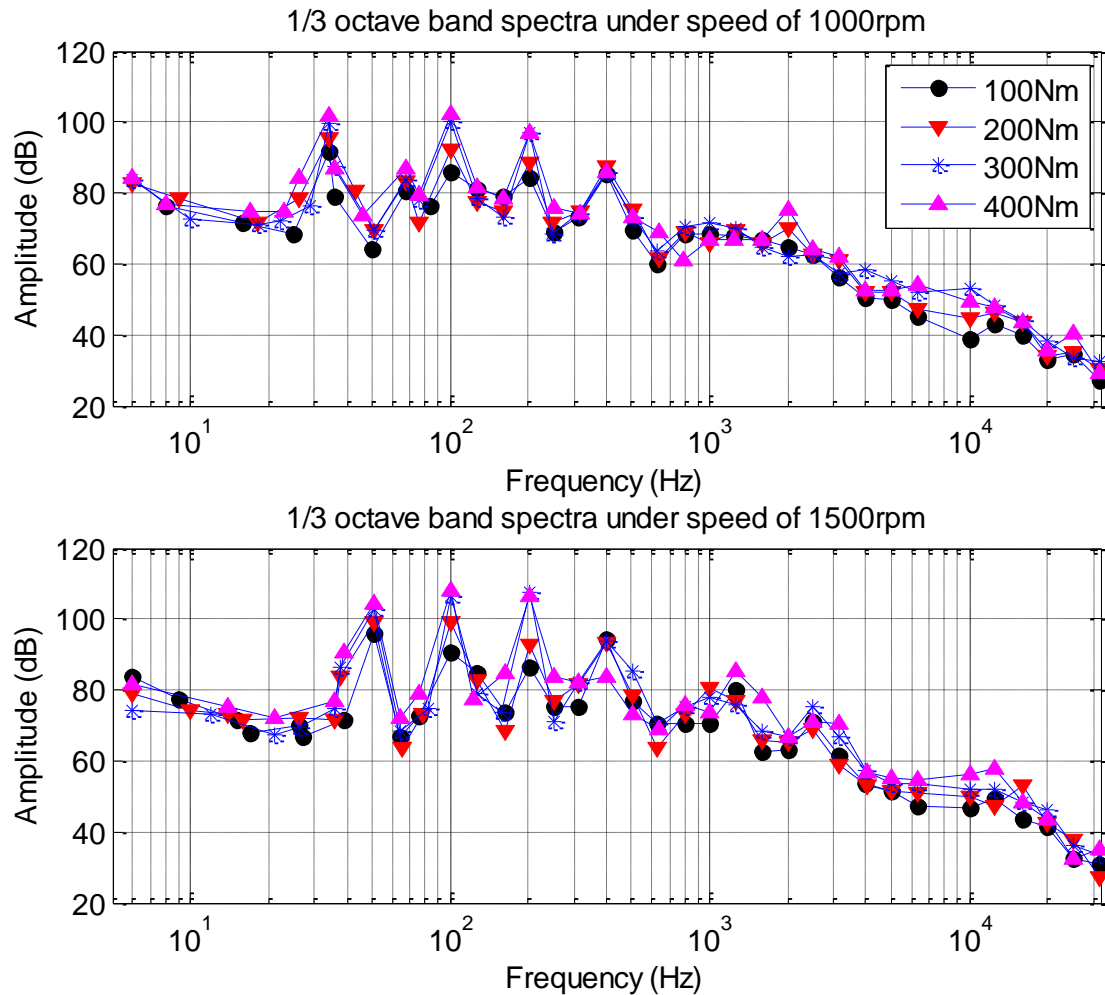


Figure 5-16 1/3 octave band spectra of acoustic signals

In Figure 5-16, the 1/3 octave band spectra assists with the comparison of the differences between the characteristics of the analyzed acoustic signals. The spectrum of load 400N m can be seen to be almost the highest and 100N m almost the lowest at both 1000rpm and 1500rpm. The spectrum of 1500rpm is higher than that of 1000rpm in most of the analyzed bands for the same load. The spectrum of some lower loads is higher than that of some higher loads in some analyzed bands. For example, the spectrum of load 200N m is lower than that of 100N m in the analyzed band of about

70Hz at both speeds. This is due to the room resonance being excited by the firing frequency and its harmonics. Most of the frequencies with higher amplitude in low frequency band are close to the room resonance frequencies as discussed in section 5.4.

5.4 Room modes

The room acoustics should be considered when analyzing engine acoustic signals because the tests were carried out in the engine test room and the room acoustic characteristics could affect the measured signals. The room modes and its eigenfrequencies are based on the room's size. So far as the test engine room dimensions 4.8m×4.2m×2.8m are concerned, and the room modes and its eigenfrequencies lower than 200Hz are listed in table 5-8.

Table 5-8 Lower order room modes

Room Mode (n_x, n_y, n_z)	Frequency (Hz) (f_n)	Room Mode (n_x, n_y, n_z)	Frequency (Hz) (f_n)
0, 1, 0	34	1, 2, 1	101
1, 0, 0	40	0, 0, 2	121
1, 1, 0	51	0, 1, 2	127
0, 0, 1	61	1, 1, 2	133
0, 1, 1	70	0, 2, 2	141
0, 2, 0	71	0, 0, 3	182
1, 0, 1	73	0, 1, 3	186
1, 1, 1	81	1, 0, 3	187
1, 2, 0	82	0, 2, 3	195
0, 2, 1	93	2, 0, 3	199

If one of the modes is excited by external forces, resonance may be induced and the sound level at that mode frequency will be increased accordingly. By comparing the firing frequencies with the room mode resonance frequencies, it can be seen that the firing frequency of 1000rpm has the same frequency as that of room model 010 which is 34Hz. It is therefore expected that this particular room mode is excited by the engine

rotation speed of 1000rpm. Similarly, the room mode 110 with a frequency of 51 Hz has a similar frequency to that of the firing frequency at 1500rpm which is 50Hz.

Noting that the room modes in table 5-8 are calculated based on a simple rectangular room in theory. Experiments need to be carried out for accurate analysis of the test engine room modes, because the presence of the diesel engine will affect the room modes. In this research work, the main frequency band of engine acoustics used for analysis is higher frequency which is above 1 kHz, and the effect of room modes on acoustics is in the lower frequency band, so room modes are not measured based on experiment here.

Figure 5-17 shows the spectrum of the acoustic signals while the engine operates under speeds of 1000rpm and 1500rpm and loads of 300N m and 400N m. It can be seen that with the engine rotation speed of 1000rpm, its firing frequency (33.3Hz) and its third harmonic frequency (99.9Hz) are similar to room modes 010 (34Hz) and 121 (101Hz) respectively. The amplitudes of these frequency components, therefore, are higher than those of its other harmonics both at loads of 300N m and 400N m. Similarly, when the engine rotates at a speed of 1500rpm, its firing frequency is 50Hz and second and fourth harmonic frequencies are 100Hz and 200Hz. These are similar to the room modes resonance frequencies 110 (51Hz), 121 (101Hz) and 203 (199Hz). All of the amplitudes of these frequency components can be influenced by the room mode resonance.

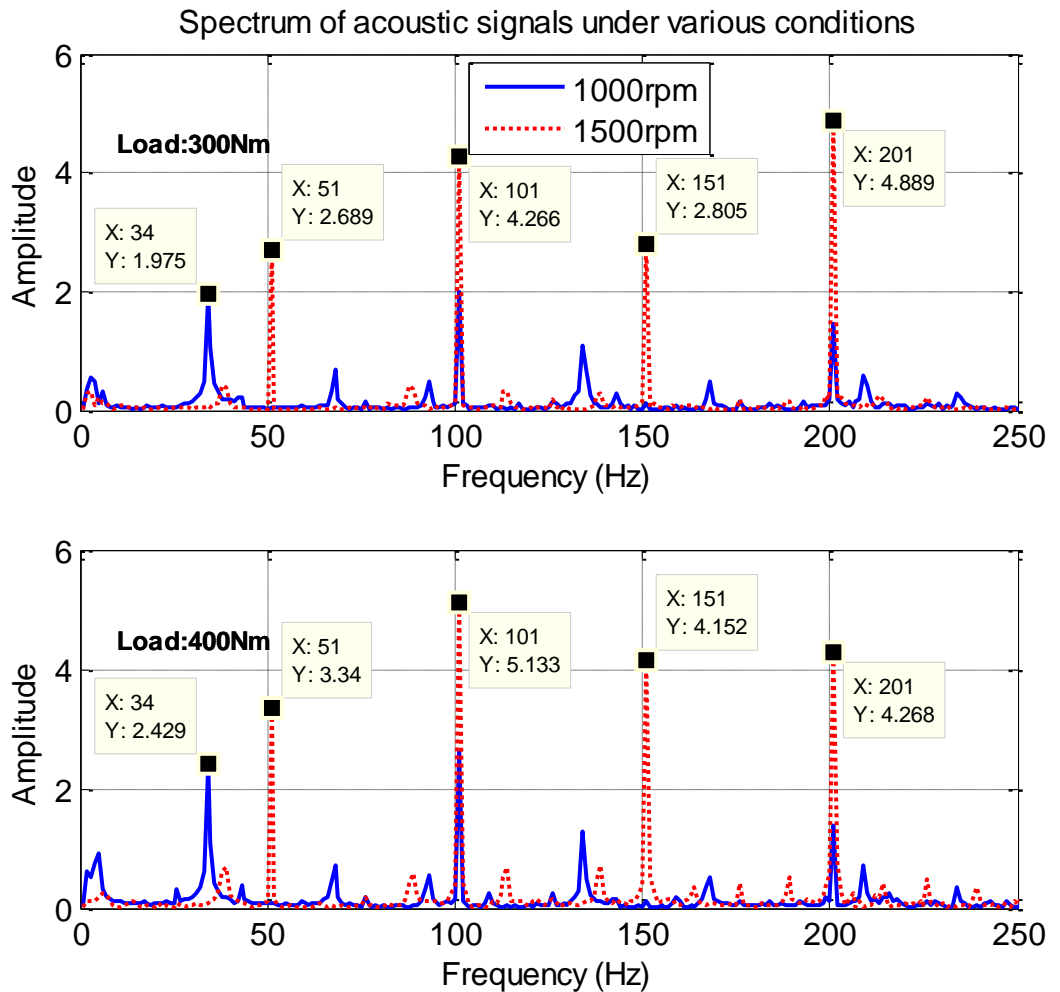


Figure 5-17 Difference spectrum of acoustic signals under different speeds

5.5 Fuel monitoring based on engine acoustics

In the first engine test, the acoustic signals are measured from the test engine operating under the different speeds of 1000rpm and 1500rpm under different loads of 0, 100, 200, 300 and 400N m, and fuelled by biodiesel with different percentages 25% (B25), 50%(B50) and 100%. (B100). The purpose of this section is to reveal the differences between different types of fuels through analysis of the engine acoustic signals and to investigate an easy way to monitor the fuels of the engine founded on acoustic based condition monitoring.

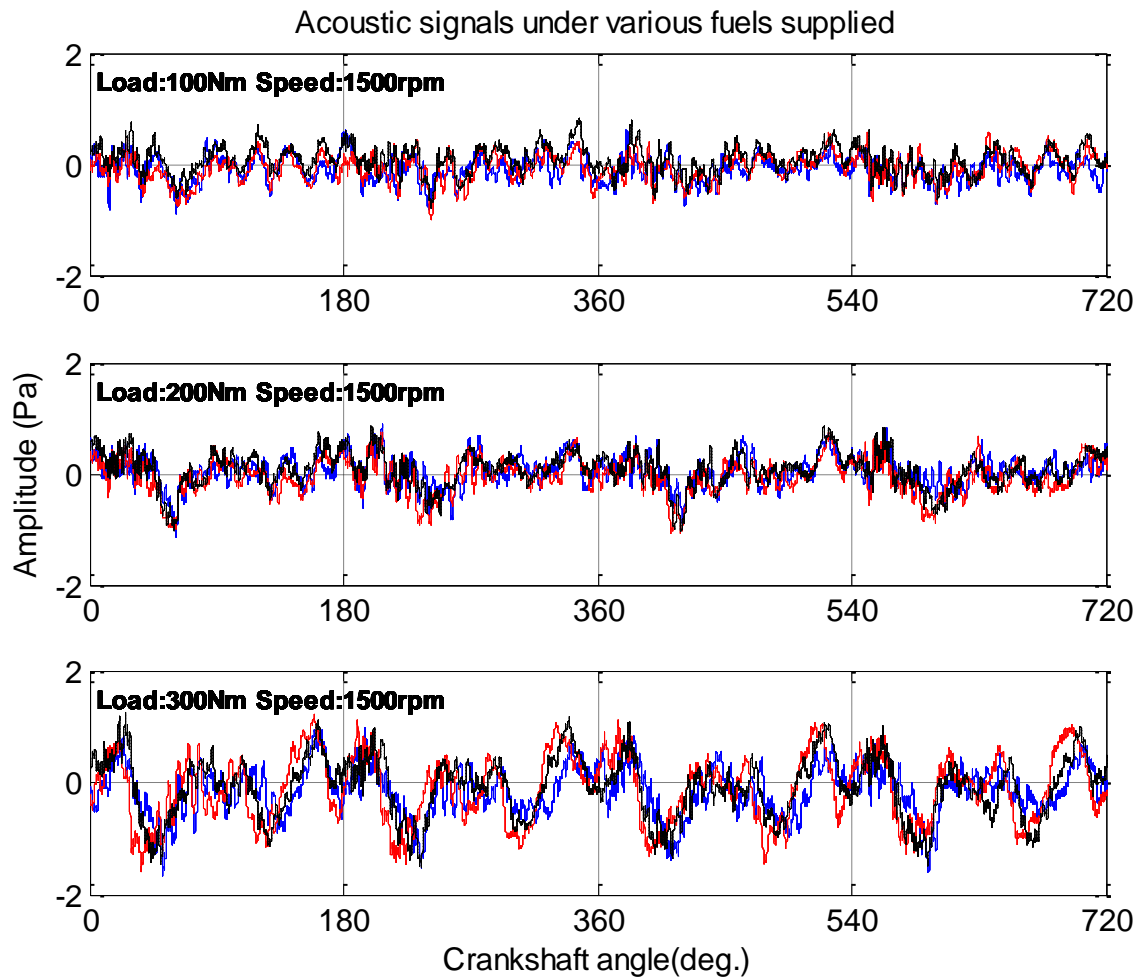


Figure 5-18 Acoustic signals under various fuels supplied in one cycle
— : B25 - - - : B50 - · - · : B100

Figure 5-18 shows the acoustic signals of the test engine operating under different conditions in one combustion cycle. It can be clearly seen that the amplitude of the acoustic signals increases and that the temporal pattern becomes clearer according to the increase of the engine loads for all types of fuels. However, the differences in the amplitudes of the acoustic signals between different supplied fuels are so small that it is difficult to distinguish the different types of fuels used. The sound pressure level levels of the measured acoustic signals under different conditions are calculated and shown in figure 5-19. It can be seen that as the loads increase under the speeds of 1000rpm and 1500rpm, the sound pressure level values increase accordingly. In addition, upon comparing the sound pressure level values at a certain load, we see that

they also increase correspondent with the increase of the speed. The differences of the sound pressure level values between different supply fuels are not obvious enough for fuel monitoring and distinguishing.

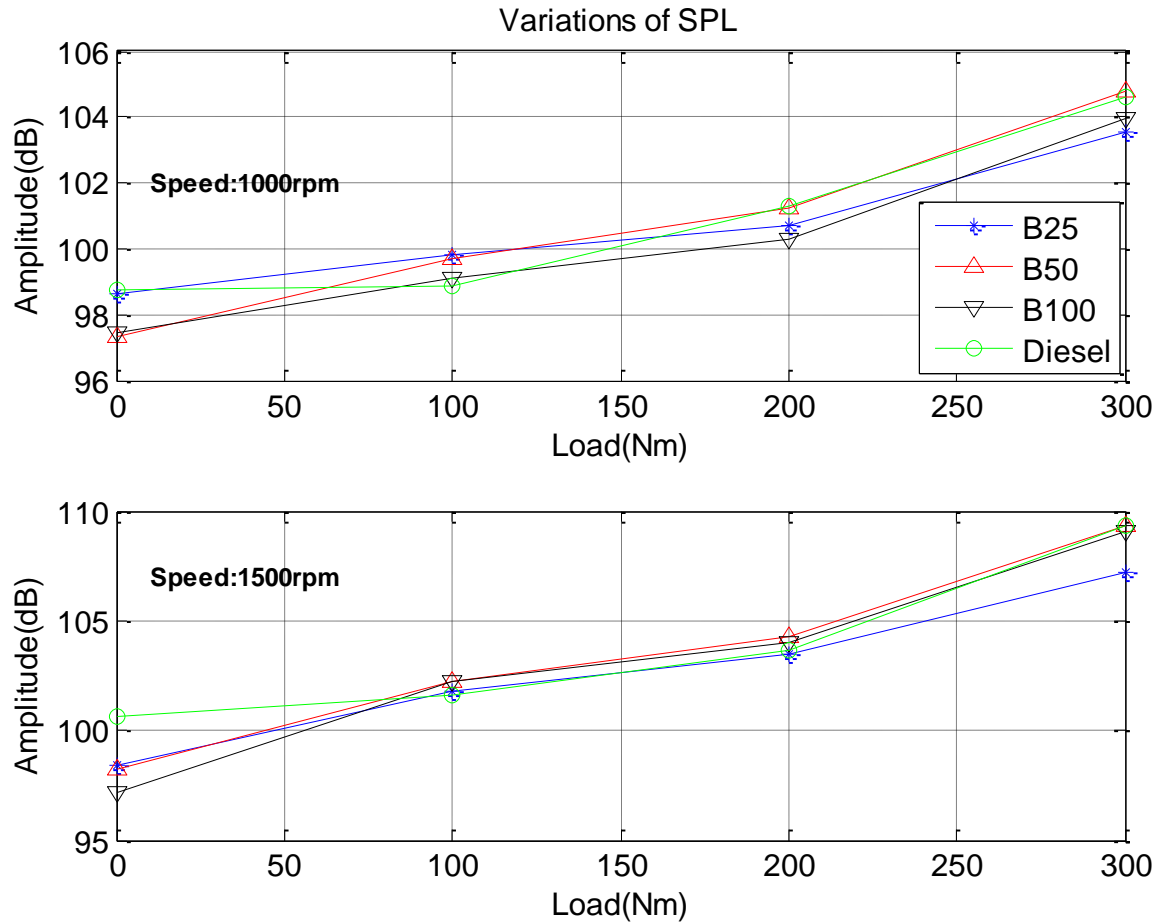


Figure 5-19 Variations of SPL under different operating conditions

Considering the effect of room modes applies mainly to the lower frequency band of the acoustic signals, a high-pass filter of 1 kHz was designed to process the engine acoustic signals and reduce the effect of the room modes on the feature extraction from the engine noise. Figure 5-20 illustrates the sound pressure level of the engine noise after processing by the high-pass filter. It can be seen that the sound pressure level values decrease once the low frequency components of the engine noise have been eliminated, and the distinguishing of the differences between fuels is improved. It can

be seen that monitoring results can be obtained through the analysis of the engine noise in a higher frequency band for fuel evaluation.

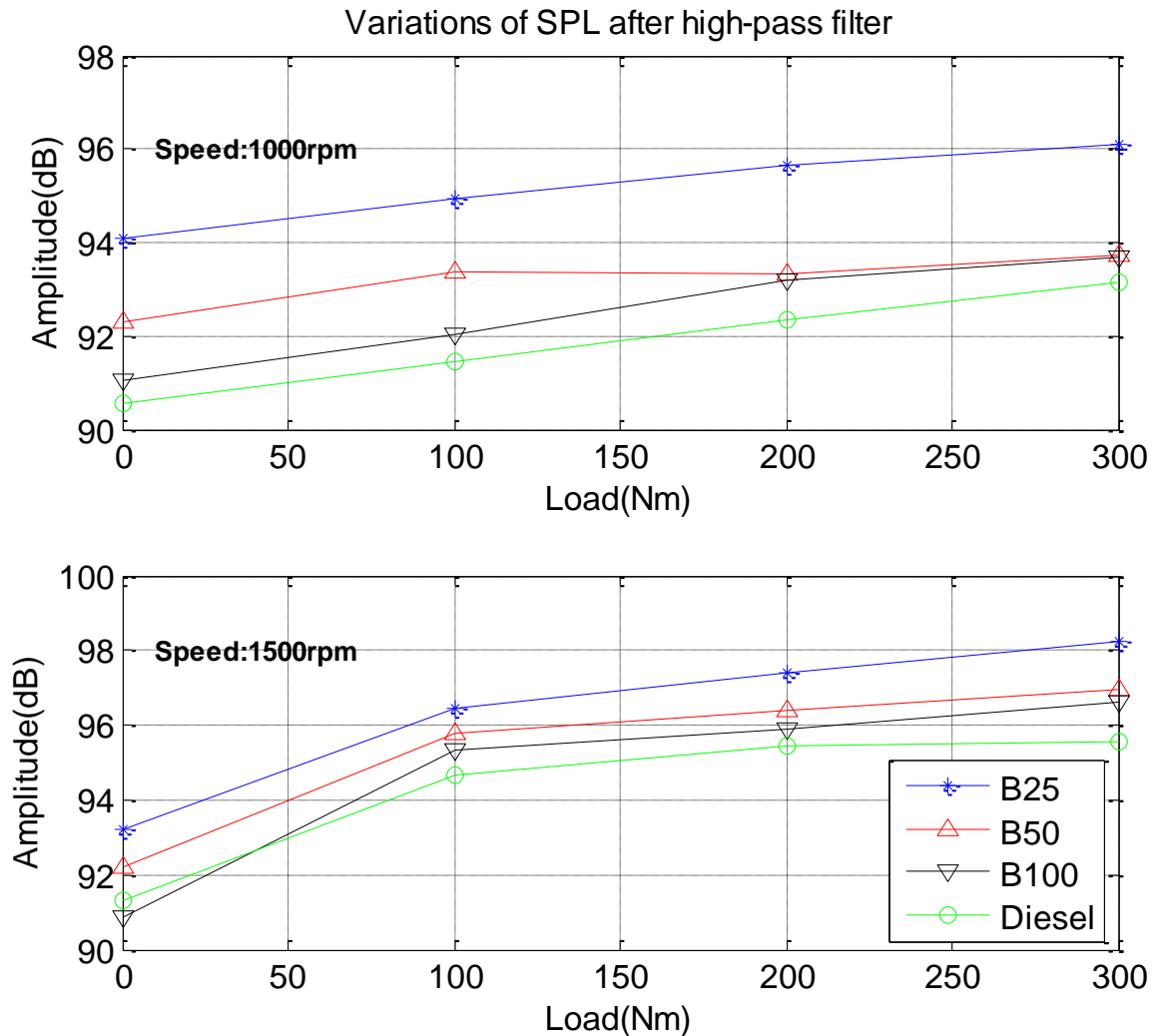


Figure 5-20 Variations of SPL filtered by high-pass filter

The 1/3 octave band spectra of the acoustic signals under the same speed of 1000rpm but supplied by different fuels are calculated and shown in Figure 5-21. It can be seen that the spectra do not give much information with respect to the energy levels and supplied fuels in the low frequency band below 1 kHz. The energy levels change greatly according to the frequency, the peak values appearing at frequencies of about 33Hz, 100Hz, and 200Hz. This is due to the room resonance, which is excited by the firing frequency and its harmonics.

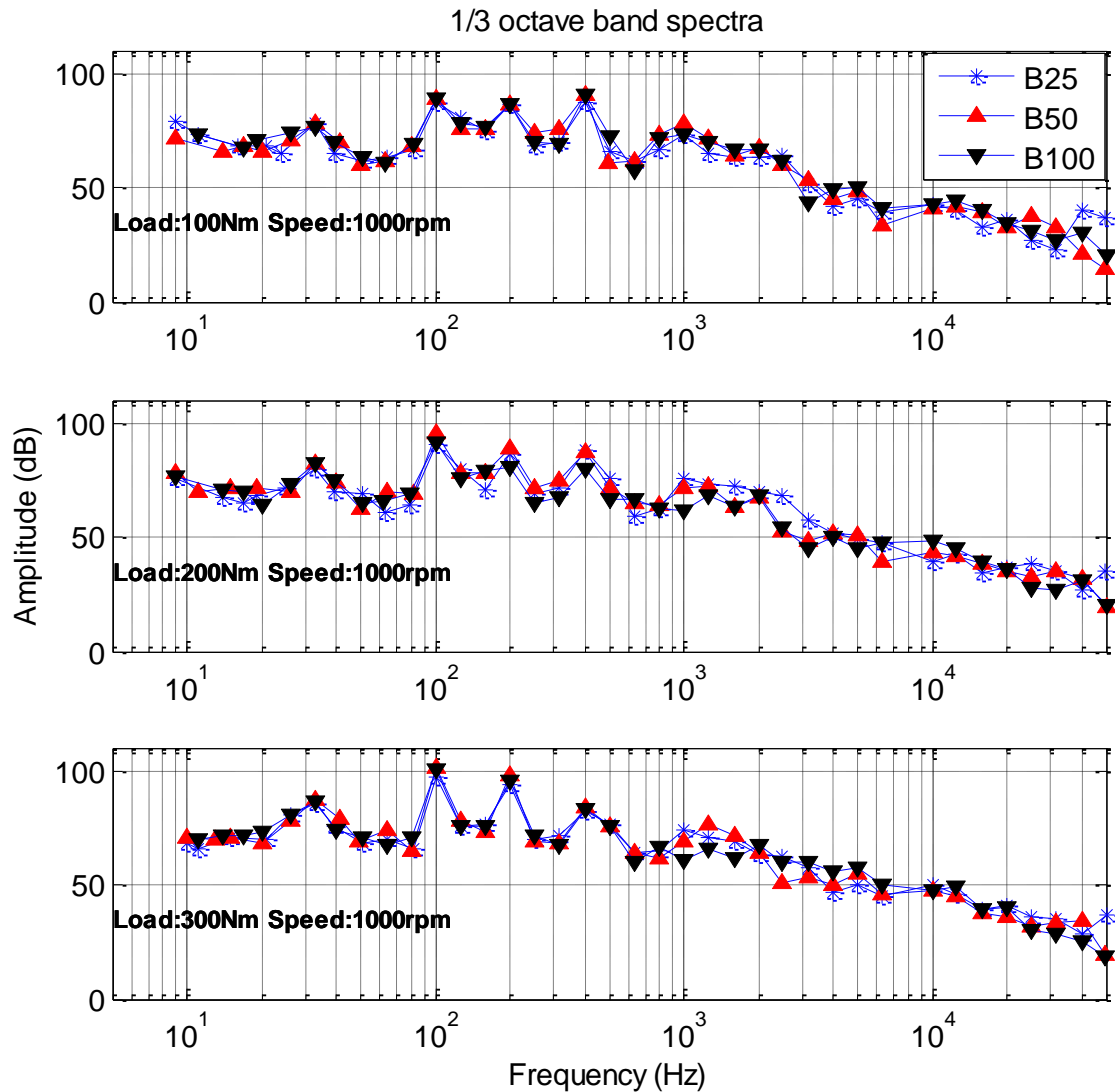


Figure 5-21 1/3 octave band spectra of acoustic signals

Conversely, spectra above 1 kHz show relative stable energy levels with the loads and supplied fuels. This indicates that the higher frequency bands are less influenced by the room resonance. It can be seen that the room eigenfrequencies and reverberation can affect the measured acoustic signals. Its impacts are mainly on the lower frequency band of the engine noise, meaning that room reverberation needs to be suppressed in order to enhance the signal so that more accurate detection results for monitoring the operating condition of the engine are achieved. As well as this, more accurate or better monitoring results can be obtained through analysis of the engine acoustic signals in a higher frequency band.

CHAPTER 6

COMBUSTION AS THE SOURCE OF VIBRO-ACOUSTICS FROM AN ENGINE FUELLED BY BIODIESEL BLENDS

This chapter will investigate the combustion process of the test diesel engine fuelled by different types of fuels. The combustion parameters including cylinder pressure, heat release rate, and ignition delay are analysed based on the measured data from the engine test. In addition, the vibration and noise generation mechanisms are studied in association with the complex combustion process and complicated engine structures. The analysis indicates that the combustion induced vibration and acoustics are closely related to the variation of the cylinder pressure, and can be used to investigate the combustion process instead of cylinder pressure data which is both intrusive and costly to obtain.

6.1 Researches on the performance of engine fuelled by biodiesel

The demand for petroleum-based fuel has risen recently, whilst resources have declined [95]. Consequently, a demand to develop alternative fuels which are cheaper and environmentally acceptable has been considered to reduce the dependency on fossil fuels. Previous research [96–98], has shown that biodiesel is one of the most promising renewable alternative and environmentally friendly fuels. Biodiesel is composed of fatty acid methyl or ethyl esters from vegetable oils or animal fats and its properties are similar to petroleum-based fuel [97]. It is renewable, biodegradable, oxygenated and can be used in diesel engines without any modification of engine structures [93]. As diesel engines are not specifically manufactured for biodiesel fuel, the impact of biodiesel on the performance and condition of diesel engines need to be analysed.

Engine combustion is a complex process due to the combustion mechanism. The performance and emission of the engine is dependent on the characteristics of the engine combustion process. Numerous studies [85–92] have been conducted to research engine performance, especially the combustion and emission characteristics of diesel engines fuelled with biodiesel compared with petroleum-based diesel. Dorado et al. [104] studied the effect of waste olive oil methyl ester on exhaust emissions using a direct injection (DI) diesel Perkins engine. *“They concluded that lower emissions of CO, CO₂, NO and SO₂ can be obtained by using biodiesel, but emissions of NO₂ increased”*. Tashtoush et al. [103] tested the combustion performance and emission of a water-cooled furnace with diesel fuel and ethyl ester of a waste vegetable oil. Their results demonstrated that *“biodiesel burned more efficiently with higher combustion efficiency and exhaust temperature and lower energy consumption rates. At higher energy input conditions, biodiesel combustion performance deteriorated and was inferior to diesel fuel as a result of high viscosity, density and low volatility”*. Therefore, it is important to analyse the combustion characteristics to evaluate the performance and influence of biodiesel when used in diesel engines. Combustion

analysis is also a critical step in engine condition monitoring and fuel quality evaluation.

6.2 Combustion parameters

The main parameters used for analysing the characteristics of the combustion process are cylinder pressure, ignition time delay, and heat release rate (HRR) [95]. All these parameters are based on the variations of cylinder pressure. Hence the combustion parameters can be calculated based on the in-cylinder pressure data. The other important combustion parameters, such as combustion duration and intensity, can be estimated from the heat release rate variation over an engine cycle. The heat release rate can be used to identify the start of combustion, indicating the ignition delay time of the combustion process, the fraction of fuel burned in the premixed mode, and differences in combustion rates of fuels [105].

The heat release rate can be calculated from a simplified approach derived from the first law of thermodynamics [106] as expressed in Equation (6-1).

$$\frac{dQ}{d\theta} = \frac{1}{\gamma-1} \left(\gamma P \frac{dV}{d\theta} + V \frac{dP}{d\theta} \right) \quad (6-1)$$

where, $dQ/d\theta$ is the heat release rate across the system boundary into the system, P is the in-cylinder gas pressure, V is the in-cylinder volume, γ is the ratio of specific heats and an appropriate range for γ for heat release analysis is 1.3 to 1.35 [106]. θ is the crank angle. $P(dV/d\theta)$ is the rate of work transfer done by the system due to system boundary displacement [107]. In addition, the cumulative heat release rate, Q_c , can be obtained from the heat release rate in Equation (6-2). The cumulative heat release is the gross heat release due to combustion.

$$Q_c = \int \frac{dQ}{d\theta} d\theta \quad (6-2)$$

The ignition delay is an important parameter for analysing the combustion process of an engine and can be obtained by calculating the heat release rate of the engine combustion process. Ignition delay is defined as the time interval between the start of

fuel injection into the combustion chamber and the commencement of combustion. The ignition delay determines the quantity of premixed flame contributing to the rate of pressure increase and its maximum value [95]. It corresponds to the period between the beginning of fuel injection until the cylinder pressure rises. Theoretically, a longer ignition delay means more fuel is available for ignition resulting in more energy release during the premixed combustion stage. Reduction in ignition delay may result in earlier combustion leading to slightly higher peak pressures, whereas an increase in the delay period results in poor combustion and may lead to lower peak pressure [100].

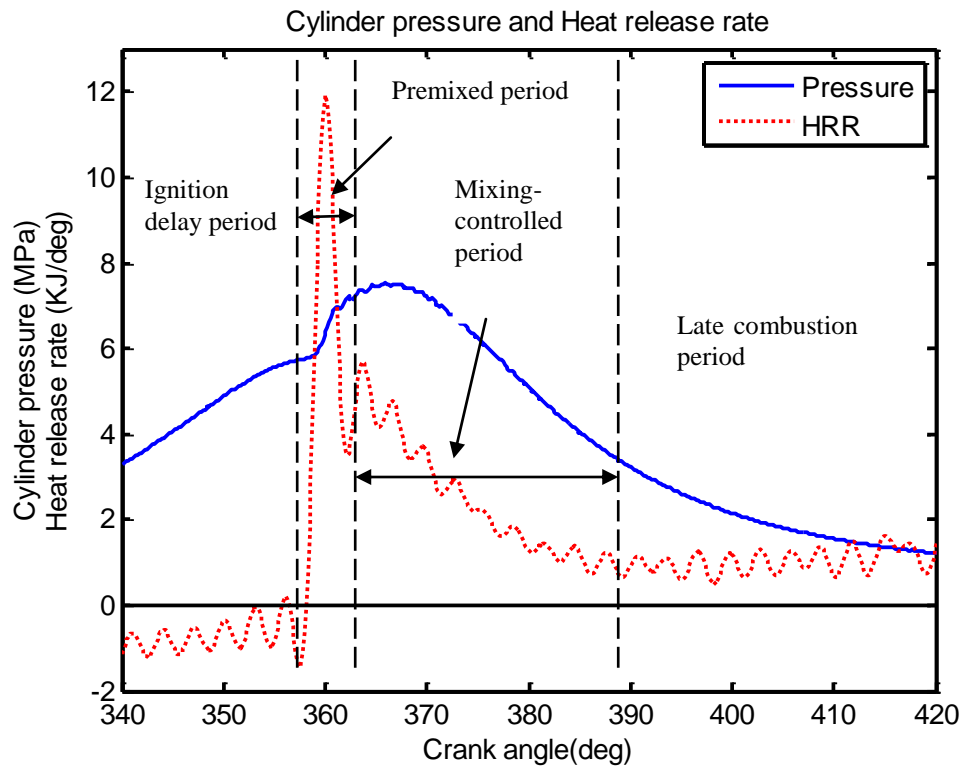


Figure 6-1 Cylinder pressure, heat release rate for diesel engine

Figure 6-1 shows the cylinder pressure and heat release rate of a diesel engine. It indicates that the combustion process can be divided into three distinguishable stages. The first stage is the premixed period, where the rate of burning is very high, combustion time is short (for only a few crank angle degrees), and the cylinder pressure rises rapidly. The second stage is the mixing controlled period and is the main heat release period corresponding to a period of gradually decreasing heat release rate

and lasting about 30 crank degrees. The third stage is the late combustion period which corresponds to the tail of the heat release diagram in which a small but distinguishable heat release rate occurs throughout much of the expansion stroke.

6.2.1 Cylinder pressure

Cylinder pressure versus crank angle over the compression and expansion strokes of the engine running cycle can be used to obtain quantitative information on the progress of combustion [107]. Figure 6-2 shows the cylinder pressures versus crank angle for different fuels (Diesel, B50, and B100), engine loads (105N m, 210N m, 315N m and 420N m) and at the constant engine speed of 1300rpm. Figure 6-3 presents the cylinder pressure versus crank angle for different fuels (Diesel, B50, and B100), engine speeds (900rpm, 1100rpm and 1300rpm) and at the constant engine load of 420N m.

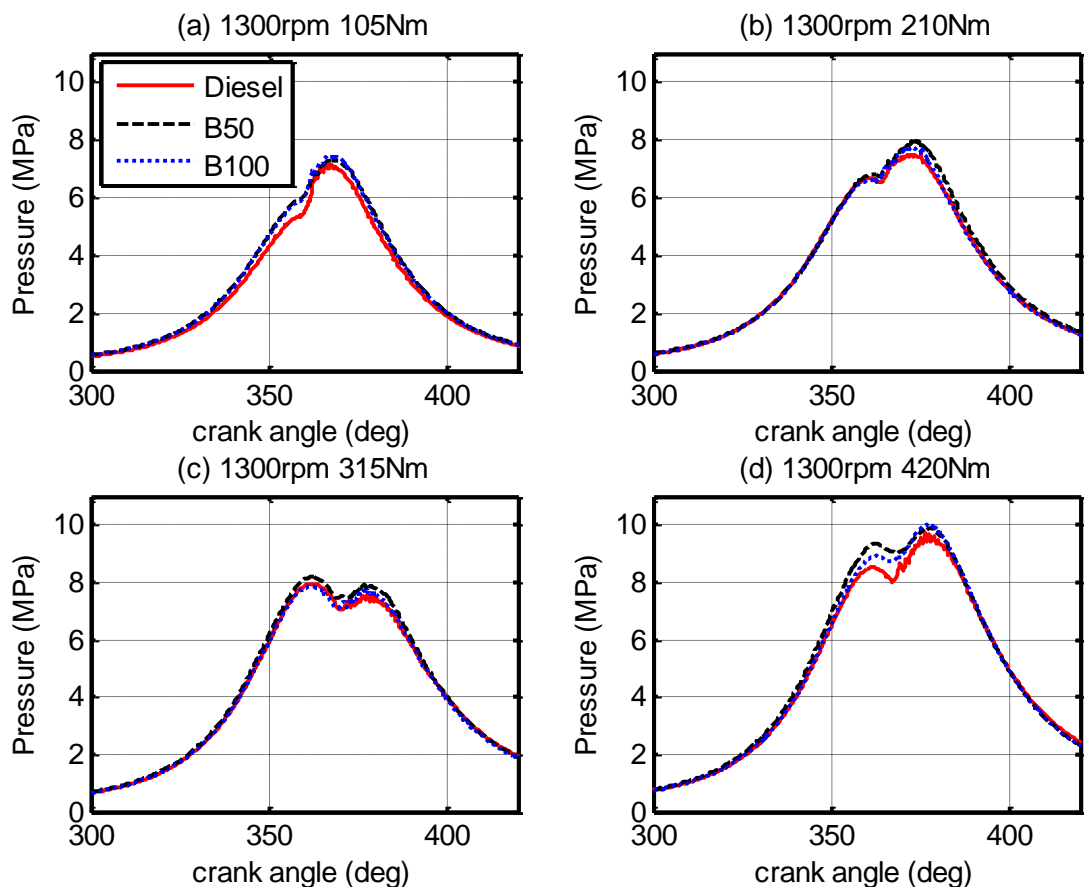


Figure 6-2 Cylinder pressure at a speed of 1300rpm under different loads

From both the Figures it can be seen that the peak cylinder pressure was higher for rapeseed oil biodiesel at all tests. The higher viscosity of biodiesel can enhance fuel spray penetration and thus improve air-fuel mixing [108]. A higher viscosity of biodiesel can also lead to bad fuel injection atomization. The peak cylinder pressure of B50 is slightly higher than that of B100, especially at high loads, and may be due to the higher viscosity of B100. The viscosity of the biodiesel increases with increased biodiesel percentage in the blends, and higher viscosity decreases combustion efficiency due to bad fuel injection atomization [96].

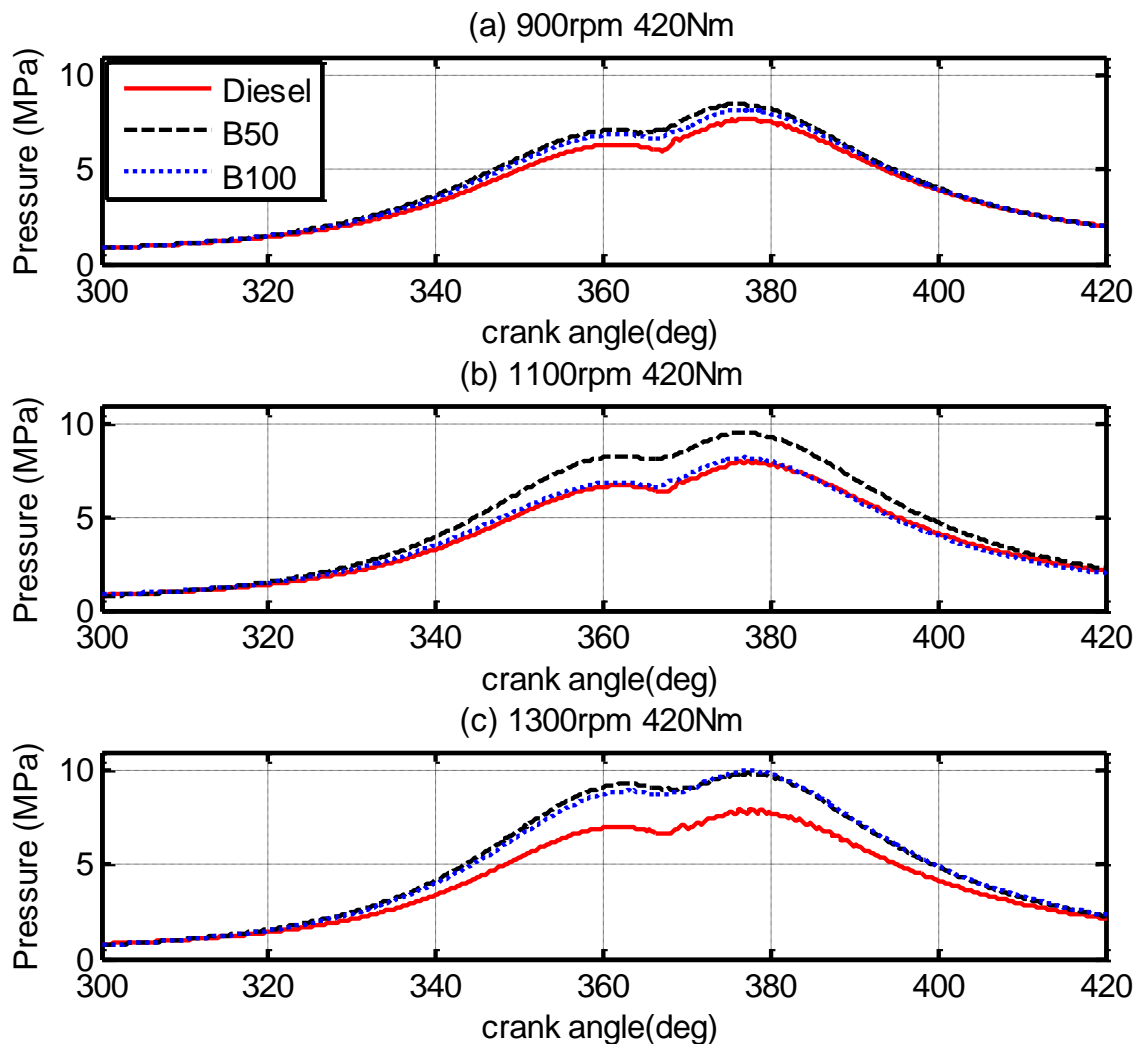


Figure 6-3 Cylinder pressure at a load of 420N m under different speeds

From Figures 6-2 and 6-3, it can be seen that, the peak cylinder pressures for both diesel and biodiesel and its blends were slightly increased when the engine loads and speeds increased. This is due to longer ignition delay which results in more fuel being available for ignition and more energy being released during the premixed combustion stage [96]. Figures 6-5 and Figure 6-6 show that the ignition delay is longer under higher loads and speeds, and the maximum heat release rate was higher than that of lower loads and speeds for both diesel and biodiesel and its blends.

6.2.2 Heat release rate

Details of the combustion process for an engine can be obtained through analysis of the heat release rate of the combustion process. The cumulative heat release rate, ignition delay and combustion duration were all determined by analysis of the heat release rate. Figures 6-4, 6-5 and 6-6 illustrate the heat release rate for the compression ignition (CI) engine used in the current investigation operating with diesel, biodiesel and its blends at speeds of 900rpm, 1100rpm and 1300rpm and at four loads of 105N m, 210N m, 315N m and 420N m respectively.

As shown in Figure 6-4, a negative heat release rate was observed initially, which was due to the vaporization of the fuel accumulated during ignition delay [109]. It can be seen that combustion starts earlier for biodiesel and its blends and the start point of the combustion crank angle decreases with the percentage increase of biodiesel under all engine operating conditions. From Figure 6-4 it can be seen that the combustion start angles for pure diesel, B50 and B100 are 358.8, 357.6 and 357 crank degrees respectively at a speed of 1100rpm and load of 105N m. Figure 6-4 also demonstrates that at lower loads of 105N m and 210N m, the premixed combustion heat release rate is higher for diesel due to the longer ignition delay leading to more fuel accumulation in the combustion chamber at the time of the premixed combustion stage. The heat release rate of biodiesel was higher at the higher loads of 315N m and 420N m even with a shorter ignition delay.

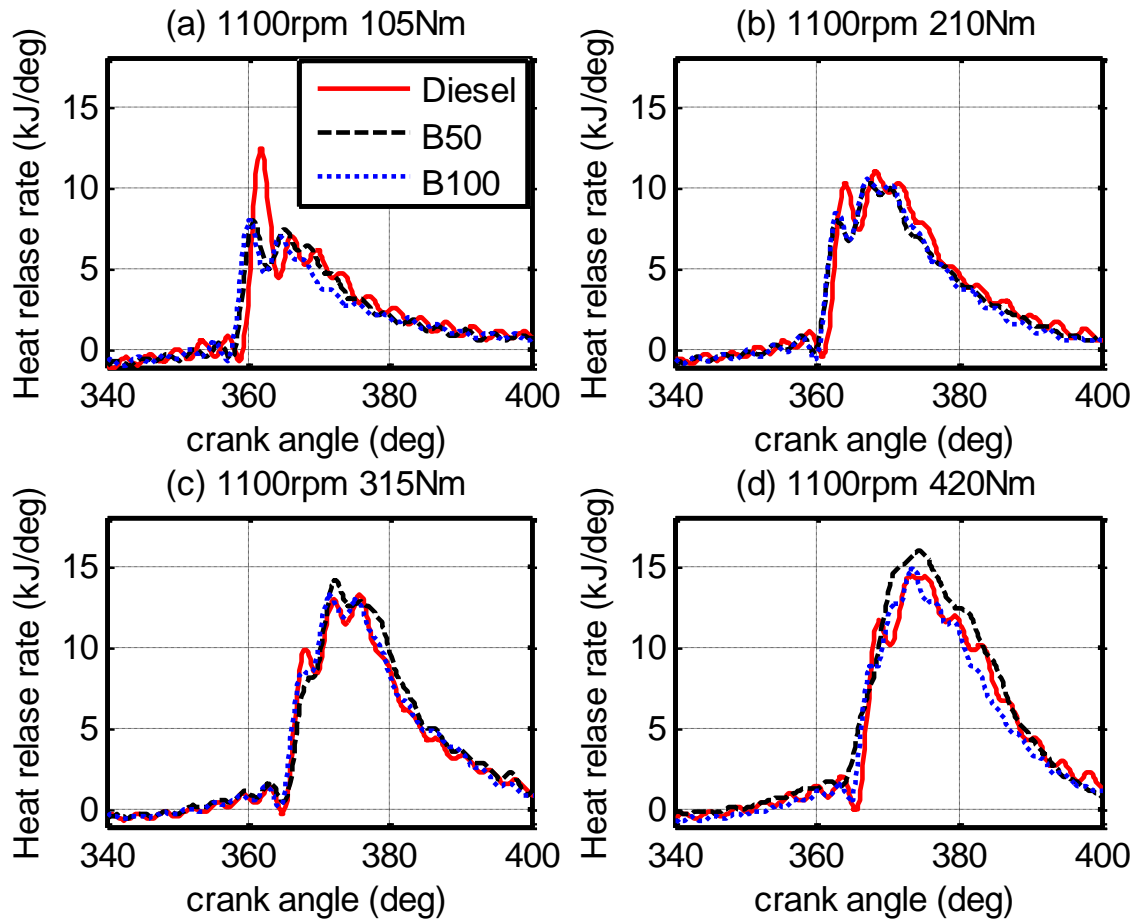


Figure 6-4 HRR at speed of 1100rpm and under different loads

The heat release rate for diesel, biodiesel and its blends (B50 and B100) at 210N m load with speeds of 900rpm, 1100rpm and 1300rpm are illustrated in Figure 6-5. It can be seen that the combustion starts earlier for reduced engine speeds by comparing the starting point of heat release rate increasing in crank angle. This means that a longer ignition delay is required at higher speeds for both diesel and biodiesel blends. Figure 6-6 shows the heat release rate of diesel, biodiesel and its blends at loads of 105N m, 210N m, 315N m and 420N m with a constant speed of 1100rpm. The figure illustrates that ignition delay increases alongside engine load for all types of fuel and leads to the maximum heat release rate occurring sooner. Maximum heat release rate increased at higher engine loads due to the increase in the quantity of fuel injected into the cylinder [110].

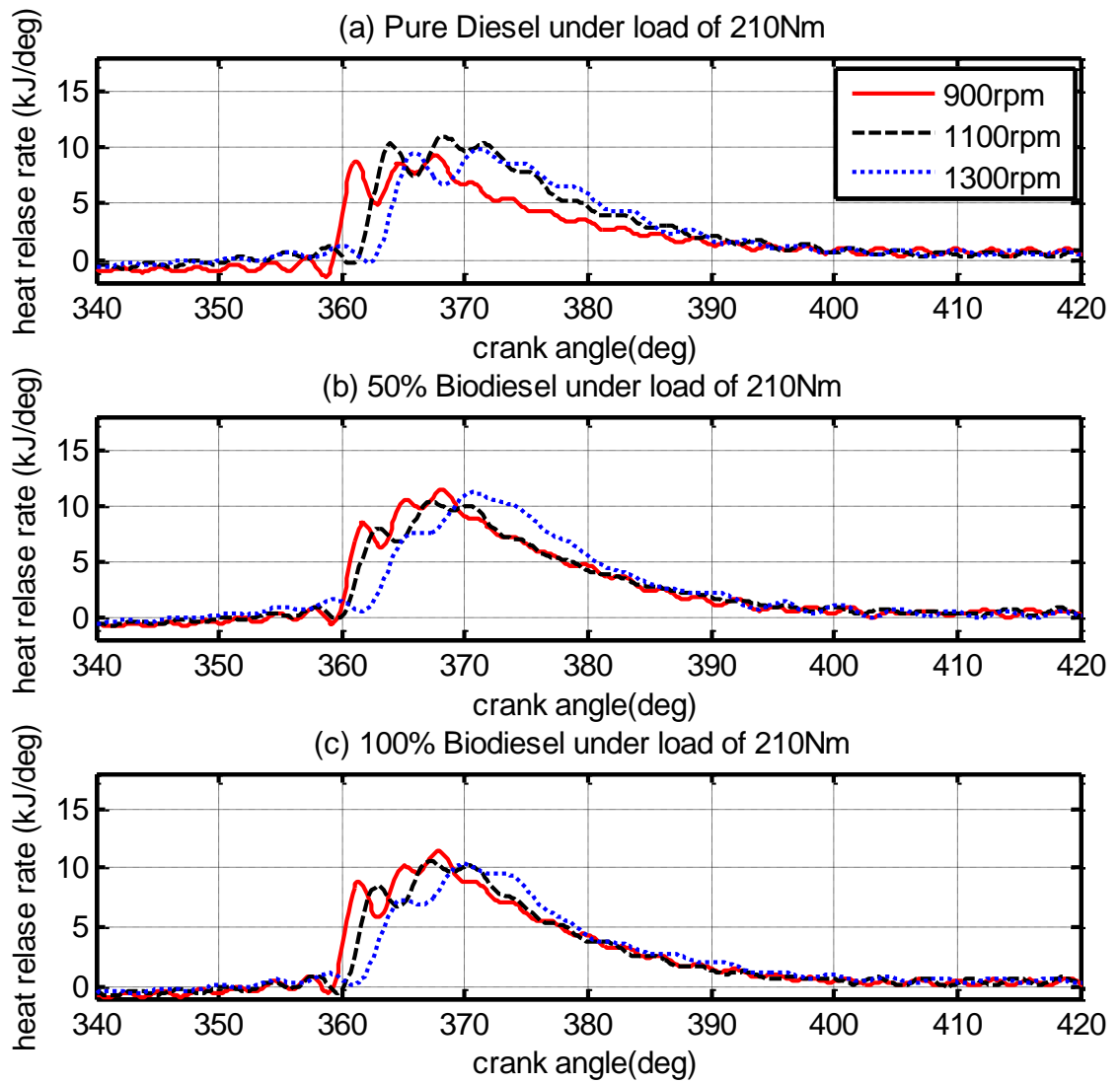


Figure 6-5 HRR at 210 N m load under different speeds for biodiesels

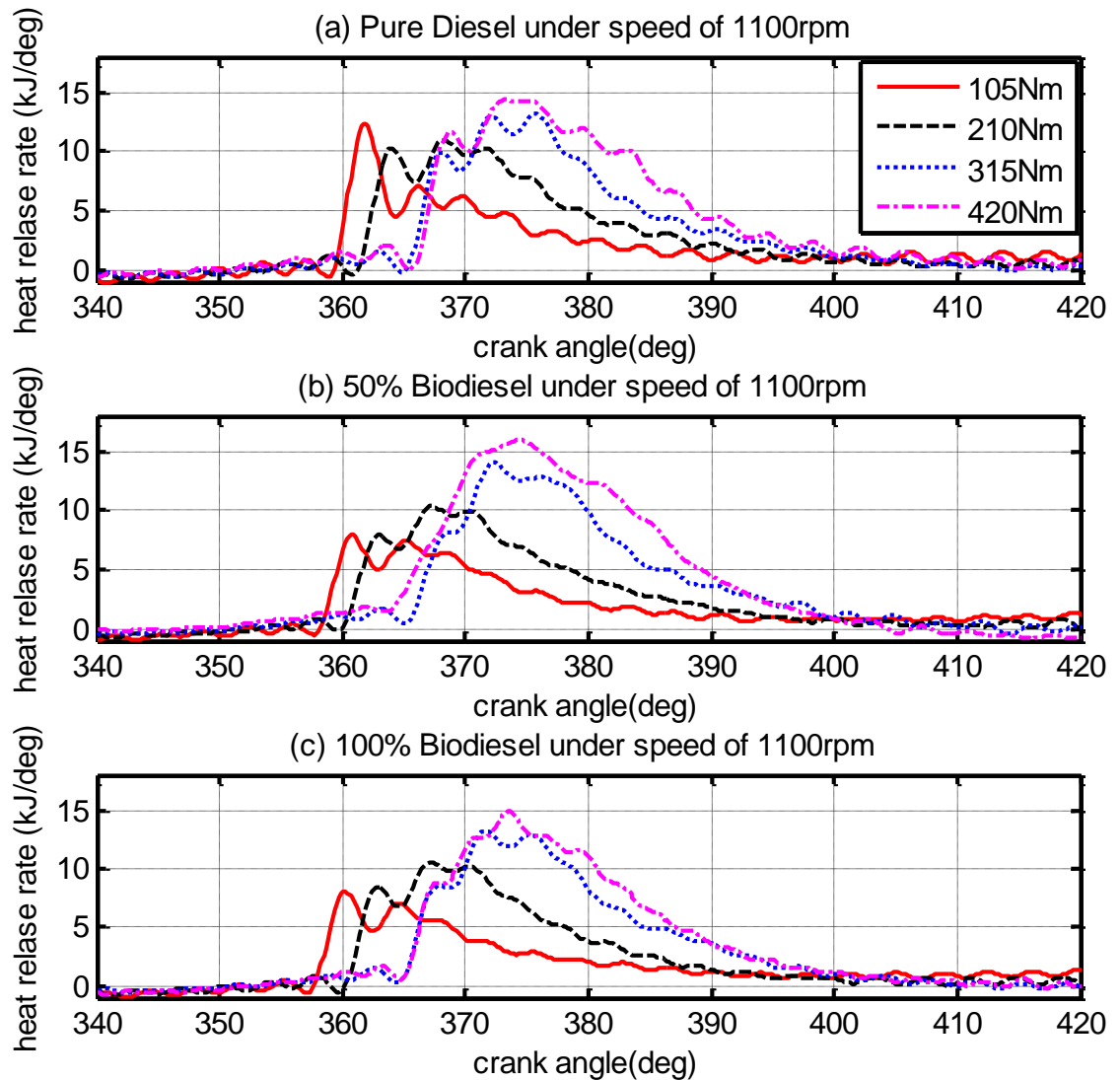


Figure 6-6 HRR at a speed of 1100rpm under different loads for biodiesel blends

6.2.3 Ignition delay

Ignition delay is an important parameter in engine combustion analysis. This property is useful in determining diesel engine operating characteristics such as noise, vibration, misfire, and smoke emissions. The ignition quality of a fuel is defined by its cetane number [110] and fuels with a low cetane number have a long ignition delay. In this instance, most of the fuel is injected before ignition occurs and results in very rapid burning rates once combustion starts with high rates of pressure increase and high peak

pressures, sometimes leading to audible knocking noises and resulting in incomplete combustion [107]. Fuels with a high cetane number have a shorter ignition delay as the ignition occurs before most of the fuel is injected [111]. Hence the heat release rate and pressure rise are controlled mainly by the rate of injection and air-fuel mixing.

Table 6-1 Crank angles at the start of combustion for fuels at different engine conditions

Speed (rpm)	900				1100				1300			
	105	210	315	420	105	210	315	420	105	210	315	420
Diesel	358.1	359.3	362.8	364.8	359.3	361.2	365.2	365.6	360	362.5	365	368
B50	357.5	359	362	364	358.2	360	363.5	365	358.3	362	364.5	366
B100	356.2	358	361	363	357.6	359.6	363	364.6	357.4	361	364	365

The crank angles at the start of combustion for the test fuels at different engine operating speeds of 900rpm, 1100rpm and 1300rpm and loads of 105N m, 210N m, 315N m and 420N m are shown in Table 6-1. It can be seen that ignition delay increased with increased engine load and speed due to the longer vaporization time of the fuel in terms of crank angle [102]. Ignition delays decreased as increasing amounts of biodiesel were added to the diesel fuel blends. This was due to the higher percentage of high cetane number biodiesel in the fuel [111] and higher viscosity [112], resulting in a shorter ignition delay.

6.2.4 Cumulative heat release

The cumulative heat release indicates the total heat released during the combustion stage. The cumulative heat values calculated from the present investigation on the engine running with pure diesel, biodiesel and its blends (B50 and B100) are shown in Figure 6-7. It can be seen that B50 resulted in higher cumulative heat release as compared to the diesel and B100.

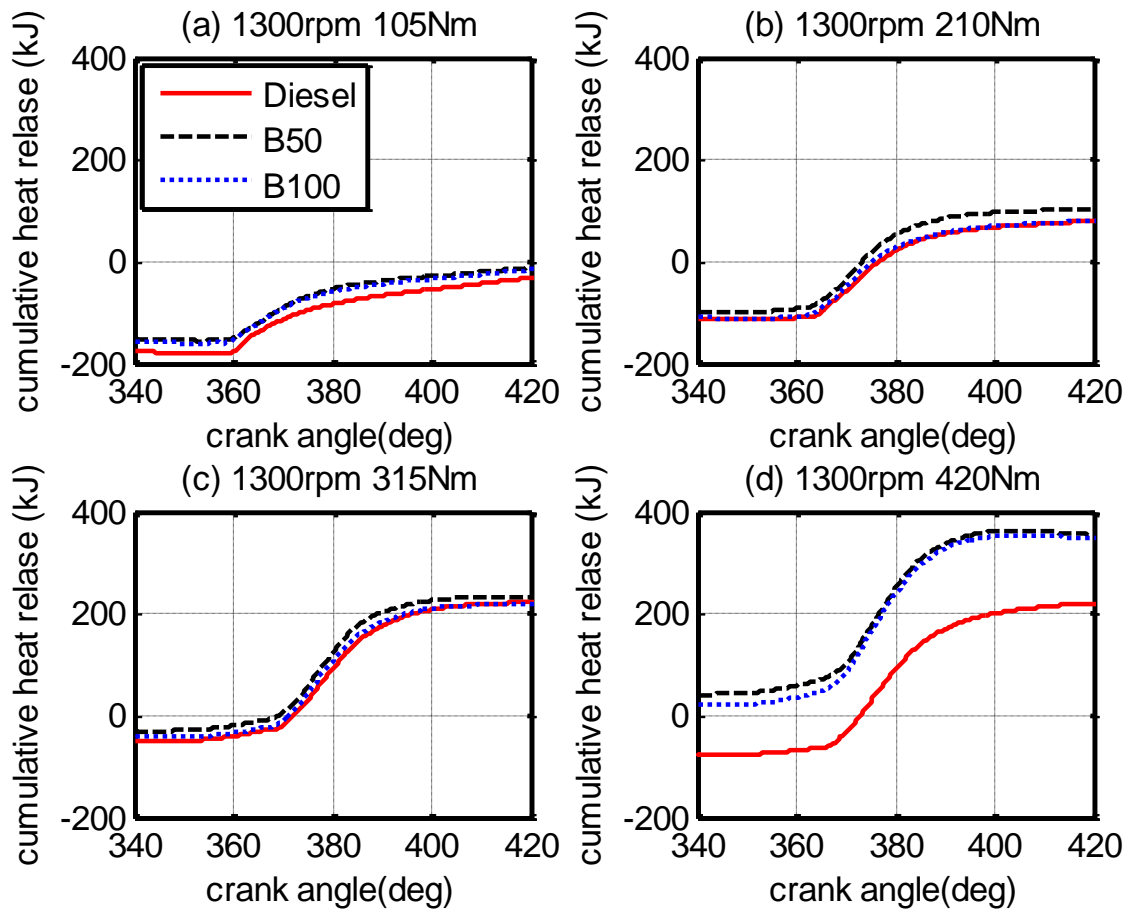


Figure 6-7 Cumulative heat release at a speed of 1300rpm and different loads

6.3 Vibration and noise from combustion

The vibration and acoustic signals of the test engine were related to the combustion process. Figure 6-8 shows the acoustic signals monitored in relation to body vibration and cylinder pressure on the test engine. It can be seen that higher cylinder pressures and fast pressure changing result in higher engine vibration and subsequently higher level acoustic signals. The variation of engine acoustics and vibration is related to the changing of in-cylinder pressure. When the combustion occurred in the cylinder, the cylinder pressure increased quickly, leading to the vibration of the engine body and generated radiated acoustic accordingly.

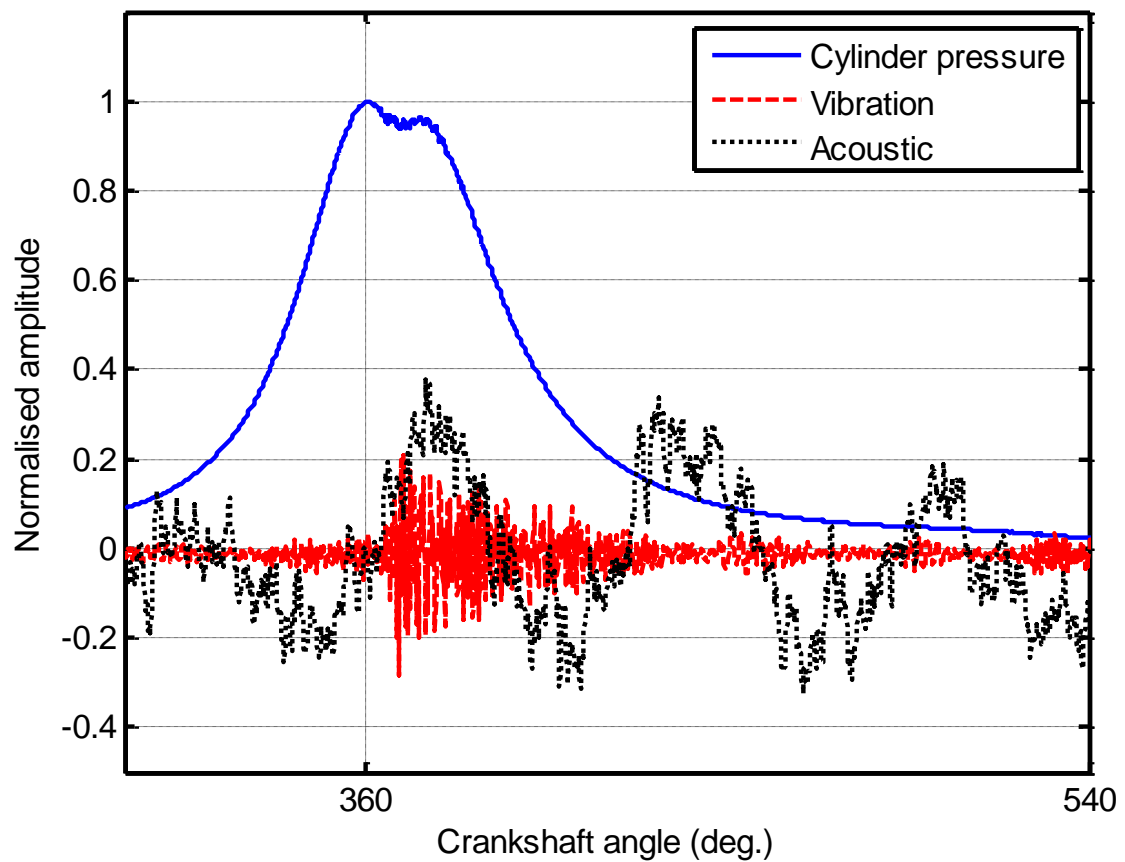


Figure 6-8 Normalised cylinder pressure, body vibration and engine acoustic

Diesel engines produce a complex noise whose level and sound quality are strongly dependent on the fuel combustion, as the primary source. This noise is the so-called combustion noise [113]. The complex noise of diesel engines is due to the harsh and irregular self-ignition of the fuel. Self-ignition occurs towards the end of the compression stroke and subsequent expansion stroke. The rapid pressure change due to combustion transmits through the engine structures and forms part of the airborne acoustic signal. The change of pressure causes vibration of the engine components such as the cylinder head, pistons, connecting rods and engine body; the vibrations of which all contribute to the overall engine noise level [114]. Together these noise sources account for over 80% of total engine noise. The combustion noise is the dominant source. A general description of the diesel engine noise generation from the combustion process is shown in Figure 6-9.

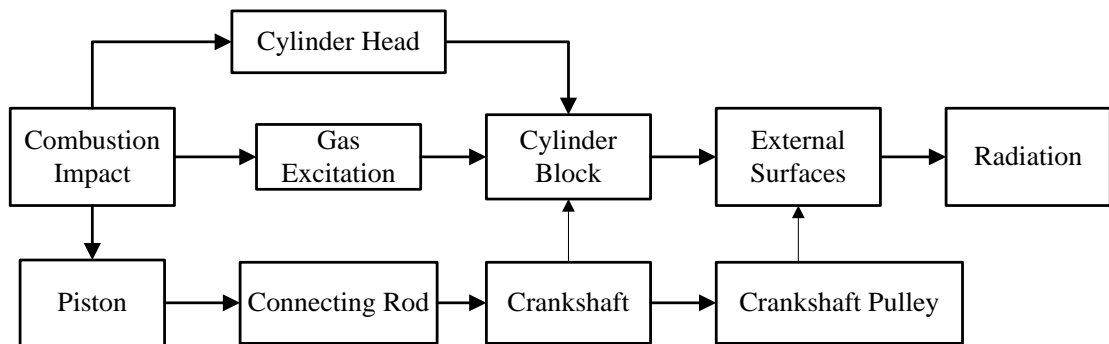


Figure 6-9 Combustion noise generation diagram

Figure 6-9 shows that noise is transmitted through three paths from the combustion impact, namely:

- The cylinder head
- Cylinder block
- The mechanical parts, including piston, connecting rod and crankshaft

In the first path, the noise is radiated from the cylinder head to the cylinder block and then directly into the air. Secondly, the gas explosion directly excites the cylinder block through which the noise is transmitted, and finally, noise is induced from the mechanical paths. Figure 6-9 is only shows the noise related to the combustion process. Another part of noise of diesel engine is the exhaust noise which is radiated from the exhaust pipe to the air.

There are a number of factors that could affect the combustion pressure characteristics and accordingly the combustion noise. The first is the cylinder bore dimension. Challen and Croker [86] found experimentally that measured noise levels increased proportionally with increases in the cylinder bore dimension. The reason for this is that the piston slap forces inside the cylinder are proportional to the piston bore dimension.

Another factor that could affect the combustion noise is the fuel injection system. Fuel injection characteristics and the types of injector nozzles could significantly affect combustion development. These characteristics include the fuel delivery, injection timing, injection pattern, spray formation, swirl level and residual gas which should all

be carefully controlled to appropriate levels [115]. Different types of nozzles affect combustion by changing the spray formation characteristics. There are also different types of combustion chambers, but their influence on combustion performance can be ignored [115].

The speeds and loads of the engine are additional factors which could affect noise. Tung, Challen and Croker [86][116] studied the effect of the speeds and loads on the engine noise, and found that the engine noise levels are quite sensitive to the changes in speed. Surprisingly, the effect of load variations on noise levels is not as influential as expected. It was observed that combustion noise decreased when the percentage of load was increased [86].

The engine output power, cylinder swept volume and the number of cylinders are also factors which influence combustion induced noise levels to a certain degree. In the following chapters, the engine vibro-acoustic signals are analysed using various non-stationary signal processing methods in the lower and higher frequency band respectively. The features extracted are used for the identification of engine conditions, diagnosis of combustion and evaluation of supply fuel quality.

CHAPTER 7

ANALYSIS OF ENGINE VIBRO-ACOUSTIC SIGNAL BASED ON FRACTIONAL FOURIER TRANSFORM

This chapter investigates the effects of biodiesel on the combustion process and the characteristics of the engine's vibro-acoustic signals produced by the combustion process. Firstly, the statistic characteristics of the engine vibration and noise and their relationships are studied by employing coherent power spectrum analysis technology. Secondly, the Wigner-Ville distribution is used to analyse the energy distribution of engine noise in the time-frequency domain. Finally, a band-pass filter based on fractional Fourier transform is developed to extract the main combustion related noise for fuel evaluation and diesel engine operating condition monitoring. The classification based on sound pressure level indicator shows that the combustion induced acoustic can be extracted for the identification of the combustion process and engine condition monitoring.

7.1 Researches on engine vibro-acoustics

The generation of sound is usually attributed to the vibration of solid objects and sound is explained as vibration of the air [17]. The solid borne noise that is transmitted through the objectives is responsible for producing the vibration and inducing noise. The study of engine vibration and noise has been carried out since the early stages of engine development and numerous noise level prediction researches have been proposed during recent decades.

Fujimoto [117] investigated the effect of the oil film on the piston slap induced noise, and found that *“the oil film formed between the piston skirt and the cylinder reduced the clearance and acted as a damper, therefore reducing the piston slap force to some extent”*. Periede *et al.* [84] also carried out a similar investigation and concluded that *“the piston slap noise was also proportional to the cylinder bore dimension.”* S. H. Cho *et al.* [118] present an analytical model which can predict the impact forces and vibratory response of an engine block surface induced by the piston slap of an internal combustion engine. *“The equivalent parameters such as mass, spring constant and damping constant of the piston and cylinder inner wall are estimated by using measured point mobility.”* The results are compared with experimental results to verify the model and to reach the conclusion that *“prediction of overall vibration level shows a similar tendency to the measured noise level close to the surface of the engine block.”* Shu and Liang [119] analyzed the complex engine noises using coherent power spectrum analysis and concluded that *“the noise of the low-frequency belt is primarily machinery noise, while the noise of the high-frequency belt is mainly combustion noise”*. Most engine noise is produced by the combustion process, but additional noise, such as the injection, inlet and exhaust noise as a result the injection of fuel and the intake and exhaust valves all make up a fraction of the overall noise [120].

Vibration and acoustic signals from an engine are usually noisy and non-stationary. It is essential to develop an appropriate analysis tool in order to extract accurate features from the non-stationary signals for engine condition monitoring, combustion diagnostics and fuel evaluation. Time-frequency analysis has been developed as a

more reliable and effective method for machinery condition monitoring as it can be used to observe the frequency variation according to the time. In this chapter, The Wigner-Ville distribution is employed to analyse the energy distribution of engine noise in time-frequency domain based on the limitation of the conventional methods in time or frequency domain. Taking into account the novel properties of the fractional Fourier transform (FRFT), a band-pass filter based on fractional Fourier transform has been developed to extract the combustion induced noise from the engine noise for combustion diagnostic and fuel evaluation.

7.2 Statistical characteristics of vibration and acoustic signals

7.2.1 Variations of engine vibro-acoustic signals

As previously discussed, engine noise is linked to engine vibration, and both are dependent on the variation of the in-cylinder pressure of the engine during the combustion process. This means that the trend of the engine vibration and noise should correspond to the changing of the in-cylinder pressure as determined by the fuel combustion characteristics for different type of fuels and by the engine operating conditions including speeds and loads.

Figure 7-1 shows the engine vibration signals at a speed of 1300rpm and at different loads of 210N m, 315N m and 420N m fuelled by different fuels of diesel, B50 and B100. It is presented based on one complete combustion cycle (720 degree) which is a simple and fundamental way of presenting data in the angular domain. This indicates that the amplitudes of the vibration signals increase alongside the increasing loads from 210N m to 420N m at a constant speed. Consequently, the acoustic signals should be increased accordingly. Figure 7-2 demonstrates the acoustic signals at a speed of 1300rpm and under different loads of 210N m, 315N m and 420N m. From this, it can be seen that the amplitude of the acoustic signals increases according to the increase of engine loads under all types of fuels.

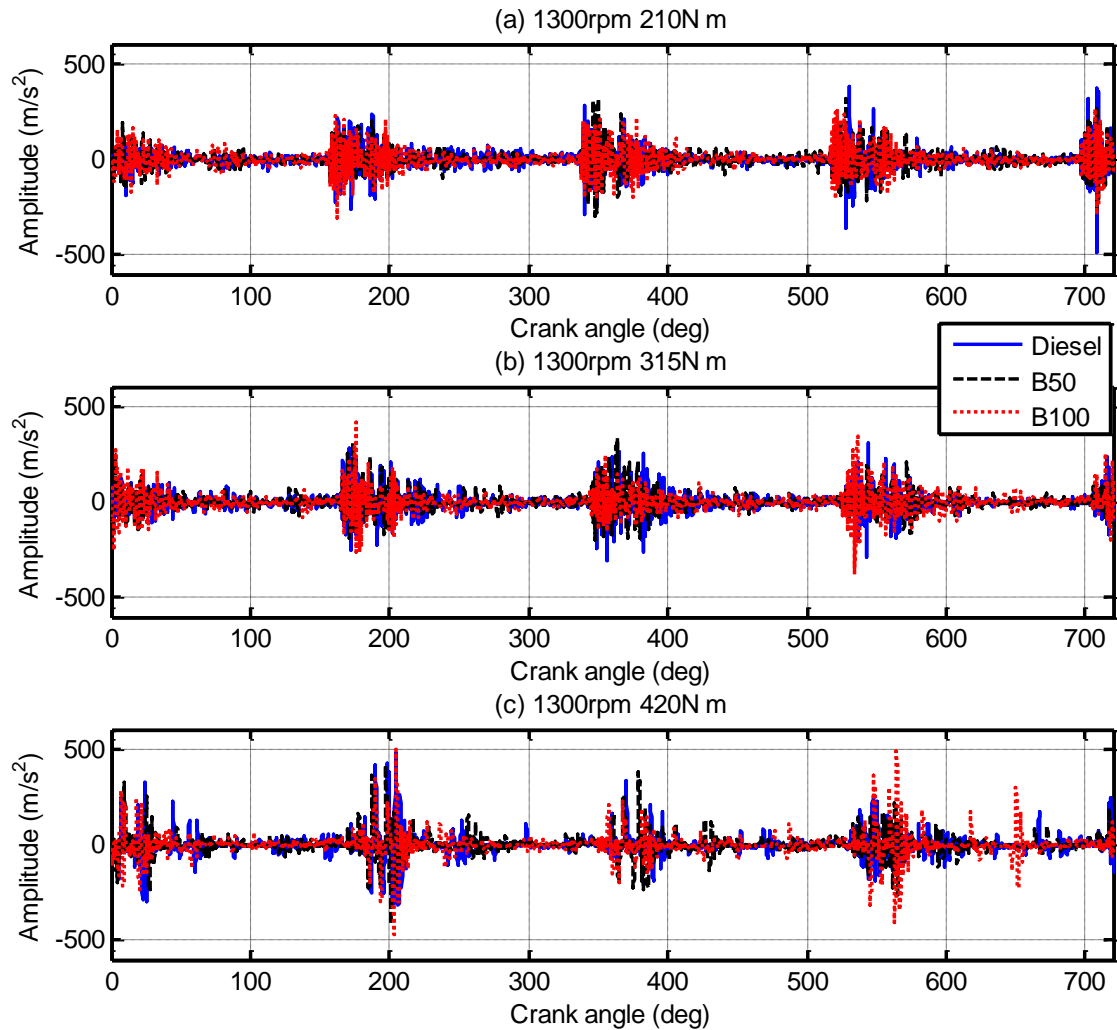


Figure 7-1 Vibration signals at a speed of 1300rpm under different loads

Even though the variation of the engine vibration and the noise corresponding to the loads and speeds can be indicated simply in the time domain waveform as is seen in Figure 7-1 and 7-2, it is difficult to observe clear features between different fuels. This is due to the complexity of engine noise sources and their mutual interference during the operation of the engine. The non-stationary characteristics of the engine vibration and noise also increase the difficulty of feature extraction between different fuels in the time domain. Based on the previous study [119], the main sources of noise within an engine are machinery noise and combustion noise. While the engine noise of a low-frequency belt is mainly the machinery noise of the oil pump, gear and valve mechanism which radiate from a thin-walled part such as the gear or valve cover. The

combustion noise can be seen in the high-frequency band of the engine noise which radiates from the combustion process.

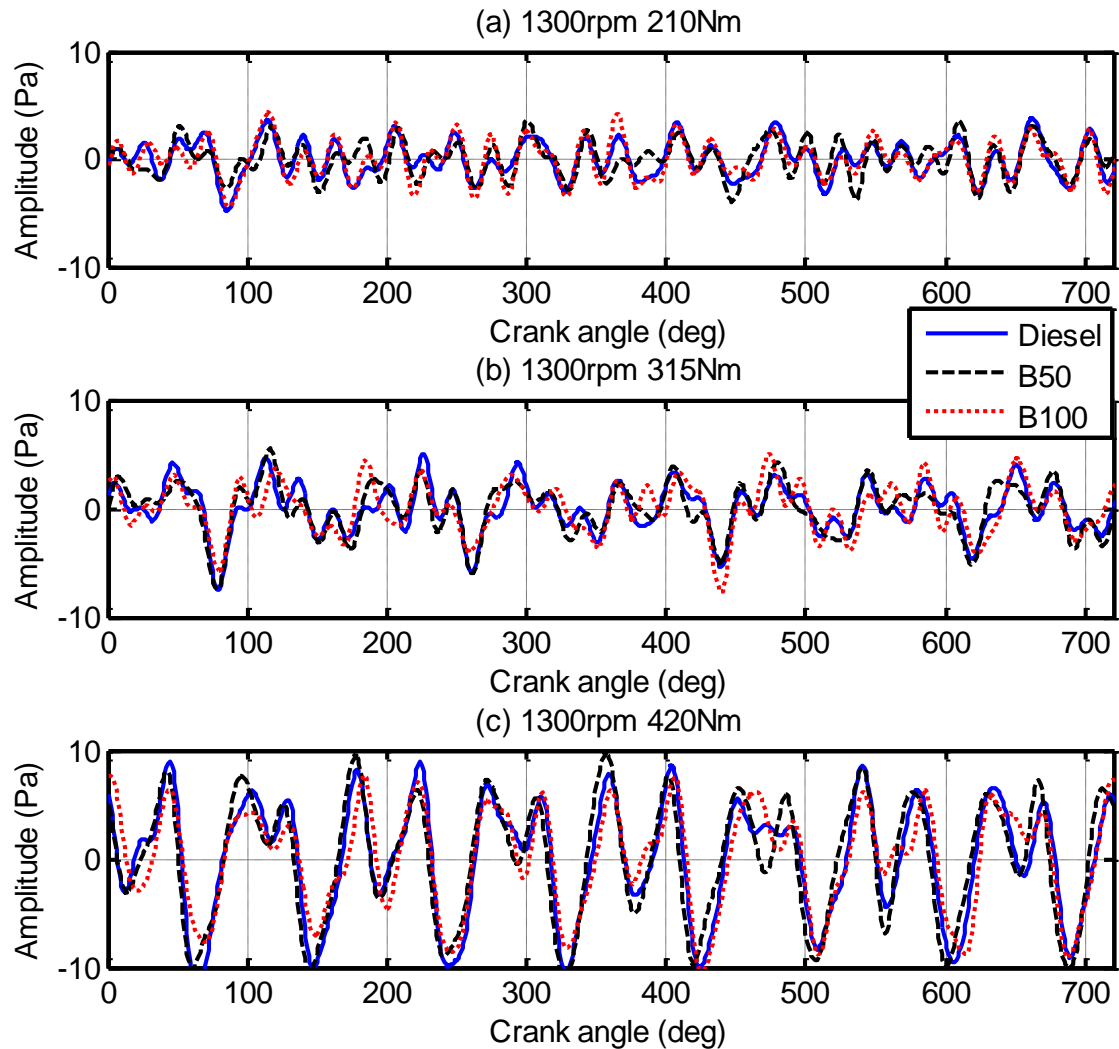


Figure 7-2 Acoustic signals at a speed of 1300rpm under different loads

Figure 7-3 and Figure 7-4 show the spectrum of vibration and acoustic signals in a low operating condition at speed of 900rpm with a load of 105N m, and a high operating condition at speed of 1300rpm with a load of 420N m, respectively. It can be seen that the energy of vibration and acoustic signals increase alongside the load and speed. The amplitudes of the spectrum of the engine noise are higher in the low-frequency band compared to that of the high-frequency band. This is potentially due to the resonance of the engine room modes being excited by the test engine noise. The main frequency

components of the machinery noise and vibration in the low frequency band are related to the firing frequencies and their harmonics which correspond to the engine speeds. It is also difficult to distinguish the fuels from the spectrum of the vibration and acoustic signals according to the Figure 7-3 and Figure 7-4. Based on the generation mechanism of the acoustic signals, engine noise is excited by the vibration of the engine, and the vibration is produced by the in-cylinder pressure changing during the combustion process. Therefore, the engine noise should be related to the engine vibration and the engine combustion process, even if it is also polluted by the background noise and affected by the resonance of the engine room modes. Hence, the combustion process and fuel quality should be revealed through analysis of the engine vibration or noise signals using proper signal processing methods.

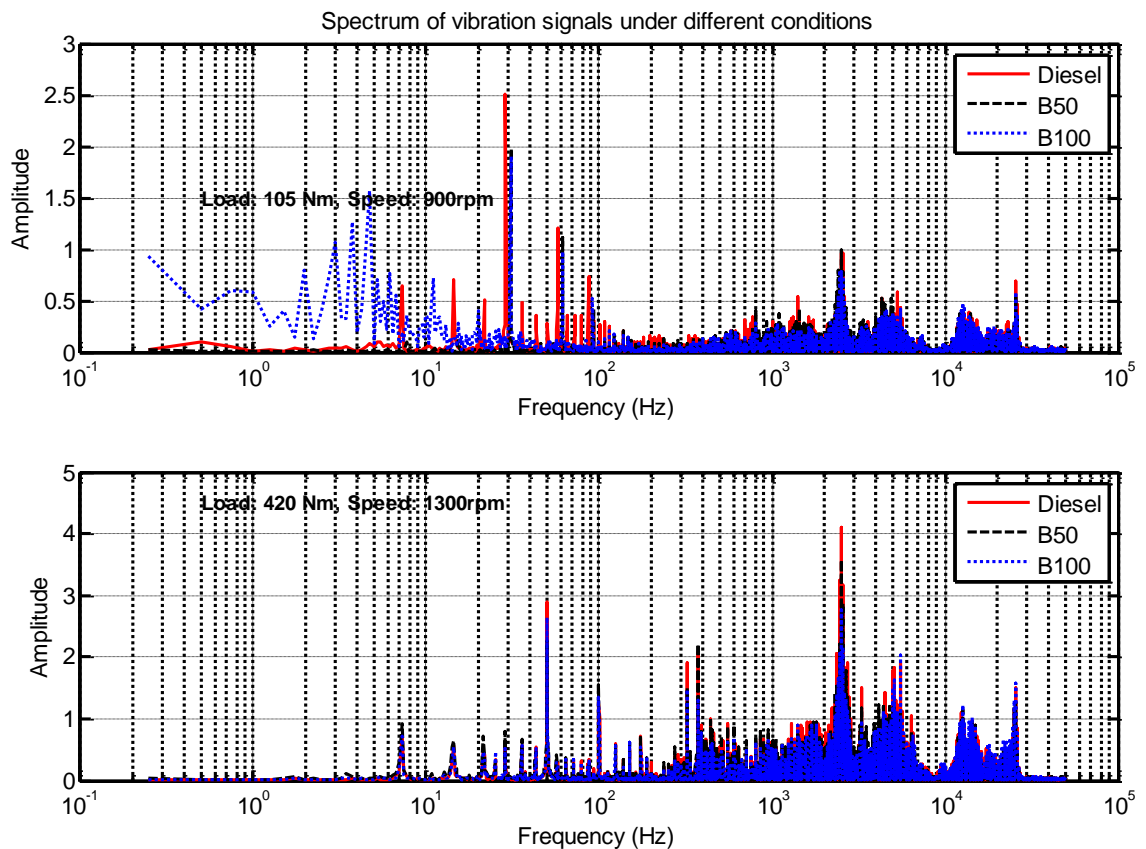


Figure 7-3 Spectrum of vibration signals under different conditions

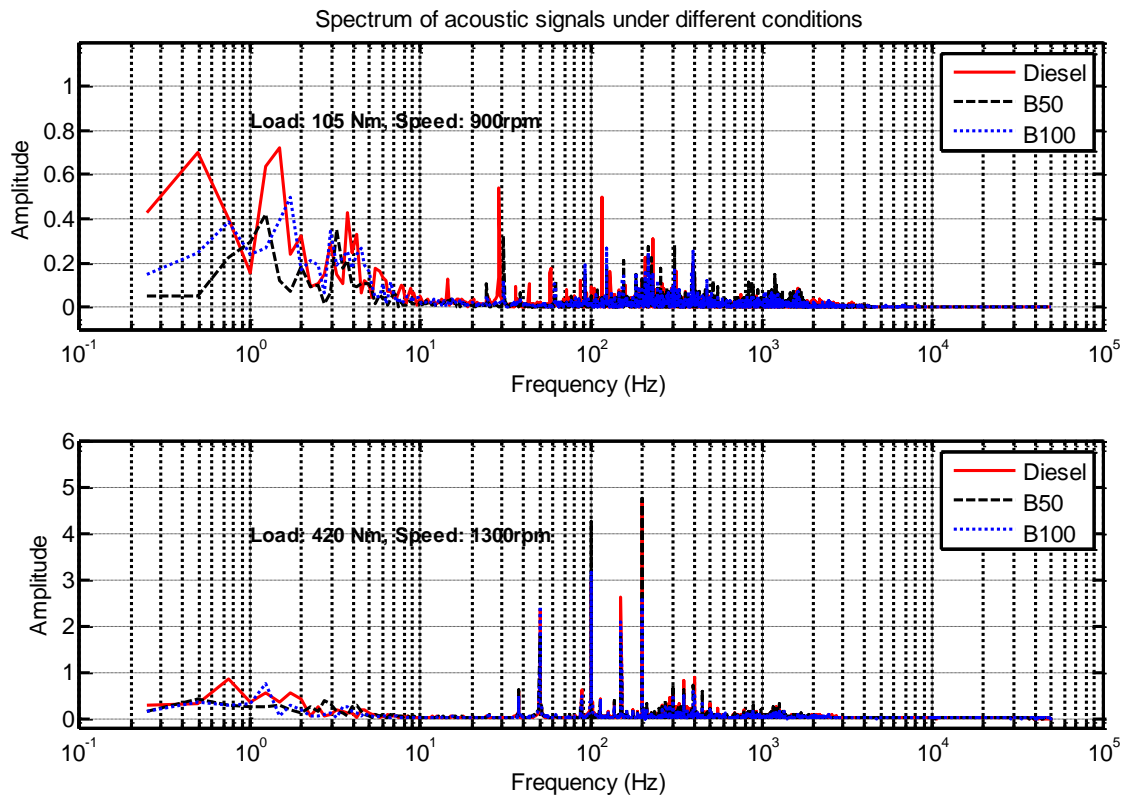


Figure 7-4 Spectrum of acoustic signals under different conditions

7.2.2 Coherent power spectrum analysis

The engine noise measured by an acoustic transducer is the total noise generated by the engine, which also includes a number of noise sources such as combustion, injection, intake and exhaust noise [14]. In order to analyse the frequency components of the engine noise, which is closely related to the combustion process, the correlation of the engine noise and the vibration should be analysed as acoustic is derived from vibration [17].

For analysing the correlation of the engine noise, engine vibration and combustion process, the coherent power spectrum analysis should be employed in order to recognise the noise sources or vibration sources that are related to the combustion process. It is because the vibration is related to the in-cylinder pressure changing during the combustion process. The noise generated by an engine can be modelled as a linear time system with multiple inputs and a single output as shown in Figure 7-5.

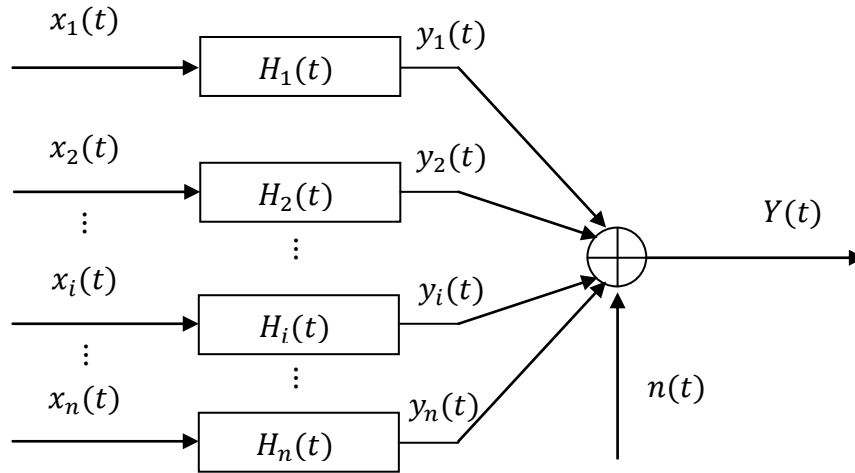


Figure 7-5 Engine noise source model

Assuming the complex engine noise sources system has n noise sources, which produce a signal $x_i(t)$, The signal measured by accelerator sensor is s_i . The function $H_i(t)$ is a scalar transfer function between the input $x_i(t)$ and the output $y_i(t)$ of the system. The measured output $Y(t)$ contains the output $y_i(t)$ and the uncorrelated background noise $n(t)$.

The measured acoustic signal $Y(t)$ can be formulated as follows:

$$Y(t) = \sum_{i=1}^n x_i(t) * H_i(t) + n(t) \quad (7-1)$$

where $*$ denotes the convolution operation.

Assuming that there is no correlation among different input signals $x_i(t)$, this model can be used regarding a frequency independent system [121]. The cross power spectrum between input $x_i(t)$ and output $Y(t)$ can be expressed as

$$G_{x_i Y}(f) = H_i(f) G_{x_i x_i}(f) \quad (7-2)$$

The coherence function of input $x_i(t)$ and output $Y(t)$ can be computed by

$$\gamma_{x_i Y}^2 = \frac{|G_{x_i Y}(f)|^2}{G_{x_i x_i}(f) G_{Y Y}(f)} \quad (7-3)$$

The input coherent power spectrum can be defined as the product of the coherent function and the input power spectrum [119],

$$G_{x_i Y}(f) = \gamma_{x_i Y}^2 G_{x_i x_i}(f) \quad (7-4)$$

where x_i can be considered as the input signal, and Y denotes the output signal of a measurement system. $G_{x_i x_i}$ and G_{YY} are the self-power spectrum of x_i and Y respectively. $G_{x_i Y}$ is the cross power spectrum between the input signal x_i and the output Y . $\gamma_{x_i Y}^2$ represents the coherent function of the input signal x_i and the output signal Y .

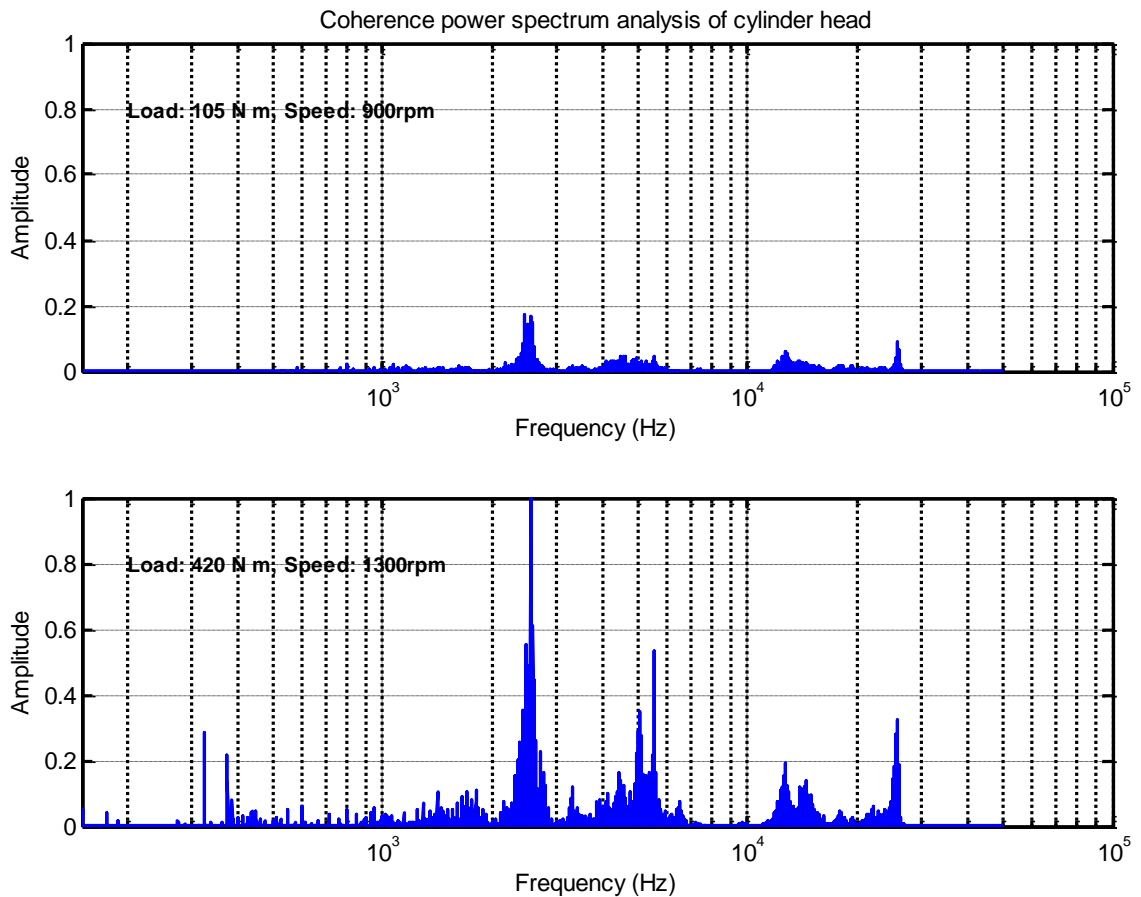


Figure 7-6 Coherent power spectrum analysis of engine noise

In this study, the signal measured by the accelerator sensor from the cylinder head of the engine is used as the input signal for coherent power spectrum analysis, while the

output signal is the signal measured by the microphone. Figure 7-6 shows the coherence power spectrum analysis results of the cylinder head vibration and engine acoustic. It indicates that the vibration of the cylinder greatly contributes to the engine noise at the frequency band of 2 kHz - 3 kHz and shows that the noise at the frequency around 5 kHz is also related to the vibration of cylinder head. It also can be seen from Figure 7-6 that the amplitude of the coherent power spectrum increases with the engine load and speed, leading to the increase of engine noise accordingly.

7.3 The time-frequency distribution of engine acoustics

7.3.1 The Wigner-Ville distribution

Wigner-Ville distribution (WVD) is a simple and effective time-frequency analysis method, it gives the instantaneous power of the analysed signal at the time t and the frequency ω . The continuous Wigner-Ville distribution of a general signal $x(t)$ can be defined by Equation (7-5) [37].

$$W_f(t, \omega) = \int_{-\infty}^{+\infty} x(t + \tau/2) x(t - \tau/2) e^{-j\omega\tau} d\tau \quad (7-5)$$

where $x(t)$ is the real-valued time signal and t and ω are the time and frequency indices, respectively. τ is the radius extending from time t . It can be seen from Equation (7-5) that the instantaneous power relies on the nature of the signal being far away from the time t due to the integral requiring an infinite signal length. As a result, localisation characteristics of the Wigner-Ville distribution are reduced to some extent. In application, a time window $w(t)$ is often added to the analysed signal before the transform is carried out [37].

$$x_w(t) = x(t)w(t) \quad (7-6)$$

The length of the added window in equation (7-6) is much shorter than that of the analytical signal, and the window has the ability to slide along the time axis so that its centre is always located at time t [40]. This short-timed window makes the transform

capable of capturing transients with a better resolution. The Wigner-Ville distribution of the windowed signal as shown in equation (7-6) can be expressed by:

$$W_{f_w}(t, \omega) = \frac{1}{2\pi} \int_{-\infty}^{+\infty} W_f(t, \eta) W_w(0, \omega - \eta) d\eta \quad (7-7)$$

where W_f and W_w are the Wigner-Ville distribution of the analytical signal and the window function respectively. In fact the Wigner-Ville distribution of a signal according to equation (7-7) is a low-pass smoothed version of the original Wigner-Ville distribution in the frequency domain [40].

7.3.2 Wigner-Ville distribution analysis of engine acoustics

Figure 7-7 shows the Wigner-Ville distribution of the test engine noise at loads of 105N m and 420N m for different fuels. The length of the window for the Wigner-Ville distribution was determined based on one complete combustion cycle (720 degrees). It can be seen that the main energy of the engine noise is located in the low frequency band which is below 1 kHz at low engine load of 105N m as shown in Figure 7-7 (a), (c) and (e). With the increase of the percentage of biodiesel, the energy level at the high frequency band (2 kHz-3 kHz) increases as well. At a high engine load of 420N m according to Figure 7-7 (b), (d) and (f), the main energy of the engine noise is located at a frequency of around 1 kHz and 2 kHz. Wigner-Ville distribution of engine noise at the frequency band of 2 kHz to 3 kHz particularly contributed by the combustion process as discussed through the coherence analysis of cylinder head vibration and engine acoustic. The strength of the acoustic energy in the frequency band of 2 kHz to 3 kHz can be used to monitor the combustion process and engine supply fuels. A band pass filter based on fractional Fourier transform is designed for the extraction of the acoustic signal at the frequency band of 2 kHz to 3 kHz.

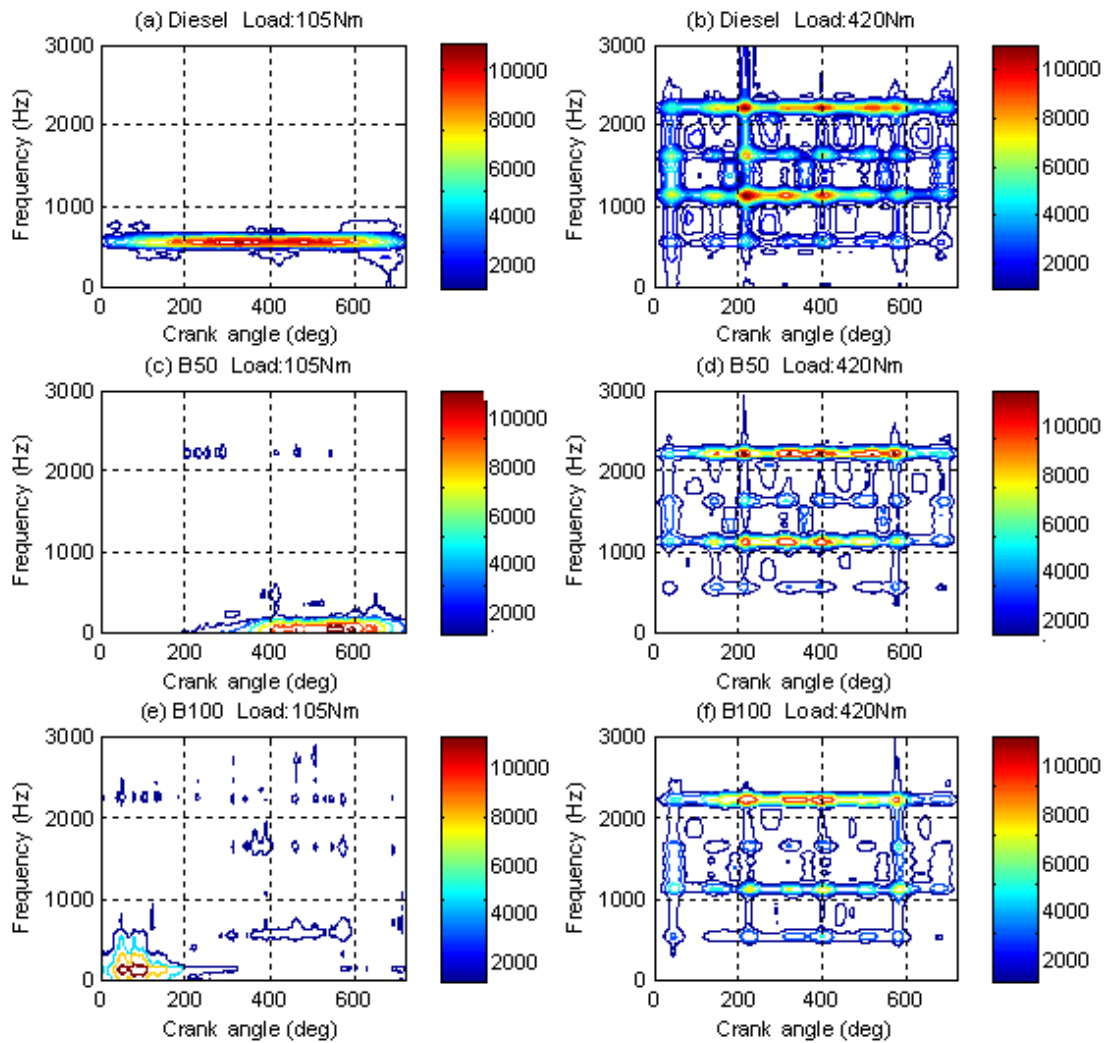


Figure 7-7 WVD of engine noise at loads of 105N m and 420N m

7.4 The fractional Fourier transform

The fractional Fourier transform (FRFT) is a generation of the classical Fourier transform, introduced from the mathematic aspect and applied in many areas [50]. The fractional Fourier transform provides a time-frequency distribution which extends from the conventional Fourier theory for the analysis of non-stationary signals, especially linear chirp signals. fractional Fourier transform is a technique which rotates the conventional time-frequency domains to a specified angle α allowing the designer to have more flexibility for extracting the useful signals or decreasing noisy signals [122].

7.4.1 Definition of fractional Fourier transform and its properties

The α^{th} order fractional Fourier transform of a signal $x(t)$ can be defined as [50].

$$X_\alpha(u) = \int_{-\infty}^{+\infty} x(t)K_\alpha(t, u)dt \quad (7-8)$$

$$\alpha = p \frac{\pi}{2} \quad (7-9)$$

The kernel function $K_\alpha(t, u)$ can be expressed as

$$K_\alpha(t, u) = \begin{cases} \sqrt{\frac{1-j\cot\alpha}{2}} e^{j(\frac{1}{2}u^2\cot\alpha + \frac{1}{2}t^2\cot\alpha - ut\csc\alpha)}, & \alpha \neq n\pi \\ \delta(t - u), & \alpha = 2n\pi \\ \delta(t + u), & \alpha = (2n + 1)\pi \end{cases} \quad (7-10)$$

where α is the rotation angle of the transformed signal for fractional Fourier transform and p is the transform order of the fractional Fourier transform. It is found that the fractional Fourier transform of the signal $x(t)$ at the order $\alpha = 0$ is the input signal $x(t)$, and the order $\alpha = \pi/2$ corresponds to the Fourier transform of the signal $x(t)$ while the order $\alpha = \pi$ is the inverse of the signal $x(-t)$. The order $\alpha = 3\pi/2$ is the Fourier transform of the signal $x(-t)$. Obviously, the fractional Fourier transform is periodic with period of 4. Let $u = u/\sqrt{2\pi}$ and $t = t/\sqrt{2\pi}$. Then the equation (7-8) equivalent to:

$$X_\alpha(u) = \int_{-\infty}^{+\infty} x(t)K_\alpha(t, u)dt$$

$$= \begin{cases} \sqrt{\frac{1-j\cot\alpha}{2\pi}} e^{j\frac{1}{2}u^2\cot\alpha} \int_{-\infty}^{+\infty} x(t) e^{j\frac{1}{2}t^2\cot\alpha - ut\csc\alpha}, & \alpha \neq n\pi \\ x(t), & \alpha = 2n\pi \\ x(-t), & \alpha = (2n + 1)\pi \end{cases} \quad (7-11)$$

In the time-frequency representations, a plane with two orthogonal axes corresponding to time and frequency is used to present the analytical signal as shown in Figure 7-8 [123]. The Fourier transform of a signal is a counter-clockwise axis rotation of $\pi/2$ rad from the time axis t to the frequency axis ω . The fractional Fourier transform is a representation of the signal along an axis u making an angle of α with the time axis t .

The rotation of the angle α is from 0 to 2π rad and is presented by the transformation kernel $K_\alpha(t, u)$ as shown in equation (7-10). The operator of fractional Fourier transform can be defined as R^α .

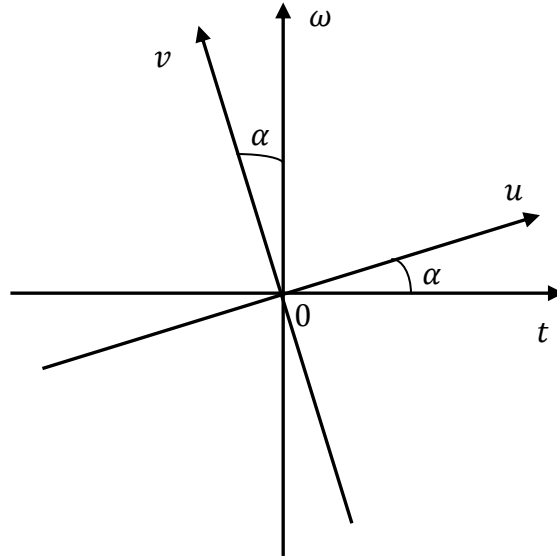


Figure 7-8 Time-frequency plane and a set of coordinates (u, v) rotated by an angle α relative to the original coordinates (t, ω)

The operator R^α has the following properties [123]:

1. When $\alpha = 0$, $R^0 = I$
2. When $\alpha = \frac{\pi}{2}$, $R^{\pi/2} = F$
3. Additively of rotations: $R^\alpha R^\beta = R^{\alpha+\beta}$
4. When $\alpha = 2\pi$, $R^{2\pi} = I$

where F in property 2 means the Fourier transform, and I in properties 1 and 4 indicates the signal itself.

From the properties of the fractional Fourier transform operator, the inverse of an fractional Fourier transform with an angle α is the fractional Fourier transform with angle $-\alpha$:

$$x(t) = \int_{-\infty}^{+\infty} X_\alpha(u) K_{-\alpha}(t, u) du \quad (7-12)$$

where $x(t)$ is expressed by a class of basic functions $K_{-\alpha}(t, u)$ with weight factors $X_{\alpha}(u)$. The basic functions are complex exponentials with linear frequency modulation. For different values of u , they differ only by a time shift and by a phase factor that depends on u [50]:

$$K_{-\alpha}(t, u) = e^{-j\frac{1}{2}u^2 \tan\alpha} K_{\alpha}(t - u \sec\alpha, 0) \quad (7-13)$$

7.4.2 Band-pass filter based on fractional Fourier transform

Based on the definition and the properties of the fractional Fourier transform, a band-pass filter can be designed for useful or interesting signal extraction from the raw measured signal. This is beneficial for the extraction of accurate features for machinery condition monitoring or fault diagnosis. The filtering process based on fractional Fourier transform should be described as follows:

1. Calculation of the fractional Fourier transform of the analytical signal according to the variation of the order $\alpha = p \frac{\pi}{2}$. The range of p is from 0.5 to 1.5, so the energy distribution of the analytical signal on the fractional plane can be obtained as shown in Figure 7-9 (a).
2. Search for the peak point (p_0, u_0) on the fractional plane, u acting as a parameter for spanning the set of basic functions, and p is related to the angle, then calculate the fractional Fourier transform of the analytical signal at the order of $\alpha_0 = p_0 \frac{\pi}{2}$.
3. Filter the analytical signal in the fractional domain using a band-pass filter. The centre frequency of the filter is based on the localization of the peak point u_0 on the fractional plane. The energy distribution of the filtered signal on the fractional plane is shown in Figure 7-9 (b).
4. The extracted signal in the time domain can be obtained by calculating the fractional Fourier transform of the filtered signal at the order of $\alpha_0 = -p_0 \frac{\pi}{2}$.

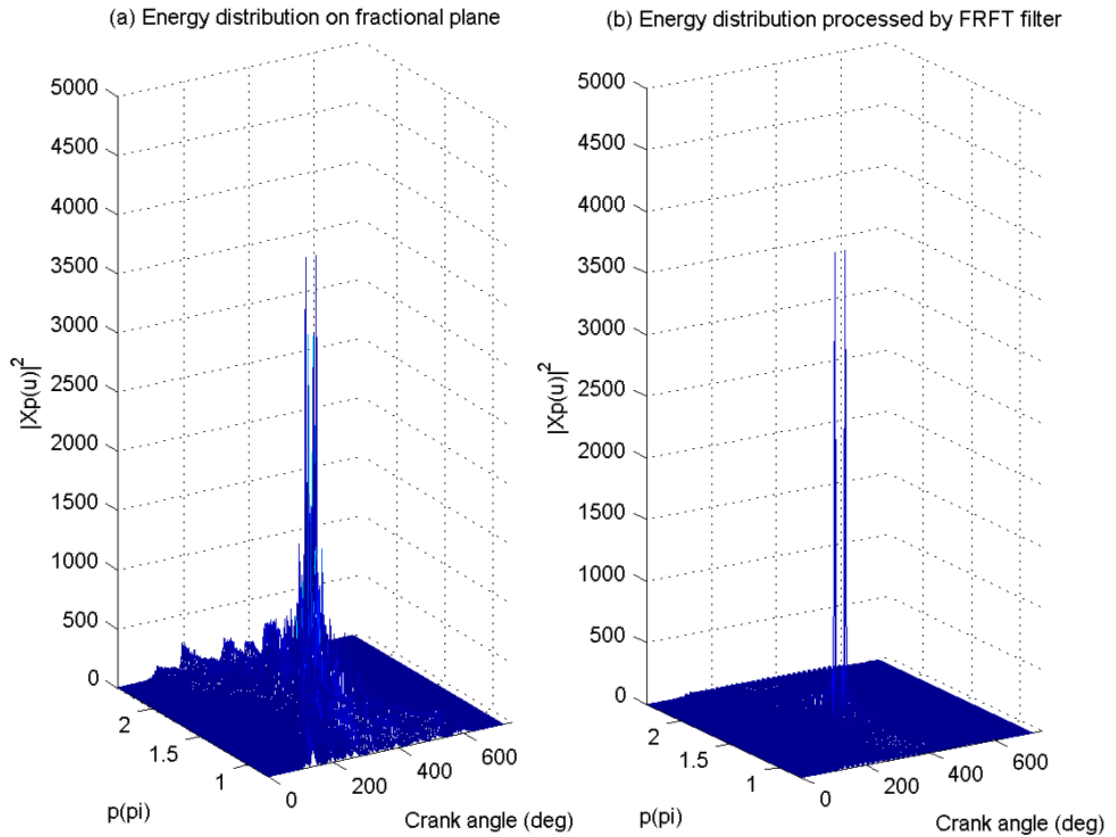


Figure 7-9 Energy distributions on the fractional plane

7.4.3 Combustion noise extraction

From the Wigner-Ville distribution analysis of the engine noise signal in section 7.3.2, it can be concluded from figure 7-7 that the frequency of engine noise, which is around 2 kHz to 3 kHz, has higher energy and can be used to reveal the differences between different types of fuels. Based on the coherent power spectrum analysis of the engine noise, it can be seen that the frequency of the combustion related noise is mainly located between 2 kHz and 3 kHz. Therefore, the band-pass filter based on the fractional Fourier transform under the criteria of the maximum peak value is used to extract the engine noise components located around 2.5 kHz for fuel evaluation and combustion monitoring.

Figure 7-10 (b), (d) and (f) show the Wigner-Ville distribution of the combustion induced noise extracted by the band-pass filter based on fractional Fourier transform.

For comparison, Figure 7-10 (a), (c) and (e) show the Wigner-Ville distribution of the unfiltered engine noise at the load of 420N m for different fuels, B50 and B100. It can be seen that the engine acoustic contributed by the combustion process at the frequency band of 2 kHz to 3 kHz is extracted from the total engine noise, and its energy level and strength on the time-frequency plane reflected the differences of the fuels. A linear classifier based on sound pressure level calculation can be designed based on the differences indication for the different operating condition separation, including fuel quality, speed and load.

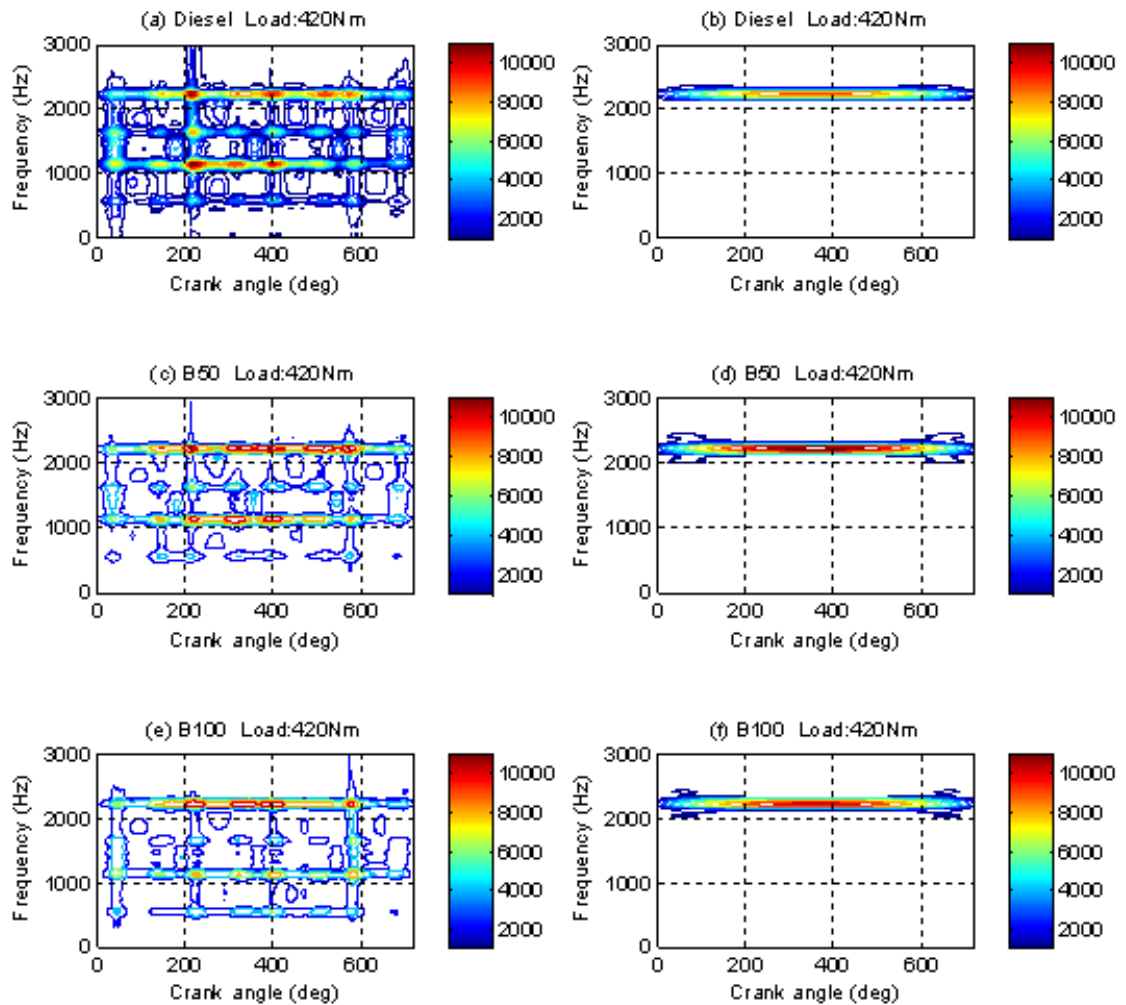


Figure 7-10 WVD of engine noise processed by FRFT filter

7.5 Feature extraction and classification

Sound pressure level is calculated from the filtered engine noise at all test conditions, and is used as a feature value for the separation and classification of different fuels for engine fuel evaluation. Figure 7-11 shows variations of the sound pressure level (SPL) and combustion induced noise under different engine operating conditions, including: different fuels (diesel, B50 and B100), different speeds (900rpm and 1300rpm) and different loads (105N m 210N m, 315N m and 420N m).

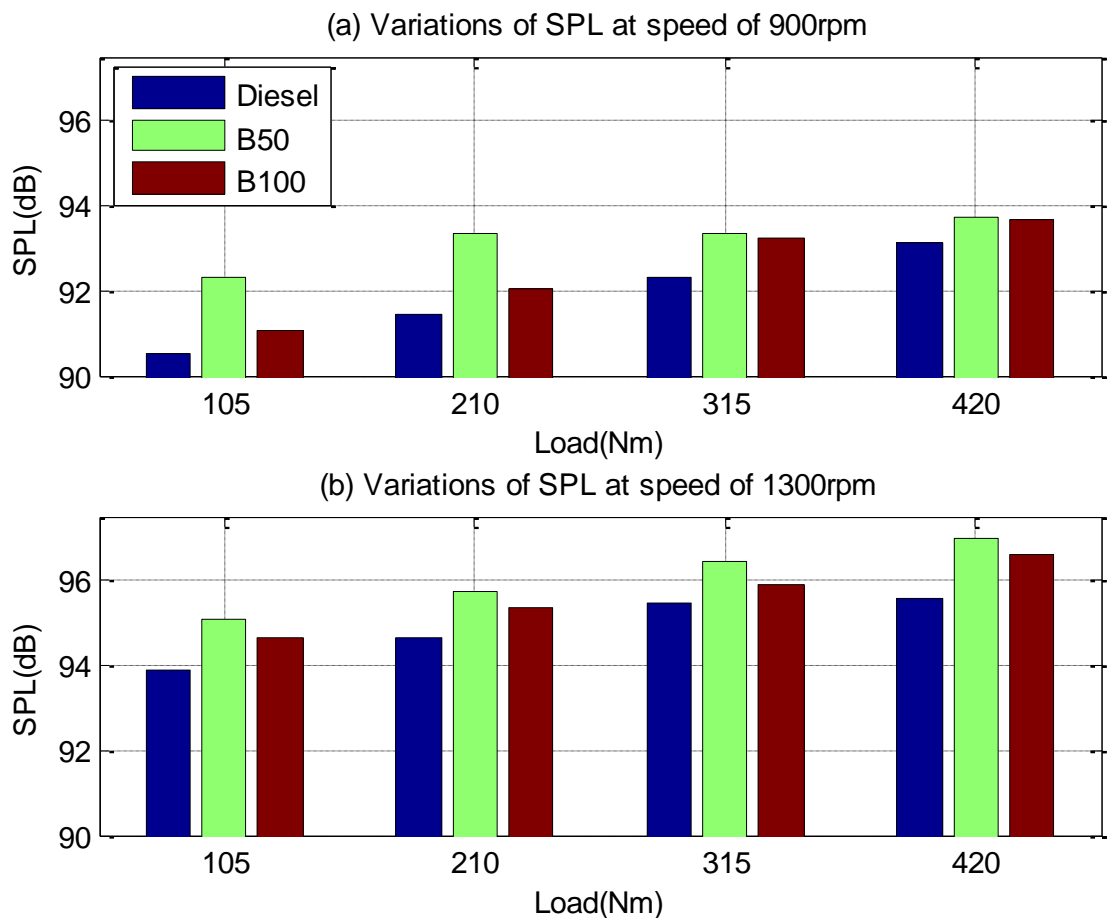


Figure 7-11 Variations of SPL for different fuels

From figure 7-11, it can be seen that the sound pressure level increased with the increase of speeds and loads under all engine fuelled conditions. The sound pressure level of the engine fuelled by biodiesel and its blends (B50 and B100) was slightly higher than that fuelled by diesel. The sound pressure level of the engine fuelled by

B50 is higher than that of the engine fuelled by B100 under all test engine speeds and loads. This is because of higher peak pressures and heat release rates obtained during the combustion process when the engine was fuelled by B50 according to the combustion parameters analysis. It can therefore be concluded that higher pressure with fast changing produces higher engine vibration and noise, so the engine vibration and acoustic can be used to monitor the engine combustion monitoring instead of using in-cylinder pressure. It is a non-contact and practical measurement method.

In the present study, an experimental investigation was carried out on the combustion process, vibration and noise analysis of a CI engine operating with rapeseed biodiesel and its blends under steady state operating conditions. Based on the experimental study, the main results are summarized as follows:

- The peak cylinder pressure was higher for rapeseed oil biodiesel than that for diesel at all test conditions. The peak cylinder pressures for both diesel and biodiesel and its blends were increased with increased engine loads and speeds as a result of longer ignition delay resulting in more fuel being made available for ignition and more energy being released during the premixed combustion stage.
- The ignition delay increased alongside engine loads and speeds for all types of fuels as a result of the extension of the vaporization time of the fuel in terms of the crank angle leading to the maximum heat release rate occurring later. The maximum heat release rate increased with the rise of the engine loads as a result of the increase in the quantity of fuel injected into the cylinder.
- Combustion started earlier for biodiesel and its blends and decreased as increased percentages of biodiesel were introduced under all engine operating conditions.
- The heat release rate of biodiesel was higher at higher loads even with a shorter ignition delay.
- The amplitude of the engine acoustic signals increased alongside the engine loads and speeds due to higher engine vibration.

- The SPLs of combustion induced noise when the engine was fuelled by biodiesel and its blends were slightly higher than those fuelled by diesel due to higher in-cylinder pressure producing higher vibration during the combustion process.

Based on the coherent power analysis of engine vibration and acoustics, it can be seen that the frequency of the combustion related noise is mainly located between 2 kHz and 3 kHz. The engine acoustic components during this low frequency band can be extracted for the identification of the combustion process and engine condition monitoring by a sound pressure level indicator based on a band-pass fractional Fourier transform filter. If the engine acoustic components in the higher frequency band can be used for combustion process diagnosis and engine condition monitoring, chapter 8 presents the analysis of engine acoustics in the higher frequency band for the combustion diagnosis and engine condition monitoring.

CHAPTER 8

COMBUSTION DIAGNOSIS BASED ON ENGINE ACOUSTICS USING WAVELET ANALYSIS

In this chapter, the continuous wavelet transform and time synchronous average will be applied with respect to engine noise processing for non-intrusive combustion diagnosis. Firstly, the mathematical characteristics and properties of continuous wavelet transform are briefly explained. Secondly, the principle of time synchronous average and its performance on processing the engine acoustic signals are discussed. Thirdly, the analysis results using the continuous wavelet transform and time synchronous average are presented and a summary of the results is given at the end of the chapter. The RMS linear classification shows that the RMS values of continuous wavelet transform coefficients can be used to evaluate the fuel for engine combustion and to indicate engine operating conditions.

8.1 Introduction to engine acoustics analysis using continuous wavelet transform

Time domain based statistical analysis can be used to observe the variations in signal energy trend development. Frequency domain based spectral analysis can reveal the compositional information of the acoustic signals in terms of frequency components. Acoustic signals from diesel engines are very complicated and difficult to analyse both in the sources of the sound, and the mechanism by which it is generated. The vibration and acoustic signals from diesel engines are usually noisy and non-stationary with wide frequency band. Furthermore, all the signals have distinctive time properties related characteristics regarding the structure of diesel engines. For example, combustion occurs once at the top dead centre (TDC) position in every two revolutions for diesel engines with four cylinders, and the pressure will be changed quickly, serious vibration will be generated, then produce noise radiated to the air from the engine structure.

Using conventional signal processing methods (see Section 2.3 and 2.4) based on the time or frequency domain it is not possible to reveal the non-stationary characteristics of these signals effectively. It is essential to develop effective methods (see Section 2.5) to extract accurate features from the non-stationary signals for machinery condition monitoring and fault diagnosis. Continuous wavelet transform (see Section 8.2) has the ability to capture the transient events present the high frequency band details and can reveal time-frequency characteristics of a non-stationary signal. Continuous wavelet transform is a typical and powerful time-frequency tool widely used in machinery condition monitoring and diagnostics as it is capable of displaying results in both the time and frequency domains at the same time.

In this chapter, continuous wavelet transform is employed to analyse the engine acoustic signals for the combustion diagnosis of a diesel engine fuelled by both pure diesel and biodiesel blends. The characteristics of the engine noise are investigated in relation to the variation of the in-cylinder pressure during the combustion process in

order to analyse the relationship between the engine acoustic characteristics and the combustion process of the diesel engines. In addition, as diesel engines are rotating machinery, the time synchronous average (TSA) can be used to pre-process the engine acoustic signals in order to enhance the signal-to-noise ratio (SNR) so that accurate analysis results can be obtained.

8.2 The continuous wavelet transform

Wavelet transform is an effective time-frequency analysis technique with high resolution and localisation characteristics. The width of the time window used in the transform can be adjusted; for instance, a wide time window is selected for analysing the low frequency band in order to collect complete cyclic information, whilst a narrow time window is chosen to extract the short time transient signals of interest in the high frequency band. Wigner-Ville distribution cannot adjust the time window width once a window has been selected for analysis. This means that the wavelet transform is more flexible for processing signals in the time-frequency domain.

There are two main categories of wavelet transform, namely the discrete wavelet transform and the continuous wavelet transform [21]. The discrete wavelet transform is suitable for data compression and signal reconstruction while the continuous wavelet transform is a better method for signal detection and feature extraction [124]. For the discrete wavelet transform, the relevant parameters must be discrete, and dyadic discretization is the most popular method using fast algorithms [125]. Although discrete wavelet transform saves computing time, it has some limitations making it unsuitable for feature extraction. Firstly, the orthogonal of the wavelet is required - it is therefore difficult to find a proper wavelet for feature extraction according to this restriction. Secondly, the sampling grids in the time-scale plane are rather sparse, meaning that the feature components cannot be separated from the irrelevant components. Finally, the time shift invariant is very important for feature detection and the discrete wavelet transform is not shift invariant [126]. This means that the discrete wavelet transform is not suitable for feature extraction, thus the continuous wavelet transform is employed in this study for feature extraction from engine acoustic signals.

8.2.1 Definition of continuous wavelet transform

The continuous wavelet transform of a signal $x(t)$ is defined as the inner product between signal $x(t)$ and the wavelet family as expressed in equation (8-1)[127][128].

$$WT_x(a, b) = \langle \psi_{a,b}(t), x(t) \rangle = |a|^{-1/2} \int x(t) \psi_{a,b}^*(t) dt \quad (8-1)$$

where $WT_x(a, b)$ denotes the wavelet transform coefficient, $\psi_{a,b}^*(t)$ represents the complex conjugate of the wavelet function, a is known as a dilation parameter and b gives the location of the wavelet and is known as a translation parameter.

The family functions are defined as [129]:

$$\psi_{a,b}(t) = |a|^{-1/2} \psi\left(\frac{t-b}{a}\right) \quad (8-2)$$

where $\psi(t) \in L^2(R)$ denotes a mother wavelet function and its Fourier transform $\hat{\psi}(f)$ which should be subjected to the admissibility condition in equation (8-3),

$$C_\psi = \int_{-\infty}^{\infty} \frac{|\hat{\psi}(\omega)|^2}{|\omega|} d\omega < \infty \quad (8-3)$$

Where ω is the angular frequency and $L^2(R)$ is the space of the square integral complex functions. The corresponding family of a wavelet consists of daughter wavelets as shown in Equation (8-2). They are derived from the wavelet function by dilation and translation through adjustment of the parameters a and b .

For a discrete sequence x_m , let $a = m\delta t$ and $b = n\delta t$, where $m, n = 0, 1, 2, \dots, N - 1$, N is the sampling point number and δt is the sampling interval. The continuous wavelet transform of x_m can be defined as:

$$WT_n(a_j) = \sum_{m=0}^{N-1} x_m \psi^* \left[\frac{(m-n)\delta t}{a_j} \right] \quad (8-4)$$

The amplitude of the feature corresponding to the scale and how this amplitude varies with time can be presented through variation of the index j and n corresponding to the scale factor a and time location b , respectively.

Wavelet coefficients obtained from the wavelet transform can be used to measure the similarity between the interesting signal and daughter wavelets. It is noted that the more similar the daughter wavelet is to the feature component the more interesting the signal; the corresponding wavelet coefficients are consistent [130]. The wavelet has oscillating wave-like characteristics and allows simultaneous analysis in the time and frequency domains with the flexible wavelet functions. In the continuous wavelet transform, the wavelet has finite energy concentrated around a limited time interval [131]. In addition, it can also represent a sharp feature in the signal and hence the original signal can be completely reconstructed or recomposed.

8.2.2 Properties of continuous wavelet transform

The scale factor a and time location b determine the time-frequency localisation characteristics of the continuous wavelet transform [129]. The window width of the wavelet depends on the variation of the scale parameter a , and the changes of the translation parameter b represents the position of the wavelet in both the time domain and frequency domain. In fact, the window widths in the time domain and the frequency domain rely on equations (8-5) and (8-6) [129].

$$[b + at_0 - a\Delta_\psi, b + at_0 + a\Delta_\psi] \quad (8-5)$$

$$\left[\frac{\omega_0}{a} - \frac{\Delta_{\hat{\psi}}}{a}, \frac{\omega_0}{a} + \frac{\Delta_{\hat{\psi}}}{a}\right] \quad (8-6)$$

where t_0 and ω_0 are the centres of the windows in the time domain and the frequency domain respectively. Δ_ψ and $\Delta_{\hat{\psi}}$ are the window radius. Hence, the area of the window in the time-frequency plane is given by:

$$A = 4\Delta_\psi\Delta_{\hat{\psi}} \quad (8-7)$$

A larger dilation scale a produces a wider time window but a narrower frequency window. This type of wavelet is suitable for analysing the signal in lower frequency bands in which the signal changes slowly, so that complete cyclic information can be obtained.

Conversely, a smaller dilation scale a will generate a narrower time window but a wider frequency window. It is used to capture the fast changing transient events in higher frequency bands. Therefore, the width of the window can be adjusted by the scale parameter a according to the frequency band being analysed.

The minimum window width for any wavelet should be no smaller than 2 according to the uncertainty principle [129]. This principle demonstrates that it is impossible to obtain the highest resolutions in both the time domain and the frequency domain. A higher resolution in the time domain leads to lower resolution in the frequency domain, and vice versa.

8.2.3 Morlet wavelet

The performance of the continuous wavelet transform analysis relies mainly on the selection of the types of wavelet functions. There are a number of wavelet functions which can be chosen for different applications, including Gabor, Haar, Daubechies, Mexican hat, Mallat and Morlet, etc. Different wavelet functions result in different analysis results. The choice of an appropriate wavelet function depends on the signal itself and the purpose of the analysis. In the application of condition monitoring and fault diagnostics, transient signals or impulses are always the symptoms of faults in a number of dynamical signals, and the Morlet wavelet is very similar to such impulse or transient component. Based on the general conclusion [21], more compactly supported and less smooth wavelet functions are better suited to analysing non-stationary and irregular signals, such as transient signals. On the contrary, less compactly supported and smoother wavelet functions are better suited to processing stationary and regular signals, such as periodic signals. The Morlet wavelet function is suitable for analysing engine acoustic and vibration signals and should give superior results in its application. This is because the vibration and acoustic signals of the machine include periodic impulses components when a fault occurs, which have a shape similar to a Morlet wavelet as shown in Figure 8-1.

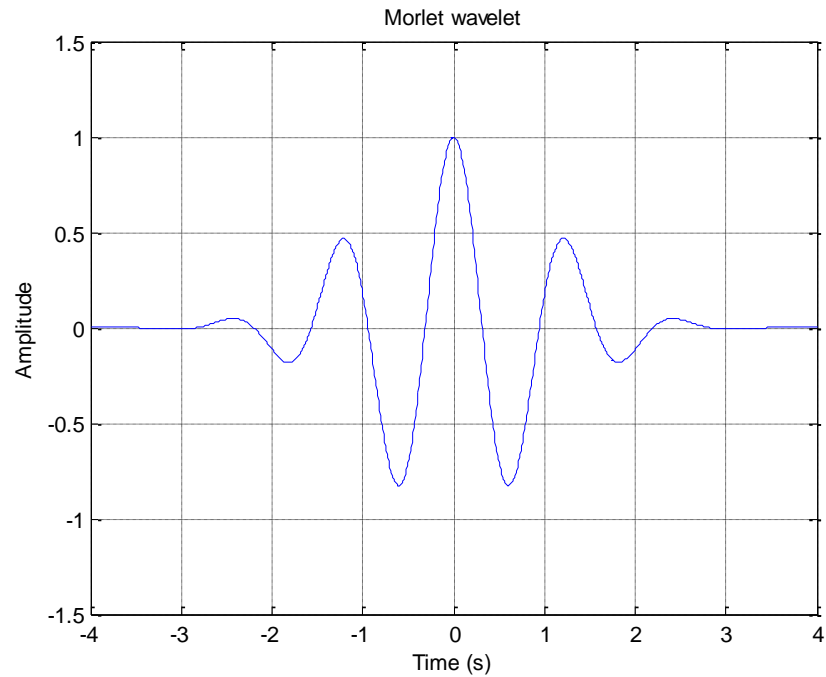


Figure 8-1 The Morlet wavelet

A Morlet wavelet function is defined in the time domain as [125]:

$$\psi(t) = e^{-t^2/2} e^{j\omega_0 t} \quad (8-8)$$

And its function in the frequency domain is given by:

$$\hat{\psi}(\omega) = \sqrt{2\pi} e^{-(\omega-\omega_0)^2/2} \quad (8-9)$$

where ω_0 is the centre frequency which determines the location of the Morlet wavelet. In order to maintain the admissibility condition, a correction term should be added to the Morlet wavelet function equations. The correction term expressed in the frequency domain is:

$$\hat{\eta}(\omega) = -e^{-(\omega^2+\omega_0^2)/2} \quad (8-10)$$

The correction term is often neglected if the centre frequency is chosen as $\omega_0 \geq 5$, because the maximum value of the correction is very small in this range. In practice, the analysis results are not affected significantly and the computation time is reduced

after neglecting the correction term. For application, less computation time means easier to use in real-time.

8.3 Time synchronous average

time synchronous average is an effective technique in the time domain to remove the noise in a repetitive signal and is widely used in rotating machine monitoring and fault diagnosis [132]. The signal-to-noise ratio (SNR) of a repetitive signal can be improved significantly by suppressing the components which are asynchronous with the parameters of interest. time synchronous average is based on the knowledge of the revolution specifications of the rotating part. Traditionally, this requirement is met by using an external trigger signal provided by a shaft encoder, and the revolution period of rotating machinery can then be obtained. The measured signal is then divided into small segments according to the revolution period of the rotating part, and all the segments are summed together so that no coherent components and asynchronous components are cancelled out. Normally, vibration and acoustic signals from rotating machinery are a combination of periodic signals with random noise. Assuming a signal $x(t)$ consists of a periodic signal $x_T(t)$ and a noisy component $n(t)$, the period of $x_T(t)$ is T_0 whose corresponding frequency is f_0 , thus the signal can be expressed as [133]:

$$x(t) = x_T(t) + n(t) \quad (8-11)$$

The synchronous average of the signal $x(t)$ by using time synchronous average can be expressed as

$$y(t) = \frac{1}{M} \sum_{i=0}^{M-1} x(t + iT_0) \quad (8-12)$$

where M is the number of the average segments, $y(t)$ is the averaged signal.

In practice, the vibration and acoustic signals collected are commonly contaminated by different noises such as those from the dynamotor and ventilation fan. This noise is unavoidable and is usually introduced into signals by various disturbances such as the

disturbance from the external environment and from the testing instrument itself. Generally, the fault and condition information included in the measured signals of the monitored machine are weak and polluted by various noises. Therefore, the de-noising and the extraction of the weak signals are critical for fault diagnostics, especially for the early fault detection where features are often very weak and masked by the noise.

In the present study, time synchronous average was used to pre-process the engine acoustic signals for further analysis. A Hengler RS58 speed sensor was used to collect the engine speed and provided revolution information for the test engine for time synchronous average processing. The time interval of the pulses in the speed signal was not constant due to oscillation of the shaft speed. Based on this consideration, assuming the shaft speed is undergoing constant angular acceleration [134]. The angular acceleration was calculated using the arrival times of the three adjacent pulses obtained from the sampling of the speed signal. The correct placement of the resample on the time axis was then carried out based on constant angular acceleration. In this study, the time axis resampling was processed in sections with each section length having 1000 points - 5 lengths were selected. Once the resample times are calculated, the vibration signal was resampled according to the resampled time axis for synchronous average.

Figure 8-2 shows the averaged acoustic signals using time synchronous average processing for one complete combustion cycle. The engine was operating under different loads and fuel types at speed of 1300rpm. It can be seen that the amplitude of the acoustic signals increases with increased load for all fuel types, and the periodic characteristic of the acoustic signals is better understood.

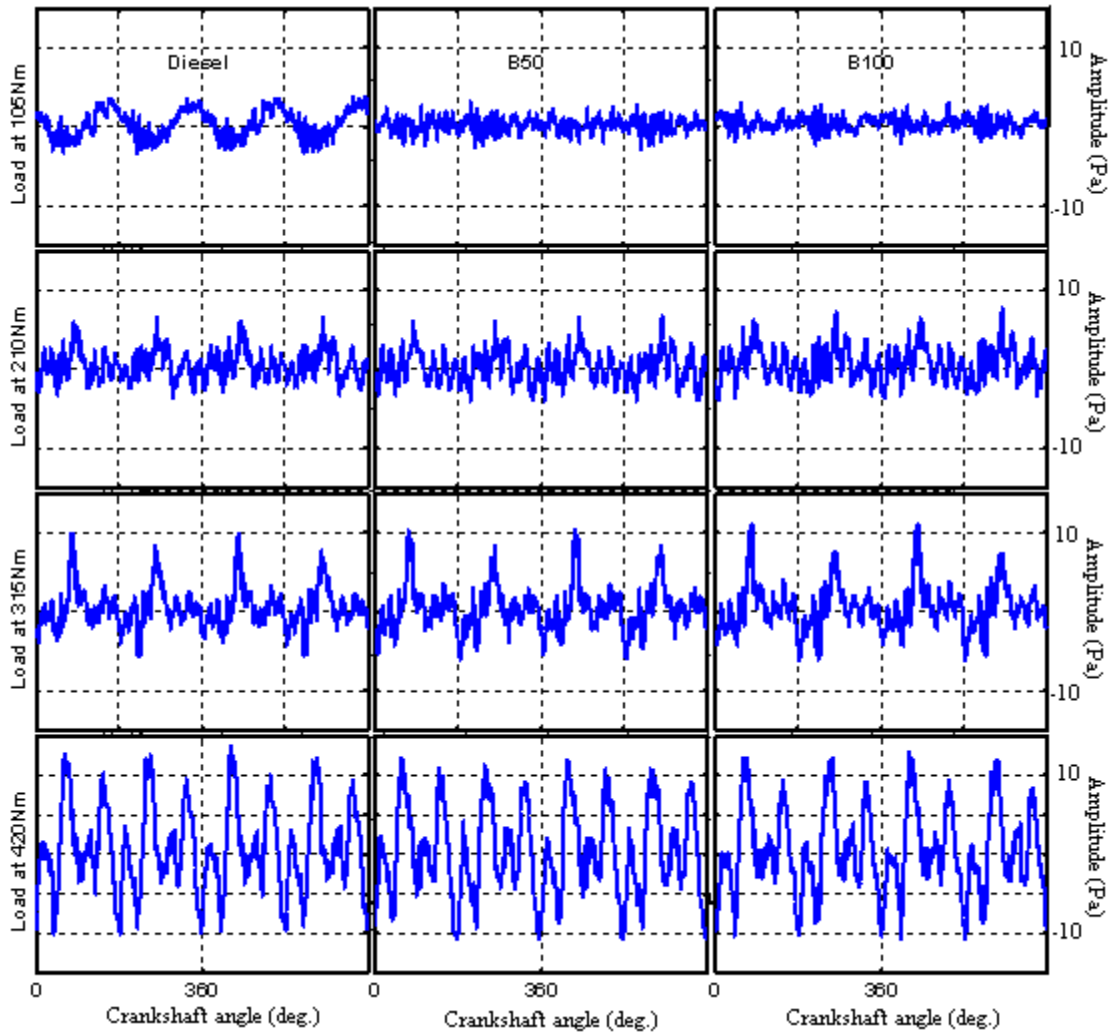


Figure 8-2 TSA acoustic signals under different operating conditions and fuel types

Root mean square (RMS) values were calculated from the time synchronous average acoustic signals as a feature parameter for comparative analysis. As presented in Figure 8-3, RMS values of time synchronous average acoustic signals have shown similar trends for the three fuel causes over different loads. The RMS values increase with the increase of the engine loads and speeds. However, RMS values cannot separate the three fuel cases over different loads, especially under low loads such as 105N m and 210N m.

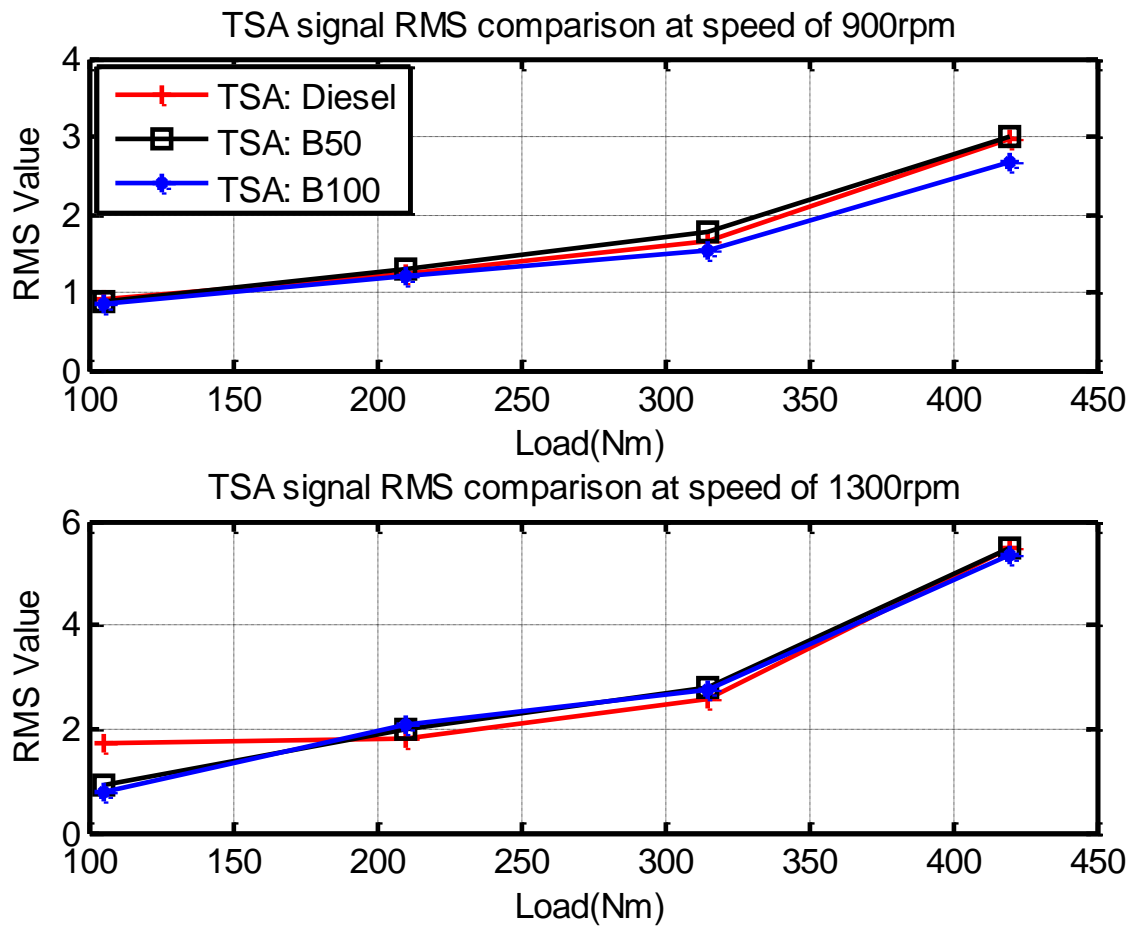


Figure 8-3 RMS values of TSA acoustic signals under different fuel types

8.4 Feature extraction and RMS linear classification

To obtain more details of the combustion events for different fuel cases, the continuous wavelet transform with Morlet wavelet function is used to analyse the time synchronous average acoustic signals collected under different types of diesel, B50 and B100 in the higher frequency band (from 10 kHz to 40 kHz). The scale ranges from 0.5 to 2 are selected for continuous wavelet transform analysis application in this study to investigate the time-frequency properties of the engine acoustic signals.

Figure 8-4 shows the contour plots of the continuous wavelet transform coefficients for the time synchronous average acoustic signals at 900rpm with varying loads and

different fuel types. It can be seen the contour shapes of the continuous wavelet transform in the high frequency band give a superior representation of the start, strength and duration of each combustion event. There are four events in every two revolutions for diesel engine with four cylinders. It can be indicated in Figure 8-4 in every 720 crank degrees. The strength of the combustion events can give sufficient information for different fuel types.

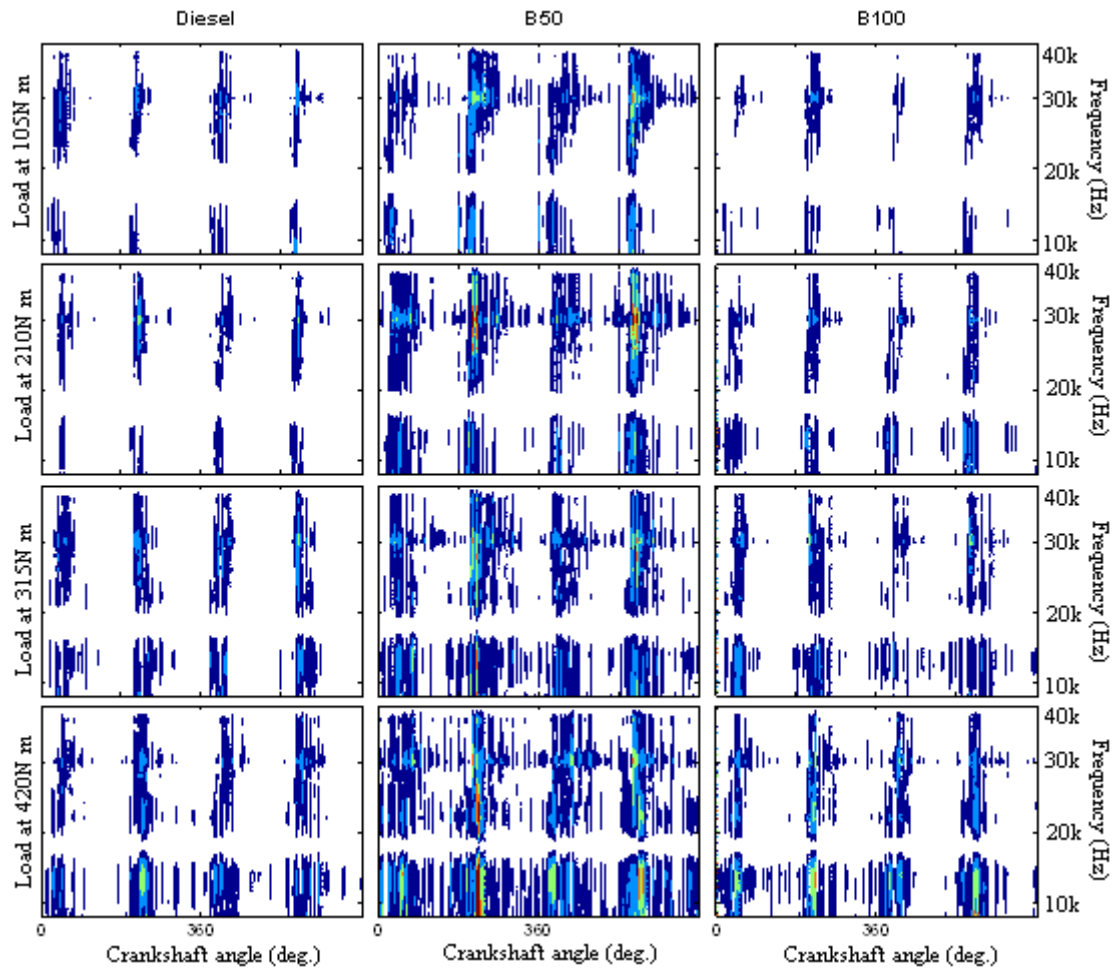


Figure 8-4 Contour plots of the results for different fuel types at the speed of 900rpm

Figure 8-5 shows the continuous wavelet transform coefficients are analogous to those shown in Figure 8-4. Comparison of the continuous wavelet transform coefficients at a lower speed (900rpm) and then also at a higher speed (1300rpm), shows that the strength of the combustion events is higher at a higher speed. It is worth noting that the

continuous wavelet transform coefficient results of Figures 8-4 and 8-5 also show uniformity in the combustion between cylinders as it can identify the combustion events properly.

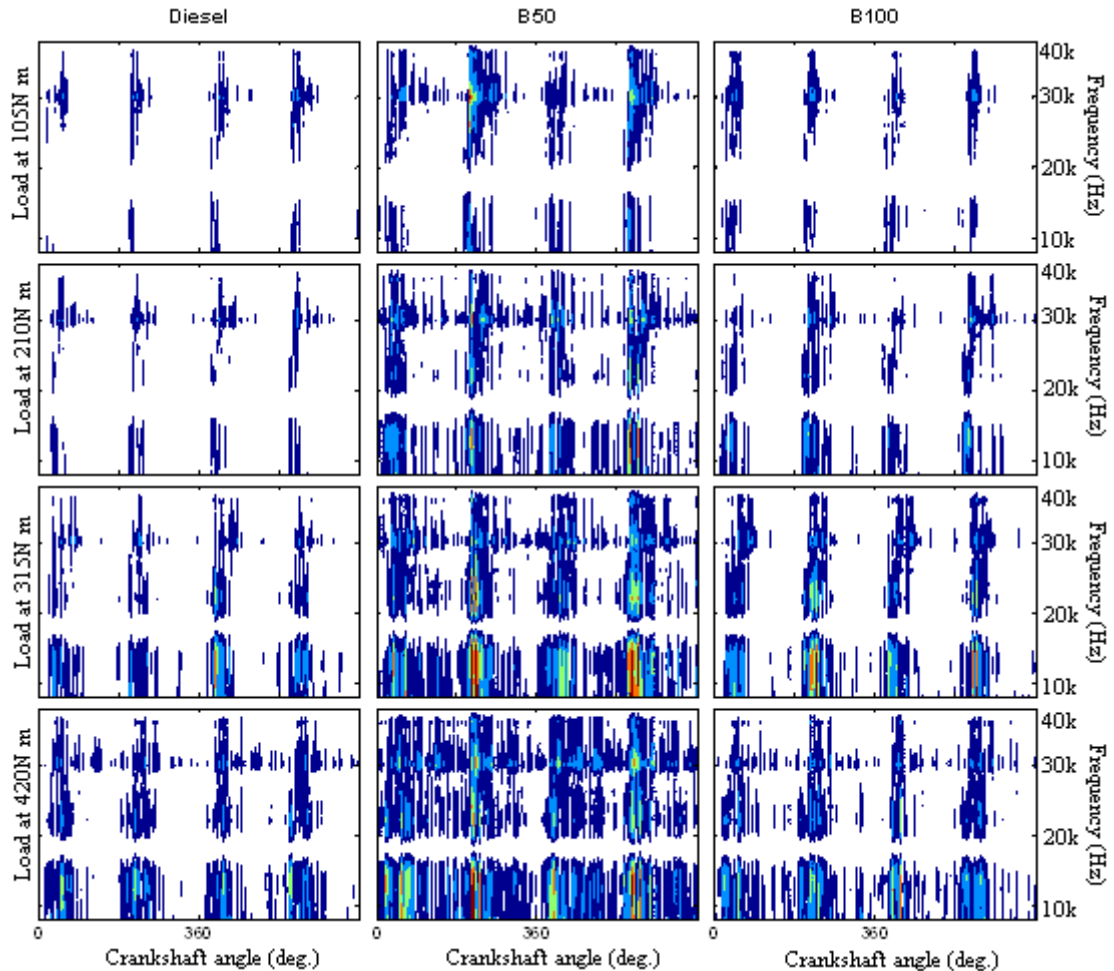


Figure 8-5 Contour plots of the results for different fuel types at the speed of 1300rpm

A common feature parameter, RMS values of the wavelet transform coefficient, is extracted from the continuous wavelet transform coefficient results for fuel types. This detection approach involves minimal computational effort, making it suitable for use as an on-line condition monitoring technique which is a more practical application. As a measure of overall sound level intensity, the average RMS value of the multi-cycle acoustic signal is calculated over the four load settings and the three fuel types. Figure 8-6 presents a comparison of the RMS value of the continuous wavelet transform

results under varying loads and different fuel types at speeds of 900rpm and 1300rpm respectively.

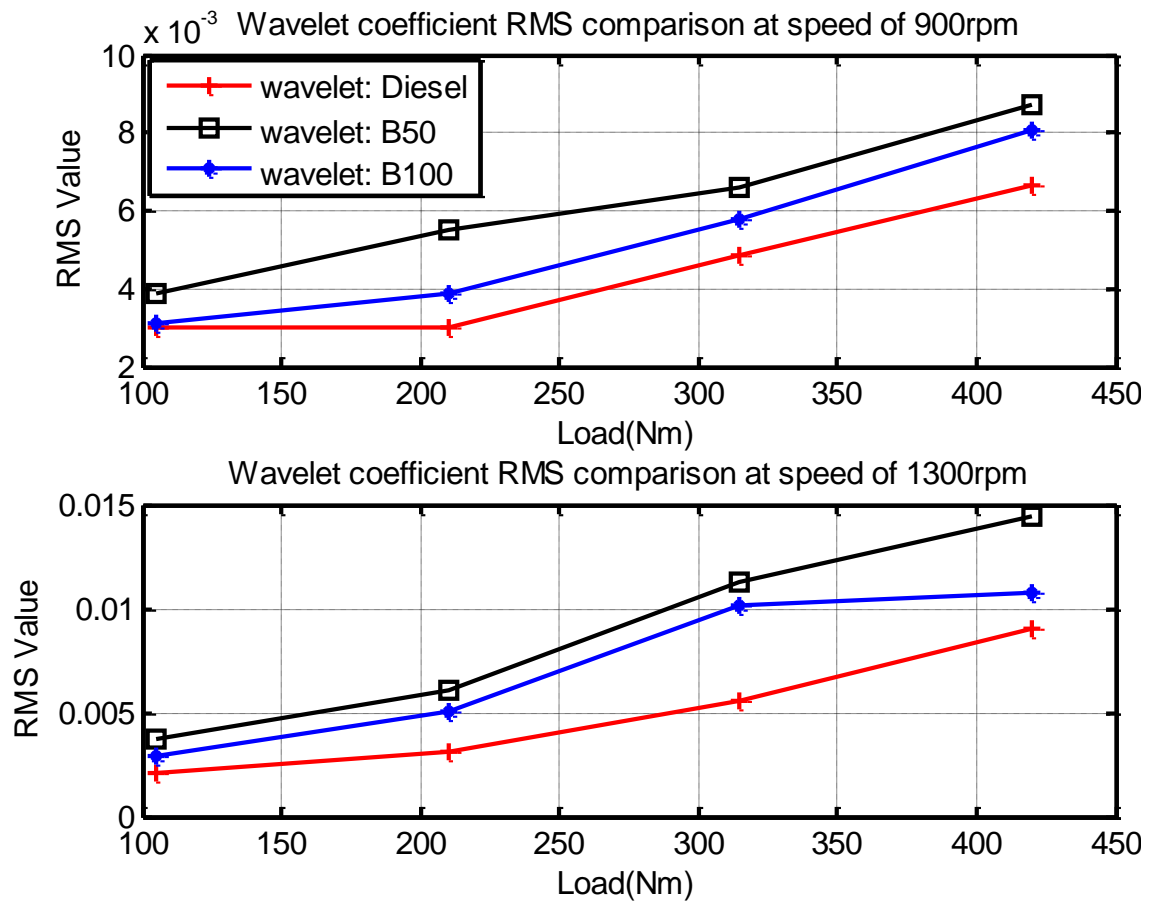


Figure 8-6 Comparison of the RMS values between different loads and fuel types

It can be seen from Figure 8-6 that the RMS values increase alongside engine load and speed. The RMS values of the continuous wavelet transform coefficient results for biodiesel and its blends (B50 and B100) are slightly higher than those for pure diesel. Focusing on the fuel cases of B50 and B100, shows that the RMS values for B50 are slightly higher than those of B100 in all test conditions. These behaviours correspond to the variation of the in-cylinder pressure, which indicates that the peak cylinder pressure for B50 is the highest and the peak cylinder pressure for diesel is the lowest over almost all the test conditions. It can, therefore, be concluded that a higher in-cylinder pressure with faster change produces higher engine vibration and noise.

Based on the time synchronous average pre-processing and the continuous wavelet transform analysis of the experimental noise of the engine, the main results can be summarized as follows:

- The peak cylinder pressure is higher when the engine is run with rapeseed oil biodiesel in comparison with regular diesel over almost all tests.
- The peak cylinder pressures for both diesel and biodiesel and its blends increased alongside the engine load and speed. This was because a longer ignition delay results in more fuel being available for ignition and more energy being released during the premixed combustion stage.
- The sound in the higher frequency band is less influenced by the measurement environment than the sound in the lower frequency equivalent in some ways.
- The continuous wavelet transform coefficient analysis in the higher frequency range is able to represent the combustion details for fuel monitoring.
- The RMS values of the continuous wavelet transform coefficients of the engine acoustic signal correspond to the variation of the in-cylinder pressure, while the changes of the in-cylinder pressure depend on the properties of the fuels.
- The effect of fuel types on combustion can be extracted from the continuous wavelet transform contour plots and the RMS values of the continuous wavelet transform coefficients.

CHAPTER 9

CONCLUSIONS AND FUTURE WORK

This chapter summarizes the achievements of this research and draws conclusions based on the results obtained from the entire research project. It then contains a summary of the novel contributions of the research conducted by the author. Finally, suggestions are given for future work which could advance the investigations presented in this thesis.

9.1 Review of thesis objectives and achievements

This section outlines the objectives and the achievements which have been made throughout this study and research contributions which have been made as part of this work. This research has focused on the study of non-stationary signal processing for machinery condition monitoring. It started with an initial overview of maintenance strategies, and particularly focusing on condition based maintenance strategies. The key to condition based maintenance is the knowledge of the machine condition which can be obtained through various condition monitoring techniques. Widely used condition monitoring techniques are outlined in Section 1.3 of this thesis.

Condition monitoring is defined as the continuous and periodic measurement and interpretation of data to indicate the condition of a system or plant which is used to guide maintenance. It is concerned with gathering data to enable better understanding of the health, or condition of an item of machinery. Condition monitoring is used to assess the current condition of a machine through analysis of measured signals. Various signal processing techniques are employed to predict potential failure in a timely manner and facilitate economic maintenance. Hence, the selection of measured signals and associated processing techniques is important for accurate assessment of the current condition of a machine.

Non-stationary signals have been widely used for condition monitoring and damage assessment in mechanical applications. In particular, the primary fault information is contained in the non-stationary components of the measured signals when machinery faults occur. The key challenge and focus of this work has been how to extract useful information from the non-stationary signals measured from the monitored machine for useful condition monitoring and fault diagnostic purposes.

According to the aims of this research work (see Section 1.4), various signal processing techniques, such as dynamic time warping (DTW) (see Section 3.2 and 4.4), Wigner-Ville distribution (WVD) (see Section 7.3), wavelet transform (WT) (see Section 8.2), and fractional Fourier transform (FRFT) (see Section 7.4) have been

employed and developed in order to process the non-stationary signals measured from the monitored objects based on a diesel engine (see Section 5.2) and a two-stage reciprocating compressor test rig (see Section 4.2). The typical non-stationary signals, such as electrical current (see Section 4.3), engine vibration and acoustic (see Section 5.3), have been analysed for fault diagnosis and condition monitoring of the test compressor and diesel engine. The main objectives of this research work are stated as follows:

1. Survey of signal processing methods and monitoring techniques.

The review of maintenance strategies (see Section 1.1), condition monitoring techniques (see Section 1.2) and main signal processing techniques (see Chapter 2) used in machinery condition monitoring were presented. Development of acoustic-based condition monitoring was reviewed and introduced in Section 1.3. Finally, non-stationary signal processing methods and their development in machinery condition monitoring were reviewed in Section 2.5.

2. Test rig design and set-up

In order to analyse the electrical current signal for condition monitoring and fault diagnosis of a two-stage reciprocating compressor, a measurement instrumentation system based on a compressor was set up. Both the hardware and experimental procedures used are provided in Section 4.2. In addition, an acoustic based instrumentation system was set up and integrated with the existing engine test facilities in the laboratory. The details of the test rig, acoustic instrumentation and data acquisition system are given in Section 5.2. The two test rigs and associated measurement instrumentation systems were then used to collect all the corresponding data sets used for later analysis in this research work.

3. Electrical current signal processing

Electrical current is a typical weak non-stationary signal for the condition monitoring of downstream equipment of an induction machine. It contains the nonlinear effects due to the faults in the rotor machine (see Section 4.3). A variety of fault information can be extracted through analysis of the sideband components of the current signal. In

this research, dynamic time warping (DTW) was employed to pre-process the electrical current signal for the fault diagnosis of the two-stage compressor (see Section 4.5). The theory of dynamic time warping was introduced in Chapter 3 and through use of the phase properties of the measured electrical current signal, the improvement of the classical dynamic time warping for the compressor fault diagnosis was developed in Sections 4.4. This method was then used to identify and detect faults and classification based on the modified dynamic time warping method and its comparison with the detection results based on the Fourier transform based methods was outlined in Section 4.5.

4. Vibro-acoustic signal processing

In the subsequent chapters (5, 6, 7 and 8), a variety of non-stationary signal processing methods were explored to analyse the measured vibration and acoustic signals for assessment of the test diesel engine condition. Initially, the characteristics of engine noise and vibration were investigated based on the time domain and frequency domain analysis (see Section 5.3). The effects of laboratory acoustics on the measured engine acoustic signals were also studied to determine the overall characteristics of the engine noise (see Section 5.4). The process of combustion in the test engine and combustion induced acoustics and vibration was then investigated through analysis of the engine vibration and acoustic signals (see Section 6.2 and 6.3). A series of non-stationary signal processing methods, such as Wigner-Ville distribution (see Section 7.3), fractional Fourier transforms (see Section 7.4), and continuous wavelet transform (see Section 8.2) were used to analyse the data. Initial results have been outlined at the end section of each chapter.

The achievements described above demonstrate that the outlined objectives of this research work have been fulfilled successfully.

9.2 Conclusions

This research has investigated, developed and validated the signal processing methods used for analysing the non-stationary signals for machinery condition monitoring and

fault diagnosis. Specially, the research has focused on the condition monitoring and fault diagnosis of a two-stage reciprocating compressor and a diesel engine. The research work was carried out through analysis of typical non-stationary signals measured from these two test rigs and a variety of signal processing methods were employed. Conclusions arising from the work carried out are summarised in the following sections.

9.2.1 Conclusions regarding the fault diagnostics of the compressor using the motor electrical current signal

Conclusion 1: The electromagnetic force and corresponding nonlinear current signal in the stator are produced as a result of the fault in the rotor system and its downstream equipment. Analysis of the electromagnetic relationship to the electrical current signal in Section 4.3 showed that the motor current signal could be employed widely for condition monitoring of the induction machine and its downstream equipment. Fault information of various types can be obtained through analysis of the sideband components of the current signal.

Conclusion 2: Analysis of the characteristics of the electrical current signal, as given in Section 4.3, is a reliable and effective method for fault diagnosis of the compressor. Combination of this with the analysis of phase properties of dynamic time warping method (see Section 3.5), demonstrates that phase compensation based dynamic time warping (see Section 4.4) is an effective method for processing the electrical current signal for accurate feature extraction and compressor fault diagnosis.

Conclusion 3: The analysis of electrical current signals based on the proposed dynamic time warping method has significant potential for the detection and identification of the presence of incipient faults in the two-stage compressor (see Section 4.5). The analysis results indicate that the dynamic time warping method can be employed to extract accurate features of the current signals. The RMS values of the residual signals can also be used to differentiate between faulty and healthy signals and to identify the difference between other fault types under various loads and discharge pressures.

Conclusion 4: Compressor fault detection and classification based on the modified dynamic time warping methods were discussed in Section 4.5 and overcame the limitation of the Fourier transform based analysis method. From this work, it can be concluded that the accuracy and reliability of detection and classification using dynamic time warping based analysis is higher than that from Fourier transform based spectrum and envelope analysis (see Section 4.5.3). In addition, the dynamic time warping processing procedure based entirely on the time domain analysis is easier to apply in real-time monitoring processes.

9.2.2 Conclusions regarding the condition monitoring of diesel engines

Conclusion 5: In this research work, vibro-acoustic signals were adopted as the main indicator of engine condition. Experimental analysis of results confirmed that the vibro-acoustic based analysis was effective and useful for the condition monitoring of engines. The vibro-acoustic based analysis has potential advantages for implementation in online condition monitoring systems.

Conclusion 6: Analysis of engine noise and vibration characteristics in the time domain and spectrum analysis (see Section 5.3) shows that the variation of the engine vibration and noise depends on the engine operating speed and load, and also on the variation of the combustion cylinder pressure. Therefore, it can be concluded that engine vibration and noise variation has the potential for use as an indicator of combustion process instead of using in-cylinder pressure.

Conclusion 7: The analysis of fuel monitoring based on engine noise in Section 5.5 demonstrated that the effects of room acoustics on engine acoustic signals (see Section 5.4) influences the analysis of acoustic signals in the low frequency domain below 1 kHz. A number of resonant frequencies and harmonics are introduced which cause difficulties in feature extraction from the measured engine acoustic signals. Therefore, room acoustic effects need to be suppressed and signal to noise ratios enhanced in order to obtain accurate detection results for monitoring the operating conditions of the

engine. Analysis results shows that engine operating conditions can be monitored through analysing the engine acoustic signals in the higher frequency band.

Conclusion 8: Engine vibration and acoustic signals are typical non-stationary signals which contain a large number of short time transient events (see Section 5.3). Based on the signal processing analysis of the non-stationary components of the engine vibration and acoustic signals (see Section 7.5 and 8.4) it has been shown that useful features can be extracted from the engine vibration and acoustic signals for engine condition monitoring and fuel evaluation.

Conclusion 9: The analysis of engine vibro-acoustic signals using coherent power spectrum analysis, Wigner-Ville distribution (WVD) (see Section 7.3) and fractional Fourier transform (FRFT) (see Section 7.4) methods in chapter 7 demonstrated that combustion induced noise is located in the frequency range from 2 kHz to 3 kHz (see Section 7.4.3), and can be used to identify fuel quality and for fuel evaluation of the diesel engine (see Section 7.5).

Conclusion 10: Analysis of engine acoustic signals using time synchronous average (TSA) (see Section 8.3) and continuous wavelet transform (see Section 8.2) techniques in chapter 8 has shown that peak cylinder pressure is higher when the engine is operated using rapeseed oil biodiesel rather than diesel. The RMS values of the continuous wavelet transform coefficients of the engine acoustic signal corresponded to the variation of the in-cylinder pressure and indicated the variation of engine operating conditions (see Section 8.4). Therefore, it is possible, using the continuous wavelet transform coefficients analysis technique in the higher frequency range, to evaluate fuel combustion characteristics and engine condition monitoring.

9.3 Research contributions to new knowledge

This thesis has many new elements which have not been considered in previous research and has made significant contribution to the knowledge in the area of non-stationary signal processing for machinery condition monitoring and fault diagnosis. A summary of these contributions is given below:

Contribution 1: The application of the dynamic time warping method used for detection and diagnosis of the compressor faults is novel (see Section 4.5). No work has been found in the literature that describes the use of dynamic time warping for machinery fault diagnosis and condition monitoring.

Contribution 2: The algorithm improvement using phase compensation for dynamic time warping is novel (see Section 4.4). Phase estimation and compensation has not been used previously for the improvement of the singularity effects of dynamic time warping. In this research work, a phase compensation method has been developed to improve the classical dynamic time warping algorithm and applied to process electrical current signals for fault diagnosis of a two-stage compressor.

Contribution 3: The application of diesel engine vibration and acoustic signals for analysis of the characteristics of the engine combustion process has been investigated. Determination of the relationship between the variations of engine acoustic, vibration and in cylinder pressure for the combustion diagnosis is a novel approach (see Section 6.3).

Contribution 4: The combustion and vibro-acoustic characteristics of a CI engine fuelled with biodiesel blends have been investigated (see Section 5.5, 7.5 and 8.4). This is a new method of monitoring fuel quality through non-contact measurement and analysis of the engine acoustic signals.

Contribution 5: Coherent power spectrum analysis was used to identify the relationship between the engine acoustic and cylinder head vibration (see Section 7.2.2). Two time-frequency analysis techniques, Wigner-Ville distribution (WVD) (see Section 7.3) and fraction Fourier transform (FRFT) (see Section 7.4), were then applied for analysis of the energy distribution of the engine acoustic and extraction of the combustion induced noise (see Section 7.5). This was a novel approach for combustion diagnosis and fuel evaluation.

Contribution 6: The application of time synchronous average (TSA) (see Section 8.3) and continuous wavelet transform methods (see Section 8.2) for extraction of

condition-indicating information from the measured engine acoustic signals has been demonstrated. An RMS linear classifier (see Section 8.4) has been designed for the classification of engine operating conditions and fuel types for combustion process monitoring and fuel evaluation.

9.4 Suggestions for further research

A great deal of preliminary research work has been undertaken as part of this study to investigate signal processing techniques for analysis of non-stationary signals in condition monitoring of machinery. If a wider and more extensive study was to be undertaken, some key recommendations should be considered for future work in this research area.

Recommendation 1: Several novel methods have been employed and developed within the current study for the processing of non-stationary signals for machinery condition monitoring. Other new methods may be developed for accurate feature extraction from the non-stationary signals for machinery condition monitoring and fault diagnosis and these should be considered.

Recommendation 2: With regards to online condition monitoring implementation, powerful and effective signal processing techniques must be developed for feature extraction. Methods should be efficient and easy to implement using the measured signals. Reliability, cost-effectiveness and accuracy of the monitoring system also need to be developed for online applications.

Recommendation 3: Condition monitoring of diesel engines using non-contact measurement, requires further investigation, particularly of the relationship between the combustion process and the engine vibro-acoustic signals. Research should be based on both experimental and theoretical studies.

Recommendation 4: Acoustic measurements are heavily affected by background noise and the accuracy of the analysis results is limited due to low signal-to-noise ratios (SNR) of the measured signals. Therefore, more effective pre-processing methods need

to be developed to enhance the signal-to-noise ratio of the measured acoustic signals for more accurate analysis of the results obtained.

Recommendation 5: Combination of the method developed in this research work with other condition monitoring methods in order to improve the detection performance and to research new information about the combustion process used for engine condition monitoring.

Recommendation 6: Further experimental work needs to investigate the use of multi-microphones, such as microphone array, for the collection of engine acoustic signals. It contains sufficient information for feature extraction with high accuracy and time efficiency for the implement of online condition monitoring system.

APPENDIX A

The Sound Pressure Level

The sound pressure level (SPL) is defined as:

$$SPL = 20 \log \frac{P_{rms}}{P_{ref}} \quad (A-1)$$

where P_{rms} is the RMS value of sound pressure and P_{ref} is the reference pressure with $P_{ref} = 2.0 \times 10^{-5} Pa$. The unit of the sound pressure level is in decibels (dB) as standard. The selection of this reference value corresponds to the minimum threshold of human hearing for the sound pressure at 1 kHz pure tone. The safety threshold of sound pressure level for safe hearing is 120 dB [7].

The sound intensity level (SIL) is defined as the logarithmic scale of the sound intensity,

$$SIL = 10 \log \frac{I}{I_{ref}} \quad (A-2)$$

where I is the sound intensity in Wm^{-2} , and I_{ref} is the reference intensity with $I_{ref} = 1.0 \times 10^{-12} Wm^{-2}$.

The sound intensity is calculated as the average rate of flow of sound energy through a unit area. Expressing the definition in mathematical format gives [17]:

$$I = \frac{1}{T} \int_0^T p u dt \quad (A-3)$$

where p and u are the wave pressure and velocity, respectively.

The relationship between the sound intensity and pressure can be expressed as:

$$I = \frac{p_{rms}^2(r)}{Z} = \frac{p_{rms}^2(r)}{\rho c} \quad (A-4)$$

where $p_{rms}(r)$ is the RMS pressure value at the distance r from the source. Z is the impedance with $Z = \rho c$, where ρ is the air density, and c is the speed of the sound in the air with $c = 340ms^{-1}$ normally.

Similarly the sound power level is defined as:

$$SWL = 10 \log \frac{W}{W_{ref}} \quad (A-5)$$

where W_{ref} is the reference sound power with $W_{ref} = 1.0 \times 10^{-12}W$.

The total power radiating from a source in a spherical wave at the radius r can be calculated by [7],

$$W = \int_S \bar{I} \cdot d\bar{S} = \frac{p_{rms}^2(r)}{Z} 4\pi r^2 \quad (A-6)$$

where \bar{I} is the intensity vector and S is the area enclosing the source at r .

The relationship between the above three levels can be expressed using equations (A-4) and (A-6), thus:

$$SIL = SPL - 0.16 \quad (A-7)$$

and

$$SWL = SPL + 20 \log \frac{r}{r_{ref}} - 0.16$$

where $r_{ref} = 0.282 m$.

APPENDIX B

Compressor Experimental Set Up

B.1 Test rig facilities

A two-stage, single-acting Broom Wade TS9 reciprocating compressor was available for the test in the school of computing and engineering at the University of Huddersfield. Figure B-1 shows the test compressor, which has two cylinders in the form of a “V”, and which delivers compressed air at up to 8.3 bar (0.8 M Pa) to a horizontal air receiver tank with a maximum working pressure of about 13.8 bar (1.38 M Pa) [135].

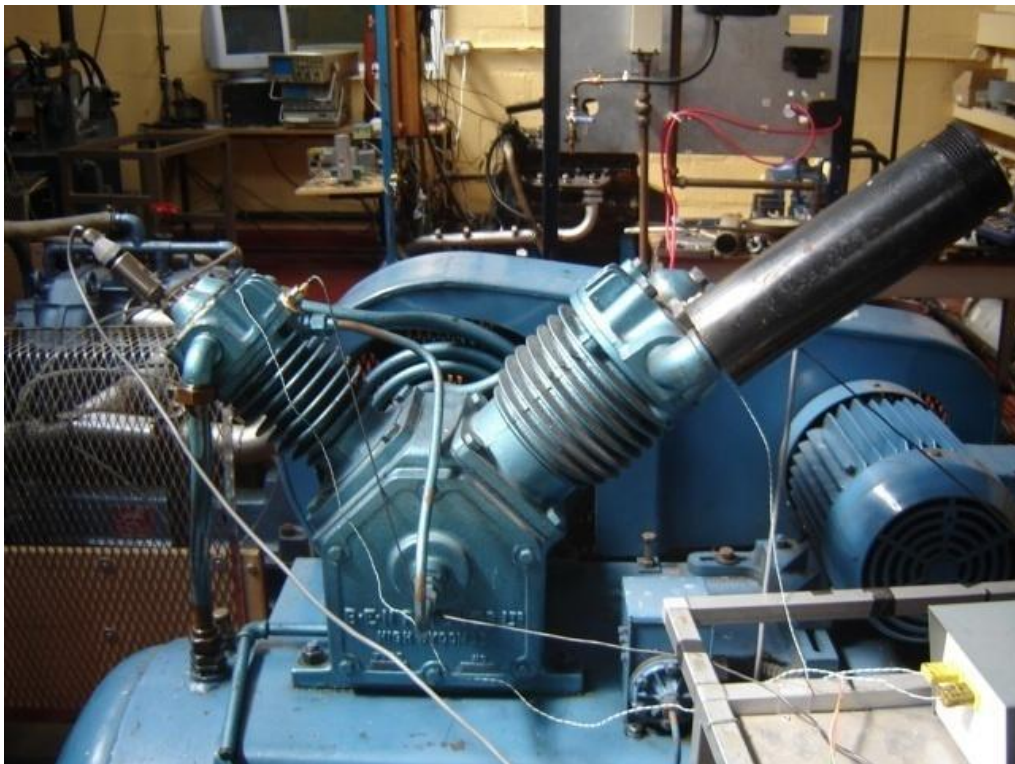


Figure B-1 Broom Wade TS9 reciprocating compressor [136]

The compressor motor is a foot mounted, squirrel cage, air cooled, type KX-C184. Its specification is given in Table B-1 in detailed [136].

Table B-1 Compressor and induction motor specification

Broom Wade TS9 Compressor and Motor	
Max working pressure	13.8 bar (1.38 MPa)
Number of cylinders	2 (90° opposed)
Piston stroke	76 mm
Speed	420 rpm
Motor power	2.2 kW
Voltage	380/420V
Motor speed	1420 rpm
Current	4.1/4.8 Amp

B.2 Measurement transducers

As the test rig would be used for several condition monitoring research projects, various different transducers were fitted on the compressor, including accelerometers, pressure sensors, thermocouples and an angular speed encoder. Each of these transducers produces a voltage output proportional to the amplitude of the measured parameters and each is connected to a data acquisition system for data recording. For more details of the transducers, refer to [136] in chapter 4.

B.3 Fault simulation [136]

Three common faults, valve leakage, intercooler leakage and belt looseness, were seeded into the test compressor separately. The compressor performance is monitored with only one fault present at a time. A base-line signature is obtained of the healthy compressor operating normally for reference. This was achieved by first having the compressor thoroughly inspected by qualified technician staff and then recording a healthy base-line signature [136]. The compressor was then seeded with each of the three faults in turn. The signal from each transducer with each fault was then compared

to that under base-line. The differences in the signal between the faulty and base-line conditions enabled three fault signatures to be developed for each fault.

B.3.1 Valve leakage simulation

In this study, valve leakage was seeded by drilling a small hole in the valve plate of the second stage discharge valve as shown in Figure B-2. The hole was 2mm diameter, which was 2% of the area of the flow cross-section [136].



Figure B-2 Leakage in second stage valve plate

B.3.2 Intercooler leakage

The loose intercooler joint is seeded into a compression joint close to the second cylinder as shown in Figure B-3. The pipeline screw nut, shown on the photo, was loosened to create the leakage. A small leakage was achieved by turning the nut through one turn. Whilst this represented a realistic leakage, it was not possible to quantify the leakage as a proportion of the area of the flow cross-section.



Figure B-3 Intercooler leakage

B.3.3 Belt looseness

To simulate a belt looseness arising from belt wear due to friction the separation of the centres of the two pulleys was reduced from 169 mm to 167 mm, equivalent to a 0.5 % increase in belt length.

B.4 Compressor performance analysis under different fault cases

During the test, the performance of the compressor was monitored with only one fault present in each experiment. Before the next experiment was carried out, the temperature and tank pressure were checked and the receiver was also drained to make sure each experiment was carried out based on the same operating conditions. The tank charge duration in time and the discharge pressure were measured in every experiment. The discharge pressure was increased from about 1 bar to 8.3 bar in the experiment. Figure B-4 shows the tank charge duration against discharge pressure under different fault cases. It can be seen that the curves have the same general shape for both the healthy and faulty conditions, but there is a significant difference of time interval

between faulty and healthy conditions. In healthy condition, the discharge pressure can reach the target pressure quickly with shorter tank charge duration, while in the faulty condition it needs more time to reach the same target pressure with healthy condition. It demonstrates that the performance of the compressor is affected by the impact of faults and declined.

Based on the compressor performance analysis in Figure B-4, it can be seen that even the differences of the time interval between faulty and health condition are small, there is a substantial difference in tank charge duration due to different faults. This suggests that the faults on the compressor can be properly diagnosed even the simulated faults are small from a mechanical point of view.

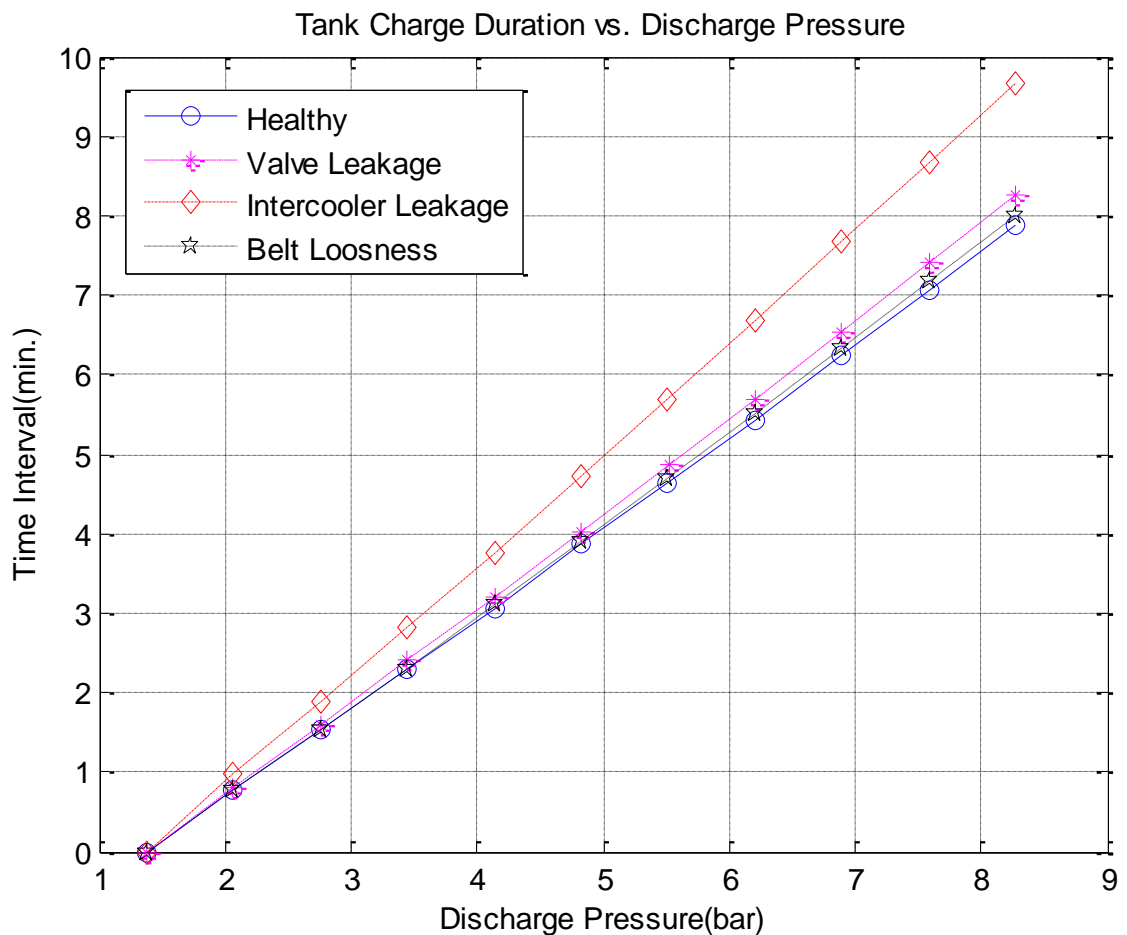


Figure B-4 Tank charge duration versus discharge pressure under different faults

REFERENCES

- [1] A. K. S. Jardine, D. Lin, and D. Banjevic, "A review on machinery diagnostics and prognostics implementing condition-based maintenance," *Mechanical Systems and Signal Processing*, vol. 20, no. 7, pp. 1483–1510, Oct. 2006.
- [2] J. H. Williams, A. Davies, and P. R. Drake, *Condition-Based Maintenance and Machine Diagnostics*. Springer, pp. 22-40, 1994.
- [3] A. Kelly, *Maintenance Strategy*. Elsevier, pp. 19-141, 1997.
- [4] T. McGrail, "Condition monitoring-a user perspective," in *HV Measurements, Condition Monitoring and Associated Database Handling Strategies (Ref. No. 1998/448)*, *IEE Colloquium on*, 1998, pp. 1/1 –1/3.
- [5] H. Austerlitz, *Data Acquisition Techniques Using PCs*. Academic Press, 2002.
- [6] K. Jemielniak, "Commercial Tool Condition Monitoring Systems," *The International Journal of Advanced Manufacturing Technology*, vol. 15, no. 10, pp. 711–721, 1999.
- [7] W. Li, *A Study of Diesel Engine Acoustic Characteristics*. PhD thesis, chapter 1, 2000.
- [8] E. P. Carden and P. Fanning, "Vibration Based Condition Monitoring: A Review," *Structural Health Monitoring*, vol. 3, no. 4, pp. 355–377, Dec. 2004.
- [9] C. R. Farrar, S. W. Doebling, D. A. Nix, C. R. Farrar, S. W. Doebling, and D. A. Nix, "Vibration-Based Structural Damage Identification," *Phil. Trans. R. Soc. Lond. A*, vol. 359, no. 1778, pp. 131–149, Jan. 2001.
- [10] D. Mba, "Development of Acoustic Emission Technology for Condition Monitoring and Diagnosis of Rotating Machines: Bearings, Pumps, Gearboxes, Engines, and Rotating Structures," *The Shock and Vibration Digest*, vol. 38, no. 1, pp. 3–16, Jan. 2006.
- [11] C. Chang and C. T. Sun, "Acoustic emissions and transient elastic waves in an orthotropic laminate plate," *Composites Science and Technology*, vol. 33, no. 3, pp. 213–236, 1988.
- [12] A. M. Al-Ghamd and D. Mba, "A comparative experimental study on the use of acoustic emission and vibration analysis for bearing defect identification and estimation of defect size," *Mechanical Systems and Signal Processing*, vol. 20, no. 7, pp. 1537–1571, Oct. 2006.
- [13] W. Li, R. M. Parkin, J. Coy, and F. Gu, "Acoustic based condition monitoring of a diesel engine using self-organising map networks," *Applied Acoustics*, vol. 63, no. 7, pp. 699–711, Jul. 2002.
- [14] F. Gu, A. Ball, and W. Li, "The Condition Monitoring of Diesel Engines Using Acoustic Measurements-Part 1: Acoustic Characteristics of the Engine and Representation of the Acoustic Signals," *SAE Technical Papers*, Mar-2000. [Online]. Available: <http://www.sae.org/technical/papers/2000-01-0730>. [Accessed: 30-May-2012].

- [15] S. Nandi, H. A. Toliyat, and X. Li, "Condition monitoring and fault diagnosis of electrical motors-a review," *Energy Conversion, IEEE Transactions on*, vol. 20, no. 4, pp. 719 – 729, Dec. 2005.
- [16] P. Tavner, L. Ran, J. Penman, and H. Sedding, *Condition Monitoring of Rotating Electrical Machines*. The Institution of Engineering and Technology, Michael Faraday House, Six Hills Way, Stevenage SG1 2AY, UK: IET, 2008.
- [17] F. Fahy, *Foundations of Engineering Acoustics*. Academic Press, 2001.
- [18] J. Benesty, J. Chen, and Y. Huang, *Microphone Array Signal Processing*. Springer, 2008.
- [19] A. Albarbar, F. Gu, A. D. Ball, and A. Starr, "Acoustic monitoring of engine fuel injection based on adaptive filtering techniques," *Applied Acoustics*, vol. 71, no. 12, pp. 1132–1141, Dec. 2010.
- [20] J. Jiang, F. Gu, R. Gennish, D. J. Moore, G. Harris, and A. D. Ball, "Monitoring of diesel engine combustions based on the acoustic source characterisation of the exhaust system," *Mechanical Systems and Signal Processing*, vol. 22, no. 6, pp. 1465–1480, Aug. 2008.
- [21] Z. K. Peng and F. L. Chu, "Application of the wavelet transform in machine condition monitoring and fault diagnostics: a review with bibliography," *Mechanical Systems and Signal Processing*, vol. 18, no. 2, pp. 199–221, Mar. 2004.
- [22] M. Haag, "Stationary and Nonstationary Random Processes," *Connexions*. [Online]. Available: <http://cnx.org/content/m10684/latest/>.
- [23] W. A. Gardner, A. Napolitano, and L. Paura, "Cyclostationarity: Half a century of research," *Signal Processing*, vol. 86, no. 4, pp. 639–697, Apr. 2006.
- [24] F. Gu, Y. Shao, N. Hu, A. Naid, and A. D. Ball, "Electrical motor current signal analysis using a modified bispectrum for fault diagnosis of downstream mechanical equipment," *Mechanical Systems and Signal Processing*, vol. 25, no. 1, pp. 360–372, Jan. 2011.
- [25] D. Zhen, H. L. Zhao, F. Gu, and A. D. Ball, "Phase-compensation-based dynamic time warping for fault diagnosis using the motor current signal," *Measurement Science and Technology*, vol. 23, no. 5, p. 055601, May 2012.
- [26] G. Dalpiaz, A. Rivola, and R. Rubini, "Effectiveness and sensitivity of vibration processing techniques for local fault detection in gears," *Mechanical Systems and Signal Processing*, vol. 14, no. 3, pp. 387–412, May 2000.
- [27] O. Henniger and S. Muller, "Effects of Time Normalization on the Accuracy of Dynamic Time Warping," in *Biometrics: Theory, Applications, and Systems, 2007. BTAS 2007. First IEEE International Conference on*, 2007, pp. 1 –6.
- [28] V. M. Velichko and N. G. Zagoruyko, "Automatic recognition of 200 words," *International Journal of Man-Machine Studies*, vol. 2, no. 3, pp. 223–234, Jul. 1970.
- [29] H. Sakoe and S. Chiba, "Dynamic programming algorithm optimization for spoken word recognition," *Acoustics, Speech and Signal Processing, IEEE Transactions on*, vol. 26, no. 1, pp. 43 – 49, Feb. 1978.
- [30] C. Myers, L. Rabiner, and A. Rosenberg, "Performance tradeoffs in dynamic time warping algorithms for isolated word recognition," *Acoustics, Speech and Signal Processing, IEEE Transactions on*, vol. 28, no. 6, pp. 623 – 635, Dec. 1980.

- [31] N. E. Huang, Z. Shen, S. R. Long, M. C. Wu, H. H. Shih, Q. Zheng, N.-C. Yen, C. C. Tung, and H. H. Liu, "The empirical mode decomposition and the Hilbert spectrum for nonlinear and non-stationary time series analysis," *Proc. R. Soc. Lond. A*, vol. 454, no. 1971, pp. 903–995, Mar. 1998.
- [32] Y. Xu and H. Zhang, "Recent mathematical developments on empirical mode decomposition," *Advances in Adaptive Data Analysis*, vol. 01, no. 04, pp. 681–702, Oct. 2009.
- [33] R. B. Randall, J. Antoni, and S. Chobsaard, "The relationship between spectral correlation and envelope analysis in the diagnostics of bearing faults and other cyclostationary machine," *Mechanical Systems and Signal Processing*, vol. 15, no. 5, pp. 945–962, Sep. 2001.
- [34] J. R. Stack, R. G. Harley, and T. G. Habetler, "An amplitude Modulation detector for fault diagnosis in rolling element bearings," *Industrial Electronics, IEEE Transactions on*, vol. 51, no. 5, pp. 1097 – 1102, Oct. 2004.
- [35] D.-M. Yang, A. F. Stronach, P. Macconnell, and J. Penman, "Third-order spectral techniques for the diagnosis of motor bearing condition using artificial neural networks," *Mechanical Systems and Signal Processing*, vol. 16, no. 2–3, pp. 391–411, Mar. 2002.
- [36] B. Eugene Parker JR, H. A. Ware, D. P. Wipf, W. R. Tompkins, B. R. Clark, E. C. Larson, and H. Vincent Poor, "Fault diagnostics using statistical change detection in the bi-spectral domain," *Mechanical Systems and Signal Processing*, vol. 14, no. 4, pp. 561–570, Jul. 2000.
- [37] J.-D. Wu and P.-H. Chiang, "Application of Wigner–Ville distribution and probability neural network for scooter engine fault diagnosis," *Expert Systems with Applications*, vol. 36, no. 2, Part 1, pp. 2187–2199, Mar. 2009.
- [38] D. Dragoman, "Applications of the Wigner distribution function in signal processing," *EURASIP J. Appl. Signal Process.*, vol. 2005, pp. 1520–1534, Jan. 2005.
- [39] W. J. Staszewski, K. Worden, and G. R. Tomlinson, "Time-frequency analysis in gearbox fault detection using the Wigner-Ville distribution and pattern recognition," *Mechanical Systems and Signal Processing*, vol. 11, no. 5, pp. 673–692, Sep. 1997.
- [40] T. Classen and W. Mecklenbrauker, "The Wigner Distribution: A Tool for Time-Frequency Signal Analysis - Part 2: Discrete-Time Signals," *Philips Journal of Research*, vol. 35, pp. 276–350, 1980.
- [41] A. Albarbar, F. Gu, and A. D. Ball, "Diesel engine fuel injection monitoring using acoustic measurements and independent component analysis," *Measurement*, vol. 43, no. 10, pp. 1376–1386, Dec. 2010.
- [42] P. Bonato, R. Ceravolo, A. De Stefano, and M. Knaflitz, "Bilinear time-frequency transformations in the analysis of damaged structures," *Mechanical Systems and Signal Processing*, vol. 11, no. 4, pp. 509–527, Jul. 1997.
- [43] F. GU and A. D. BALL, "use of the smoothed pseudo wigner ville distribution in the interpretation of monitored vibration data," *Maintenance*, vol. 10, no. 2, pp. 16–20, Mar. 1995.
- [44] R. K. Young, *Wavelet Theory and Its Applications*. Springer, pp. 19-50 1993.

- [45] W. J. Staszewski and G. R. Tomlinson, "Application of the wavelet transform to fault detection in a spur gear," *Mechanical Systems and Signal Processing*, vol. 8, no. 3, pp. 289–307, May 1994.
- [46] R. Rubini and U. Memeghetti, "Application of the envelope and wavelet transform analysis for the diagnosis of incipient faults in ball bearings," *Mechanical Systems and Signal Processing*, vol. 15, no. 2, pp. 287–302, Mar. 2001.
- [47] N. Baydar and A. Ball, "Detection of gear failures via vibration and acoustic signals using wavelet transform," *Mechanical Systems and Signal Processing*, vol. 17, no. 4, pp. 787–804, Jul. 2003.
- [48] V. Namias, "The Fractional Order Fourier Transform and its Application to Quantum Mechanics," *IMA J Appl Math*, vol. 25, no. 3, pp. 241–265, Mar. 1980.
- [49] D. Mendlovic and H. M. Ozaktas, "Fractional Fourier transforms and their optical implementation: I," *J. Opt. Soc. Am. A*, vol. 10, no. 9, pp. 1875–1881, 1993.
- [50] R. Tao, B. Deng, and Y. Wang, "Research progress of the fractional Fourier transform in signal processing," *Science in China Series F: Information Sciences*, vol. 49, no. 1, pp. 1–25, 2006.
- [51] L. Qi, R. Tao, S. Zhou, and Y. Wang, "Detection and parameter estimation of multicomponent LFM signal based on the fractional fourier transform," *Science in China Series F: Information Sciences*, vol. 47, no. 2, pp. 184–198, 2004.
- [52] D. Zhen, J. Gu, T. Wang, F. Gu, and A. Ball, "Diagnostic Feature Development based on Dynamic Time Warping of Dynamic Signals under Variable Machine Operating Condition." In: CM 2010 and MFPT 2010: The Seventh International Conference on Condition Monitoring and Machinery Failure Prevention Technologies, 22-Jun-2010.
- [53] E. J. Keogh and M. J. Pazzani, "Derivative Dynamic Time Warping." In Proc. of the First Intl. SIAM Intl. Conf. on Data Mining, Chicago, Illinois, 2001.
- [54] R. Bellman and R. Kalaba, "On adaptive control processes," *Automatic Control, IRE Transactions on*, vol. 4, no. 2, pp. 1-9, Nov. 1959.
- [55] B. Huang and W. Kinsner, "ECG frame classification using dynamic time warping," in *Electrical and Computer Engineering, 2002. IEEE CCECE 2002. Canadian Conference on*, 2002, vol. 2, pp. 1105 – 1110 vol.2.
- [56] T. Syeda-Mahmood, D. Beymer, and F. Wang, "Shape-based Matching of ECG Recordings," in *Engineering in Medicine and Biology Society, 2007. EMBS 2007. 29th Annual International Conference of the IEEE*, 2007, pp. 2012 – 2018.
- [57] V. Tuzcu and S. Nas, "Dynamic time warping as a novel tool in pattern recognition of ECG changes in heart rhythm disturbances," in *Systems, Man and Cybernetics, 2005 IEEE International Conference on*, 2005, vol. 1, pp. 182 – 186 Vol. 1.
- [58] J. Aach and G. M. Church, "Aligning Gene Expression Time Series with Time Warping Algorithms," *Bioinformatics*, vol. 17, no. 6, pp. 495–508, Jun. 2001.
- [59] F. Hermans and E. Tsiorkova, "Merging Microarray Cell Synchronization Experiments Through Curve Alignment," *Bioinformatics*, vol. 23, no. 2, pp. e64–e70, Jan. 2007.
- [60] M. Faundez-Zanuy, "On-line signature recognition based on VQ-DTW," *Pattern Recognition*, vol. 40, no. 3, pp. 981–992, Mar. 2007.

- [61] T. M. Rath and R. Manmatha, "Word image matching using dynamic time warping," in *Computer Vision and Pattern Recognition, 2003. Proceedings. 2003 IEEE Computer Society Conference on*, 2003, vol. 2, p. II-521 – II-527 vol.2.
- [62] K. Gollmer and C. Posten, "Supervision of bioprocesses using a dynamic time warping algorithm," *Control Engineering Practice*, vol. 4, no. 9, pp. 1287–1295, Sep. 1996.
- [63] P. Senin, "Dynamic Time Warping Algorithm Review." Information and Computer Science Department University of Hawaii at Manoa Honolulu, USA, 2008.
- [64] D. Zhen, A. Alibarbar, X. Zhou, F. Gu, and A. D. Ball, "Electrical Motor Current Signal Analysis using a Dynamic Time Warping Method for Fault Diagnosis," *Journal of Physics: Conference Series*, vol. 305, p. 012093, Jul. 2011.
- [65] J. B. Kruskall and M. Liberman, "The symmetric time warping algorithm: From continuous to discrete." *Time Warps, String Edits and Macromolecules*. Addison-Wesley, 1983.
- [66] J. Antoni, J. Daniere, and F. Guillet, "Effective vibration analysis of IC engines using cyclostationarity. Part I-A methodology for condition monitoring," *Journal of Sound and Vibration*, vol. 257, no. 5, pp. 815–837, Nov. 2002.
- [67] Y. Xie and B. Wiltgen, "Adaptive Feature Based Dynamic Time Warping," *IJCSNS International Journal of Computer Science and Network Security*, vol. 10, no. 1, pp. 264–273, 2010.
- [68] F. Itakura, "Minimum prediction residual principle applied to speech recognition," *Acoustics, Speech and Signal Processing, IEEE Transactions on*, vol. 23, no. 1, pp. 67 – 72, Feb. 1975.
- [69] S. Chu, E. Keogh, D. Hart, and M. Pazzani, "Iterative deepening dynamic time warping for time series." *In Proc 2 nd SIAM International Conference on Data Mining*, 2002.
- [70] E. J. Keogh and M. J. Pazzani, "Scaling up dynamic time warping for datamining applications," in *Proceedings of the sixth ACM SIGKDD international conference on Knowledge discovery and data mining*, New York, NY, USA, 2000, pp. 285–289.
- [71] M. E. H. Benbouzid, "A review of induction motors signature analysis as a medium for faults detection," in *Industrial Electronics Society, 1998. IECON '98. Proceedings of the 24th Annual Conference of the IEEE*, 1998, vol. 4, pp. 1950 – 1955 vol.4.
- [72] J. R. Stack, T. G. Habetler, and R. G. Harley, "Bearing fault detection via autoregressive stator current modeling," *Industry Applications, IEEE Transactions on*, vol. 40, no. 3, pp. 740 – 747, Jun. 2004.
- [73] R. R. Obaid, T. G. Habetler, and R. M. Tallam, "Detecting load unbalance and shaft misalignment using stator current in inverter-driven induction motors," in *Electric Machines and Drives Conference, 2003. IEMDC'03. IEEE International*, 2003, vol. 3, pp. 1454 – 1458 vol.3.
- [74] M. T. Chen, "Digital algorithms for measurement of voltage flicker," *Generation, Transmission and Distribution, IEE Proceedings-*, vol. 144, no. 2, pp. 175 –180, Mar. 1997.

- [75] F. Zhang, Z. Geng, and W. Yuan, "The algorithm of interpolating windowed FFT for harmonic analysis of electric power system," *Power Delivery, IEEE Transactions on*, vol. 16, no. 2, pp. 160–164, Apr. 2001.
- [76] D. Lyon, "The Discrete Fourier Transform, Part 4: Spectral Leakage.," *The Journal of Object Technology*, vol. 8, no. 7, p. 23, 2009.
- [77] Y. F. Li and K. F. Chen, "Eliminating the picket fence effect of the fast Fourier transform," *Computer Physics Communications*, vol. 178, no. 7, pp. 486–491, Apr. 2008.
- [78] A. Naid, F. S. Gu, Y. M. Shao, S. Al-Arbi, and A. Ball, "Bispectrum Analysis of Motor Current Signals for Fault Diagnosis of Reciprocating Compressors," *Key Engineering Materials*, vol. 413–414, pp. 505–511, Jun. 2009.
- [79] F. Filippetti, G. Franceschini, C. Tassoni, and P. Vas, "AI techniques in induction machines diagnosis including the speed ripple effect," *Industry Applications, IEEE Transactions on*, vol. 34, no. 1, pp. 98–108, Feb. 1998.
- [80] A. Bellini, F. Filippetti, G. Franceschini, C. Tassoni, and G. B. Kliman, "Quantitative evaluation of induction motor broken bars by means of electrical signature analysis," *Industry Applications, IEEE Transactions on*, vol. 37, no. 5, pp. 1248–1255, Oct. 2001.
- [81] R. R. Schoen, T. G. Habetler, F. Kamran, and R. G. Bartfield, "Motor bearing damage detection using stator current monitoring," *Industry Applications, IEEE Transactions on*, vol. 31, no. 6, pp. 1274–1279, Dec. 1995.
- [82] R. W. Wall, "Simple methods for detecting zero crossing," in *Industrial Electronics Society, 2003. IECON '03. The 29th Annual Conference of the IEEE*, 2003, vol. 3, pp. 2477–2481 Vol.3.
- [83] E. A. Feilat, "Detection of voltage envelope using Prony analysis-Hilbert transform method," *IEEE Transactions on Power Delivery*, vol. 21, no. 4, pp. 2091–2093, Oct. 2006.
- [84] T. Priede, "In Search of Origins of Engine Noise - an Historical Review," SAE International, Warrendale, PA, 800534, Feb. 1980.
- [85] M. Hosseini Fouladi, M. J. M. Nor, and A. K. Ariffin, "Spectral analysis methods for vehicle interior vibro-acoustics identification," *Mechanical Systems and Signal Processing*, vol. 23, no. 2, pp. 489–500, Feb. 2009.
- [86] B. J. Challen and D. M. Croker, "A Review of Recent Progress in Diesel Engine Noise Reduction," SAE International, Warrendale, PA, 820517, Feb. 1982.
- [87] C. M. P. Chan and D. Anderton, "The effect of engine bore and engine noise, surface vibration and combustion for a six-cylinder engine." ISVR report No. 74/2, University of Southampton, 1974.
- [88] A. G. Bell, "The effect of combustion system on engine noise," presented at the Proceedings of the Diesel Engine Noise Conference, Society of Automotive Engineers, SP-397, August 1975., 1975.
- [89] R. R. Schoen and T. G. Habetler, "Effects of time-varying loads on rotor fault detection in induction machines," *Industry Applications, IEEE Transactions on*, vol. 31, no. 4, pp. 900–906, Aug. 1995.
- [90] Z. Liu, X. Yin, Z. Zhang, D. Chen, and W. Chen, "Online rotor mixed fault diagnosis way based on spectrum analysis of instantaneous power in squirrel cage

- induction motors,” *Energy Conversion, IEEE Transactions on*, vol. 19, no. 3, pp. 485 – 490, Sep. 2004.
- [91] R. G. T. Almeida, S. A. Da Silva Vicente, and L. R. Padovese, “New technique for evaluation of global vibration levels in rolling bearings,” *Shock and Vibration*, no. Volume 9, Numbers 4–5/2002, pp. 225–234.
- [92] “JCB 444 Turbocharged Diesel Engine.” JCB Power Systems Ltd.
- [93] B. Tesfa, R. Mishra, F. Gu, and A. D. Ball, “Water injection effects on the performance and emission characteristics of a CI engine operating with biodiesel,” *Renewable Energy*, vol. 37, no. 1, pp. 333–344, Jan. 2012.
- [94] D. D. Reynolds, *Engineering Principles of Acoustics: Noise and Vibration Control*. Pearson Allyn & Bacon, 1981.
- [95] C. C. Enweremadu and H. L. Rutto, “Combustion, emission and engine performance characteristics of used cooking oil biodiesel—A review,” *Renewable and Sustainable Energy Reviews*, vol. 14, no. 9, pp. 2863–2873, Dec. 2010.
- [96] H. Aydin and H. Bayindir, “Performance and emission analysis of cottonseed oil methyl ester in a diesel engine,” *Renewable Energy*, vol. 35, no. 3, pp. 588–592, Mar. 2010.
- [97] H. Hazar, “Effects of biodiesel on a low heat loss diesel engine,” *Renewable Energy*, vol. 34, no. 6, pp. 1533–1537, Jun. 2009.
- [98] S. Murillo, J. L. Míguez, J. Porteiro, E. Granada, and J. C. Morán, “Performance and exhaust emissions in the use of biodiesel in outboard diesel engines,” *Fuel*, vol. 86, no. 12–13, pp. 1765–1771, Aug. 2007.
- [99] J. Xue, T. E. Grift, and A. C. Hansen, “Effect of biodiesel on engine performances and emissions,” *Renewable and Sustainable Energy Reviews*, vol. 15, no. 2, pp. 1098–1116, Feb. 2011.
- [100] L. C. Meher, D. Vidya Sagar, and S. N. Naik, “Technical aspects of biodiesel production by transesterification—a review,” *Renewable and Sustainable Energy Reviews*, vol. 10, no. 3, pp. 248–268, Jun. 2006.
- [101] K. Hamasaki, H. Tajima, K. Takasaki, K. Satohira, M. Enomoto, and H. Egawa, “Utilization of Waste Vegetable Oil Methyl Ester for Diesel Fuel,” SAE International, Warrendale, PA, 2001-01-2021, May 2001.
- [102] M. Canakci, A. N. Ozsezen, and A. Turkcan, “Combustion analysis of preheated crude sunflower oil in an IDI diesel engine,” *Biomass and Bioenergy*, vol. 33, no. 5, pp. 760–767, May 2009.
- [103] G. Tashtoush, M. I. Al-Widyan, and A. O. Al-Shyoukh, “Combustion performance and emissions of ethyl ester of a waste vegetable oil in a water-cooled furnace,” *Applied Thermal Engineering*, vol. 23, no. 3, pp. 285–293, Feb. 2003.
- [104] M. . Dorado, E. Ballesteros, J. . Arnal, J. Gómez, and F. . López, “Exhaust emissions from a Diesel engine fueled with transesterified waste olive oil☆,” *Fuel*, vol. 82, no. 11, pp. 1311–1315, Jul. 2003.
- [105] M. F. J. Brunt, H. Rai, and A. L. Emtage, “The Calculation of Heat Release Energy from Engine Cylinder Pressure Data,” SAE International, Warrendale, PA, 981052, Feb. 1998.
- [106] R. van Basshuysen and F. Schaefer, “Internal combustion engine handbook - basics, components, systems and perspectives,” no. R-345, 2004.

- [107] J. Heywood, *Internal combustion engine fundamentals*. McGraw-Hill, pp. 1-60, 1988.
- [108] B.-F. Lin, J.-H. Huang, and D.-Y. Huang, "Experimental study of the effects of vegetable oil methyl ester on DI diesel engine performance characteristics and pollutant emissions," *Fuel*, vol. 88, no. 9, pp. 1779–1785, Sep. 2009.
- [109] M. Gumus, "A comprehensive experimental investigation of combustion and heat release characteristics of a biodiesel (hazelnut kernel oil methyl ester) fueled direct injection compression ignition engine," *Fuel*, vol. 89, no. 10, pp. 2802–2814, Oct. 2010.
- [110] A. N. Ozsezen, M. Canakci, A. Turkcan, and C. Sayin, "Performance and combustion characteristics of a DI diesel engine fueled with waste palm oil and canola oil methyl esters," *Fuel*, vol. 88, no. 4, pp. 629–636, Apr. 2009.
- [111] X. Meng, G. Chen, and Y. Wang, "Biodiesel production from waste cooking oil via alkali catalyst and its engine test," *Fuel Processing Technology*, vol. 89, no. 9, pp. 851–857, Sep. 2008.
- [112] M. Lapuerta, O. Armas, R. Ballesteros, and J. Fernández, "Diesel emissions from biofuels derived from Spanish potential vegetable oils," *Fuel*, vol. 84, no. 6, pp. 773–780, Apr. 2005.
- [113] L. Pruvost, Q. Leclère, and E. Parizet, "Diesel engine combustion and mechanical noise separation using an improved spectrofilter," *Mechanical Systems and Signal Processing*, vol. 23, no. 7, pp. 2072–2087, Oct. 2009.
- [114] W. Li, F. Gu, A. D. Ball, A. Y. T. Leung, and C. E. Phipps, "A study of the noise from diesel engines using the independent component analysis," *Mechanical Systems and Signal Processing*, vol. 15, no. 6, pp. 1165–1184, Nov. 2001.
- [115] K. Schmillen and J. Wolschendorf, *Cycle-to-cycle variations of combustion noise in diesel engines*. Society of Automotive Engineers, pp. 1-11, 1989.
- [116] V. T. C. Tung and M. J. Crocker, "Diesel Engine Noise and Relationship to Cylinder Pressure," SAE International, Warrendale, PA, 820237, Feb. 1982.
- [117] Y. Fujimoto, T. Suzuki, and Y. Ochiai, "Some new results concerning parameters influencing piston slap in reciprocating machinery," *Mechanical Engineering Publications Limited*, pp. 33-38, 1979.
- [118] S.-H. Cho, S.-T. Ahn, and Y.-H. Kim, "A simple model to estimate the impact for induced by piston slap," *Journal of Sound and Vibration*, vol. 255, no. 2, pp. 229–242, Aug. 2002.
- [119] G. Shu and X. Liang, "Identification of complex diesel engine noise sources based on coherent power spectrum analysis," *Mechanical Systems and Signal Processing*, vol. 21, no. 1, pp. 405–416, Jan. 2007.
- [120] T. Priede, "Problems and Developments in Automotive Engine Noise Research," SAE International, Warrendale, PA, 790205, Feb. 1979.
- [121] J. S. Bendat and A. G. Piersol, *Engineering Applications of Correlation and Spectral Analysis*, 2nd ed. Wiley-Blackwell, 1993.
- [122] H. M. Ozaktas, O. Arikan, M. A. Kutay, and G. Bozdogat, "Digital computation of the fractional Fourier transform," *Signal Processing, IEEE Transactions on*, vol. 44, no. 9, pp. 2141–2150, Sep. 1996.

- [123] L. B. Almeida, "The fractional Fourier transform and time-frequency representations," *Signal Processing, IEEE Transactions on*, vol. 42, no. 11, pp. 3084–3091, Nov. 1994.
- [124] A. Y. T. LEUNG and W. LI, "Using Acoustic Signals in Machine Condition Monitoring." Proceedings of International Conference on Vibration Engineering, Dalian, China, 1998.
- [125] J. Lin and L. Qu, "Feature extraction based on morlet wavelet and its application for mechanical fault diagnosis," *Journal of Sound and Vibration*, vol. 234, no. 1, pp. 135–148, Jun. 2000.
- [126] M. Lang, H. Guo, J. E. Odegard, C. S. Burrus, and J. Wells, R.O., "Noise reduction using an undecimated discrete wavelet transform," *Signal Processing Letters, IEEE*, vol. 3, no. 1, pp. 10–12, Jan. 1996.
- [127] H. Zheng, Z. Li, and X. Chen, "Gear fault diagnosis based on continuous wavelet transform," *Mechanical Systems and Signal Processing*, vol. 16, no. 2–3, pp. 447–457, Mar. 2002.
- [128] P. M. Bentley and J. T. E. McDonnell, "Wavelet transforms: an introduction," *Electronics Communication Engineering Journal*, vol. 6, no. 4, pp. 175–186, Aug. 1994.
- [129] C. K. Chui, *An Introduction to Wavelets*. Academic Press, pp. 23-74, 1992.
- [130] O. Rioul and P. Duhamel, "Fast algorithms for discrete and continuous wavelet transforms," *Information Theory, IEEE Transactions on*, vol. 38, no. 2, pp. 569–586, Mar. 1992.
- [131] G. Niu, A. Widodo, J.-D. Son, B.-S. Yang, D.-H. Hwang, and D.-S. Kang, "Decision-level fusion based on wavelet decomposition for induction motor fault diagnosis using transient current signal," *Expert Systems with Applications*, vol. 35, no. 3, pp. 918–928, Oct. 2008.
- [132] F. Combet and L. Gelman, "An automated methodology for performing time synchronous averaging of a gearbox signal without speed sensor," *Mechanical Systems and Signal Processing*, vol. 21, no. 6, pp. 2590–2606, Aug. 2007.
- [133] W. Wu, J. Lin, S. Han, and X. Ding, "Time domain averaging based on fractional delay filter," *Mechanical Systems and Signal Processing*, vol. 23, no. 5, pp. 1447–1457, Jul. 2009.
- [134] K. R. Fyfe and E. D. S. Munck, "Analysis of computed order tracking," *Mechanical Systems and Signal Processing*, vol. 11, no. 2, pp. 187–205, Mar. 1997.
- [135] B. Wade, "Operating Maintenance and Parts Manual." Bucks, England.
- [136] A. Amar M Naid, *Fault Detection and Diagnosis of Reciprocating Compressors using Motor Current Signature Analysis*. PhD thesis, chapter 4, 2009.